

Imperial College London  
National Heart and Lung Institute  
November 2020

---

**Paracrine crosstalk between  
endothelial cells and cardiomyocytes  
during inflammation**

Jerome Fourre

---

*A thesis submitted for the degree of Doctor of Philosophy (PhD)*

*For my parents.*

## **Statement of originality**

I hereby certify that this submission and its content are the products of my own work. To the best of my knowledge, it includes no material which is the result of a collaboration, or material provided and/or published by others, unless it is explicitly acknowledged and authorised.

Any assistance I have received, and all sources have been fully acknowledged.

Jerome Fourre

## **Copyright declaration**

The copyright of this thesis rests with the author. Unless otherwise indicated, its contents are licensed under a Creative Commons Attribution-Non-Commercial-No Derivatives 4.0 International Licence (CC BY-NC-ND).

Under this licence, you may copy and redistribute the material in any medium or format on the condition that; you credit the author, do not use it for commercial purposes and do not distribute modified versions of the work.

When reusing or sharing this work, ensure you make the licence terms clear to others by naming the licence and linking to the licence text.

Please seek permission from the copyright holder for uses of this work that are not included in this licence or permitted under UK Copyright Law.

## Abstract

Endothelial cells (EC) release paracrine factors which can modulate the survival, morphology, and function of neighbouring cardiomyocytes (CM), e.g. contraction and relaxation. In multiple cardiomyopathies, as well as in heart failure, EC dysfunction correlates strongly with severity and prognosis, and moreover, endothelial inflammation is thought to precede this dysfunction. While it is known that EC functions are modified by inflammation, the paracrine effects of this response on neighbouring CM are poorly understood and too often confused with those of endothelial dysfunction. I hypothesised that calcium handling and contractile properties of CM were differently regulated by inflamed EC.

To investigate this, a co-culture system was first validated as a model of the paracrine EC-CM crosstalk. A pro-inflammatory cocktail of TNF $\alpha$ , IL-1 $\beta$  and hIL-6 ("Cytomix") was then validated as a pre-conditioning treatment for cardiac microvascular EC. Adult ventricular CM were co-cultured with untreated or Cytomix-treated EC. Calcium transients were then analysed in CM using Fluo-4 and Fura-2. Cell contractility and relaxation were also studied using an automated CytoCypher™ system. Finally, living rat myocardial slices were used to investigate the effects of Cytomix in a more complex heterocellular model.

Co-culture with Cytomix-treated EC induced a significant shortening of calcium transients in CM compared to untreated EC (thus validating the hypothesis). This was due to an increase in SERCA activity. However, the cell shortening amplitude and rate of relaxation were unaffected by co-culture or Cytomix treatment, while data also suggests that the myofilament sensitivity to calcium was unchanged. In cultured myocardial slices, Cytomix treatment increased force but not the passive tension, although this was limited to high levels of stretch and kinetics were unchanged compared to untreated slices.

Further work is required to better define and understand these mechanisms. This could help determine the therapeutic potential of controlling EC function in inflammatory heart diseases.

## Acknowledgements

First, I cannot express enough gratitude to Prof. Justin Mason and Prof. Cesare Terracciano, for placing their trust in me, for investing so much in my learning, and in guiding me throughout my MRes and PhD. Their mentorship, support, encouragement, patience, and openness have been absolutely exemplary from beginning to end, and it has been an honour to work for them.

I have also been incredibly fortunate to have met Charis Pericleous and Rob Maughan. These fantastic scientists have helped me repeatedly in difficult times, and I must thank them for their expert advice regarding flow cytometry, ELISAs, and bioinformatics, as well as their extremely generous feedback for many of my other experiments. My PhD would not have been the same without them. I also address my thanks to Damien Calay, who supervised my first steps in this project with great talent and an inspiring professionalism. I am very thankful to Peter O’Gara for isolating cardiomyocytes, and to Brian Wang for isolating and providing cardiac fibroblasts. I am also very thankful to Stephen Rothery (FILM facility) for providing his expert assistance and trainings in microscopy. Finally, I am immensely grateful to the British Heart Foundation, who funded this work as part of an MRes/PhD 1+3 years studentship (FS/15/65/32036).

The overall experience of this PhD has truly been alleviated by my peers, with whom frequent talks and occasional collaborations have brightened many days. In that, Marie Lang deserves a special thank you. It has been a pleasure going through this long journey at the side of this incredibly talented scientist, whom I predict has started a great career. Thank you also to Sam Kit-Anan, Ifigeneia Bardi, Filippo Perbellini, and Oisín King for their support, great feedback, and their friendship all these years, and with whom I had the most stimulating and entertaining discussions of my life.

Finally, I would like to thank my family and friends, in France and elsewhere, who have been all so supportive since the very beginning. A huge thank you to my parents, in particular, for their many selfless sacrifices. Thank you, most of all, to Emy, for giving me so much strength, encouragement, support, and love, whatever I choose to do and whatever happens.

# TABLE OF CONTENTS

<b><i>Statement of originality</i></b>	<b>3</b>
<b><i>Copyright declaration</i></b>	<b>4</b>
<b><i>Abstract</i></b>	<b>5</b>
<b><i>Acknowledgements</i></b>	<b>6</b>
<b><i>Table of contents</i></b>	<b>7</b>
<b><i>List of figures</i></b>	<b>13</b>
<b><i>List of tables</i></b>	<b>15</b>
<b><i>List of Uncommon Abbreviations and Acronyms</i></b>	<b>16</b>

## CHAPTER 1

<b>INTRODUCTION</b>	<b>21</b>
<b>1.1 HEART FAILURE AND INFLAMMATION .....</b>	<b>22</b>
1.1.1 Heart failure with preserved ejection fraction .....	22
1.1.2 Ischemic heart disease and myocardial infarction .....	24
1.1.3 The role of inflammation in non-ischemic cardiomyopathies .....	25
1.1.4 Inflammatory cardiomyopathy .....	26
<b>1.2 ENDOTHELIAL INFLAMMATION AND DYSFUNCTION .....</b>	<b>27</b>
1.2.1 Inflammatory cytokines and endothelial cells .....	27
1.2.2 Vascular permeability and inflammation .....	29
1.2.3 Differential secretion of cardiotropic agents .....	30
<b>1.3 EXCITATION-CONTRACTION COUPLING IN CM AND ITS MODULATION BY EC-     DERIVED CARDIOTROPES .....</b>	<b>33</b>
1.3.1 Effects of nitric oxide on contractility and relaxation .....	33
1.3.2 Effects of endothelin-1 on contractility and relaxation .....	34
1.3.3 Pacemaker activity and ventricular rhythmicity .....	35
1.3.4 Action potential (AP) .....	36
1.3.5 Calcium-induced calcium release (CICR) .....	39
1.3.6 Sarco-endoplasmic reticulum Ca <sup>2+</sup> -ATPase (SERCA) .....	40
1.3.7 Sodium-calcium exchanger (NCX) .....	41
1.3.8 Additional mechanisms of calcium extrusion .....	43
1.3.9 Sarcomeres and myofilament sensitivity to calcium .....	45
1.3.10 Bowditch, Frank-Starling and Anrep effects .....	46

1.3.11	Other mediators of EC activity on CM, and the pitfalls of transitive logic .....	48
1.3.12	Conclusions.....	52
<b>1.4</b>	<b>HYPOTHESIS .....</b>	<b>53</b>
<b>1.5</b>	<b>AIMS .....</b>	<b>53</b>
<b>1.6</b>	<b>STUDY DESIGN .....</b>	<b>54</b>

## CHAPTER 2

<b>MATERIAL AND METHODS</b>	<b>57</b>
<b>2.1 ANIMAL MODELS .....</b>	<b>58</b>
2.1.1 Sprague-Dawley.....	58
2.1.2 Myocardial infarction (MI) model in rats .....	58
<b>2.2 SOLUTIONS .....</b>	<b>59</b>
<b>2.3 CELL CULTURE.....</b>	<b>62</b>
2.3.1 Culture of human EC.....	62
2.3.2 Isolation and culture of human adult cardiac fibroblasts .....	62
2.3.2 Isolation of adult rat ventricular myocytes (ARVM) .....	63
2.3.3 Culture of ARVM .....	64
2.3.4 Transwell co-culture of EC and CM .....	64
<b>2.4 SDS-PAGE AND WESTERN BLOTTING .....</b>	<b>66</b>
2.4.1 Sample preparation .....	66
2.4.2 Quantification of protein concentration .....	66
2.4.3 SDS-PAGE.....	67
2.4.4 Protein transfer and blotting .....	67
2.4.5 Imaging and quantification .....	68
<b>2.5 ENDOTHELIAL CELLS STUDIES .....</b>	<b>69</b>
2.5.1 Flow cytometric characterisation of HCMEC .....	69
2.5.2 Cell cycle progression .....	70
2.5.3 Endothelial permeability .....	70
2.5.4 Thrombin-induced calcium transients .....	71
2.5.5 Endothelial NO bioavailability.....	72
<b>2.6 CELL SECRETOME CHARACTERISATION .....</b>	<b>74</b>
2.6.1 Human XL Cytokine Profiler™ Array .....	74
2.6.2 Enzyme-Linked Immunosorbent Assay (ELISA).....	74
<b>2.7 CARDIOMYOCYTE STUDIES.....</b>	<b>76</b>



2.7.1	Immunofluorescent staining, confocal microscopy, and CM planimetry .....	76
2.7.2	Normal calcium transient analysis .....	77
2.7.3	Fractional release of calcium .....	78
2.7.4	Differentiating the mechanisms of calcium extrusion .....	78
2.7.5	Contractility and relaxation of isolated ARVM .....	80
2.7.6	Calcium transients with Fura-2.....	80
2.7.7	Calcium sensitivity of myofilaments .....	81
2.7.8	Bioinformatic meta-analysis of gene expression.....	82
<b>2.8</b>	<b>LIVING MYOCARDIAL SLICES.....</b>	<b>83</b>
2.8.1	Rat myocardial slice preparation and culture .....	83
2.8.2	Rat myocardial slice contractility .....	84
<b>2.9</b>	<b>ANTIBODIES .....</b>	<b>86</b>
<b>2.10</b>	<b>STATISTICS .....</b>	<b>87</b>

### CHAPTER 3

	<b>CO-CULTURE MODEL TO TEST THE PARACRINE EFFECTS OF CARDIAC MICROVASCULAR ENDOTHELIAL CELLS ON ADULT VENTRICULAR CARDIOMYOCYTES</b>	<b>89</b>
<b>3.1</b>	<b>INTRODUCTION.....</b>	<b>90</b>
<b>3.2</b>	<b>METHODS .....</b>	<b>92</b>
3.2.1	Experimental design for co-cultures .....	92
3.2.2	Coronary ligation in rat .....	93
3.2.3	Calcium transient analysis by Optical Mapping .....	93
3.2.4	Flow cytometry with intracellular staining.....	93
3.2.5	Immunostaining and confocal microscopy .....	94
3.2.6	Statistics .....	94
<b>3.3</b>	<b>RESULTS.....</b>	<b>95</b>
3.3.1	There is lack of consensus on the basic methodology for EC-CM co-cultures .....	95
3.3.2	Transwell co-culture system is the optimal model to study the paracrine effects of EC on CM .....	98
3.3.3	Cardiac and non-cardiac EC might regulate calcium handling of CM differently.....	103
3.3.4	HCMEC did not induce remodelling of cell dimensions and sarcomeres in ARVM after 24 hours in Transwell co-culture .....	103
3.3.5	HCMEC produced the same paracrine effects on calcium handling in ARVM after 4 or 24 hours of Transwell co-culture .....	107

3.3.6	HCMEC conserved their paracrine effects on calcium handling of ARVM isolated after myocardial infarction .....	107
3.3.7	Use of the custom designed co-culture media did not induce transdifferentiation of HCMEC into lymphatic EC or fibroblasts .....	109
<b>3.4</b>	<b>DISCUSSION .....</b>	<b>111</b>
3.4.1	Limitations and failures of published research with EC-CM co-cultures.....	111
3.4.2	Transwell inserts are most appropriate to study the paracrine interaction of EC and CM without mechanical or electrophysiological interference, or loss of secretome .....	112
3.4.3	HCMEC are most relevant for co-cultures with CM due to high EC heterogeneity .....	114
3.4.4	Using ARVM, a custom co-culture medium and a short time-point to circumvent the limitations of in vitro co-culture of EC and CM .....	116
3.4.5	No hypertrophy of ARVM was detected after co-culture with HCMEC .....	118
3.4.6	MI did not affect the response of ARVM to EC co-culture .....	119
3.4.7	Summary the effects of EC on ARVM in these co-culture conditions.....	120

## CHAPTER 4

<b>PRO-INFLAMMATORY TREATMENT OF CARDIAC MICROVASCULAR</b>		
<b>ENDOTHELIAL CELLS WITH TNF ALPHA, IL-1 BETA AND HYPER-IL-6</b>		<b>121</b>
<b>4.1</b>	<b>INTRODUCTION.....</b>	<b>122</b>
<b>4.2</b>	<b>METHODS .....</b>	<b>124</b>
4.2.1	Cell culture, cytokine treatments, and co-cultures.....	124
4.2.2	SDS-PAGE and western blotting .....	125
4.2.3	Cell cycle analysis by flow cytometry .....	125
4.2.4	Endothelial permeability, by transmural diffusion of FITC-Dextran.....	126
4.2.5	Thrombin-induced calcium transients in EC – Optical Mapping .....	126
4.2.6	Confocal imaging of DAF-2 DA fluorescence .....	127
4.2.7	Human XL Cytokine Profiler™ Array .....	127
4.2.8	Enzyme-Linked Immunosorbent Assay (ELISA).....	127
4.2.9	Meta-analysis .....	129
4.2.10	Statistics.....	129
<b>4.3</b>	<b>RESULTS.....</b>	<b>130</b>
4.3.1	Inflammatory signalling in EC after treatment with TNF $\alpha$ , IL-1 $\beta$ or hIL-6 alone.....	130
4.3.2	Protein expression of inflammatory markers in EC is cytokine-dependent and distinct in the cytokine co-treatment (Cytomix) .....	132
4.3.3	Cell cycle progression was arrested at G1 in HCMEC after Cytomix treatment.....	134
4.3.4	Effect of Cytomix on basal and thrombin-induced endothelial permeability .....	136

4.3.5	Effect of Cytomix on thrombin-induced calcium transients in HCMEC .....	138
4.3.6	Effect of Cytomix on basal and thrombin-induced NO synthesis in HCMEC.....	140
4.3.7	Screening for EC-secreted inflammatory markers and candidate mediators for the paracrine effects of EC on CM .....	142
4.3.8	Quantitative validation of soluble factors identified with the array as potentially enriched by Cytomix treatment on HCMEC.....	146
4.3.9	Meta-analytical assessment of ligand-receptor interactions in CM, based on the expression of specific receptors in published large datasets .....	149
<b>4.4</b>	<b>DISCUSSION .....</b>	<b>152</b>
4.4.1	Modelling the trans-signalling of IL-6 in EC in vitro with hIL-6 .....	153
4.4.2	hIL-6 interfered with the TNF $\alpha$ and IL-1 $\beta$ signalling in EC .....	154
4.4.3	Anti-proliferative properties of Cytomix treatment in HCMEC, recapitulating the pathophysiology of microvascular inflammation .....	155
4.4.4	Lack of effect of Cytomix treatment on endothelial permeability .....	156
4.4.5	Cytomix impaired the calcium release in EC after acute thrombin treatments .....	158
4.4.6	On the “paradoxical” thrombin-induced increase of NO in Cytomix-treated EC .....	159
4.4.7	Screening and differential release by EC of markers of endothelial inflammation after treatment with Cytomix.....	161
4.4.8	Are the soluble factors secreted by Cytomix-treated HCMEC likely to affect the function of ARVM in co-culture? .....	164
4.4.9	Conclusions on the effects of Cytomix in EC .....	165

## **CHAPTER 5**

<b>EFFECTS OF CYTOMIX-TREATED CARDIAC MICROVASCULAR ENDOTHELIAL CELLS ON CO-CULTURED ADULT RAT VENTRICULAR MYOCYTES</b>	<b>167</b>
<b>5.1 INTRODUCTION.....</b>	<b>168</b>
<b>5.2 METHODS .....</b>	<b>170</b>
5.2.1 Cell culture, cytokine treatments, and co-cultures .....	170
5.2.2 Optical Mapping, fractional release, and quantification of SERCA/NCX activity .....	170
5.2.3 Western blotting .....	171
5.2.4 CytoCypher™ MultiCell system – Contractility and calcium dual measurements .....	171
5.2.5 Calcium-contraction hysteresis loops and calcium sensitivity of myofilaments .....	172
5.2.6 Adult living ultrathin myocardial slices and force transducer .....	172
5.2.7 Statistics .....	172
<b>5.3 RESULTS.....</b>	<b>173</b>
5.3.1 Shortening of calcium transients in CM after co-culture with Cytomix-treated EC .....	173
5.3.2 Efficiency of calcium release from the SR of CM after co-culture with EC .....	175

5.3.3	Cytomix-induced shortening of calcium transients in EC-CM co-cultures is due to higher SERCA activity .....	177
5.3.4	Changes of protein expression and phosphorylation in CM after co-culture .....	177
5.3.5	Co-culture with untreated or Cytomix-treated EC did not alter CM contractility .....	179
5.3.6	Co-culture of CM with untreated or Cytomix-treated EC did not alter the calcium sensitivity of myofilaments .....	181
5.3.7	Cytomix only affected the contractility of cardiac tissue at high levels of preload .....	181
<b>5.4</b>	<b>DISCUSSION .....</b>	<b>185</b>
5.4.1	Differential effects of untreated and Cytomix-treated EC on calcium extrusion in co-cultured CM: lost function or new function? .....	185
5.4.2	Increased SERCA activity mediates the lusitropic effects of Cytomix-treated EC on calcium handling in co-cultured CM .....	186
5.4.3	Inotropic effect of Cytomix-treated EC at the level of SR Ca <sup>2+</sup> release .....	188
5.4.4	On the dissociation of calcium transient kinetics and contraction kinetics .....	189
5.4.5	On the load-dependent effect of Cytomix on whole tissue contractility .....	190
5.4.6	Conclusion on the effect of Cytomix on the paracrine EC-CM crosstalk .....	192

## CHAPTER 6

<b>GENERAL DISCUSSION</b>	<b>193</b>	
<b>6.1 RECAPITULATION AND IMPLICATIONS OF RESULTS .....</b>	<b>194</b>	
6.1.1	Limitations of interpreting changes of CM function in co-culture with EC .....	195
6.1.2	Potential mediators of the paracrine effects of untreated and Cytomix-treated EC on calcium handling in CM .....	196
6.1.3	Additional remarks .....	197
<b>6.2 COMPARISON WITH A RECENTLY PUBLISHED STUDY .....</b>	<b>198</b>	
6.2.1	Comparison of general methods .....	198
6.2.2	The effects of pro-inflammatory treatment on endothelial NO bioavailability .....	200
6.2.3	The effects of co-culture and EC pre-conditioning on CM contractility .....	201
6.2.4	Conclusions from this comparison .....	204
<b>6.3 STRENGTHS AND LIMITATIONS .....</b>	<b>205</b>	
<b>6.4 FUTURE WORK .....</b>	<b>207</b>	
<b>6.5 CONCLUDING REMARKS .....</b>	<b>210</b>	
 <i>References</i>	 <b>211</b>	
<i>Appendix</i>	<b>243</b>	

## List of Figures

<b>Figure 1.1:</b> Inflammatory cascade and NO in the pathogenesis of HFpEF .....	24
<b>Figure 1.2:</b> Canonical signalling pathways and relevant target genes of TNF $\alpha$ , IL-1 $\beta$ and IL-6 in endothelial cells .....	28
<b>Figure 1.3:</b> Calcium transport and the excitation-contraction coupling in CM.....	35
<b>Figure 1.4:</b> Ventricular action potential, with ion currents and after-depolarisations.....	38
<b>Figure 1.5:</b> EC-CM paracrine crosstalk and its plasticity.....	49
<b>Figure 1.6:</b> Schematic summary of the study design .....	55
<b>Figure 2.1:</b> Transwell co-culture systems.....	65
<b>Figure 2.2:</b> Calcium transient recording and analysis of calcium extrusion mechanisms.....	79
<b>Figure 2.3:</b> Calcium-contraction interpolation and hysteresis loops .....	81
<b>Figure 2.4:</b> Preparation, culture and mechanical stimulation of rat living myocardial slices.....	85
<b>Figure 3.1:</b> Distribution of published EC-CM co-culture models per parameter .....	98
<b>Figure 3.2:</b> Schematic view of the two main Transwell insert applications for use as EC-CM co-culture model	103
<b>Figure 3.3:</b> Cardiac and non-cardiac EC might regulate calcium handling differently in adult rat CM .....	104
<b>Figure 3.4:</b> Co-culture with HCMEC for 24 hours did not induce a remodelling of dimensions or sarcomere structures in ARVM .....	105
<b>Figure 3.5:</b> EC induced the same effects on calcium handling of co-cultured CM after 4 and 24 hours.....	106
<b>Figure 3.6:</b> EC induced the same effects on the calcium handling of co-cultured CM after myocardial infarction .....	108
<b>Figure 3.7:</b> HCMEC did not transdifferentiate into lymphatic EC or fibroblasts after 24 hours of incubation with the custom medium used for co-cultures.....	110
<b>Figure 4.1:</b> Induction of pro-inflammatory markers validating the use of TNF $\alpha$ , IL-1 $\beta$ and hIL-6 at tested concentrations in HCMEC in vitro .....	132
<b>Figure 4.2:</b> Expression profiles of markers of cytokine activity were cytokine-specific, and the effect of cytokines co-treatment was not additive or synergistic .....	133
<b>Figure 4.3:</b> Cytomix treatment induced cell cycle arrest at G1 in HCMEC .....	135
<b>Figure 4.4:</b> Cytomix treatment did not affect basal permeability in HCMEC monolayers but might affect the response of EC to thrombin .....	137
<b>Figure 4.5:</b> Cytomix treatment attenuated both the amplitude and duration of thrombin-induced calcium transients in HCMEC .....	140

<b>Figure 4.6:</b> Cytomix treatment increased the synthesis of NO in vitro after thrombin or after L-NAME application in HCMEC, but not the basal levels of intracellular NO .....	141
<b>Figure 4.7:</b> Cytomix treatment stimulated the secretion of 10 pro-inflammatory proteins by HCMEC in vitro .	143
<b>Figure 4.8:</b> Optimisation of sample dilution for ELISA quantification of candidate EC-secreted factors.....	147
<b>Figure 4.9:</b> CXCL5 and G-CSF, but not ET-1, CXCL1 and GM-CSF, were differentially released by EC alone and during EC:CM co-culture after Cytomix treatment .....	148
<b>Figure 4.10:</b> RNA expression of candidate ligands (identified with the Profiler Array) and their canonical receptors in mouse and rat CM .....	150
<b>Figure 5.1:</b> Cytomix-treated EC shortened the calcium transients in co-cultured CM compared to untreated EC .....	174
<b>Figure 5.2:</b> Efficiency of SR Ca <sup>2+</sup> release was improved in CM co-cultured with Cytomix-treated EC compared to untreated EC.....	175
<b>Figure 5.3:</b> Ca <sup>2+</sup> extrusion involving SERCA but not NCX was increased in CM after co-culture with Cytomix-treated HCMEC .....	176
<b>Figure 5.4:</b> Protein expression profile of CM after 4 hours of co-culture with EC.....	178
<b>Figure 5.5:</b> Lack of effect of co-culture with untreated or Cytomix-treated EC on contractility of CM, using CytoCypher™ .....	180
<b>Figure 5.6:</b> Dual measurement of calcium and contractility in CM showed no significant effect of co-culture and Cytomix treatment on the sensitivity of myofilaments to Ca <sup>2+</sup> .....	182
<b>Figure 5.7:</b> Stretch-dependent effects of Cytomix on the contractility, but not passive tension of cultured rat myocardial slices.....	183
<b>Figure 5.8:</b> Morphology of contractions at 20% and 23% isometric stretch of slices .....	184
<b>Figure 6.1:</b> Time-dependency of CM contraction decline duration with the CytoCypher set-up .....	200
<b>Figure 6.2:</b> Published effects of Transwell co-culture and of TNFα pre-conditioning of EC on the contractility and relaxation rate of contractions in CM .....	202

## List of Tables

<b>Table 1.1:</b> <i>Effects of neuregulin-1, apelin, endothelin-1 and nitric oxide on CM function</i> .....	50
<b>Table 2.1:</b> <i>List of antibodies mentioned in the thesis</i> .....	86
<b>Table 3.1:</b> <i>Classification of published and theoretical in vitro and ex vivo systems to study the EC-CM crosstalk</i> .....	99
<b>Table 4.1:</b> <i>Analytes detected in the Proteome Human XL Cytokine Profiler™ Array kit</i> .....	128
<b>Table 4.2:</b> <i>Treatment with Cytomix or individual cytokines produced different profiles of secreted inflammatory proteins in HCMEC in vitro</i> .....	144
<b>Table 6.1:</b> <i>Comparison of methodology for cell culture, co-culture, and characterisation of CM functions in this project and in Juni et. al. (2019)</i> .....	199

## List of Uncommon Abbreviations and Acronyms

<b><math>\alpha</math>-SMA</b>	Alpha-smooth muscle actin
<b>ACCT</b>	Ascorbate, Creatine, Carnitine, Taurine (culture medium formulation)
<b>ADM</b>	Adrenomedullin
<b>Ang-II</b>	Angiotensin-II
<b>AP</b>	Action potential
<b>ARVM</b>	Adult rat ventricular myocyte
<b>BSA</b>	Bovine serum albumin
<b>CAD</b>	Coronary artery disease
<b>cAMP / cGMP</b>	Cyclic adenosine/guanosine monophosphate
<b>CICR</b>	Calcium-induced calcium release
<b>CM</b>	Cardiomyocyte
<b>CMOS</b>	Complementary Metal Oxide Semiconductor
<b>CTL</b>	Control
<b>DMEM</b>	Dulbecco's Modified Eagle Medium
<b>EAD</b>	Early after-depolarisation
<b>EC</b>	Endothelial cell
<b>ECGS</b>	Endothelial cell growth supplement
<b>ECL</b>	Enhanced chemiluminescence
<b>EGM-MV2</b>	Endothelial cell growth medium – MV (microvascular) 2



<b>eNOS</b>	Endothelial nitric oxide synthase
<b>ERK1/2</b>	Extracellular signal-regulated kinases 1/2
<b>ESC-CM</b>	Embryonic stem-cell derived cardiomyocytes
<b>ET-1</b>	Endothelin-1
<b>ET<sub>A/B</sub></b>	Endothelin receptor subtypes A and B
<b>FBS</b>	Foetal bovine serum
<b>FSTL-1</b>	Follistatin-related protein 1
<b>GAPDH</b>	Glyceraldehyde 3-phosphate dehydrogenase
<b>G-CSF</b>	Granulocyte-colony stimulating factor
<b>GM-CSF</b>	Granulocyte-macrophage colony-stimulating factor
<b>hACF</b>	Human adult cardiac fibroblasts
<b>HAEC</b>	Human aortic endothelial cells
<b>HCMEC</b>	Human cardiac microvascular endothelial cells
<b>HF</b>	Heart failure
<b>HFpEF / HF<sub>r</sub>EF</b>	Heart failure with preserved (p) or reduced (r) ejection fraction
<b>HO-1</b>	Heme oxygenase
<b>HRP</b>	Horseradish peroxidase
<b>HUVEC</b>	Human umbilical vein endothelial cells
<b>Hyper-IL-6 / hIL6</b>	Hyper-interleukin-6 (IL-6/sIL-6R $\alpha$ chimeric compound)
<b>ICAM-1</b>	Intercellular adhesion molecule 1
<b>I<sub>K1</sub></b>	Inward rectified potassium current

<b><math>I_{Kr}</math> / <math>I_{Ks}</math></b>	Rapid (r) and slow (s) components of the delayed rectifier potassium current
<b>IL1RL1</b>	Interleukin-1 receptor-like 1
<b>IL-x</b>	Interleukin-x
<b>iNOS</b>	Inducible nitric oxide synthase
<b>iPSC-CM</b>	Induced pluripotent stem-cells derived cardiomyocytes
<b><math>I_{to}</math></b>	Transiently outward potassium current
<b>KH</b>	Krebs-Henseleit solution
<b>LMS</b>	Living myocardial slices
<b>L-NAME</b>	N( $\omega$ )-nitro-L-arginine methyl ester
<b>LPS</b>	Lipopolysaccharides
<b>LTCC</b>	L-type calcium channel
<b>LVEF</b>	Left ventricular ejection fraction
<b>MI / MINOCA</b>	Myocardial infarction / ... with non-obstructive coronary arteries
<b>MnSOD</b>	Manganese superoxide dismutase
<b>NCX</b>	Sodium-calcium exchanger
<b>NHE1</b>	Sodium-hydrogen exchanger 1
<b>nNOS</b>	Neuronal nitric oxide synthase
<b>NO / NOS</b>	Nitric oxide / Nitric oxide synthase
<b>NRG-1</b>	Neuregulin-1
<b>NRVM</b>	Neonatal rat ventricular myocytes

<b>PAR</b>	Protease-activated receptors
<b>PBS</b>	Phosphate buffered-saline
<b>PI</b>	Propidium iodide
<b>PKA / PKD / PKG</b>	Protein kinases A, D, G
<b>PLB</b>	Phospholamban
<b>ROI</b>	Region of interest
<b>ROS</b>	Reactive oxygen species
<b>RyR2</b>	Ryanodine receptor 2
<b>SERCA</b>	Sarco-endoplasmic reticulum Ca <sup>2+</sup> -ATPase
<b>sIL-6R<math>\alpha</math></b>	Soluble interleukin-6 receptor alpha
<b>SL</b>	Sarcomere length
<b>SOCE</b>	Store operated calcium entry
<b>SR</b>	Sarcoplasmic reticulum
<b>STAT3</b>	Signal transducer and activator of transcription 3
<b>TGF-<math>\beta</math></b>	Transforming growth factor-beta
<b>TNF<math>\alpha</math></b>	Tumour necrosis factor-alpha
<b>TRAF6</b>	Tumour necrosis factor receptor (TNFR)-associated factor 6
<b>UT</b>	Untreated
<b>VCAM-1</b>	Vascular cell adhesion molecule 1
<b>VEGF</b>	Vascular endothelial growth factor



# 1.

## **Introduction**

## 1.1 Heart failure and inflammation

### 1.1.1 Heart failure with preserved ejection fraction

Heart failure (HF) refers to a life-threatening dysfunction of the myocardium which can impair the contractility or relaxation of the cardiac tissue, and its adaptability to stress or exercise. As such, this definition actually covers a range of disorders, with a variety of clinical presentations, aetiologies, and effective therapeutics. Clinically, these are first categorised by the efficiency of the left ventricle to eject blood during each beat (systole), forming two categories: HF with a reduced ejection fraction (HFrEF), where the left ventricular ejection fraction is below 40%, and HF with a preserved ejection fraction (HFpEF). The boundaries of these categories and the relevance for such a distinction are still being discussed. An intermediate category (i.e. HF with mid-range, or moderately reduced, ejection fraction, HFmrEF) has even been created as part of the 2016 European Society of Cardiology HF guidelines<sup>1</sup>, for patients with an ejection fraction of the left ventricle (LVEF) comprised between 40% and 50%.

Studies have determined that between 22% and 73% of all HF patients fall into the category of HFpEF, depending on the assessment criteria applied and the year of publication<sup>1-4</sup>. While the symptoms of HFpEF resemble those of HFrEF (breathlessness, intolerance to exercise, fatigue), it is now accepted that these are distinct clinical entities. Indeed, common treatments for HFrEF fail to improve cardiac function in HFpEF patients<sup>5</sup>. To date, there are no approved treatment, which further increases the urgency to validate new therapeutic strategies to benefit these patients. Yet, clinically defining HFpEF is still up for debate, with current definitions being challenged by practical and semantical limitations. Indeed, current assessment scores for HF (e.g. Framingham criteria or the Braunwald definition) are either not sensitive enough, biased towards older patients, or demand an invasive test of ventricular function under exercise<sup>6</sup>.

Because systolic function (as measured by the ejection fraction) is largely normal in HFpEF, it is generally considered that HFpEF is the result of diastolic dysfunction. In other words, the

filling of the ventricle is impaired, as opposed to HFrEF where the emptying of the ventricle is impeded. However, HFpEF and diastolic dysfunction are not interchangeable as most HFrEF patients also present diastolic dysfunction<sup>7</sup>, which can also be seen without HF. Moreover, the limited ability to increase the stroke volume in conditions of stress or exercise (as is seen in HFpEF) could well be interpreted as systolic dysfunction<sup>8</sup>, further increasing its confusion with HFrEF.

HFpEF is associated with many risk factors, including aging, gender (female patients are more prevalent in the HFpEF group than in HFrEF), ethnicity, and sedentarism<sup>6</sup>. It is also linked with comorbidities which include coronary artery disease, overweight or obesity, diabetes mellitus, hypertension, chronic obstructive pulmonary disease, and chronic kidney disease<sup>6,9</sup>. These factors have been proposed as the first step of pathogenesis for HFpEF, in the new paradigm published by Paulus & Tschöpe (2013)<sup>9</sup>. To summarise it briefly, the presence of multiple or severe comorbidities induces a chronic systemic pro-inflammatory response which provokes a coronary microvascular endothelial inflammation. This, in turn, results in a reduced nitric oxide (NO) bioavailability, negatively affecting the cyclic guanosine monophosphate (cGMP) levels and protein kinase G (PKG) activity in cardiomyocytes (CM). Finally, this leads to hypertrophic remodelling in CM, as well as the hypophosphorylation of titin, stiffening the cell and hindering relaxation during diastole. These steps are detailed and explained further in other sections of this introduction, but it should be noted that inflammation (particularly coronary microvascular endothelial inflammation) is a pivotal element to this paradigm, as illustrated in Figure 1.1. The remodelling of myocardial architecture during HFpEF is extensive and not limited to hypertrophy and CM stiffening. CM apoptosis, interstitial fibrosis, arteriolar wall thickening and capillary rarefaction are thought to contribute to the pathogenesis of HFpEF as well, and can result from inflammation of the myocardium (myocarditis) or of cardiac endothelial cells (EC)<sup>9-13</sup>.

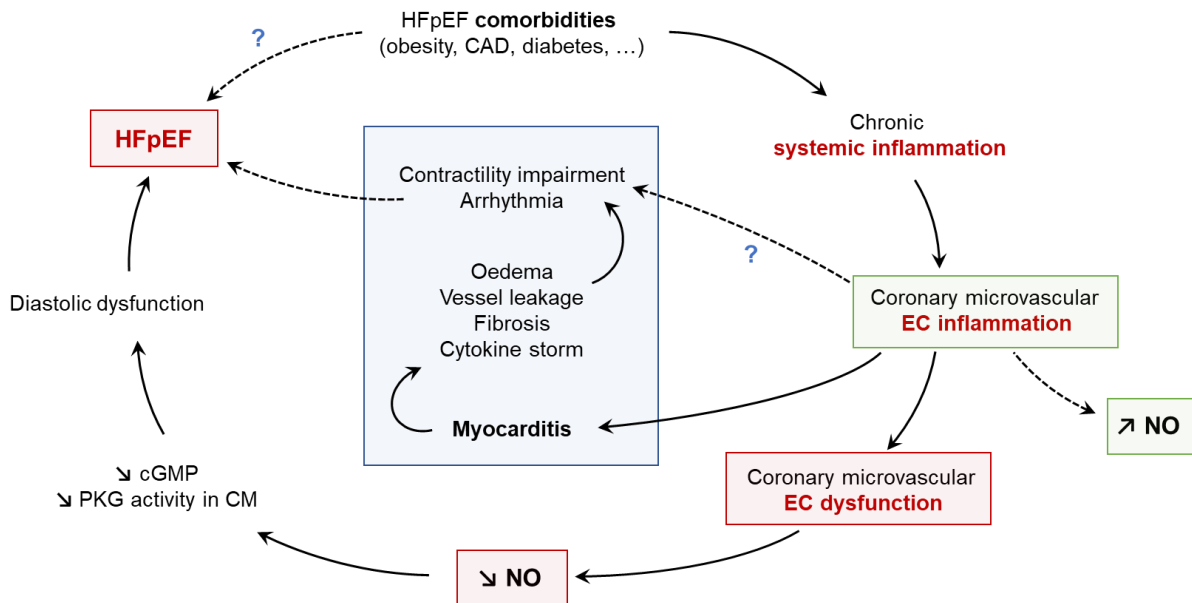


**Figure 1.1: Inflammatory cascade and NO in the pathogenesis of HFpEF**

### 1.1.2 Ischemic heart disease and myocardial infarction

Ischemic heart disease has a prominent role in both types of HF<sup>14</sup>, although it is more prevalent in HFrEF patients. Indeed, between 50 and 70% of all HF cases in Europe and in the United States are caused by or associated with an underlying coronary artery disease (CAD), which is a risk factor for ischemia<sup>15</sup>. Ischemia can be chronic (e.g. obstructive epicardial stenosis) or acute (e.g. after a sudden thrombotic occlusion of a coronary artery), but also non-obstructive, as described below. If sustained, this results in a loss of contracting CM, fibrosis, hypertrophy, necrosis, arrhythmia, and inflammation<sup>16</sup>. This is known as a myocardial infarction (MI), which begets a severe remodelling of the left ventricle, culminating in a dilated cardiomyopathy and HF<sup>17</sup>.

Infarction is essentially the result of an imbalance between oxygen supply and demand, and is therefore not necessarily of obstructive origin. A severe hypertension, hypotension or shock, hypertrophy, respiratory failure, anaemia, severe tachycardia or bradycardia, coronary spasm,



coronary microvascular dysfunction, coronary artery dissection, Takotsubo syndrome, as well as myocarditis have the potential to disrupt this supply/demand equilibrium, to cause an acute infarction (this would be classified as a type 2 MI)<sup>18</sup>. Obstructive (type 1 MI) and type 2 MI can be distinguished from each other based on the presence of myocardial injury, which clinically is detected by an elevated level of circulating cardiac troponin<sup>18</sup>. Recently, however, MI with nonobstructive coronary arteries (MINOCA) has been better defined<sup>19</sup> and fails to fall into the traditional type 1-2 groups of MI, as cardiac troponin levels are elevated in these patients. This is a complicated issue, as MINOCA patients also present myocarditis<sup>20</sup> and coronary spasm<sup>21</sup>, pointing to endothelial inflammation and dysfunction. Interestingly, biomarkers of inflammation were found at higher levels in MINOCA patients 3 months after MI than in MI-CAD patients<sup>22</sup>, indicating that perhaps anti-inflammatory treatments may offer some protection.

For MI-CAD patients, revascularisation procedures (percutaneous coronary intervention, PCI, and coronary artery bypass grafting, CABG) have long been adopted to limit myocardial injury, improve survival, and reduce the occurrence of future MI<sup>23</sup>. Such procedures are however not adapted for type-2 MI or MINOCA patients, for whom a therapeutic control of vascular function may be preferable. Relevant clinical trials have yet to be performed to fully test this hypothesis.

### **1.1.3 The role of inflammation in non-ischemic cardiomyopathies**

Cardiomyopathies, whether they transform into HF or not, are not limited to ischemic events. Indeed, numerous pathophysiological or environmental factors can induce cardiomyopathies. These include genetic mutations, viral infections, cardiac amyloid deposition, cardiotoxic drugs (e.g. chemotherapy), physical trauma, pulmonary or systemic hypertension, sustained stress (Takotsubo syndrome), and systemic inflammatory diseases, such as rheumatoid arthritis<sup>24-26</sup>. The mechanisms of pathogenesis, in each case, are too complex and irrelevant to be detailed in this thesis. It is interesting to note, however, that inflammation (e.g. vasculitis, myocarditis, and pericarditis) is a common cause and feature of cardiomyopathy<sup>27</sup>.

In western countries, case reports indicate that viral infections are responsible for the majority of myocarditis cases<sup>28</sup>. Many viruses have been associated with inflammatory heart disease, including parvovirus B19, human herpes virus 6, coxsackievirus, adenovirus, cytomegalovirus, and Epstein-Barr virus<sup>29</sup>. SARS-CoV-2 (severe acute respiratory syndrome coronavirus 2) has also been associated with myocarditis<sup>30,31</sup>, which was identified as the cause of death for some patients<sup>32</sup>. Direct cardiotoxic effects of viral load and the host immune response contribute to the pathogenesis of viral myocarditis<sup>33</sup>. Viral infection leads to myocardial injury, partly due to the cytotoxic activity of T-lymphocytes, which are recruited and stimulated by a cytokine storm involving predominantly interleukin-6 (IL-6)<sup>33,34</sup>. Although this has the potential to affect cardiac cell viability and CM functions, by mechanisms elaborated below, non-specific immunity may also directly impair the function and survival of myocardial cells<sup>27</sup>.

#### **1.1.4 Inflammatory cardiomyopathy**

To recapitulate the role of inflammation in cardiac dysfunctions: 1) systemic inflammation and coronary microvascular inflammation have been proposed as the pivotal elements of HFpEF pathogenesis, 2) myocarditis is prevalent in non-obstructive MI, and 3) it is also dominant in non-ischemic cardiomyopathies. Myocarditis can disrupt multiple functions of the myocardium, inducing interstitial oedema, leakage of capillary vessels, and fibrosis, in addition to impairing CM contractility and promoting arrhythmia<sup>27</sup>. The mechanisms are still poorly understood, and further complicated by the highly dynamic nature of the pathogenesis. Inflammatory cytokines are undoubtedly involved in disease progression towards HF, with local and systemic levels of Tumour Necrosis Factor- $\alpha$  (TNF $\alpha$ ), Interleukin-1 $\beta$  (IL-1 $\beta$ ), IL-6, IL-8, IL-10, IL-1 $\alpha$ , IL-2, Interferon- $\gamma$  (IFN- $\gamma$ ) and Transforming Growth Factor- $\beta$  (TGF- $\beta$ ) found elevated in correlation to the severity of HF, for example in diastolic dysfunction<sup>35</sup>. Systemic inflammatory diseases (e.g. rheumatoid arthritis) are also known to evolve into myocarditis<sup>24</sup>, with studies suggesting that endothelial dysfunction plays an important role in this transition<sup>36</sup>.

## 1.2 Endothelial inflammation and dysfunction

To better understand the contribution of the endothelium to the pathogenesis of inflammatory cardiomyopathies, and why it might be an interesting therapeutic target for HF, we must first establish how EC respond to pro-inflammatory stimuli and how they transition to dysfunctional EC. I will focus this review to IL-6, IL-1 $\beta$ , and TNF $\alpha$ , which have all important roles in the acute phase response, in chronic inflammation, in cardiomyopathies and HF, and are able to affect EC functions in these conditions.

First, the activation of EC by pro-inflammatory cytokines is considered a Type-II activation, as opposed to Type-I which is mediated by G-protein coupled receptor activation. Although both types of EC activation lead to an increased blood flow, vascular permeability, and binding and extravasation of leucocytes, the time scale of these responses are different. Indeed, Type-I is much more transient than Type-II (10-20 minutes, compared to hours or even days in Type-II activation). In addition, Type-I is independent of protein synthesis, unlike Type-II activation. If the stimulus of EC activation is maintained, this response can evolve into chronic inflammation of EC (although EC can display features of acute and chronic inflammation simultaneously)<sup>37</sup>.

### 1.2.1 Inflammatory cytokines and endothelial cells

IL-6 is an important cytokine in cardiovascular diseases, and said to be pivotal in the transition from acute to chronic inflammation<sup>38</sup>. It mediates the activation of T cells and B cells, involved in the immune response which accompanies inflammation. IL-6 also contributes to endothelial dysfunction in the coronary vasculature, in the metabolic syndrome, an effect that was shown to be dependent on TNF $\alpha$  signalling, decreasing the phosphorylation and activity of eNOS (endothelial NO synthase)<sup>39</sup>. The activity of IL-6 is more nuanced than TNF $\alpha$  or IL-1 $\beta$ , as it might be anti-inflammatory in the right conditions. Indeed, a lack of IL-6 *in vivo* was associated with an increase of TNF $\alpha$  levels<sup>40</sup>, and was identified as protective against angiotensin-II (Ang-II)-induced EC dysfunction<sup>41</sup>. IL-6 also confers protection against apoptosis and endothelial

dysfunction after MI<sup>42</sup>. However, the inflammatory response to localised tissue damage was found defective in IL-6 deficient mice<sup>43</sup>.

To activate EC, IL-6 requires binding to a protein complex composed of the transducer protein gp130 and IL-6R $\alpha$ . If EC express gp130, they lack the constitutive expression of IL-6R $\alpha$ , and therefore are unable to transduce IL-6 signals on their own. IL-6R $\alpha$  can however be secreted by neutrophils, for example in response to EC-produced IL-8. In this case, this soluble IL-6R $\alpha$  (sIL-6R $\alpha$ ) can reach EC and allow for IL-6 signal transduction to occur (as seen in Figure 1.2). This is known as the *trans*-signalling of IL-6<sup>44</sup>. Where this is allowed, IL-6 activates multiple pathways, including the Janus-associated kinases (JAK) and signal transducer and activator of transcription (STAT) pathway (though primarily JAK1/2-STAT3 in EC), as well as the extracellular signal-regulated kinases (ERK1/2), mitogen-activated protein kinases (MAPK), and the phosphatidylinositol-3-kinase (PI3K/Akt) pathways<sup>45</sup>. Known target genes of IL-6 in EC include MCP-1 (monocyte chemoattractant protein-1, or CCL2), which is pro-inflammatory

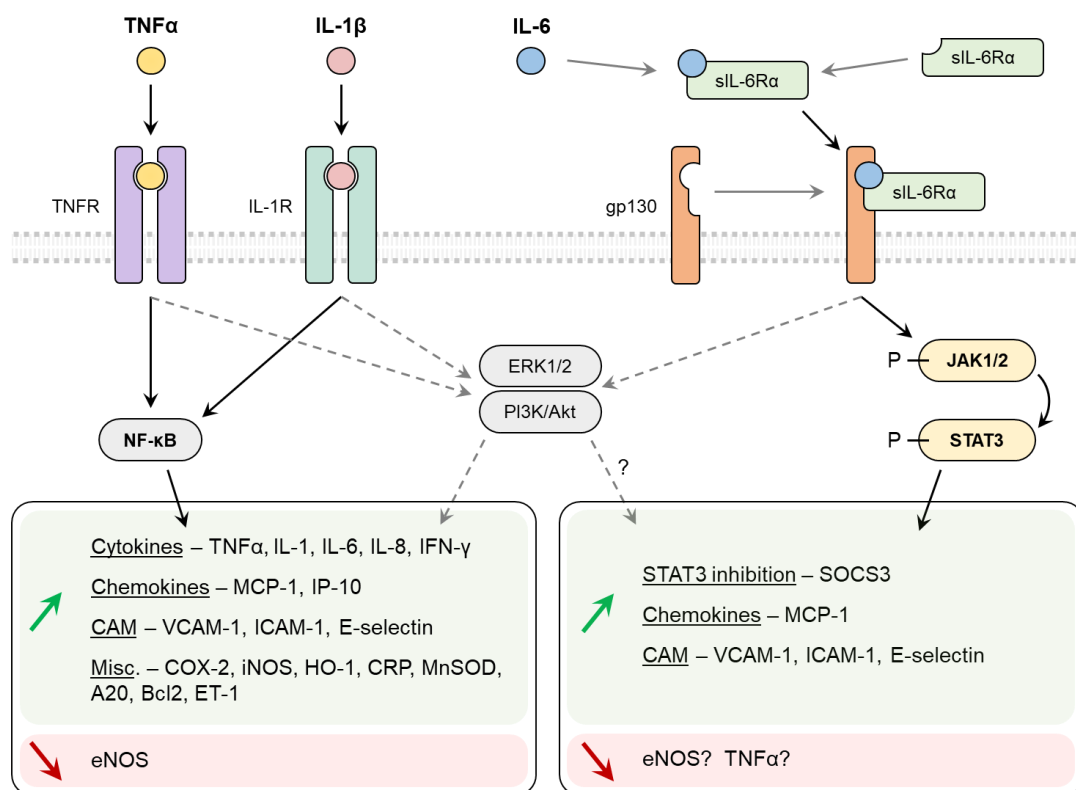


**Figure 1.2: Canonical signalling pathways and relevant target genes of TNF $\alpha$ , IL-1 $\beta$  and IL-6 in endothelial cells**

as it promotes macrophage infiltration to the site of inflammation, and SOCS3 (suppressor of cytokine signalling 3), which conversely is anti-inflammatory as it rapidly inactivates STAT3. IL-6 also stimulates the surface expression of cell adhesion molecules (e.g. ICAM-1, VCAM-1 and E-selectin) in EC, promoting leucocyte attachment<sup>46,47</sup>. Finally, the inhibition of eNOS activity by IL-6 has been proposed at multiple occasions<sup>48,49</sup>. However, NO bioavailability was not quantified in these studies, and a possible shift to iNOS (inducible NOS) expression and activity has yet to be addressed.

Both TNF $\alpha$  and IL-1 $\beta$  activate the nuclear factor- $\kappa$ B (NF- $\kappa$ B) pathway, which involves inducible transcription factors (NF- $\kappa$ B1/p50, NF- $\kappa$ B2/p52, RelA/p65, RelB, and c-Rel), as seen in Figure 1.2. This pathway is well known and has been detailed expertly by others<sup>50</sup>. It is important to note that NF- $\kappa$ B holds a central role in inflammatory diseases (e.g. rheumatoid arthritis, inflammatory bowel disease, and atherosclerosis), inducing the local and systemic release of cytokines (e.g. TNF $\alpha$ , IL-1, IL-6, IL-8, and interferon- $\gamma$ ), chemokines (e.g. MCP-1, IP-10), and stimulating the cell surface expression of cell adhesion molecules. Other target proteins include COX-2 (cyclooxygenase-2), iNOS, HO-1 (heme oxygenase-1), and CRP (C-reactive protein)<sup>50</sup>. Not all targets regulated by NF- $\kappa$ B activation are pro-inflammatory or detrimental to cellular function. Indeed, MnSOD (manganese superoxide dismutase), A20, and Bcl2, for example, have anti-oxidant properties, help suppress NF- $\kappa$ B activation, and have anti-apoptotic properties (respectively). As for IL-6, multiple other signalling pathways are activated by TNF $\alpha$  or IL-1 $\beta$  (including PI3K/Akt, ERK1/2, and other MAPK pathways)<sup>51</sup>.

### **1.2.2 Vascular permeability and inflammation**

The main function of the vascular endothelium is to form a physical barrier between the blood and the underlying tissues, restricting the diffusion (or leak) of large molecules (the cut-off size has been described between 20 and 40 kDa<sup>52</sup>) or even cells. In pro-inflammatory conditions, the endothelium becomes more permeable<sup>53</sup>. *In vivo*, a transient increase of permeability was indeed reported in venules in the early stage of an inflammatory response, albeit chemically

induced<sup>54</sup>. This promotes leucocyte extravasation, amplifying the inflammatory response. But a chronic increase in permeability can also lead to oedema, or changes in the neurohormonal environment of perivascular cells, and overall contribute to disease progression, for instance in HF<sup>53,55</sup>.

TNF $\alpha$  was shown to stimulate endothelial permeability<sup>56</sup>, although this effect may not involve changes in eNOS or iNOS expression. Similarly, other pro-inflammatory factors are known to induce EC permeability, e.g. histamine, vascular endothelial growth factor (VEGF), bradykinin, and thrombin<sup>57-59</sup>. While the effects of TNF $\alpha$  and thrombin are mainly mediated by an increase of intracellular Ca<sup>2+</sup>, that is transient<sup>56,60-63</sup>, histamine, VEGF, and bradykinin have been shown to primarily activate Akt<sup>58</sup>. Both pathways however result in the phosphorylation of eNOS, and this stimulates NO synthesis<sup>58</sup>. Multiple downstream targets of this NO synthesis have been proposed: 1) S-nitrosylation of  $\beta$ -catenin causing the disassembly of VE-cadherin and thus of cell-cell junctions<sup>58,64</sup>, and 2) a reversal of stress fibre formation<sup>62</sup>, thus facilitating intercellular gap formation and further destabilising cytoskeletal cell-cell junctions. IL-6 also increases EC permeability, but this is protein kinase C (PKC)-dependent and the study which demonstrated this relationship makes no mention of calcium transients or NO synthesis<sup>65</sup>.

It is unclear how EC behave mechanistically in more complex pro-inflammatory environments. It has been reported that TNF $\alpha$  and thrombin can have synergistic effects on the duration of calcium transients in EC, and on vascular permeability, but the interplay of other cytokines has not been investigated<sup>61</sup>. Of note, the contribution of iNOS-mediated NO on the control of EC permeability has never been seriously studied, limiting our understanding of this phenomenon.

### **1.2.3 Differential secretion of cardiotropic agents**

As described above, endothelial dysfunction can negatively affect the function of CM and is now considered a hallmark of HFpEF, as well as a candidate of choice for novel therapeutics. In other words, the paracrine activity of EC on CM is considered an important feature of cardiac

remodelling and a system which might be exploited clinically. First, we must understand how EC can communicate with CM.

Although separated by a basement membrane and interstitial extracellular matrix, the distance between microvascular EC and CM can be smaller than 1  $\mu\text{m}$ <sup>66</sup>. This allows for soluble factors to diffuse rapidly from one cell to the other, and this is of importance for paracrine mediators with a short half-life in physiological conditions (such as NO)<sup>67</sup>. It is now recognised that the secretome is not just limited to small molecules or proteins but can include lipids, mRNA, microRNA, exosomes, macroparticles, etc<sup>68</sup>. Furthermore, the composition of cell types in the heart has been reassessed in recent years, to demonstrate that there are between 2 to 3 single EC per CM<sup>66,69,70</sup> (although CM take up most of the space, due to their size). This cell ratio is physiologically balanced, as a rarefaction of capillary or excessive CM hypertrophy are susceptible to affect the efficiency of EC-CM crosstalk. Moreover, it could be speculated that an excessive deposition of extracellular matrix (as is seen in interstitial fibrosis) could physically increase the distance between EC and CM, and impair their paracrine exchange. The soluble component of this crosstalk has been studied for decades. However, it should be noted that other types of EC-CM communications can occur (e.g. biomechanical forces or electrophysiological communication).

Endothelial function is highly plastic, and susceptible to change in inflammatory conditions, as described above. The secretion of potential paracrine factors by EC is no exception. Indeed, endothelin-1 (ET-1), which is a potent vasoconstrictor and increasingly considered a mediator of inflammation<sup>71</sup>, was found expressed and secreted at greater rates by EC treated *in vitro* by chemokines (MCP-1) or cytokines (except IL-8)<sup>72</sup>. This is consistent with circulating levels of ET-1, which are increased in CAD, atherosclerotic, and HF patients<sup>73</sup>. There is evidence to suggest that an elevated ET-1 secretion may contribute to or even initiate coronary vasospasm (and thus play an important role in MINOCA)<sup>73</sup>. The release of ET-1 is however under control by NO<sup>74</sup>. In endothelial dysfunction, the reduced bioavailability of NO might be a primary mean of upregulating ET-1 release from EC. Finally, EC-derived ET-1 is able to affect CM function.

This is detailed in Section 1.3, but it should be observed here that a pro-hypertrophic effect of EC-derived ET-1 on CM was identified using EC-CM co-cultures<sup>75</sup>.

Pro-inflammatory cytokines such as TNF $\alpha$  and IL-1 $\beta$  have also been shown to affect NO levels and synthesis by EC. This involves four main changes: 1) a decreased eNOS expression<sup>76,77</sup>, 2) an upregulation of iNOS<sup>78,79</sup>, 3) an uncoupling of eNOS (which becomes Ca<sup>2+</sup>-independent and more likely to synthesise reactive oxygen species, ROS)<sup>80,81</sup>, and 4) a scavenging of NO by cytokine-mediated ROS generation or the NF- $\kappa$ B target gene MnSOD. It is still controversial that iNOS might be upregulated during inflammation. And even if this is the case, it is unclear if this would result in the increase of NO synthesis and activity which was predicted decades ago. However, as introduced in Section 1.2.2, a cytokine-induced synthesis of NO is essential to the stimulation of vascular permeability. This is therefore likely to be a distinct cellular state than endothelial dysfunction, which is defined solely by the pathologically reduced synthesis of NO, and the resulting stiffening of the vasculature. NO has many effects on CM, which I will describe in the next section.



### **1.3 Excitation-contraction coupling in CM and its modulation by EC-derived cardiotropes**

The action potential (AP), cyclic release of  $\text{Ca}^{2+}$  in the cytosol (calcium transients) and calcium-induced shortening of myofilaments are three functions of CM which connect stimulus and cell contractions, in a sequence of mechanisms which is called excitation-contraction coupling. Briefly, a small depolarisation of the plasmalemma of CM (trigger) induces a sequence of ionic currents which further depolarise the cell before returning it to resting membrane potentials; a process known as the action potential (AP). During the AP, a small entry of  $\text{Ca}^{2+}$  via the L-type calcium channel (LTCC) induces a large release of  $\text{Ca}^{2+}$  from the sarcoplasmic reticulum (SR), mediated by the ryanodine receptor (RyR2). This is known as calcium-induced calcium release (CICR).  $\text{Ca}^{2+}$  then interacts with myofilaments, which results in actin and myosin binding within contractile units of myofilaments (known as sarcomeres), i.e. driving contraction.  $\text{Ca}^{2+}$  is then removed from the cytosol to the extracellular space via the sodium-calcium exchanger (NCX) and, in the majority, re-sequestered to the SR lumen through the sarco-endoplasmic reticulum  $\text{Ca}^{2+}$ -ATPase (SERCA). The excitation-contraction coupling is illustrated in Figure 1.3.

These mechanisms are finely regulated in health and disease. It is now well recognised that crosstalk of non-CM with CM contributes extensively to regulation of the excitation-contraction coupling<sup>82</sup>, and therefore controlling the kinetics, amplitude, and duration of CM contractions. How each element of this coupling is modulated by EC or by EC-derived paracrine factors is detailed below.

#### **1.3.1 Effects of nitric oxide on contractility and relaxation**

Endocardial ablation, using Triton X-100 or physical rubbing, provided the first evidence that EC can affect CM contractility<sup>83</sup>, decreasing papillary muscle twitch tension (i.e. amplitude) in the cat<sup>84</sup>. Co-culture of papillary muscles deprived of endocardium with endocardial cells was able to restore baseline contractility, but this was inhibited by haemoglobin (known to bind and

inhibit NO activity)<sup>85</sup>. The effect of NO was however limited to accelerating relaxation, in this study and in others<sup>86</sup>, without affecting systolic performance. However, a coronary infusion of substance P in the human heart (stimulating NO release from the coronary vasculature) led to a decrease of systolic force in addition to increasing diastolic stretch<sup>87</sup>. This can be replicated *in vitro* on isolated CM with NO donors<sup>88,89</sup>. Using this approach of donors, some have also reported an acceleration of the calcium transient decay<sup>90</sup>. These effects have been associated with cGMP/PKG activity in CM, suggesting that EC-derived NO is synthesised and diffused at sufficient concentrations to activate the cGMP/PKG signalling pathway. This is consistent with the hypophosphorylation of titin that occurs as a response to endothelial dysfunction<sup>91</sup>, during which NO release by EC is reduced along with the cGMP/PKG-mediated phosphorylation of target proteins such as titin in adjacent CM. The effect of NO on contractility (inotropy) and on relaxation (lusitropy) implicates multiple proteins of the excitation-contraction system in CM, as described in the following sections.

### **1.3.2 Effects of endothelin-1 on contractility and relaxation**

As for NO, the effects of ET-1 on contractility and relaxation were first studied using papillary muscles stripped of their endocardium. In this case, an exogenous application of ET-1 induced an increase of twitch tension<sup>92</sup>, which was attributed to a release of catecholamines (i.e. having an indirect effect). However, this inotropic effect was reproduced in co-cultures of endocardial EC and adult rat ventricular CM (ARVM)<sup>93</sup>, demonstrating the ability of EC-derived ET-1 to control CM contractility. An intracoronary injection of ET-1 has a positive inotropic effect, mediated by the ET<sub>A</sub> receptor, and a negative lusitropic effect (i.e. a prolonged relaxation) mediated by the ET<sub>B</sub> receptor<sup>94</sup>. This is therefore diametrically opposed to the effects of NO, interestingly in accordance with their respective effects on the vascular tone (vasorelaxation for NO and vasoconstriction for ET-1). Although an acute blockade of ET<sub>A</sub> in healthy rats has been reported to lack effect on cardiac contractility<sup>95</sup>, a chronic blockade of the ET-1 system *in vivo* was shown to depress significantly contractility and lusitropy<sup>96</sup>. Curiously, both inotropy

and lusitropy can be improved by a chronic inhibition of ET-1 when performed in a murine model of myocarditis, where ET-1 release is elevated<sup>96</sup>. This contradiction may arise from indirect effects of ET-1 inhibition (e.g. preventing CM damage and toxicity). It remains unclear how NO and ET-1 interact to regulate CM functions in physiological conditions, as these pathways are usually studied in isolation.

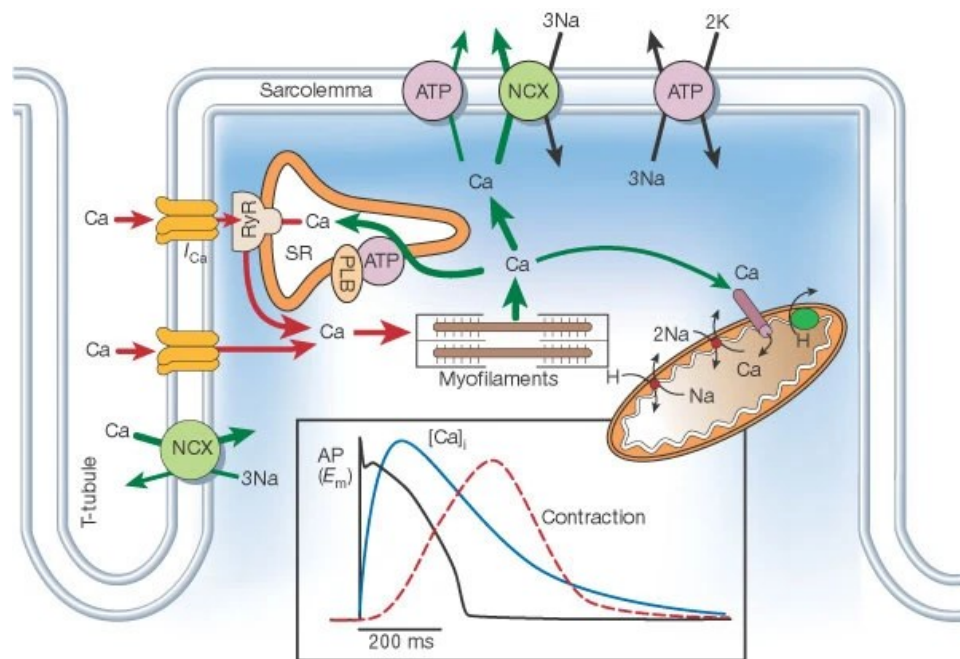


**Figure 1.3: Calcium transport and the excitation-contraction coupling in CM**

Reproduced from Bers *et. al.* (2002). Inset shows the time course of an action potential (AP), the resulting calcium transient and myofilament contraction measured in a rabbit ventricular CM at 37°C. NCX, Na<sup>+</sup>/Ca<sup>2+</sup> exchange; ATP, ATPase; PLB, phospholamban; SR, sarcoplasmic reticulum.

### 1.3.3 Pacemaker activity and ventricular rhythmicity

In adult ventricular CM, depolarisation of the membrane is predominantly caused by external stimuli (e.g. electrical field stimulation, or intercellular propagation of depolarised voltages via gap junctions). This lack of internal pacemaker activity contrasts with other *in vitro* models of CM, such as neonatal CM or induced pluripotent stem cells-derived CM (iPSC-CM), both of which spontaneously depolarise above the threshold of activation due to the high expression

of the hyperpolarisation-activated cyclic nucleotide-gated potassium channel (HCN4) responsible for the funny current ( $I_f$ )<sup>97</sup>. NCX is also electrogenic and depolarises the membrane when extruding  $Ca^{2+}$ , hence contributing to pacemaker activity in CM<sup>98</sup>. However, NCX-induced depolarisations are not sufficiently rapid to override sinus rhythm under normal physiology conditions.

The effects of EC on the ventricular rhythm are difficult to pin-point. Coronary EC dysfunction is a known risk factor for atrial fibrillation<sup>99</sup> and potentiates ventricular arrhythmia after MI, with evidence implicating an increase of ET-1<sup>100</sup> and a loss of NO bioavailability<sup>101</sup>. This is supported by other studies identifying anti-arrhythmic roles for NO<sup>102–104</sup>. The chronotropic effects of NO on pacemaker currents might be location specific, as studies have shown that it increased sinus rhythm<sup>103,105</sup>, while another study reported negative chronotropic effects of endogenous NO on isolated CM<sup>106</sup>. These can be difficult to differentiate from indirect effects, e.g. baroreceptor-mediated reflex tachycardia in response to the fall in arterial blood pressure<sup>105</sup>, or NO-mediated inhibition of  $\beta$ -adrenergic signalling, therefore limiting positively chronotropic effects<sup>107</sup>. Finally, Giacomelli *et. al.* (2017) produced 3D constructs with co-cultured CM and EC, where the electrophysiological properties of CM and the spontaneous beating rate of the tissue were unchanged compared to constructs with only CM<sup>108</sup>. However, in this study, CM and EC were co-differentiated from induced-pluripotent stem cells, and the relevance of such EC models is still up for debate. Conversely, primary human umbilical vein EC (HUVEC) led to an increased beating frequency of co-cultured neonatal rat ventricular CM (NRVM) in a separate study<sup>109</sup>.

#### **1.3.4 Action potential (AP)**

The AP of ventricular CM is a well-regulated sequence of inward and outward currents carried by  $Na^+$ ,  $K^+$  and  $Ca^{2+}$ -permeable voltage-sensitive ion channels situated on the plasmalemma, depolarising the membrane potential of CM from -80 mV in resting conditions to +20 mV, and returning to baseline within 250-400 ms. Such depolarisations propagate actively where these

channels are expressed, i.e. along cell membranes and across gap junctions of excitable cells, but can also propagate passively through non-excitable cells (e.g. up to 300  $\mu\text{m}$  across *in vitro* cultures of fibroblasts connected by gap junctions<sup>110</sup>).

The role of AP in the myocardium, beyond propagating anisotropically, is to induce a calcium release from the SR via an inward  $\text{Ca}^{2+}$ -current, implicating the L-type calcium channel. This current opposes a repolarising  $\text{K}^+$  current in phase 2 of the AP, thus slowing down the return to resting membrane potential (Figure 1.4A). While an increased LTCC current stimulates a larger CICR from the SR<sup>111</sup>, as is the case in response to  $\beta$ -adrenergic agonists, it can also delay the membrane repolarisation beyond the refractory period of sodium channels and thus potentiate early after-depolarisations (EAD). This is due to  $\text{Na}^+$  channels re-activating during phases 2-3 of the AP, and is an important risk factor for ventricular arrhythmia. Endogenous NO can inhibit the LTCC-mediated pro-inotropic effects of the  $\beta$ -adrenergic response, and therefore help prevent EAD<sup>107</sup>. This effect might be directly caused by S-nitrosylation of LTCC subunits<sup>112</sup> or indirectly by preventing the synthesis of cAMP, as a result of cGMP synthesis<sup>113</sup>. NO has also been associated with increased  $I_{\text{Ks}}$  and  $I_{\text{K1}}$  currents<sup>114,115</sup>, i.e. shortening phase 3 of AP and hyperpolarising the resting membrane potential in CM. In addition, NO inhibits  $I_{\text{to1}}$  and  $I_{\text{Kr}}$  currents<sup>116,117</sup>, shortening the AP plateau (therefore shortening the activity of LTCC) and reducing the amplitude of CICR as a result.

ET-1, again in contrast to the effects of NO, can increase the expression of LTCC via activation of the extracellular signal-regulated kinases 1/2 (ERK1/2)<sup>118</sup>, and inhibit the delayed rectifier  $\text{K}^+$  current responsible for the repolarisation during phase 3 of the AP<sup>119</sup>, resulting in an increased amplitude of calcium transients<sup>120</sup>. Some inotropic effects of ET-1 may also be attributed to a stimulated release of endogenous catecholamines in the myocardium, eliciting a traditional  $\beta$ -adrenergic response in CM<sup>92</sup>. The effects of other known EC-derived paracrine factors on AP morphology in CM remain to be demonstrated and, to date, how AP morphology is modulated in CM after co-culture with EC is still unclear.

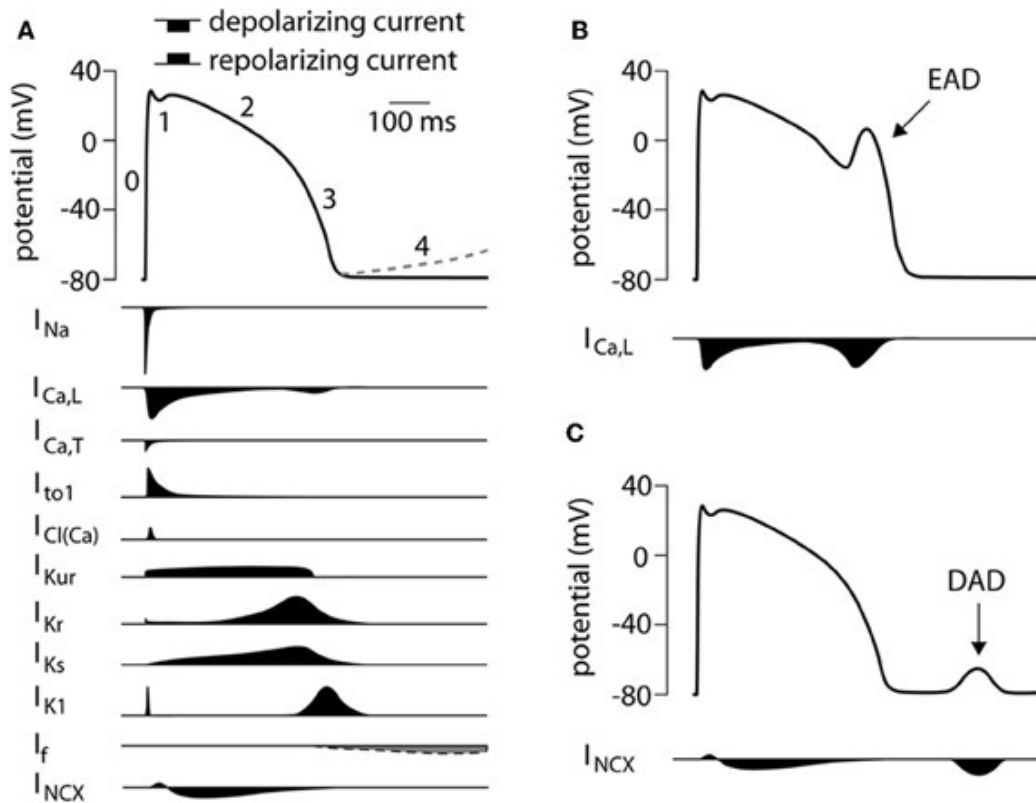


**Figure 1.4: Ventricular action potential, with ion currents and after-depolarisations**

Reproduced from Hoekstra *et. al.* (2012). Original legend: “**A.** Schematic representation of a human ventricular action potential (top panel). Numbers denote the different phases of the ventricular action potential. The dashed line represents phase 4 depolarization normally present in cells from the conduction system and not in ventricular CMs. Underlying ionic membrane currents and their schematic time course are depicted below. **B.** Schematic representation of an early afterdepolarization (EAD) and its underlying mechanism. **C.** Schematic representation of a delayed afterdepolarization (DAD) and its underlying mechanism.  $I_{Na}$ ,  $Na^+$  current;  $I_{Ca,L}$ , L-type  $Ca^{2+}$  current;  $I_{Ca,T}$ , T-type  $Ca^{2+}$  current;  $I_{to1}$ , transient outward current type 1;  $I_{Cl(Ca)}$ ,  $Ca^{2+}$  activated  $Cl^-$  current, also called  $I_{to2}$ ;  $I_{Kur}$ , ultra-rapid component of the delayed rectifier  $K^+$  current,  $I_{Kr}$ , rapid component of the delayed rectifier  $K^+$  current;  $I_{Ks}$ , slow component of the delayed rectifier  $K^+$  current;  $I_{K1}$ , inward rectifier  $K^+$  current;  $I_f$ , funny current;  $I_{NCX}$ ,  $Na^+/Ca^{2+}$  exchange current.” (Under CC Attribution License © 2012 Hoekstra, Mummery, Wilde, Bezzina and Verkerk)

### 1.3.5 Calcium-induced calcium release (CICR)

By far, the most widely accepted mechanism of  $\text{Ca}^{2+}$  release from the SR is LTCC-mediated CICR, whereby  $\text{Ca}^{2+}$  influx through LTCC activates the opening of neighbouring RyR2, and as a result leads to a large release of SR  $\text{Ca}^{2+}$  into the cytosol. Such CICR requires LTCC and RyR2 to be juxtaposed, in a protein complex (which includes many others) known as a dyad.  $\text{Ca}^{2+}$  release is moreover concentrated to a narrow space formed between the plasmalemma and the SR membrane: the junctional cleft. T-tubules are invaginations of the plasmalemma which allow for this CICR to occur nearer to myofilaments, i.e. further away from cell surface (Figure 1.3). A disruption of the tubular network is a common feature of CM remodelling during HF, impairing the efficiency and synchrony of CICR across CM<sup>121,122</sup>. It is not known whether factors secreted by EC contribute to this disruption during myocardial remodelling, or inversely prevent it by stabilising the tubular network.

A NCX-mediated CICR has been proposed<sup>123</sup>, as the result of extruding  $\text{Na}^+$  from phase 0 near dyads, but this has been challenged experimentally<sup>124,125</sup>. In addition, there is little evidence for NCX and even sodium channels to be expressed sufficiently close to dyads and contribute to CICR<sup>126</sup>. Therefore, EC-mediated changes in NCX or  $\text{Na}^+$  channels are not thought to affect the CICR directly.

$\text{Ca}^{2+}$  released at the dyad through LTCC binds to and activates RyR2, which is normally closed at diastolic concentrations of cytosolic calcium ( $[\text{Ca}^{2+}]_i$ ). Binding of  $\text{Ca}^{2+}$  increases the open probability of the channel and results in SR  $\text{Ca}^{2+}$  flowing to the cytosol<sup>127</sup>. The amount of  $\text{Ca}^{2+}$  released is a function of both  $I_{Ca}$  and SR  $\text{Ca}^{2+}$  load. The LTCC and RyR2 then close to terminate the CICR, allowing the SR to reload and  $[\text{Ca}^{2+}]_i$  to decrease to diastolic levels<sup>111</sup>. This is an intricate negative feedback mechanism, as the open probability of both channels decreases with increasing cytosolic  $[\text{Ca}^{2+}]$ . RyR2 has been identified as a target of NO-mediated S-nitrosylation, with which NO can increase RyR2 activity<sup>128,129</sup>. Yet, this has been linked to an nNOS-mediated local synthesis of endogenous NO<sup>129</sup> and the presence of such regulation of RyR2 by EC-derived NO remains to be confirmed. Furthermore, cAMP-mediated

PKA activity has been shown to increase the sensitivity of RyR2 to cytosolic  $\text{Ca}^{2+}$ , i.e. facilitating CICR but also pro-arrhythmic SR leaks during diastole<sup>130,131</sup>, via direct phosphorylation of RyR2. The effects of NO on the  $\beta$ -adrenergic response (mediated by cGMP) have not been well characterised for this section of the excitation-contraction coupling. In addition, while ET-1 can increase the amplitude of calcium transients, at least via LTCC<sup>120</sup>, it is still unclear whether ET-1 regulates directly the function of RyR2 or the properties of CICR downstream of LTCC. The paracrine effects of EC on the CICR and SR  $\text{Ca}^{2+}$  leaks in CM have never been appropriately tested experimentally, with co-cultures or other models.

### **1.3.6 Sarco-endoplasmic reticulum $\text{Ca}^{2+}$ -ATPase (SERCA)**

Once released from the SR during the CICR,  $\text{Ca}^{2+}$  is cleared from the cytosol via at least three mechanisms. In the adult rat and human ventricular CM, the dominant mechanism of extrusion is the SERCA pump. This protein is abundantly expressed at the SR membrane, allowing for  $\text{Ca}^{2+}$  to be reloaded in the SR within milliseconds. The dominant isoform of SERCA in the adult cardiac muscle is SERCA2a, and it requires the hydrolysis of ATP to transport  $\text{Ca}^{2+}$  to the SR lumen (against concentration gradients)<sup>132</sup>. SERCA is directly regulated by a protein known as phospholamban (PLB) which, in unstimulated conditions, inhibits the activity of SERCA. PLB phosphorylation relieves this inhibition, and therefore increases the velocity of  $\text{Ca}^{2+}$  re-uptake to the SR<sup>132</sup>. This is a known target of the  $\beta$ -adrenergic signalling, whereby a cAMP-dependent activation of PKA leads to the phosphorylation of PLB<sup>111</sup>. Importantly, a reduced expression of SERCA (mRNA and protein levels), a hypophosphorylation of PLB, and logically a decreased SR  $\text{Ca}^{2+}$  transport have been reported in patients with HF of different aetiologies<sup>133–138</sup>. SERCA downregulation also results in a reduced SR  $\text{Ca}^{2+}$  content and thus negatively impacts on the CICR, contributing to the reduced amplitude of calcium transients in HF<sup>111</sup>. However, it should be noted that not all studies have found a downregulation of SERCA or PLB expression in HF, further illustrating the heterogeneity and complexity of these dysregulations<sup>139</sup>.



Interestingly, little is known about the regulation of these mechanisms by EC-derived paracrine factors. EC-derived NO has been shown to stimulate the activity of SERCA in vascular smooth muscle cells<sup>140</sup>, although this does not involve the same isoform of SERCA as in CM (SERCA2b is predominant in smooth muscle cells<sup>141</sup>). The effects of NO on SERCA2a activity are unclear, with a study showing an nNOS-mediated inhibition of SR Ca<sup>2+</sup> uptake<sup>142</sup>, and another showing that NO-derived peroxynitrite (ONOO<sup>-</sup>) increased the activity of SERCA by S-Glutathiolation<sup>143</sup>. The regulation of SERCA activity by NO and NO-derived thiol oxidants (e.g. ONOO<sup>-</sup>) have not been well differentiated, and never confirmed in heterocellular *in vitro* models. Moreover, the effects of other known EC-derived cardiotropes on SERCA activity can only be speculated.

### 1.3.7 Sodium-calcium exchanger (NCX)

NCX is the second mechanism of calcium extrusion in CM. Unlike SERCA, NCX is expressed at the plasmalemma and thus transports Ca<sup>2+</sup> to the extracellular space<sup>111</sup>. There is evidence to suggest that NCX is preferentially localized in T-tubules, although as discussed above its expression and role within dyads is still being debated<sup>144</sup>. To maintain Ca<sup>2+</sup> homeostasis, NCX removes the same amount of Ca<sup>2+</sup> as was introduced by LTCC. Importantly, NCX exchanges 1 Ca<sup>2+</sup> for 3 Na<sup>+</sup>, which has two implications: (1) NCX activity is electrogenic, depolarising the membrane of CM when extruding Ca<sup>2+</sup>, and (2) it contributes to Na<sup>+</sup> homeostasis<sup>111,145</sup>. NCX has unsurprisingly been associated with pro-arrhythmic after-depolarisations, as well as Na<sup>+</sup> overload, in models of cardiac hypertrophy or HF, where NCX expression is increased<sup>133,146</sup>. Interestingly, NCX can work in “reverse mode”, during which Ca<sup>2+</sup> enters the cell and Na<sup>+</sup> is extruded. This occurs when the equilibrium potential of NCX (a function of the respective equilibrium potential of Na<sup>+</sup> and Ca<sup>2+</sup>) is lower than the membrane potential, thus inverting the driving force of this ion exchange<sup>111,145</sup>. As discussed above, it is unclear if the reverse mode of NCX contributes to the initiation of CICR. There is little evidence for a significant role of the reverse mode of NCX on the excitation-contraction coupling in CM with physiological [Na<sup>+</sup>]<sub>i</sub>

and  $[Ca^{2+}]_i$ . However, during HF,  $Na^+$  overload lowers the equilibrium potential of NCX, potentiating the reverse mode<sup>147</sup> and decreasing the normal (“forward”) mode. As a result, more  $Ca^{2+}$  enters the cell via NCX during the AP, and less  $Ca^{2+}$  is extruded via NCX in diastole. This slows  $Ca^{2+}$  extrusion, and therefore affects the kinetics of relaxation, but it also promotes SR  $Ca^{2+}$  loading (with SERCA gaining a relatively larger portion of  $Ca^{2+}$  to extrude than with physiological  $[Na^+]_i$ )<sup>145,147</sup>. It is also unclear whether such  $Na^+$  overload can provoke the constant leakage of SR  $Ca^{2+}$  (partial CICR) which was proposed by others<sup>146</sup>. Conversely, NCX might be part of cardioprotective compensatory mechanisms, e.g. by lowering  $[Na^+]_i$  and supplying additional  $Ca^{2+}$  in systole during its time in reverse mode. This is part of a complex mechanism, however, and the effects of NCX activity should not be fully isolated from the changes in NCX expression which are common in HF.

NCX is an important regulator of  $Ca^{2+}$  homeostasis and, as demonstrated above, an important feature of CM remodelling during HF. It is therefore surprising that the effects of EC or even of NO on NCX activity have not gathered interest so far. Studies are too scarce to make a fully comprehensive conclusion on the role of NO in the regulation of NCX activity. A study performed in 2003 showed no effect of nNOS-mediated NO synthesis on the expression and activity of NCX in CM<sup>148</sup>. More interestingly, other reports have proposed indirect effects, all consequential to changes in  $[Na^+]_i$ . Richards *et. al.* (2019) reported that the transports of the  $Na^+/H^+$ -exchanger-1 (NHE1) were increased by low [NO] and decreased by high [NO], and this was mediated by cAMP and cGMP rather than by S-nitrosylation<sup>149</sup>. Raised NHE1, as seen in HF, can evoke a rise of  $[Na^+]_i$  which, as indicated earlier, reduces the driving force of NCX fluxes in forward mode. Studies are however lacking to validate this second-degree effect of NO on NCX. Furthermore, another study has shown that NO can increase the activity of the  $Na^+/K^+$ -ATPase, hence limiting  $Ca^{2+}$  and  $Na^+$  overload in CM<sup>150</sup>. Indeed, by decreasing  $[Na^+]_i$  via the  $Na^+/K^+$ -ATPase, NO increases the equilibrium potential of NCX (i.e. increasing the forward mode of NCX while reducing the reverse mode). This is further complicated when introducing elements of the  $\beta$ -adrenergic response in CM, where cAMP-mediated activation

of PKA can activate the Na<sup>+</sup>/K<sup>+</sup>-ATPase while reducing NCX currents (via phosphorylation of their common co-factor phospholemman)<sup>151</sup>. It should be noted that PKA can also increase NCX currents, but that this is reduced significantly in HF due to direct hyperphosphorylation of the exchanger<sup>152</sup>. It is unknown how NCX phosphorylation is affected by NO or by other EC-derived cardiotropes.

Finally, the role of ET-1 on NCX function is also unclear and deserves more attention. ERK1/2 activation, as a result of ET-1 autocrine or paracrine release, has been shown to increase the activity of NHE1 in CM<sup>153</sup>. As discussed above, this modulates the activity of NCX by reducing its forward mode while increasing its reverse mode, hence contributing to both Na<sup>+</sup> and Ca<sup>2+</sup> overload in CM. However, this signalling has never been confirmed experimentally beyond the ERK1/2-mediated activation of NHE1, and needs to be tested in EC-CM co-cultures. A direct stimulation of NCX by ET-1 has also been reported, involving PKC activation<sup>154</sup>.

### **1.3.8 Additional mechanisms of calcium extrusion**

In addition to SERCA and NCX, mitochondria can also uptake Ca<sup>2+</sup> and contribute to cytosolic Ca<sup>2+</sup> clearance<sup>111</sup>. However, at steady state, this mechanism is unlikely to significantly regulate the morphology of calcium transients. Beat-to-beat changes in mitochondrial Ca<sup>2+</sup> have been demonstrated recently<sup>155</sup>, and this was enhanced in mitochondria localized near the SR. This would suggest that mitochondria contribute to calcium transient decay, but it should be noted that in the same study, intramitochondrial calcium transients decayed with a time constant too long to be compatible with steady state (approximately 5 sec). This experiment was performed at room temperature, so it remains unclear if mitochondrial calcium extrusion kinetics improve at 37°C. In neonatal rat ventricular myocytes (NRVM), the siRNA silencing or overexpression of mitochondrial Ca<sup>2+</sup> uniporter (MCU), which is responsible for mitochondrial Ca<sup>2+</sup> uptake<sup>156</sup>, respectively induced an increase and decrease of calcium transients amplitude<sup>157</sup>. This would again suggest that mitochondrial activity contributes to the beat-to-beat control of Ca<sup>2+</sup> levels, but this effect has been rejected as incompatible with steady state as well<sup>158</sup>. Furthermore,

this result is inconsistent with data obtained using adult CM where inhibition of mitochondrial  $\text{Ca}^{2+}$  had a less significant impact on the amplitude and kinetics of calcium transients<sup>159,160</sup>.

Cytosolic and mitochondrial  $\text{Ca}^{2+}$  are not independently regulated, however, as a prolonged  $\text{Ca}^{2+}$  overload can increase the mitochondrial uptake and overload mitochondria as a result<sup>161</sup>. ATP generation is calcium-dependent, so it is possible that cytosolic  $\text{Ca}^{2+}$  modulates indirectly the activity of kinases or ATPases (e.g.  $\text{Na}^+/\text{K}^+$ -ATPase) and thus multiple components of the excitation-contraction coupling machinery<sup>162</sup>. A mitochondrial  $\text{Ca}^{2+}$  overload is associated with ischemia-reperfusion injury, and is thought to be critical for cell necrosis<sup>156</sup>. However, how this is linked to the pathological remodelling of the excitation-contraction coupling is still unknown.

NO may affect mitochondrial respiration and  $\text{Ca}^{2+}$  uptake, but not in ways which are directly relevant to the excitation-contraction coupling<sup>163</sup>. The effects of EC-produced cardiotropes on mitochondrial calcium handling are still unexplored, and can only be speculated.

Finally, non-mitochondrial mechanisms of  $\text{Ca}^{2+}$  extrusion should be considered: e.g. diffusion via gap junctions, packaging in secreted vesicles, transport to other intracellular compartments (nucleoplasmic calcium transients have been reported, as reviewed by others<sup>164</sup>),  $\text{Ca}^{2+}$ -ATPase transport at the plasmalemma<sup>111</sup>, and store-operated calcium entry (SOCE)<sup>165,166</sup>. Of note, SOCE could be lost during maturation of CM<sup>167</sup>, but SOCE proteins (e.g. stromal interaction molecule 1, STIM1) could regulate the activity of SERCA and SR  $\text{Ca}^{2+}$  content even in the absence of SOCE<sup>168</sup>. In the interest of brevity, it is not necessary that these mechanisms are reviewed in this thesis. These have never been validated as potent regulators of the excitation-contraction coupling and, even if present in adult CM, would presumably not account for significant  $\text{Ca}^{2+}$  fluxes compared to SERCA or NCX activity. Evidence is also lacking to draw firm conclusions on the effects of EC-derived cardiotropes on these mechanisms.

### 1.3.9 Sarcomeres and myofilament sensitivity to calcium

When released from the SR,  $\text{Ca}^{2+}$  interacts with myofilaments and provokes a force-generating interaction of actin with myosin, i.e. shortening of the CM length<sup>169</sup>. Briefly, free  $\text{Ca}^{2+}$  binding to troponin-C induces an allosteric conformational change of the troponin-tropomyosin complex, which exposes myosin-binding sites on the actin filaments. Once myosin heads bind to actin, ATP induces a conformational change of myosin which generates force and results in myosin filaments sliding along actin filaments. This is dependent on the amount of cytosolic  $\text{Ca}^{2+}$  and the sensitivity of these myofilaments to  $\text{Ca}^{2+}$ , but also the level of cellular stretch. Actin-myosin cross-bridges are indeed regulated by the interfilament lattice spacing, which decreases when CM are stretched<sup>170</sup>. Of note, differences of lattice spacing were not observed in isometrically contracting CM<sup>171</sup>. Because cross-bridges of myosin with actin potentiate  $\text{Ca}^{2+}$  binding to actin, interfilament lattice spacing holds an important role in the length-dependent responsiveness of myofilaments to  $\text{Ca}^{2+}$  and the length-dependent development of force<sup>172</sup>.

Myofilaments are organised in symmetrical contractile blocks, known as sarcomeres, which are arranged in series and in parallel along the entire length of CM. It is beyond the scope of this introduction to describe the numerous sarcomeric proteins, but titin is noteworthy for three reasons: (1) its placement along the sarcomere increases the lattice spacing when sarcomere length decreases, thus acting as a mechanosensor<sup>173</sup>. (2) It is also responsible for the passive lengthening of CM in diastole (in conjunction with forces generated by the extracellular matrix and cardiac filling). Titin acts as a “molecular spring” that is essential to diastolic function<sup>169</sup>. (3) Hypophosphorylation of titin contributes to the development of HFpEF by lowering the elastic capacity of titin, resulting in a stiffening of CM during relaxation which can eventually lead to diastolic dysfunction<sup>91</sup>. This is strongly associated to endothelial dysfunction, as a loss of NO bioavailability in EC can lead to titin hypophosphorylation<sup>91</sup>. NO can also induce a cGMP/PKG-mediated phosphorylation of troponin-I, which increases the rate of  $\text{Ca}^{2+}$  dissociation from the myofilaments and therefore improves diastolic function and relaxation (i.e. positively lusitropic effects)<sup>174,175</sup>. Finally, cAMP-mediated activation of PKA during the  $\beta$ -

adrenergic response has been associated with the phosphorylation of troponin-I<sup>176</sup>, of the myosin binding protein C<sup>177</sup> and of titin<sup>178,179</sup>. Overall, this increases the rate of cross-bridge cycling, increasing the rate of force development and the stretch activation response<sup>180</sup>, in addition to decreasing passive tension of cardiac tissue<sup>178,179</sup>. Although interference with this signalling by NO-mediated generation of cGMP can be hypothesised, it has never been tested experimentally. ET-1 has been associated with a phosphorylation of troponin I, therefore lowering the myofilament sensitivity to Ca<sup>2+</sup>. This was attributed to PKC<sup>181</sup> and Protein Kinase D (PKD)<sup>182</sup> activation. The involvement of other known EC mediators on sarcomeric function remains undefined, and is a blind spot which should be scrutinised to better understand how endothelial plasticity can regulate cardiac contractility.

#### **1.3.10 Bowditch, Frank-Starling and Anrep effects**

The Bowditch effect (or staircase phenomenon) is a property of the myocardium to increase or decrease force in response to an increasing beating frequency. This relationship is positive in adult human myocardium<sup>111</sup> but tends to be flat or negative in small rodents, including rats<sup>183</sup>, or in the failing myocardium<sup>184</sup>. The mechanism responsible for this effect is still being debated but is thought to involve SERCA<sup>185</sup>, by which an increased frequency of calcium release acutely modifies SR Ca<sup>2+</sup> loading, as well as LTCC and NCX<sup>186</sup>. This affects the intensity of CICR and the activation of myofilaments. As shown above, EC-derived paracrine mediators (NO and ET-1 particularly) can affect the activity of SERCA, LTCC and (although this is less well studied) NCX. However, it is challenging to differentiate in HF the paracrine contribution of endothelial dysfunction from independent changes of SERCA, LTCC or NCX activity and expression. It is thus unclear if EC play a role in regulating the Bowditch effect in normal or failing myocardium. Furthermore, no *in vitro* study has to date shown a direct effect of EC on the force-frequency relationship of co-cultured CM.

CM experience two major types of mechanical load during the cardiac cycle: the end-diastolic stretch (preload), which is caused by the ventricular filling, and a systolic resistance (afterload),

which is caused by aortic pressure. These loads apply uniaxial forces on the CM and regulate CM contractility, as described below. Stroke volume (a result of force) increases with preload, a relationship known as the Frank-Starling mechanism. This has been shown to be modulated by phosphorylation of troponin I<sup>187</sup> and of the myosin binding protein C<sup>188</sup>, as well as by titin<sup>189</sup>. The most likely mechanism for this effect is an increased sensitivity of myofilaments for Ca<sup>2+</sup> at long sarcomere lengths, though this might not be associated with a change of actin-myosin cross-bridge kinetics<sup>190</sup>. As discussed in the previous section, these proteins are likely to be independently modulated by NO. However, evidence is lacking to confirm that NO activity can alter the length-dependent activation of the Frank-Starling mechanism. Furthermore, while the role of EC and endothelial dysfunction on passive tension has been well studied, their effects on length-dependency remain unknown.

The Frank-Starling mechanism can also be viewed as a rapid response to stretch. If the stretch is prolonged and uncompensated by the Frank-Starling response, a gradual increase of force will take place over 10-15 min. This is known as the slow myocardial response to stretch, and is commonly referred to as the Anrep effect<sup>191</sup>. Of note, this effect was first described as a result of aortic banding<sup>192</sup>, indicating that an increasing afterload can trigger this response. Distinctly from the Frank-Starling mechanism, the Anrep effect has been associated with an increase of calcium transient amplitude in CM<sup>191</sup>. It is beyond the scope of this section to detail this effect but, in summary, it is thought to involve a number of non-genomic events: 1) autocrine/paracrine release of angiotensin II (Ang-II), 2) activation of Ang-II type-1 receptors (AT-1), 3) autocrine release of ET-1 (ET-1 can also be provided by other cell types), 4) activation of the ET-1 receptor ET<sub>A</sub>, 5) activation of mineralocorticoid receptors (MR), 6) transactivation of epidermal growth factor receptor (EGFR), 7) mitochondrial generation of ROS, 8) phosphorylation of ERK1/2, 9) stimulation of the NHE1, 10) increase of [Na<sup>+</sup>]<sub>i</sub>, 11) entry of Ca<sup>2+</sup> via NCX in reverse mode, 12) increase of calcium transient amplitude<sup>191</sup>.

The order of these events is well understood, but not all links have been confirmed as crucial elements to the Anrep effect, while some have only been extrapolated from other models. This

limits greatly the strength of this paradigm. Furthermore, this sequence might not be the only possible pathway bridging stretch and calcium transient amplitude elevation, as some studies have proposed alternative pathways (e.g. those implicating NOS and the CICR)<sup>193</sup>. However, such pathways have so far been refuted by others<sup>194</sup>. Theoretically, EC-produced paracrine factors (again focusing on NO and ET-1) have the ability to interfere with the Anrep effect, by direct regulation of the ET-1 signalling, ROS synthesis, phosphorylation of ERK1/2, as well as NHE1 and NCX activity. However, this has never been tested and hence constitutes another blind spot of the scholarship regarding the EC-CM crosstalk.

### **1.3.11 Other mediators of EC activity on CM, and the pitfalls of transitive logic**

So far, I have focused this review of the literature on NO and ET-1 and their effects on CM for three reasons: 1) NO and ET-1 are the most relevant paracrine mediators of the EC-CM axis for the rest of this thesis, 2) they have also been studied in more detail than any other paracrine factor, and 3) both have pleiotropic activity, regulating multiple components of CM physiology. However, other paracrine factors secreted by EC can regulate the excitation-contraction coupling of CM. These include neuregulin-1 (NRG-1)<sup>195</sup> and apelin<sup>196</sup>, which have gathered considerable interest as inotropic agents. The most experimentally validated effects of EC-derived factors on CM functions are listed in Table 1.1.

This table may appear reductionist in comparison to recent reviews or meta-analytical works relating to EC-CM crosstalk. In Segers *et. al.* (2018)<sup>197</sup>, where the effects of EC-derived factors on CM have been most recently and exhaustively compiled, the EC-CM paracrine network is shown in more detail (Figure 1.5). However, not all links should be accepted at face value. For example, EC are shown secreting follistatin-like 1 (FSTL-1) during pressure overload, with anti-hypertrophic and pro-survival properties on CM. This is potentially misleading, as no direct evidence exists to suggest that EC can affect CM function via FSTL-1. The anti-hypertrophic effects of FSTL-1 were demonstrated in CM-specific gene knock-out and in NRVM<sup>198</sup>. Lara-Pezzi *et. al.* (2008) were able to confirm an elevation of FSTL-1 expression in EC in models



of pressure overload, but did not study directly the effects on CM<sup>199</sup>. Indeed overexpression of FSTL-1 in NRVM has anti-apoptotic effects<sup>200</sup>, but this cannot serve as evidence that EC-secreted FSTL-1 can affect CM survival. Other studies implicating FSTL-1 include further CM-specific experiments<sup>201</sup>, as well as analyses of its implication in vascular repair after MI. Therefore, linking EC-produced FSTL-1 with anti-hypertrophic and pro-survival effects on CM relies entirely on transitive logic.

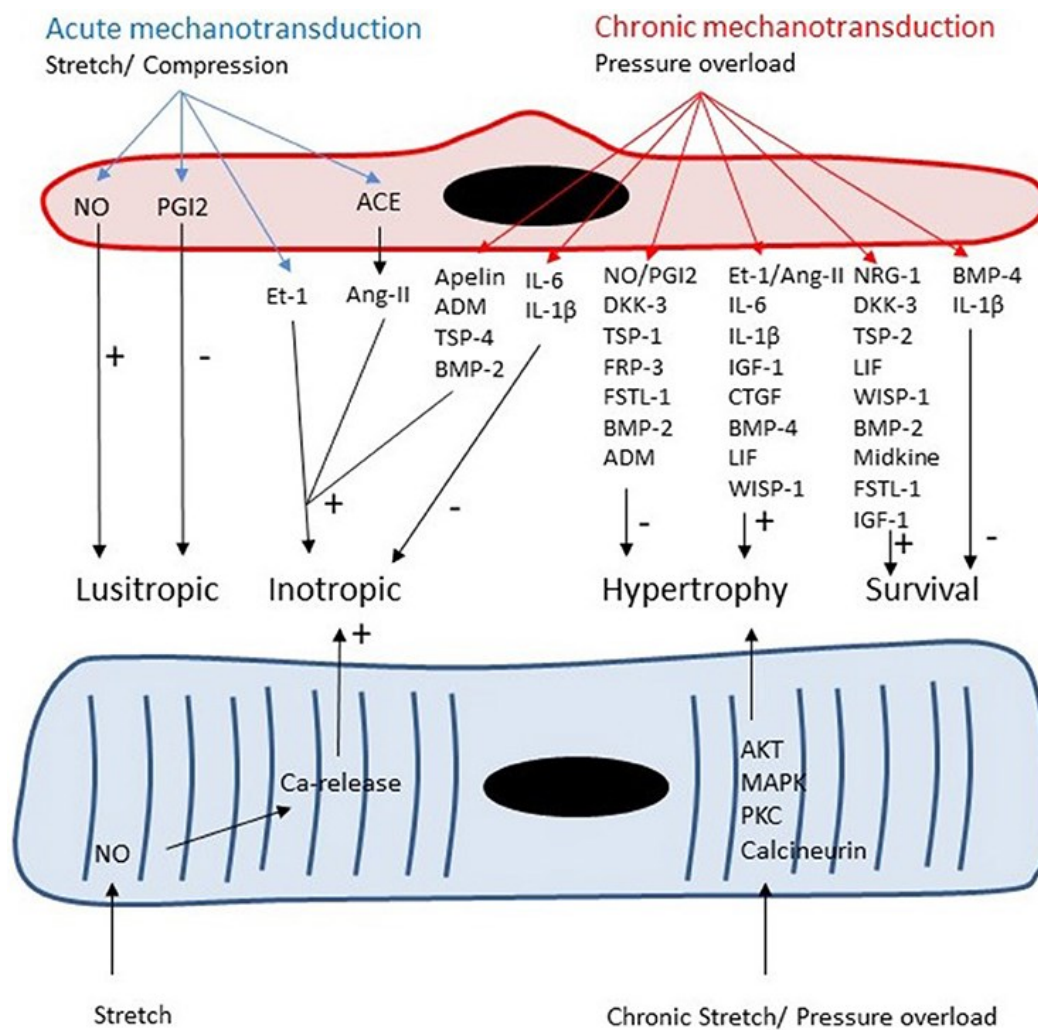


**Figure 1.5: EC-CM paracrine crosstalk and its plasticity**

Reproduced from Segers *et al.* (2018). Original legend: "Both cardiomyocytes and microvascular ECs are responsive to acute and chronic changes in loading conditions. Autocrine and paracrine signaling leads to acute changes in lusitropy and inotropy of cardiomyocytes and to chronic changes in cardiomyocyte growth and survival." (Under CC BY License © 2018 Segers, Brutsaert and De Keulenaer)

**Table 1.1: Effects of neuregulin-1, apelin, endothelin-1 and nitric oxide on CM function**

Agent	Demonstrated targets and/or effects on CM	Ref
<b>NRG-1</b>	Protects CM against hypoxia/reoxygenation injury	202
	Pro-hypertrophic	203
	Negatively inotropic	195
<b>Apelin</b>	Positively inotropic	204
<b>ET-1</b>	Positively inotropic	94,96
	Negatively lusitropic	94,96
	Cardiotoxic	96
	Pro-arrhythmic	100
	ERK1/2-mediated upregulation of LTCC	118
	Decreased $I_{Ks}$	119
	PKC-mediated stimulation of NCX	154
	PKC/PKD-mediated phosphorylation of troponin I	181,182
<b>NO</b>	Negatively inotropic	89
	Positively lusitropic	89
	cGMP-mediated inhibition of $\beta$ -adrenergic signalling	107
	Anti-arrhythmic (including a lower frequency of EAD)	103,104
	S-Nitrosylation of LTCC (inhibition)	112
	Increased $I_{Ks}$ and $I_{K1}$	114,115
	Decreased $I_{to1}$ and $I_{Kr}$	116,117
	Stimulation of RyR2	128,129
	ONOO <sup>-</sup> mediated S-Glutathiolation of SERCA (activation)	143
	Decrease NHE1 activity at high concentrations / increase NHE1 activity at low concentrations	149
	Activation of the Na <sup>+</sup> /K <sup>+</sup> -ATPase	150
	Phosphorylation of titin (decrease passive tension)	91
	Phosphorylation of troponin I (pro-lusitropic)	174,175

In other words, it implies that FSTL-1 secreted by EC has the same effects on CM as FSTL-1 produced within CM. The relevance of such logic for cell-cell interactions is debatable, but this has never been challenged in the literature. Without data from co-cultures or *in vivo* models, it remains speculative to conclude that EC affect CM via a given factor because: 1) EC can produce this factor, and 2a) this factor can affect CM function, or because 2b) CM express the receptor for this protein. Focusing on direct evidence might be too conservative, however, as too many components of EC-CM crosstalk would have to be discarded (i.e. FSTL-1, placenta growth factor, Dickkopf-related protein-3, thrombospondin-4, leukemia inhibitory factor, IL-1 $\beta$ , thioredoxin, parathyroid hormone-related protein, C1q/TNF-related protein-9, frizzled-related protein-3, secreted protein acidic and cysteine-rich (SPARC), bone morphogenetic proteins, adrenomedullin, Wnt1-inducible signalling pathway protein 1, osteopontin, midkine, tenascins, periostin, glutathione, connective tissue growth factor, and insulin-like growth factor-1). This would revert our knowledge of the EC-CM interactome back to 2003, when only NO, ET-1, NRG-1, apelin, Ang-II, and IL-6 were considered as direct contributors to the EC-to-CM axis<sup>205</sup>. The current trend to adopt transitive logic without any further or direct evidence of intercellular communication should still be considered one of the biggest limitations of the literature serving as foundation for this thesis.

Although NO and ET-1 have been confirmed as mediators of EC-to-CM signals<sup>85,92</sup>, much of what is known of their respective effects on CM physiology also relies on transitive logic. For example, the effects of NO on SERCA, LTCC and RyR2 activity (described above) have been studied in models of isolated CM or *in vivo* but non-specifically to EC, with either exogenously applied NO (using NO donors)<sup>206</sup> or a direct manipulation of NOS activity affecting endogenous NO synthesis by CM<sup>129</sup>. In these models, it is assumed that NO released by EC has the same effects on CM as endogenous NO. In light of the importance of subcellular spatial confinement for NOS isoforms and NO synthesis in CM<sup>129</sup>, and of the biphasic effects of NO on CM function based on its effective bioavailability<sup>206</sup>, this assumption deserves more scrutiny. Similarly, the effects of ET-1 on CM physiology have been studied in isolated CM, either stimulating an ET-1

autocrine release by CM or applying ET-1 exogenously at concentrations which might not be physiologically relevant to EC activity<sup>118</sup>.

### **1.3.12 Conclusions**

As described above, almost all aspects of CM physiology can be modulated by NO, ET-1, and other soluble factors known to be secreted by EC in certain conditions. Their secretion is highly dynamic, and sensitive to the environment. We now have a vast set of evidence that acute or chronic inflammation can modulate the secretome of EC, either quantitatively or qualitatively, for example disrupting the NO/ET-1 relationship.

There has been an emphasis on endothelial dysfunction and its effects on myocardial function, for years. However, even though it is well understood that inflamed and dysfunctional EC are not necessarily synonymous, the paracrine effects of inflamed EC (where NO bioavailability is not lost) on CM remain untested and theoretical. In studying this, it might be possible to bring to light contractile or electrophysiological signs of an early myocardial or vascular inflammatory response (i.e. preceding the EC dysfunction).

## 1.4 Hypothesis

The paracrine effects of EC on the excitation-contraction coupling of CM are modified by pro-inflammatory treatment of EC.

## 1.5 Aims

I address this hypothesis in three chapters of this thesis (3-5), aiming to:

1. Optimise and validate an *in vitro* co-culture system to study the paracrine effects of EC on CM, and identify a CM function which can serve as a reference point for the effects of EC-CM co-culture in Aim 3. (*Chapter 3*)
2. Characterise endothelial functions, with an emphasis on NO synthesis and the profile of protein secretion, in response to *in vitro* treatment with pro-inflammatory cytokines, and validate this treatment as relevant to cardiac vascular inflammation. (*Chapter 4*)
3. Investigate the effects of cytokine-treated EC on the excitation-contraction coupling of co-cultured CM. (*Chapter 5*)

Though the first two aims do not address the hypothesis of this thesis directly, they represent important steps in the validation of results in the third aim. Chapter 3 is also the opportunity to test the basal paracrine effect of EC on the calcium handling of co-cultured CM, a target of the crosstalk which has been theorised but never directly confirmed experimentally. While the aim of Chapter 4 is primarily to validate the pro-inflammatory treatment of EC prior to co-culture with CM, it is also the opportunity to investigate the differences of endothelial responses to different inflammatory cytokines, which is still poorly understood.

## 1.6 Study design

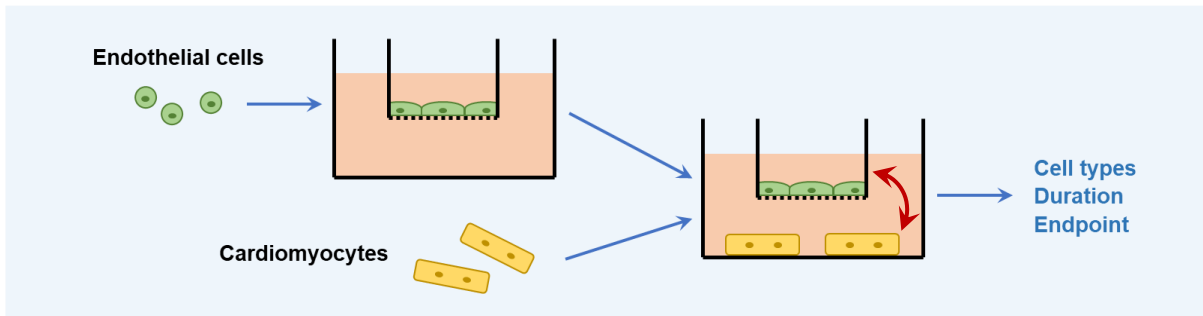
In Chapter 3, co-culture models were reviewed to determine the optimal mean of investigating EC-CM paracrine crosstalk with the highest physiological relevance and the lowest implication of other types of intercellular communication (e.g. exchanges of biomechanical forces). Next, with this model of co-culture, the effects of EC on the calcium transients in CM were assessed to confirm that this system can be used to generate a paracrine EC-CM interaction.

In Chapter 4, EC were treated with a cocktail of TNF $\alpha$ , IL-1 $\beta$  and hyper-IL-6. Cell proliferation, endothelial permeability, NO synthesis, and the secretion of inflammatory proteins were tested to assess the relevance of this treatment to model microvascular inflammation.

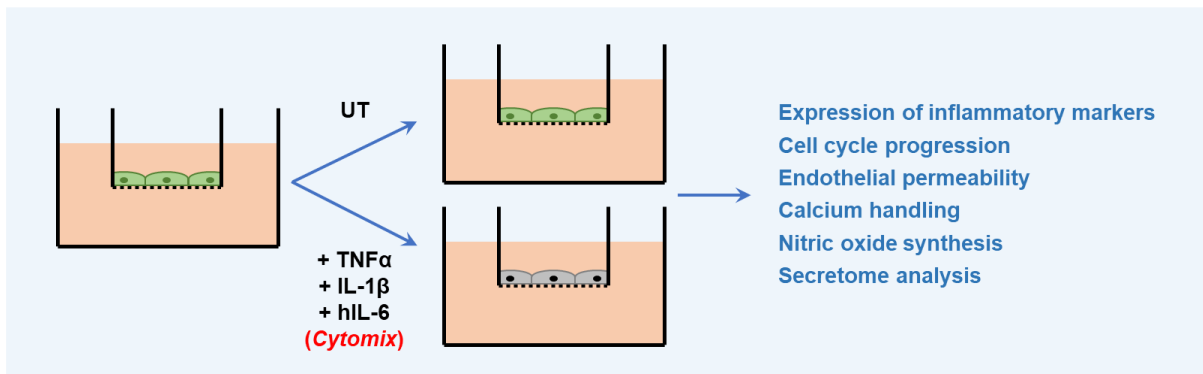
In Chapter 5, the co-culture model and the pro-inflammatory treatment established in Chapters 3 and 4 were combined. Calcium transients in CM were characterised after co-culture with EC that were pre-conditioned with cytokine treatments, compared to co-culture with untreated EC. In this Chapter, I have also laid the foundations for further experiments in *ex vivo* and ultimately *in vivo* models, which will aim to confirm the results obtained with co-cultures.

A simplified representation of this study design, divided by aims and chapters, can be found in the following page (Figure 1.6).

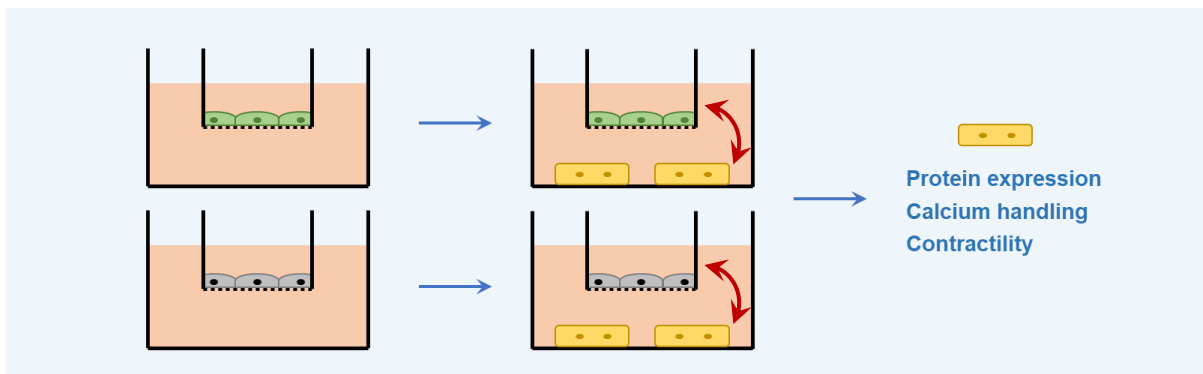
**Aim 1 – Chapter 3. Optimisation of co-culture model**









**Aim 2 – Chapter 4. Validation of pro-inflammatory treatment**



**Aim 3 – Chapter 5. Characterisation of cardiomyocytes after co-culture**



-  Endothelial cell
-  Cardiomyocyte
-  Paracrine interaction
-  Treated endothelial cell
-  Culture medium
-  Porous membrane

**Figure 1.6: Schematic summary of the study design**





# 2.

## **Material and methods**

## 2.1 Animal models

All procedures were carried out in compliance with the standards for the care and use of animal subjects as stated in the Guide of the Care and Use of Laboratory Animals (NIH publication No. 85-23, revised 1996) and following the requirements of the UK Home Office (ASPA 1986 Amendments Regulations 2012) incorporating the EU directive 2010/63/EU. Protocols were approved by the Animal Care and Use Committee of Imperial College London.

### 2.1.1 Sprague-Dawley

Adult male wild type Sprague-Dawley rats (*Rattus norvegicus*) were obtained from Charles River Laboratories (Harlow, UK) and housed in the Centre for Biological Services at Imperial College London and maintained on standard rat chow *ad libitum*. Four to five rats were housed per cage, and exposed to a 12-hour light-dark cycle at 21°C. Rats typically weighed between 150-250 g for CM isolation and 250-350 g for preparations of living myocardial slices (note: it is easier to slice larger left ventricles, which come from heavier rats). Rats were sacrificed in accordance with the Human Killing Register via Schedule 1 method, subsequent to completing the modules 1-4 of the Home Office and possession of a personal licence. Animals were briefly anaesthetised using 5% isoflurane in an anaesthetic induction box. Primary method of killing involved cervical dislocation before confirmation of death by dissection of the carotid arteries.

### 2.1.2 Myocardial infarction (MI) model in rats

To model chronic HF, the rats described in Section 2.1.1 underwent proximal coronary ligation to induce permanent MI. This model has been shown to induce severe ventricular remodelling, a loss of t-tubule structures in CM, reduced twitch amplitude, slower calcium transient kinetics, and increased frequency of  $Ca^{2+}$ , all consistent with chronic HF<sup>122</sup>. ARVM-MI were then isolated after 16 weeks, as described in Section 2.3.2. The coronary ligation and ARVM isolation were both performed by Mr Peter O’Gara.

## 2.2 Solutions

The following solutions were used throughout this study. Concentrations are described in mM unless stated otherwise. All chemicals were provided by VWR international, Sigma Aldrich, or ThermoFisher unless stated otherwise. Solutions were made up in Milli-Q water except for the low calcium solution and enzyme solution which used AnalaR water.

**Krebs-Henseleit (KH) solution:** 119 NaCl, 4.7 KCl, 0.94 MgSO<sub>4</sub>, 1.2 KH<sub>2</sub>PO<sub>4</sub>, 25 NaHCO<sub>3</sub>, 11.5 glucose, 1 CaCl<sub>2</sub>; pH-controlled and oxygenated by continuous bubbling through with 95% O<sub>2</sub> and 5% CO<sub>2</sub>

**Low calcium solution:** 120 NaCl, 5.4 KCl, 5 MgSO<sub>4</sub>, 5 Na<sup>+</sup> pyruvate, 20 glucose, 20 taurine, 10 4-(2-hydroxyethyl)-1-piperazineethanesulfonic acid (HEPES), 5 nitrilotriacetic acid (NTA), 0.04 CaCl<sub>2</sub>; pH 6.96 (NaOH)

**Enzyme buffer:** 120 NaCl, 5.4 KCl, 5 MgSO<sub>4</sub>, 5 Na<sup>+</sup> pyruvate, 20 glucose, 20 taurine, 10 HEPES, and 0.2 CaCl<sub>2</sub>; pH 7.4 (NaOH)

**Normal Tyrode's solution (for human cells preparations):** 140 NaCl, 4.5 KCl, 10 glucose, 10 HEPES, 1 MgCl<sub>2</sub>, 1.8 CaCl<sub>2</sub>; pH 7.4 (NaOH)

**Normal Tyrode's solution (for rat cells preparations):** 140 NaCl, 6 KCl, 10 glucose, 10 HEPES, 1 MgCl<sub>2</sub>, 1 CaCl<sub>2</sub>; pH 7.4 (NaOH)

**Normal Tyrode's solution (for myocardial slices):** 140 NaCl, 6 KCl, 10 glucose, 10 HEPES, 1 MgCl<sub>2</sub>, 1.8 CaCl<sub>2</sub>; pH 7.4 (NaOH)

**Na<sup>+</sup>- and Ca<sup>2+</sup>-free Tyrode's solution:** 140 LiCl, 6 KCl, 10 glucose, 10 HEPES, 1 MgCl<sub>2</sub>, 10 egtazic acid (EGTA); pH 7.4 (KOH)

**Slicing solution:** 140 NaCl, 6 KCl, 10 glucose, 10 HEPES, 1 MgCl<sub>2</sub>, 1.8 CaCl<sub>2</sub>, 30 2,3-butanedione monoxime (BDM); pH 7.4 (NaOH); Sterile-filtered (0.2 μm)

**Lysis buffer (western blotting):** Radioimmunoprecipitation assay buffer (RIPA), cComplete™ protease inhibitor cocktail (Roche, Switzerland), PhosSTOP™ phosphatase inhibitor cocktail (Roche, Switzerland)

**Tris-buffered saline Tween (TBS-T):** 20 Tris base (Trizma), 137 NaCl, Tween 20 at a 1:1,000 dilution; pH 7.8

**Loading buffer:** Bolt™ Lithium dodecyl sulfate loading buffer (LDS), 166.6 dithiothreitol (DTT)

**Blocking buffer (western blotting):** TBS-T, 5% bovine serum albumin (BSA)

**Blocking buffer (fluorescent immunostaining):** 94.7% Phosphate-Buffered Saline (PBS), 5% normal serum (species matched with the antibody), 0.3% Triton X-100

**Antibody dilution buffer:** PBS, 1% BSA, 0.3% Triton X-100

**Permeabilization buffer (cell cycle):** PBS, 50 Ethylenediaminetetraacetic acid (EDTA), 0.1% Triton X-100

**Stock RNase A solution:** 10 mg/ml RNase A (Sigma, Cat. No. R5000) dissolved in 10 mM sodium acetate buffer, pH 5.2. Heated to 100°C for 15 min, cooled to room temperature, and pH adjusted to 7.4 using 0.1 volume of 1 M Tris-HCl, pH 7.4. Stored at -20°C

**Propidium iodide (PI) staining solution:** 91% permeabilization buffer, 5% propidium iodide (1 mg/ml in dH<sub>2</sub>O; Sigma, Cat. No. P4170), 4% stock RNase A solution (v/v)

Below is the composition of culture media used throughout these experiments. All products were supplied by Gibco® (Life technologies, USA), Sigma Aldrich or PromoCell. Fresh culture medium was made in 50ml batches when required.

**Human umbilical vein endothelial cells and human aortic endothelial cells (HUVEC and HAEC) culture medium:** Medium-199 (with L-glutamine), 10% heat-inactivated bovine serum (FBS), 7.5 µg/ml endothelial cell growth supplement (ECGS), 0.2% heparin, and 100 U/ml penicillin, 100 µM streptomycin

**Human cardiac microvascular endothelial cells (HCMEC) culture medium:** Endothelial Cell Growth Medium MV2 (EGM-MV2, PromoCell; Cat. No. C-22121), with 10% FBS and 100 U/ml penicillin, 100 µM streptomycin

**Fibroblast culture medium:** Dulbecco's Modified Eagle Medium (DMEM) with high glucose, L-glutamine, and supplemented with 10% FBS and 100 U/ml penicillin, 100 µM streptomycin

**Adult rat ventricular myocytes (ARVM) culture medium (ACCT):** Medium-199 (with Earle's salts, L-glutamine, and sodium bicarbonate), 100 U/ml penicillin, 100 µM streptomycin, 0.2% BSA, 1.6 carnitine, 4.4 creatine monohydrate, 5.3 taurine, 100 µM L-ascorbate; sterile-filtered at 0.2 µm

**Cell co-culture medium:** Basal medium consisted of 50% ACCT and 50% EGM-MV2 (with supplements but not FBS); supplemented with 1% FBS, 6 µg/ml ECGS, and 0.2% heparin

**Myocardial slice culture medium:** Medium-199 (with Earle's salts, L-glutamine, and sodium bicarbonate), 300 U/ml penicillin, 300 µM streptomycin, 1:1,00 dilution of Insulin-Transferrin-Selenium (ITS) supplement (Gibco; Cat. No. 41400045)

## **2.3 Cell culture**

All biological procedures were carried out under sterile conditions in BioMat 2 class II microbial safety cabinets. Cell cultures were maintained in a humidified incubator at 37°C and 5% CO<sub>2</sub>.

### **2.3.1 Culture of human EC**

HUVEC, HAEC and HCMEC at passage 2 (P2) were purchased as cryopreserved vials from PromoCell. The EC were cultured on 1% gelatine-coated tissue culture (TC)-graded flasks, up to P6, and in their specific culture medium (see Section 2.2). Cells were split 1:3 when reaching confluency. To achieve this, the medium was removed, the culture flasks rinsed with PBS, and 1.5 ml of Trypsin-EDTA (Gibco®, Life Technologies, USA) was added to detach cells from the flask (for 5 min at 37°C). This was quenched with 4.5 ml of medium. Cells were collected and centrifuged at 500 g for 5 min, the supernatant discarded, and the pellet resuspended in fresh medium. This was distributed in new gelatine-coated flasks, or cells were counted using a Cellometer automated counter (Nexcelom Bioscience, USA) and distributed to culture wells for specific experiments.

### **2.3.2 Isolation and culture of human adult cardiac fibroblasts**

Human cardiac ventricular fibroblasts were obtained from adult donor hearts that were rejected for transplant surgery at Addenbrooke's Hospital (Cambridge). The whole heart was provided by NHS Blood and Transplant, UK (REC reference 16/LO/1568). TC Petri dishes were coated with 10 µg/ml fibronectin in PBS for 1 hour at 37°C, during fibroblast isolation. Left ventricular free wall samples were collected in ice-cold cardioplegia. Excess fat and connective tissues were removed from myocardium pieces, which were washed and minced in PBS containing 5% v/v penicillin and streptomycin (<10 mm<sup>3</sup>). Tissue pieces were transferred into a new dish of sterile PBS, minced to smaller pieces (<1 mm<sup>3</sup>), and washed in 0.05% Trypsin-EDTA for 2 min. Trypsin was quenched with an equal volume of fibroblast culture medium. Tissue pieces

were then transferred to the fibronectin-coated Petri dishes and separated from each other by at least 5 mm, to allow for cell outgrowth. These were incubated with fibroblast culture medium for 2 hours (50% normal volume) before additional medium was added to submerge the tissue explants. These were cultured for 4 days before the next change of medium. After this, media were changed every other day while cell outgrowth was monitored. At cell confluence, which was approximately 2 weeks after explant isolation, fibroblasts were trypsinised and transferred to TC flasks. The fibroblast isolation, characterisation and early cell passaging were performed by Brian Wang, PhD, with the help of Mr Oisín King. Cells were used up to passage 20.

### **2.3.2 Isolation of adult rat ventricular myocytes (ARVM)**

Following Schedule 1, incisions were made along the subcostal margin, giving access to the thoracic cavity through the diaphragm, which was dissected away. Viscera were removed and submerged in ice-cold KH solution. Blood was removed by gentle massage of the heart, which was separated from lungs and pericardial fat. The aorta was cannulated, mounting the heart on a Langendorff system for retrograde perfusion of coronary arteries with 37°C KH. Beating was allowed for approximately 2 min, to clear as much blood from the system as possible. KH was then switched to low calcium solution to stop contractions. This solution was switched to enzyme buffer containing 1 mg/ml Collagenase II and 0.6 mg/ml Hyaluronidase after 5 min, to degrade the extracellular matrix for 10 min. The left ventricle was then isolated from the other parts of the heart, minced into fresh enzymatic solution (with Collagenase and Hyaluronidase) and mechanically shaken at 35°C for 5 min. The supernatant was filtered, and the enzymatic solution replaced. Tissue was shaken for 30 min at 35°C, before replacing again the enzymatic solution, eliminating smaller cardiac cells (i.e. all but CM). Myocytes were centrifuged at 50 *g* for 1 min, the supernatant discarded, and the pellet resuspended in enzyme buffer (but without Collagenase or Hyaluronidase). This resulted in a suspension of calcium-tolerant ARVM. Both the Schedule 1 and ARVM isolation were performed by Mr Peter O’Gara.

### **2.3.3 Culture of ARVM**

After a maximum of 1 hour after isolation, ARVM were counted, centrifuged at 20 g for 1 min, resuspended in co-culture medium, centrifuged, and resuspended in co-culture medium again. Cells were plated on 13 mm diameter glass coverslips (pre-coated with 1% laminin) at 20,000 rod-shaped cells per coverslip. These were incubated at 37°C for 2 hours to let as many ARVM attach as possible, before gently washing away unattached cells and replacing the co-culture medium. Co-cultures with EC were initiated at this point, whenever applicable. Cells were thus incubated at 37°C for 4 or 24 hours before the experimental endpoints.

### **2.3.4 Transwell co-culture of EC and CM**

A Transwell co-culture model was used to investigate the paracrine interaction of EC and CM. In this system, the two cell types are separated by a porous membrane. This is done by plating one of the cell types, here EC, in culture well inserts (called Transwells) which hang at a short distance above the other cell type, cultured in the well in a traditional fashion (Figure 2.1). This allows for bidirectional paracrine exchange to occur between the cells, but not biomechanical or electrophysiological interactions.

EC were plated in sterile gelatine-coated ThinCert™ inserts, adapted for 12-well format plates (Greiner Bio-One, Austria), at 60,000 cells per insert. These were composed of a transparent polyester (PET) membrane, with capillary pores of 0.4 µm diameter at a density of  $2 \times 10^6 \text{ cm}^{-2}$ , on which the EC were plated. Cells were cultured in 0.5 ml of medium in the insert, with 1 ml in the culture well (lower compartment).

EC were grown to confluence in the inserts, for 24 hours in EGM-MV2. The medium was then removed, cells rinsed with sterile PBS, and cultured for 24 hours in co-culture medium. Inserts were then transferred in culture wells containing freshly isolated and plated CM. Empty inserts (but still gelatine-coated) were used for negative controls (i.e. ARVM alone). EC were washed



with PBS and the medium renewed before co-culture. Co-cultures were thus maintained for 4 or 24 hours, depending on the experiment.

To obtain co-cultures with Transwell inserts where EC and CM are only separated by the insert membrane, the 12-well inserts were first positioned upside-down (Figure 2.1A). HCMEC were then plated in a droplet of medium (100  $\mu$ l) on the insert membrane (Figure 2.1B). After 1 hour of sedimentation at 37°C, the medium droplet was removed, leaving a layer of EC attached at the bottom of the inserts. These were turned, placed normally in culture plates, and the other side of the membrane (upper) was coated with laminin before rod-shaped ARVM were plated at a density of  $4.4 \times 10^4$  cells/cm<sup>2</sup>.

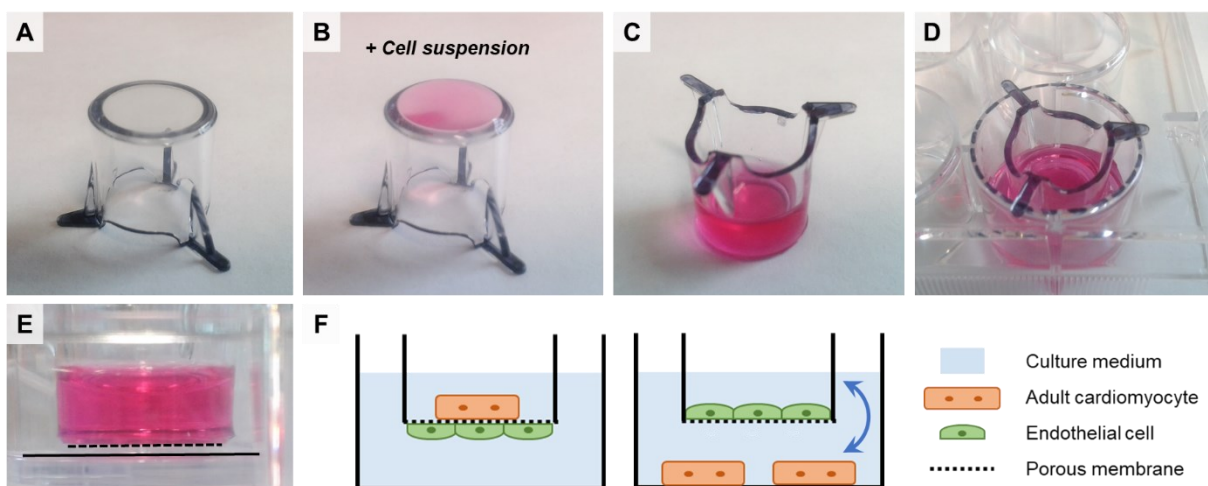


**Figure 2.1: Transwell co-culture systems**

Traditional and alternative uses of Transwell inserts for EC-CM co-culture. **A.** Picture of a single insert upside-down. **B.** Upside-down insert with a 100  $\mu$ l droplet of EC suspended in medium, during 1 hour of sedimentation in the alternative method. In the traditional method, EC are instead plated inside the insert (**C**). **D.** Picture of an insert in a culture plate well, with medium inside and outside the insert. **E.** Side view picture of an insert placed in a well, with medium inside the insert only. The plain and dotted lines represent the bottom of the well and the porous membrane of the insert, respectively. **F.** Simple schematic of the inverted (left panel) and traditional (right panel) Transwell models.

## **2.4 SDS-PAGE and western blotting**

Sodium dodecyl sulfate polyacrylamide gel electrophoresis (SDS-PAGE) and western blotting allow for semi-quantitative measurements of protein expression from cells or tissue.

### **2.4.1 Sample preparation**

To collect and purify protein samples in cell preparations, cultures were washed twice with ice-cold PBS. PBS was removed entirely, and a RIPA-based lysis buffer was used to break cellular membranes and stabilise proteins (including phosphorylation). For HCMEC samples, 80  $\mu$ l of lysis buffer was used per well of 6-well plates. For ARVM, four technical replicates were pooled from 13 mm diameter coverslips covered by 20  $\mu$ l of lysis buffer. Samples were incubated for 5 min on ice throughout, after which a cell scraper was used to ensure that all proteins were collected from the lysed preparation. Samples were collected in 0.5 ml Eppendorf tubes, then centrifuged at 14,000 *g* for 12 min and the pellet discarded to remove cellular debris from the final sample. Samples were conserved at -80°C until further use. Repeated freeze-thaw cycles were avoided whenever possible.

### **2.4.2 Quantification of protein concentration**

The concentration of proteins in lysis buffer was quantified after sampling using a detergent-compatible colorimetric protein assay (Bio-Rad, USA). BSA was used to generate a standard. Samples were loaded in triplicates in a plate of 96-well format. Proteins were detected as per manufacturer's recommendation, by reading the absorbance at 595 nm (the plate reader was from Synergy HT, BioTek, USA). Data were collected between the 15-60 min points of the colorimetric reaction. This reaction is based on the Lowry assay, and is linear for at least 2 hours. This method was used to determine the volume of protein sample corresponding to 5-10  $\mu$ g of protein.

### **2.4.3 SDS-PAGE**

Electrophoresis samples were prepared by diluting lysis protein samples into loading buffer, for a total volume of 30 µl containing 5 or 10 µg of protein per sample. Proteins were denatured through a heat cycle of 100°C for 10 min. Samples were then loaded in single wells of Bolt™ precast polyacrylamide Bis-Tris HCl buffered 4-12% gradient gels (Invitrogen). Two gel lanes were reserved for a protein standard: SeeBlue® Plus2 pre-stained standard (Invitrogen), which was used to extrapolate the approximative molecular weight of protein signals detected later. Electrophoresis was performed in Bolt™ 3-(N-Morpholino)propanesulfonic acid (MOPS)-SDS running buffer (Invitrogen) and run at 200 V for 32 min, or until the protein separation by size was judged appropriate for the detection of specific targets.

### **2.4.4 Protein transfer and blotting**

After the SDS-PAGE, proteins were transferred from the electrophoresis gels to polyvinylidene difluoride (PVDF) membranes of 0.2 µm pore size, using the dry transfer method and utilizing iBlot™ 2 premade transfer stacks (Invitrogen) with pre-activated PVDF membranes. Transfer was performed using the iBlot™ 2 Gel Transfer Device, with the following program: 20 V for 1 min, 23 V for 4 min and 25 V for 5.5 min. Membranes were then incubated at room temperature in blocking buffer containing BSA, for 1 hour on a rocking table. Proteins were probed using specific primary antibodies, at 1:3,000 to 1:1,1000 dilution in blocking buffer, at 4°C overnight and with a rocking motion. Membranes were then washed thoroughly three times with TBS-T, in cycles of 15 min on a rocking table. They were incubated for 1 hour at room temperature with horseradish peroxidase (HRP)-labelled secondary antibodies (species matched with the primary antibodies) diluted at 1:3,000 in blocking buffer. Membranes were finally washed again three times with TBS-T, as previously.

#### **2.4.5 Imaging and quantification**

Immunostaining was revealed by enhanced chemiluminescent (ECL) reaction using Pierce™ ECL substrate reagents (Amersham, GE Healthcare, USA). Radiographic images were taken in complete darkness at different exposures, using X-ray films (Thermo Scientific) which were then run through a Konica-Minolta-SRX101A film developer and scanned at 300 dpi resolution. Quantification was performed using ImageJ, after down-conversion of JPG images to 8-bits. Pixel density for specific bands was corrected for each lane to the pixel density of the loading control Glyceraldehyde 3-phosphate dehydrogenase (GAPDH). Normalised densitometric data were then compared between lanes of the same gels, but not directly between different gels.

## 2.5 Endothelial cells studies

### 2.5.1 Flow cytometric characterisation of HCMEC

To confirm that culturing HCMEC in the co-culture medium does not induce transdifferentiation of vascular EC into lymphatic EC or mesenchymal cells, the expression of EC markers (CD31, CD144), of the lymphatic marker Lyve-1 and of  $\alpha$ -smooth muscle actin ( $\alpha$ -SMA) was quantified by flow cytometry. HUVEC and hACF were used as control EC and non-EC, respectively.

Cells were cultured in 6-well plates (300,000 cells per well) in their respective culture media, and trypsinised after 48 hours. Samples were centrifuged at 300 *g* for 5 min to remove media, and cells were subsequently resuspended in PBS to be counted. PBS was removed, and cells were resuspended in Cell Staining Buffer (BioLegend, Cat. No. 420201) which contained the fluorophore-conjugated antibodies of interest (for cell surface antigens, i.e. all except  $\alpha$ -SMA), or isotype control antibodies (listed in Section 2.9). Samples were vortexed and incubated at 4°C for 30 min in the antibody solution. Cells were then washed three times with Cell Staining Buffer, each time centrifuged for 5 min, and finally resuspended in Fixation Buffer (BioLegend, Cat. No. 420801) in darkness for 20 min at room temperature. Cells were centrifuged again to remove the buffer, which was replaced by Permeabilization Wash Buffer (BioLegend, Cat. No. 421002), used to wash cells again three times with centrifugation cycles. Cells were incubated for 20 min at room temperature in Permeabilization Wash Buffer containing the intracellular primary antibodies of interest, and washed three times with the wash buffer before suspending fixed and intracellularly labelled cells in Cell Staining Buffer.

Cell suspensions were then processed through a CyAn™ APD cytometer (Beckman Coulter, USA). At least 10,000 events were recorded for each sample. Debris and cell multiplets were excluded from the datasets by a selective gating strategy from a forward-/side-scatter plot and secondly from a pulse width/forward scatter plot. Analysis was carried out using Summit 4.3 (Beckman Coulter, USA).

### **2.5.2 Cell cycle progression**

Cell cycle progression and proliferation of HCMEC were analysed by flow cytometry using a propidium iodide (PI) staining. After cell permeabilization, PI is used to stain DNA, which allows for stages of the cell cycle (G1, G2, S, M) to be differentiated by a quantitative analysis of PI fluorescence intensity. Since PI can also bind to double-stranded RNA, it is necessary to treat the cells with RNase.

EC were trypsinised and centrifuged at 300 *g* for 5 min to collect cell pellets and remove the media. Samples were then washed at room temperature with PBS three times, with a cycle of vortex and spin each time, before final resuspension in 200  $\mu$ l of PBS. Cells were fixed with 70% ice-cold ethanol for 1 hour at 4°C. To prevent cell aggregates, the ethanol was slowly added in a drip-wise manner using a micropipette, while cells were constantly vortexed at a medium speed. Next, samples were centrifuged to remove the ethanol and washed three more times with ice-cold PBS. PBS was removed and cells resuspended in PI staining solution, for 30 min at 37°C (in darkness). Cell suspensions were then processed through a CyAn™ APD cytometer (Beckman Coulter, USA), with 15,000 +/- 5,000 events recorded from each sample. Debris and cell multiplets were excluded from the datasets by a selective gating strategy from a forward-/side-scatter plot and secondly from a pulse width/forward scatter plot. Analysis was carried out in FCS Express, using the in-built analytical tool to classify cells by cell cycle stage (MultiCycle, Phoenix Flow Systems, USA), which is based on an algorithmic processing of the PI staining.

### **2.5.3 Endothelial permeability**

To measure the endothelial permeability of HCMEC, cells were plated at 60,000 cells per 12-well Transwell insert (Greiner Bio-One, Austria) and grown to confluence for 48 hours in EGM-MV2 and, in the last 24 hours, the co-culture medium. The fluorescent tracer FITC-Dextran of 40 kDa (Sigma, Cat. No. FD40) was added at 0.1 mg/ml in the luminal chamber of the inserts

(i.e. upper compartment). Immediately after adding FITC-Dextran, Thrombin (Sigma, Cat. No. T7572) was added in the upper chamber of the inserts as well, at a final concentration of 0.1 U/ml. After 1 hour of diffusion, medium from the abluminal chamber was sampled in triplicates (200  $\mu$ l). Fluorescence intensity was measured on a plate reader (Synergy HT, BioTek, USA), at 488 nm. Finally, concentrations were extrapolated from a standard curve of FITC-Dextran. Endothelial permeability ( $P(EC)$ ) was calculated as previously described<sup>207</sup>, by first calculating the volume ( $V$ ) of tracer cleared through the filter (insert membrane):

$$V = \frac{CA \cdot VA}{CL} \quad (1)$$

where ( $CL$ ) is the initial luminal concentration of FITC-Dextran, ( $CA$ ) the concentration in the abluminal compartment after diffusion, and ( $VA$ ) the abluminal volume of media. The changes of FITC-Dextran concentration in the luminal chamber can be regarded as insignificant<sup>207</sup>. The permeability ( $P$ ) of the system was expressed in  $m \cdot s^{-1}$  and calculated from the clearance rate ( $dV/dt$ ) and the surface area of insert membranes ( $S$ ) in  $m^2$ :

$$P = \frac{dV/dt}{S} \quad (2)$$

Permeability was calculated thus with EC monolayers ( $P(EC + F)$ ) and separately in gelatine-coated inserts ( $P(F)$ ), therefore isolating the transendothelial component of permeability in this system as shown in equation 3. Of note, the diffusion of FITC-Dextran is passive since there are no hydrostatic and oncotic gradients at play, nor active transport mediated by EC function.

$$\frac{1}{P(EC)} = \frac{1}{P(EC + F)} - \frac{1}{P(F)} \quad (3)$$

#### 2.5.4 Thrombin-induced calcium transients

Thrombin-induced calcium transients were investigated in HCMEC using the non-ratiometric  $Ca^{2+}$ -sensitive dye Fluo-4-acetoxymethyl ester (AM) (Invitrogen) and fluorescent microscopy (Optical Mapping). Culture medium was replaced with fresh normal Tyrode's containing 4  $\mu$ M

Fluo-4 AM (solubilised in DMSO). Next, cells were incubated for 15 min at 37°C, the Tyrode's solution was then changed to remove Fluo-4 from the bath, and further incubated for 10 min at 37°C to allow for cytosolic dye de-esterification. Cells were superfused with normal Tyrode's at 37°C throughout this experiment. Fluo-4 was excited using a LED emitting at 488 nm and signals were imaged through a  $560 \pm 35$  nm long-pass optic filter. These were recorded with WinFluor, an analogue signal acquisition software, and a Complementary Metal Oxide Semiconductor (CMOS) sensor C11440 digital camera (Hamamatsu, Japan) mounted on a Nikon Eclipse FN1 upright microscope. Fluo-4 signals were recorded for 20 min at 2 fps (33 ms interval exposure) and at 10x magnification.

After 120 seconds of recording, Thrombin was injected at different concentrations in the bath solution, using a micropipette in proximity to the area of interest. This triggers a cytosolic  $\text{Ca}^{2+}$  wave in EC translating into a higher Fluo-4 signal. Videos were converted to TIFF format, and regions of interest (ROI) delineated in ImageJ to generate TXT files of averaged fluorescence intensity for each frame. Trace morphology was then analysed in Clampfit (pClamp 10.2.0.14). The background noise was averaged in cell-free regions and subtracted from averaged signals in individual cell. Only one dish was used per thrombin-induced calcium wave.

Baseline fluorescence was defined as  $F_0$ , and fluorescence at any time-point as  $F_1$ . Traces were shown as  $F_1/F_0$ . The amplitude of thrombin-induced calcium transients was calculated at  $\text{max } F_1$ . The duration of transients ( $\text{TTD}_{80\%}$ ) was calculated in seconds, from the first point of transients to the point of the decay phase corresponding to 80% of decay from the peak.

### **2.5.5 Endothelial NO bioavailability**

To measure the intracellular levels of NO in HCMEC, the cell permeable fluorescent probe for NO, 4,5-Diaminofluorescein diacetate (DAF-2 DA, Abcam), which was added at 1  $\mu\text{M}$  in EGM-MV2 to 60,000 HCMEC (per well, on #1.5 glass in glass-bottom 12-well plates; Cellvis, USA). Cells were incubated thus for 1 hour and medium was then changed to fresh Tyrode's solution.



After 5 min of equilibration at 37°C, Thrombin (0-0.1 U/ml) and/or N( $\omega$ )-nitro-L-arginine methyl ester (L-NAME) (10  $\mu$ M) were added to the wells and incubated for 20 min at 37°C. DAF-2 DA fluorescent images were collected using a Zeiss LSM-780 inverted confocal microscope (FILM facility), at 488/515 nm (ex./em.) and at 63x magnification. The intensity of fluorescence was corrected for background noise and averaged as pixel intensity for each cell using ImageJ.

## **2.6 Cell secretome characterisation**

Culture supernatants (1 ml) were collected from the lower compartment of Transwell cultures. Samples were centrifuged at 18,000 *g* for 12 min (at 4°C) to remove floating cells, debris, and larger vesicular bodies. Processed conditioned media were stored at -80°C until used and only thawed once to limit cytokine degradation. Different samples were used for the cytokine array and the enzyme-linked immunosorbent assay (ELISA), which are described below.

### **2.6.1 Human XL Cytokine Profiler™ Array**

The culture supernatants of HCMEC (UT or cytokine-treated) were screened for inflammatory soluble proteins, mainly cytokines, chemokines and growth factors, with a Human XL Cytokine Array kit (R&D, Cat. No. ARY022B). In this array, nitrocellulose membranes have been spotted in duplicates with capture antibodies for 105 proteins (listed in Table 4.1). This array was used as per manufacturer's recommendations but, briefly, membranes were incubated with culture supernatants, washed, and incubated with a cocktail of biotinylated detection antibodies. Next, protein binding was revealed using Streptavidin-HRP, a chemiluminescent reaction, and X-ray films. As previously, the films were processed using a Konica-Minolta-SRX101A radiographic film developer and scanned at 300 dpi resolution. Pixel densities were collected and analysed using ImageJ, after down-conversion of JPG images to 8-bits. Negative control spots allowed for background noise to be corrected in the dataset. Signals were compared between samples (i.e. membranes collected on the same X-ray film and at the same exposure).

### **2.6.2 Enzyme-Linked Immunosorbent Assay (ELISA)**

A more quantitative and accurate approach than the cytokine array was required to verify the level of soluble proteins of interest in the media supernatants of HCMEC and after co-culture with CM. This was accomplished with ELISAs. All kits were purchased from R&D Systems®. ET-1 was detected using a Quantikine™ ELISA (Cat. No. DET100). DuoSet™ ELISAs were

used to detect the C-X-C motif chemokines CXCL5 (Cat. No. DY254) and CXCL1 (Cat. No. DY275), as well as the Granulocyte colony-stimulating factor (G-CSF; Cat. No. DY214) and Granulocyte-macrophage colony-stimulating factor (GM-CSF; Cat. No. DY215). For the DuoSet™ kits, an ancillary reagent kit was required (R&D, Cat. No. DY008). All arrays were used as per manufacturer's recommendations. Protein standards were provided in each kit. To determine the appropriate sample dilution for further experiments, samples were first used at different dilutions in assay diluents (1:1, 1:50, 1:100, 1:200). Samples were run in technical duplicates and data were collected using a plate reader (Synergy HT, BioTek, USA) measuring optical density at 450 nm and 562 nm. The reading at 562 nm was subtracted from the reading at 450 nm to correct for optical imperfections in the ELISA plate.

## 2.7 Cardiomyocyte studies

### 2.7.1 Immunofluorescent staining, confocal microscopy, and CM planimetry

Hypertrophy and sarcomeric remodelling of CM were investigated by confocal microscopy of  $\alpha$ -actinin, a sarcomeric protein. To accomplish this, ARVM were first fixed for 15 min with ice-cold methanol and washed with PBS three times. This fixative is adapted to preserve the cytoskeletal architecture, thus preferable to paraformaldehyde in this instance. Fixed samples were incubated for 1 hour at room temperature with blocking buffer, and overnight at 4°C with anti- $\alpha$ -actinin antibody diluted in antibody dilution buffer (see Table 2.1). Samples were rinsed with PBS and incubated for 2 hours at room temperature with the secondary antibody diluted in antibody dilution buffer. Finally, after three gentle washes with PBS, samples were mounted on glass microscope slides using Vectashield® Antifade HardSet™ mounting media containing 4',6-diamidino-2-phenylindole (DAPI) (Vector laboratories, USA, Cat. No. H-1500-10). Slides were then cured overnight at room temperature, in complete darkness, and stored at 4°C.

A single focal image of  $\alpha$ -actinin fluorescent signals was collected at 40x magnification in each cell, avoiding the nuclei, using a Zeiss LSM-780 inverted confocal microscope (FILM facility). The Alexa Fluor® 488 probe, conjugated to the secondary antibody, was stimulated at 488 nm with an argon laser, and images were collected through a 500-550 nm band-pass filter. Images of ARVM morphology were collected using brightfield microscopy, also at a 40x magnification.

Analysis was carried out in ImageJ. ARVM dimensions (planimetry) were described as follows: maximal length as “long axis”, maximal width as “short axis”, and long axis divided by the short axis as “aspect ratio”. The number of sarcomeres was counted along the long axis. Sarcomere length was averaged from >20 sarcomeres.

## 2.7.2 Normal calcium transient analysis

Calcium handling was characterised in ARVM by recording calcium transients with the Optical Mapping technique described in Section 2.5.4, but with some variations. Briefly, media were replaced with fresh normal Tyrode's solution containing 4  $\mu$ M Fluo-4 AM. Cells were incubated for 15 min at 37°C, the Tyrode's solution changed to remove Fluo-4, and further incubated for 10 min at 37°C to allow for cytosolic dye de-esterification. Cells were superfused with normal Tyrode's solution at 37°C throughout the experiment. Fluo-4 was excited using a LED emitting at 488 nm and signals were imaged through a  $560 \pm 35$  nm long-pass optic filter, with WinFluor and a C11440 digital camera (Hamamatsu, Japan) at a 40x magnification. ARVM were field-stimulated at 1 Hz with 40V bipolar pulses (of 10 ms), using a MyoPacer stimulator (IonOptix, USA) and platinum wires. Videos were collected at 250 fps, exposed 4 ms per frame, and for 5 sec minimum to ensure that the calcium transients recorded were consistent. The gain and offset of the camera were kept as constant as possible across samples and experiments.

Videos were converted to TIFF format, and regions of interest (ROI) delineated in ImageJ to generate TXT files of averaged fluorescence intensity for each frame. Trace morphology was then analysed in Clampfit (pClamp 10.2). Background noise was averaged in cell-free regions and subtracted from averaged signals in individual cell. Analysis was done manually, but in a blinded fashion to remove bias. Traces were shown as  $F1/F0$  with  $F0$  as baseline fluorescence and  $F1$  as the fluorescence at any time-point. These were used to determine the amplitude of transients ( $\max F1/F0$ ), the time to peak (TP), the rate of decay ( $\kappa$ ) and the time to 90% decline from the peak (TD90%), as shown in Figure 2.2A. The rate of decay  $\kappa$  was calculated from the time constant  $\tau$  of a mono-exponential decay curve (Equation 4) that was fitted along the decay phase of calcium transients:

$$f(t) = \sum_{i=1}^n A_i e^{-t/\tau_i} + C \quad (4)$$

$$\kappa = \frac{1}{\tau} \quad (5)$$

### **2.7.3 Fractional release of calcium**

Not all the  $\text{Ca}^{2+}$  stored in the SR is released in the cytosol during each cycle. Determining the amount of calcium released as a function of total SR calcium can serve as an indirect indicator of calcium-induced calcium release efficiency in CM. To measure this, calcium transients were first recorded as in Section 2.7.2 for 5 sec to establish the baseline amplitude ( $F1/F0$ ). Caffeine was then injected at 40 mM near the ROI, after the field-stimulation was interrupted. Caffeine is a potent agonist of RyR2, therefore inducing a maximal calcium release from the SR (which is approximated as total SR content). Caffeine was injected with a glass micropipette (Harvard Apparatus, Cat. No. 30-0058) stretched with a P-97 pipette puller (Sutter, USA). The caffeine-back-filled pipette was connected to a manual pressure syringe (to inject approximately 30  $\mu\text{l}$ ). The pipette tip was placed at the bottom of the dish and at the edge of the field of view, which was centred on the cell of interest. Fractional release of calcium corresponds to the amplitude of stimulated calcium transients divided by the amplitude of caffeine-induced transients.

### **2.7.4 Differentiating the mechanisms of calcium extrusion**

The activity of SERCA and NCX can be measured using the calcium imaging with Fluo-4, as described in Section 2.7.2. The rate of decay  $\kappa$  of stimulated calcium transients corresponds to the combined activity of all calcium extrusion mechanisms. However,  $\kappa$  of caffeine-induced transients does not integrate the activity of SERCA since the SR cannot accumulate calcium in these conditions (described in Section 2.7.3). The perfusion of normal Tyrode's solution was replaced with  $\text{Na}^+$ - and  $\text{Ca}^{2+}$ -free Tyrode's solution (0/0), which eliminates the activity of NCX. This prevents field-stimulated calcium release, but still allows for caffeine to induce a calcium release from the SR, from which the rate of decay can be measured. A direct comparison of  $\kappa$  values in the three conditions allows for the calculation of mechanism-specific  $\kappa$ , as described in Figure 2.2B and with Equations 6-8.

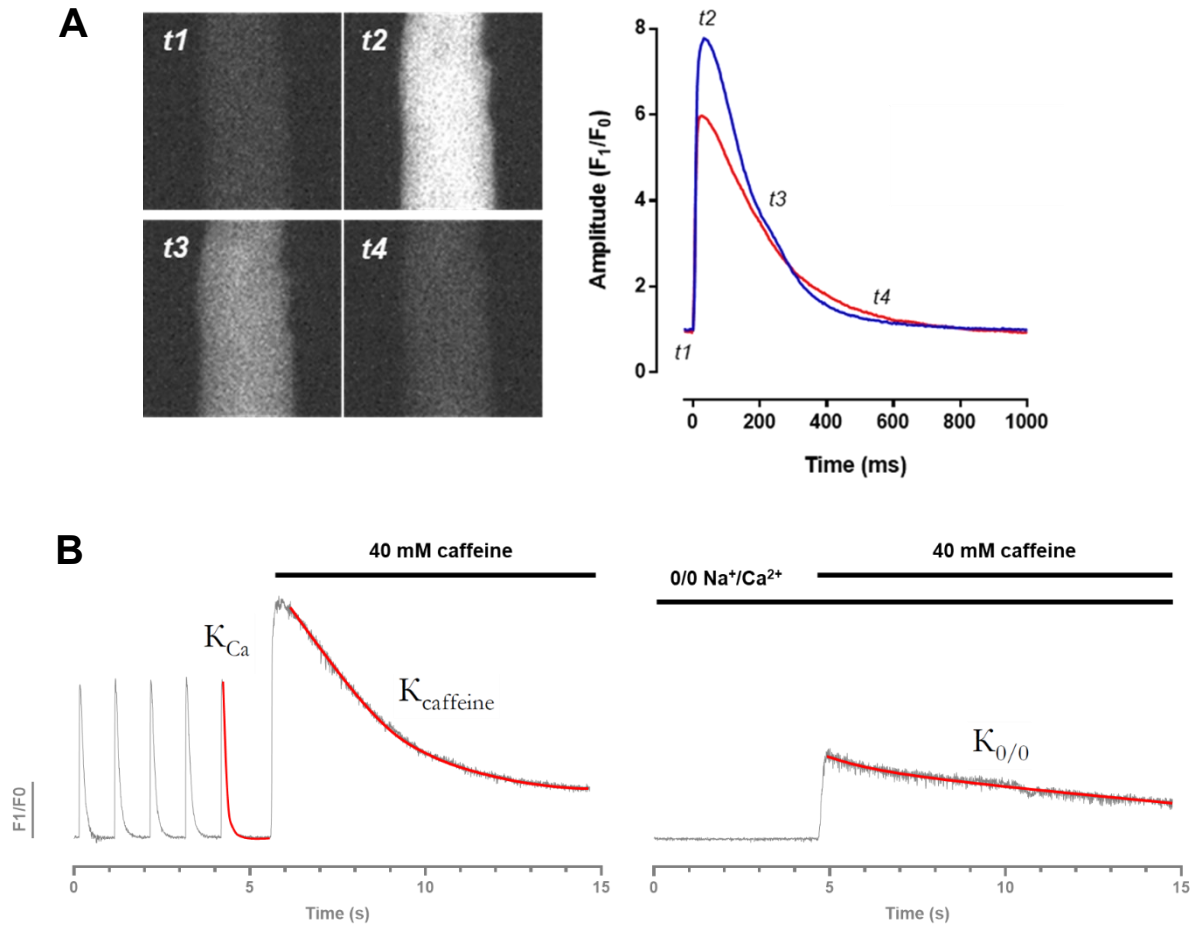


**Figure 2.2: Calcium transient recording and analysis of calcium extrusion mechanisms**

Calcium transient analysis in ARVM, by Optical Mapping recording of cytosolic Fluo-4 fluorescence intensity over time. **A.** (Left panel) images of a CM extracted from video recording, showing variations of Fluo-4 signals at different time-points ( $t_1$ - $t_4$ ). (Right panel) Traces of fluorescence over the baseline fluorescence ( $F_1/F_0$ ) for 1 sec, showing a calcium transient. **B.** Representative traces of Fluo-4 after application of the protocol described in Section 2.7.4. Exponential decay curves (shown in red) were fitted to the relevant decay phases of these transients to measure  $\kappa$  values in the three conditions.

$$K_{Ca} = K_{SR} + K_{NCX} + K_{Slow} \quad (6)$$

$$K_{Caffeine} = K_{NCX} + K_{Slow} \quad (7)$$

$$K_{0/0} = K_{Slow} \quad (8)$$

### **2.7.5 Contractility and relaxation of isolated ARVM**

The CytoCypher™ MultiCell system (Netherlands), which is a fully automated CM contractility recording system based on IonOptix technology, was used to measure fractional shortening (percentage change of cell length), TP, TD90% and the rate of decay of CM contractions. CM were transferred into a 35 mm glass bottom MatTek dish, with fresh normal Tyrode's solution, on stage of the temperature-controlled CytoCypher chamber (at 37°C). Cells were incubated for 15 min to stabilise temperature in the dish and reach a stable state of contractions, which tend to be prolonged in the first 15 min after cell transfer (see Figure 6.1). During equilibration and throughout the recording, cells were continuously field-stimulated with platinum electrodes connected to a MyoPacer stimulator (IonOptix, USA) and at 1 Hz (40 V bipolar pulses of 10 ms). While this frequency is lower than the *in vivo* beating frequency in rat, it was preferred for this experiment due to the lack of elastic recoil during diastole. At higher frequencies (e.g. >2), isolated CM tend to hypercontract, therefore reducing the relevance of fractional shortening measurements.

At the time of this experiment, not enough data had been collected between users to confirm that the automated seek-and-record capability of the system was sufficiently functional. When fully automated, non-contracting or arrhythmic CM were often included in datasets. CM were therefore selected manually, based on the following criteria: rod-shaped, contracting, and non-arrhythmic. The analysis was however performed automatically by the Transient Analysis Tool of the MultiCell system. Data points were collected at 250 fps.

### **2.7.6 Calcium transients with Fura-2**

The ratiometric fluorescent  $\text{Ca}^{2+}$  indicator Fura-2 AM allows for more accurate measurements of calcium transient amplitude than Fluo-4. Optics included in the CytoCypher MultiCell system are also designed for Fura-2 imaging, with a 340/380 nm excitation ratio for the dye. CM were incubated with 1  $\mu\text{M}$  Fura-2 AM (Invitrogen) for 15 min whilst still in co-culture with EC, before



being washed with a fresh Tyrode's solution and equilibrated on the stage of the MultiCell system for 15 min (allowing for dye de-esterification). Cells were paced, selected, and recorded at 500 fps as in Section 2.7.5. The analysis was performed automatically with the Transient Analysis Tool, providing the same parameters as with Fluo-4.

### 2.7.7 Calcium sensitivity of myofilaments

With simultaneous recordings of contractions and calcium transients, as with the CytoCypher system, it becomes possible to measure the relationship slope between  $[Ca^{2+}]_i$  concentrations and sarcomere shortening. To do this, traces of sarcomere shortening and of the 340/380 ratio for Fura-2 were processed with an interpolation macro (IonOptix), homogenising the sampling frequency of the two datasets (Figure 2.3A). Using this combined dataset, calcium-contraction hysteresis loops were constructed (Figure 2.3B). From these, the sensitivity of myofilaments to calcium was measured as the slope of the descending linear portion in hysteresis loops (red dotted line in Figure 2.3B). Data was discarded where the slope could not be fitted accurately ( $R^2 < 0.9$ )

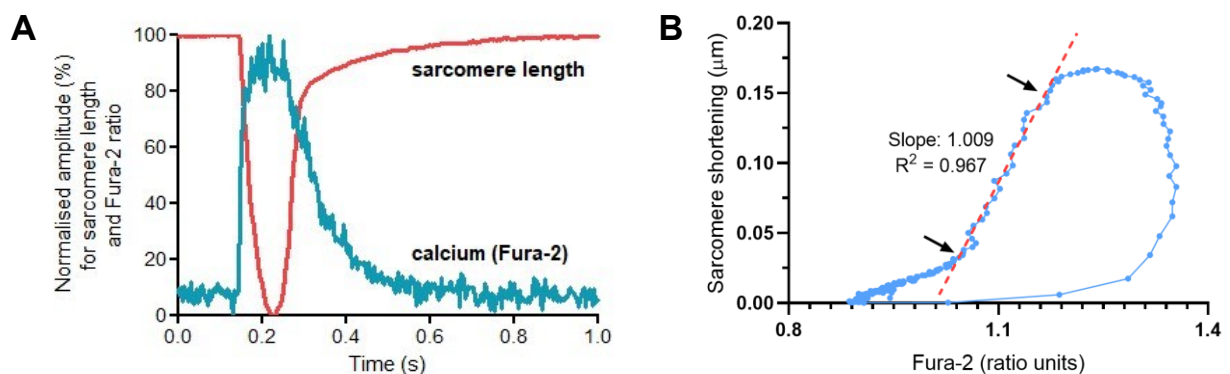


**Figure 2.3: Calcium-contraction interpolation and hysteresis loops**

Measurement of myofilament sensitivity to calcium, using MultiCell data of Fura-2 ratiometric signals and of sarcomere shortening. **A.** Superposition of calcium and sarcomere length traces over time. **B.** Representative hysteresis loop of the sarcomere shortening and Fura-2 intensity. The linear portion of this loop (i.e. delineated by the arrows) is shown with a red dotted line. The slope of this line, which corresponds to the calcium-sensitivity of myofilaments, is measured as 1.009 in this case.

### 2.7.8 Bioinformatic meta-analysis of gene expression

The mRNA expression was analysed for specific markers of CM (*TNNT2*, *MYL2*, and *ACTC1*), for *CXCL5*, *CXCL1*, *CCL2*, *CSF2* (GM-CSF), *CSF3* (G-CSF), *IL6*, *IL1RL1*, the receptors *CCR2* and *CCR4* (activated by *CCL2*), *CXCR2* (targeted by *CXCL1*, *CXCL5* and *IL-8*), *CSFR2A* (for GM-CSF), *IL6R*, *TNFRSF1A* (receptor for *TNF $\alpha$* ), *EDNRA* and *EDNRB* (ET-1 receptors). This was accomplished indirectly, by bioinformatic meta-analysis of two transcriptomic datasets.

Tabula Muris is a single-cell transcriptomic dataset obtained from 20 mouse organs (7 mice)<sup>208</sup>. Gene counts were assessed in flow cytometry-sorted cells, based on a SMART-Seq2 RNAseq library. Data were obtained from the open platform Figshare (which is found at <https://tabula-muris.ds.czbiohub.org/>). Besides the raw RNA count for each gene of interest, cells were also counted as positive for a certain gene when the cell RNA count was superior or equal to 10.

To use a different model and a distinct method of analysis, a microarray for mRNA expression in neonatal and adult Sprague-Dawley rat ventricular CM was examined<sup>209</sup>. This was performed from 6 rat samples using an Affymetrix GeneChip™ Rat Genome Array 230 2.0 (A-AFFY-43) covering 31,000 gene transcripts (Expression Atlas – E-MTAB-2832). Data were normalised by a Robust Multi-array Average using the Oligo 1.36.1 package (R). Extraction of data was done with the help of Robert Maughan, PhD.

## 2.8 Living Myocardial Slices

The following protocol is an abridged version of the protocol detailed in Watson *et. al.* (2017)<sup>210</sup>. Living myocardial slices (LMS) are preparations of cardiac tissue which can be cultured for a period of days or even weeks without the requirement for coronary blood perfusion, as slices are sufficiently thin (300 µm) to allow for nutrients to diffuse to all parts of the cultured tissue. However, to maintain cell viability, and to slow tissue remodelling or the loss of contractility over time, LMS need to be maintained under constant mechanical load<sup>211</sup>. When this is done, LMS become an ideal model to study cardiac function where the heterocellularity, architecture, extracellular matrix, and physiology of the myocardium are preserved. For this thesis, LMS were produced from adult male Sprague-Dawley rats.

### 2.8.1 Rat myocardial slice preparation and culture

Heart and lungs were excised as in Section 2.3.2 and transferred into 37°C heparinised slicing solution (2 U/ml; Fannin, UK), before gently compressing the heart to remove as much blood as possible. The heart was transferred into ice-cold heparinised slicing solution, and dissected down to a flat block of the left ventricle. The tissue block was mounted with Histoacryl<sup>®</sup> surgical glue (B. Braun Medical, UK) as flat as possible with the epicardial surface sat down on a block of 4% agarose, itself glued onto the specimen holder of a vibrating microtome 7000smz-2 (vibratome; Campden Instruments, UK). The tissue block was then sliced from the endocardial side to the epicardial side with a ceramic blade vibrating at 80 Hz, at an amplitude of 2 mm, and advancing through tissue at 0.03 mm/s. The section thickness was set to 300 µm. Tissue was sliced in ice-cold slicing solution (no heparin), constantly bubbled with 100% filtered O<sub>2</sub>. A maximum of 5 viable slices were obtained from each ventricle. Slices were trimmed to 7 x 9 mm, in slicing solution, immediately after being detached from the tissue block (Figure 2.4A). Custom-made rectangular rings, 3D printed with T-Glase filament (taulman3D, USA) using an Original+ 3D printer (Ultimaker, Netherlands), were glued at the extremities of slices (to 1 mm

of tissue) and orthogonally to the myocardial fibre direction (Figure 2.4A). These were used to apply an isometric and uniaxial mechanical load to myocardial slices, by mounting the slices on custom-designed stretchers made of stainless steel (Figure 2.4D). An isometric stretch of 17% was applied, corresponding to a physiological sarcomere length of 2.1  $\mu\text{m}$  (Figure 2.4C). Stretched LMS were placed in custom-designed slice culture chambers and fully submerged in slice culture medium. Chambers were then sealed and kept at 37°C for an incubation period of 24 hours. Medium was oxygenated (95% O<sub>2</sub>, 5% CO<sub>2</sub>) and recirculated using a peristaltic pump at 15 ml/min throughout culture. LMS were stimulated at 1 Hz for 10 ms at 12 V, in the first 2 hours, then 15 V, via carbon electrodes submerged in the medium. The % stretch was measured with calipers.

## 2.8.2 Rat myocardial slice contractility

After 24 hours in culture, LMS were removed from culture chambers and connected to a F30 isometric force transducer (Harvard Apparatus, USA). A micromanipulator was used to stretch slices, being attached to a fixed post in the bath and the force transducer using the rectangular plastic rings. LMS were continually superfused with oxygenated Tyrode's solution at 37°C and electrically field-stimulated at 1 Hz using platinum electrodes in the bath solution, with bipolar pulses of 40 V for 4 ms. LMS were left to stabilise for 5 min before gradually increasing stretch, from 0% to 30%, by increments of approximately 1%. Data were recorded using the AxoScope software (Molecular Devices, USA) and analysed with Clampfit (pClamp, Molecular Devices). The contraction amplitude was converted to force (mN) with a scale factor of 0.881, measured during calibration of the force transducer, and normalised to the cross-sectional area of slices (Equation 9). Contractility was thus expressed in mN/mm<sup>2</sup>.

$$Force = \frac{Amplitude}{0.881} / (width \times thickness) \quad (9)$$

The same equation was used to convert the averaged value measured at the end-diastole, for each stretch, into passive tension. Contractions kinetics were calculated as in Section 2.7.2.

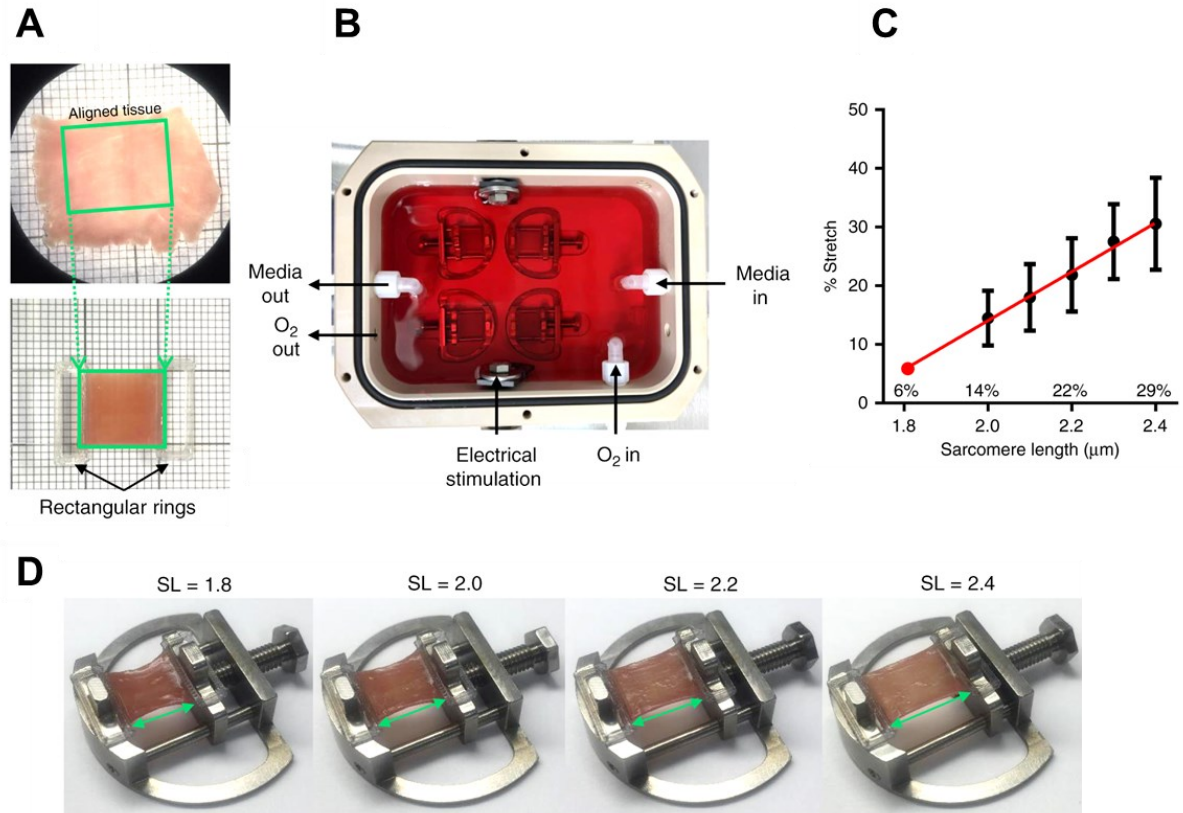


**Figure 2.4: Preparation, culture and mechanical stimulation of rat living myocardial slices**

Reproduced from Watson *et. al.* (2019). Application of electromechanical stimulation to rat myocardial slices (LMS). **A.** (*Top*) Rat LMS visualised using a macroscope. The slice is placed on a mm grid and the green rectangle highlights the portion of the tissue where myocardial fibres are aligned. (*Bottom*) Custom-made 3D-printed rings are attached to opposite ends of the aligned portion of the myocardial slice using surgical glue. **B.** Custom-made slice culture chamber, containing 4 samples on stretchers. LMS are superfused with culture media, oxygenated directly in the culture chamber. Field stimulation was provided via carbon electrodes. **C.** Percentage of stretch required to set the average diastolic rat myocardial slice sarcomere length (SL). A linear regression was used to estimate the stretch required to obtain SL of 1.8 μm (as this could not be measured accurately using the laser diffraction method). **D.** Myocardial slice attached to the posts of a custom-made stretcher, using the rings, and stretched at SL of 1.8-2.4 μm. Mean +/- standard error of the mean is shown on graphs. (*The original figure is under CC BY License – Permission is not required by Springer Nature*)

## 2.9 Antibodies

**Table 2.1: List of antibodies mentioned in the thesis**

Target	Used as	Description	Dilution
$\alpha$ -actinin	IF primary	Mouse monoclonal (clone EA-53) – Sigma A7811	1:500
$\alpha$ -SMA	Flow cytometry	Mouse monoclonal IgG2a – APC (clone 1A4) – R&D IC1420A	1:100
A20	WB primary	Rabbit monoclonal (clone D13H3) – CST #5630S	1:1,000
Akt1	WB primary	Mouse monoclonal (clone 2H10) – #2967	1:2,000
CD144	Flow cytometry	Mouse PE anti-human (clone BV9) – BioLegend #348505	1:100
CD31	Flow cytometry	Mouse FITC anti-human (clone WM59) – BioLegend #303104	1:200
eNOS	WB primary	Rabbit polyclonal – BD Transduction 610298	1:1,000
GAPDH	WB primary	Rabbit monoclonal (clone 14C10) - CST #2118S	1:3,000
HO-1	WB primary	Rabbit monoclonal (clone EP1391Y) – Abcam ab52947	1:1,000
ICAM-1	WB primary	Mouse monoclonal (clone 15.2) – from culture supernatant	1:4
iNOS	WB primary	Rabbit monoclonal (clone D6B6S) – CST #13120S	1:1,000
Lyve-1	Flow cytometry	Mouse monoclonal IgG1 APC (clone 537028) – R&D FAB20892A	1:100
MnSOD	WB primary	Rabbit polyclonal – Enzo Life Sciences #ADI-SOD-110	1:1,1000
P-PLB	WB primary	Rabbit polyclonal – Santa Cruz sr-17024-R	1:1,000
P-STAT3 (S727)	WB primary	Rabbit polyclonal – CST #9134S	1:1,000
PLB	WB primary	Mouse monoclonal (clone F-7) – sc-393990	1:1,000
RyR2	WB primary	Mouse monoclonal (clone F-1) – Santa Cruz sc-376507	1:1,000
SERCA2	WB primary	Mouse monoclonal (clone F-1) – Santa Cruz sc-376235	1:1,000
VCAM-1	WB primary	Rabbit monoclonal (clone E1E8X) – CST #13662	1:3,000
Mouse IgG	IF secondary	Goat anti-mouse – Alexa Fluor® 488 – Life Technologies #A21121	1:1,000
Mouse IgG	WB secondary	Goat anti-mouse – HRP-conjugated	1:3,000
Rabbit IgG	WB secondary	Swine anti-rabbit – HRP-conjugated	1:3,000

*IF: immunofluorescence; WB: western blotting*

## 2.10 Statistics

Data are represented in graphs as mean +/- standard error of the mean (SEM) unless specified otherwise. Graph construction and statistical analysis were performed using GraphPad Prism 8 software (GraphPad Software Inc., USA). A D'Agostino-Pearson test was used to determine the normality of sample distribution, with an  $\alpha$  critical value of 0.05 set for the level of statistical significance ( $p < 0.05$ ).

A parametric two-tailed t-test was used to compare the means of two unpaired groups, complemented by a Welch's correction when standard deviations were significantly different. When comparing >2 normally distributed groups, an ordinary one-way analysis of variance (ANOVA) with Bonferroni's or Tuckey's correction was used. For groups that were not normally distributed, however, a non-parametric Kruskal-Wallis test with Dunn's correction for multiple comparisons was preferred.

When comparing >2 groups to the same control condition, a one-way ANOVA with Dunnett's multiple comparison test (parametric), or a Welch's ANOVA with Dunnett's T3 correction (non-parametric) were used.

Sample sizes are described as n/N, with n = cells or images taken per biological replicate, and N = biological replicates, unless otherwise specified. All statistical analysis was carried out using biological replicates (i.e. N). In graphs, data points show N unless otherwise specified, and significant differences between groups were indicated by \*, \*\*, \*\*\* or \*\*\*\* for  $p < 0.05$ , 0.01, 0.001, and 0.0001, respectively.





# 3.

**Co-culture model to test the paracrine effects of cardiac  
microvascular endothelial cells on adult ventricular  
cardiomyocytes**

### 3.1 Introduction

The working hypothesis for this project can only be investigated with: (1) an appropriate model of EC-CM crosstalk and (2) a well-defined basal effect of EC on CM. In this project, in order to simplify the problem to be addressed, the focus is narrowed down to the paracrine effects of EC on CM. With no prior experience with co-cultures involving CM and EC in the Mason and Terracciano labs, the first step for this project was to review the relevant literature and test some co-culture systems. As discussed in Chapter 1 and later in this thesis, the effects of EC on CM have been rarely reported with direct evidence and remain poorly understood either *in vivo* or when using co-cultures. Protocol guidelines for the co-culture of cardiac cells are lacking, allowing for many publications to use unique and incomparable methods, resulting in inconsistent effects of EC on CM being reported. This is reviewed later in this chapter. In this project the initial challenge was therefore to optimise a model of co-culture, while not knowing the type and magnitude of effect which might serve as an indicator of success for given *in vitro* conditions.

As mentioned above there is a lack of agreement on the required characteristics of EC-CM co-cultures, as much as there is (for example) a consensus on culture media for CM or about protocols for angiogenic assays. As such, it is still not understood how these co-cultures differ in physiological relevance by using different cell types, time-points, EC:CM ratios, co-culture systems, or culture media.

It was shown that EC can transdifferentiate *in vitro*<sup>212,213</sup> and that CM remodelling occurs rapidly after isolation<sup>121,214</sup>, questioning the physiological relevance of some co-culture media and longer time-points. The marked heterogeneity of EC across all vascular beds<sup>215</sup>, including within the heart<sup>66</sup>, and the major phenotypic differences between *in vitro* models of CM<sup>97,216</sup> also question the relevance of certain cell types in co-cultures. Finally, too little is understood about the plasticity of CM in terms of their response to EC. While the current project aims to test how a change in EC can affect different functions of CM, it is still possible that a change

in CM would affect their response to co-culture with EC, for example during HF where the expression profile of CM can be extensively altered<sup>217</sup>. It will be thus of interest in this chapter to test: (1) different types of EC; (2) different time-points for co-cultures; (3) to exclude transdifferentiation of EC induced by the co-culture medium; (4) to determine whether pathological remodelling of CM impairs their response to healthy EC. Only once this is done is it possible to discuss the basal effects of EC on co-cultured CM, and how this might be altered by pro-inflammatory stimulation of EC.

## 3.2 Methods

The methods described in this chapter are described in full in Chapter 2.

### 3.2.1 Experimental design for co-cultures

For all experiments, human umbilical vein EC (HUVEC), human aortic EC (HAEC) and human cardiac microvascular EC (HCMEC) were used at passage 4-6 and cultured in their respective culture media as recommended by their supplier. Adult rat ventricular myocytes (ARVM) were isolated from male Sprague-Dawley rats (refer to Chapter 2 for the protocol). This was kindly performed by Peter O'Gara. Prior co-cultures, 60,000 EC were plated in the 12-well Transwell inserts (Greiner Bio-One) and grown to confluence for 24 hours in their maintenance medium. Media were then changed for the co-culture medium (Section 2.2) and EC were cultured for 24 hours to acclimatise to the new medium. ARVM were collected immediately after isolation. After a wash with co-culture medium, 20,000 rod-shaped cells were plated on laminin-coated 13 mm diameter glass coverslips and cultured for 2 hours to allow cell attachment. ARVM were then gently washed with medium to remove the calcium-intolerant CM, and the Transwell inserts containing EC were transferred on top of ARVM cultures. Empty inserts were used for control groups (i.e. ARVM alone). Co-cultures were used for 4 or 24 hours.

To obtain co-cultures with Transwell inserts where EC and CM are only separated by the insert membrane (Figure 3.2B), the 12-well inserts were first positioned upside-down. HCMEC were then plated in a droplet of medium on the insert membrane. After 1 hour of sedimentation the droplet was removed, leaving a layer of EC attached at the bottom of the inserts. These were turned, placed in multiwell plates, and the other side of the membrane was coated with laminin before rod-shaped ARVM were plated at a density of  $4.4 \times 10^4$  cells/cm<sup>2</sup>. In all configurations of the Transwell models, the lower compartment received 1 ml of medium and the top chamber 0.5 ml. For each biological replicate, at least 2 co-cultures were produced.

### 3.2.2 Coronary ligation in rat

Adult male Sprague-Dawley rats (250-300 g) underwent a permanent ligation of the proximal coronary system to induce chronic myocardial infarction (MI)<sup>122</sup>. ARVM were isolated 16 weeks after ligation. This was performed by Peter O'Gara.

### 3.2.3 Calcium transient analysis by Optical Mapping

Calcium transients were recorded in ARVM using the cytosolic free-calcium indicator Fluo-4 AM. ARVM were loaded for 15 min with Fluo-4 AM while still in co-culture with EC. Transwell inserts were then removed and the coverslips with ARVM were transferred on the microscope stage to equilibrate in the superfused 37°C Tyrode's solution for 5 min before the recording. Samples were paced continuously at 1 Hz. Cells were delineated in ImageJ to extract traces of Fluo-4 AM signals from individual cells. Background noise was corrected for each recording using cell-free regions. Fluo-4 AM traces were exported to Clampfit (pClamp suite) where the calcium transient parameters were measured manually. The amplitude, time to peak, time to 50% and 90% decay, as well as the time constant  $\tau$  (from which the rate of decay  $\kappa$  was calculated) were averaged for all cells within each biological replicate (20 cells minimum).

### 3.2.4 Flow cytometry with intracellular staining

Primary human adult ventricular fibroblasts (hACF) were isolated from the LV of hearts which were ruled out for transplantation. Cells were isolated, maintained and kindly provided by Brian Wang, PhD., with the help of Mr Oisín King. Fibroblasts were used under passage 20. HUVEC, HCMEC and hACF were cultured in 6-well plates (300,000 cells per well) in their optimal maintenance media or, in the case of HCMEC, the recommended bullet kit medium (EGM-MV2) or the co-culture medium (custom), for 24 hours. Briefly, cells were trypsinised, fixed, permeabilised and incubated with a panel of antibodies, at 1:100 in cell staining buffer, to stain for CD31, CD144,  $\alpha$ -SMA or Lyve-1. Isotype control antibodies were used as negative controls

for this staining. Cell suspensions were then processed through a CyAn™ APD cytometer (Beckman Coulter). At least 10,000 events were recorded for each sample. A selective gating strategy was used to ensure that debris and cell multiplets were excluded from the datasets. Analysis was carried out with Summit 4.3.

### **3.2.5 Immunostaining and confocal microscopy**

ARVM were fixed with ice-cold methanol for 15 min, while in co-culture with EC, after 24 hours of culture. Immunostaining of alpha-actinin was performed to identify sarcomeric architecture in CM and imaged using a Zeiss LSM-780 inverted confocal microscope. Planimetric data were obtained from bright-field images of CM. All images were taken with a 40x objective. Analysis was carried out with ImageJ. Sarcomere length was averaged from >20 sarcomeres per cell. The short axis of ARVM was measured at the widest point of ARVM.

### **3.2.6 Statistics**

Data are displayed as mean +/- SEM. Statistical significance was calculated with unpaired two-tailed t-test for the comparison of two groups, complemented with Welch's correction when standard deviations were not equal between groups. For the comparison of multiple groups to a single control group, one-way ANOVA with Dunnett's multiple comparison test was used. To compare >2 groups between each other, one-way ANOVA with Tukey's or Bonferroni's post-hoc corrections were preferred. Significance is shown as: \*  $p < 0.05$ . \*\*  $p < 0.01$ . Replicates are described as n/N, with n = cells or images taken per replicate, and N = biological replicates.

### 3.3 Results

#### 3.3.1 There is lack of consensus on the basic methodology for EC-CM co-cultures

The literature contains many examples of *in vitro* co-cultures with EC and CM, published in articles testing the EC-CM crosstalk and addressing hypotheses resembling that of the present study. To determine if there was a predominant model or recurring culture parameters in such papers that could be applied to this study, thus easing the process of validation for the model, the relevant literature was first scrutinised. A total of 2,219 publications were found as a result of a broad scope PubMed search using the following terms:

“endothelial AND cardiomyocyte AND [x]” - (last updated on the 05.07.2020)

“[x]” was replaced by one of the following terms, thus panning basic elements of the co-culture lexicon as well as the protein name of paracrine factors that have been associated with the EC-CM crosstalk (independently of isoforms): “paracrine”, “co-culture”, “secretome”, “nitric oxide”, “interleukin”, “TNF”, “Ang-II”, “ET-1”, “IGF”, “neuregulin”, “glutathione”, “PGF”, “BMP”, “adrenomedullin”, “apelin”, “thioredoxin”, “thrombospondin”, “CTGF”, “PTHrP”, “midkine”, “follistatin”, “periostin”, “osteopontin”, “CTRP9”, “LIF”, “SPARC”, “tenascin”, “WISP”, or “CCN”.

In order to reduce the number of articles to those that are relevant to the problem of EC-CM co-culture methodology, all abstracts were read and eliminated from the list if: (1) experiments using EC or CM could not be found\*, (2) the role of EC was only attributed to mechanical properties of the endothelium or the vasculature (e.g. focusing on barrier function or control of coronary flow capacity), (3) not peer-reviewed, (4) written in another language than English, or (5) not containing an *in vitro* co-culture model. All the articles which satisfied these criteria were then categorised for each element of co-culture methodology. As seen in Figure 3.1A and 3.1B, co-cultures with EC and CM in this selection of articles included predominantly EC of non-cardiac origin (57%) and of human origin (52%). EC isolated from microvascular beds

---

\* The search terms did not discriminate papers where EC or CM were used in experiments to papers where EC or CM were only mentioned

accounted for 38% of all EC, followed by EC of venous origin (23%; note that HUVEC were included in the venous section) as well as of other origin (e.g. derived from pluripotent stem-cells; 21%). The CM in contrast were largely isolated from rat tissue (64%), while mouse (19%) and human (17%) were much less represented. Perhaps accounting for the challenges in maintaining adult CM phenotype after isolation, CM were mostly used at the foetal to neonatal stage (48%). Adult CM only accounted for 22% of cells used for EC-CM co-cultures. Although a growing trend in cardiovascular research, the use of iPSC-CM or ESC-CM was still poorly represented (16%), barely surpassing the controversial use of immortalised lines of CM (14%).

While DMEM was the most recurrent base component among all media variants (36%) there was a worrying 25% of articles where the media components could not be identified (Figure 3.1D). Of note, only 5% contained a custom culture medium, often the maintenance media of both EC and CM in various respective proportions. No less than 30% of all EC-CM co-cultures removed serum from the media completely (Figure 3.1E), while the rest used FBS at various concentrations, though mostly at 10% (in 20% of cases). Here again, this analysis is hindered by 25% of articles in which it was not specified if serum was included in the media.

Co-cultures of EC and CM were found to be used for any duration between 15 min and 30 days (Figure 3.1G). Studies of paracrine crosstalk were notably collecting data at  $12\text{h} \pm 12$ , with longer time-points being almost exclusively reserved to studies developing engineered heart tissues or vascularised 3D constructs. Another aspect of co-culture design, the ratio of cell numbers (Figure 3.1F), was surprisingly poorly communicated with nearly 40% of relevant articles not providing this crucial information. Of the rest, the most common case (17% of co-cultures) was seen with EC and CM used in equal proportions (1:1).

Finally, no guidance can be found in the literature as to which co-culture system should be used to model the EC-CM crosstalk. The transfer of conditioned medium (which admittedly barely qualifies as a co-culture,) accounted for 19% of all *in vitro* studies on the subject (Figure 3.1C). More complex models, e.g. using 3D suspensions and/or organotypic features such as vasculature, were included in 21% of all articles. The use of indirect co-cultures (i.e. paracrine



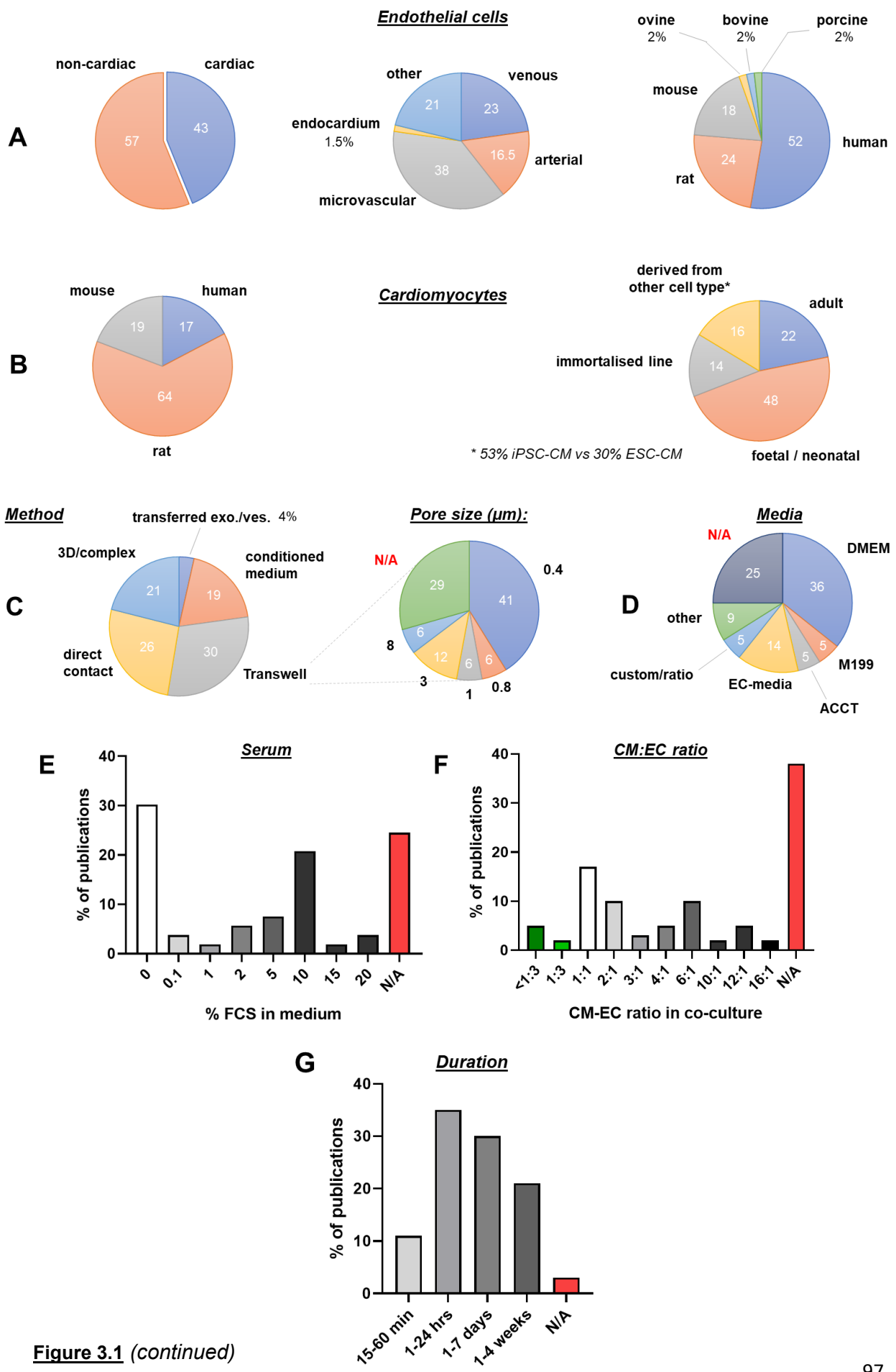


Figure 3.1 (continued)

### **Figure 3.1: Distribution of published EC-CM co-culture models per parameter**

Numbers of articles describing the use of each co-culture parameters, expressed as a percentage of all articles which include EC-CM co-cultures, and categorised as follows: **A.** Origin of EC, by organ, type of vascular bed and species. **B.** Origin of CM, by species and nature of differentiation. **C.** Method of co-culture, and pore size of Transwell inserts (in  $\mu\text{m}$ ). **D.** Base for culture medium. **E.** Percentage of FCS in the complete culture medium. **F.** CM:EC ratio. **G.** Duration of co-culture before the endpoint experiments. N/A: information not available.

bidirectional activities only) or direct co-cultures (i.e. with contact and therefore biomechanical interactions allowed) accounted respectively for 30% and 26% of all articles screened for this review. Indirect co-culture is synonymous with the use of porous well inserts (commonly called Transwells). For these, 0.4  $\mu\text{m}$  was the preferred diameter for the pores in the membrane of inserts (41% of articles with Transwells).

According to this literature overview, a stereotypical EC-CM model would be to co-culture non-cardiac human microvascular EC with foetal/neonatal rat CM for up to 24h at a 1:1 ratio, with EC in Transwell inserts of 0.4  $\mu\text{m}$  pores, and in serum-free DMEM. As expected, not a single article was found to fully match this stereotype. However, all parameters considered, 63% of the relevant articles did not provide sufficient information to help define their model. Although this brief review will help contextualise the methodology to be used later in this study, it was not used as a primary mean to select co-culture properties.

#### **3.3.2 Transwell co-culture system is the optimal model to study the paracrine effects of EC on CM**

It was not immediately obvious which co-culture system could be used for this study. To clarify which *in vitro* or *ex-vivo* multicellular model would allow the current hypothesis to be tested, the most widely published co-culture systems to date were first reviewed (Table 3.1).

**Table 3.1: Classification of published and theoretical in vitro and ex vivo systems to study the EC-CM crosstalk**

Name	Classification	Brief methodology	Strengths	Weaknesses	Throughput (n) & Cost (c)*	Physiological relevance*	Notes	References
<b>Transfer of a specific portion of the secretome</b>	Unidirectionally paracrine with selected mediators only	Culture cell A with media supplemented with exosomes or vesicles isolated from cell B supernatant	High control over the nature of the interaction and easy to manipulate	Not representative of full secretome; concentrations are often arbitrary or supraphysiological	n + + + c -	- - -	N/A	218,219
<b>Conditioned medium</b>	Unidirectionally paracrine	Culture cell A with cell B supernatant	High control over the nature of the interaction and easy to manipulate	Some soluble mediators will lose activity due to poor half-life in medium (e.g. NO)	n + + + c - -	- - -	N/A	68,220–224
<b>Transwell inserts (or “Boyden chamber”)</b>	Paracrine	Cells are separated by a porous membrane	Cell types can be separated easily after bidirectional co-culture	Endpoints often require separating the two cells types	n + + c - / +	- -	- Microscopic imaging of cells in the insert can be difficult† - Approach of a patch-clamp pipette or upright imaging of cells in the lower compartment requires removal of the insert	68,75,225–227
<b>Membrane separation</b>	Paracrine	Cells are plated on opposite sides of a porous membrane	Models the effect of the basement membrane on cell-to-cell interaction	- Low practicality† - Adult CM detach too easily from the membrane†	n + + c - / +	- -	- Cells must be scraped separately for molecular studies - Imaging is hindered by membrane material† - Endpoints are also limited by the shape of the insert	75,228
<b>2D co-plating</b>	Direct contact	Cells are mixed prior plating	Simplicity of model	- When required, cells can only be separated by FACS - Cell phenotyping and discrimination is challenging	n + + + c - -	-	Competition and outgrowth of cell populations may occur. Cells will also reorganise uncontrollably†	108,229–236
<b>Sequential plating (2D)</b>	Direct contact	Cell B is plated on top of cell A monolayer	- Interface between cell types is highly controlled - Cell A monolayer is well formed before co-culture	Adult CM can only be plated onto EC monolayers (i.e. facing the apical membrane), and they will detach easily†	n + + + c - -	-	N/A	226

Name	Classification	Brief methodology	Strengths	Weaknesses	Throughput (n) & Cost (c)*	Physiological relevance*	Notes	References
<b>Cell sheets</b>	Direct contact	Multiple cell monolayers are detached and stacked	Highly controlled cell-to-cell interface	Sheets are difficult to manipulate and may curl†	n - c +	- / +	N/A	237
<b>3D suspension</b>	3D	Cells are mixed in polymerizable 3D gel	Improved functions & cell-cell contact and communication	- Requires greater cell numbers than 2D co-cultures - No cell specificity for treatments - No control over the cytoarchitecture	n + + c -	- / +	Negative controls for co-culture (without cell type A) should either keep the initial density of cell B, or the total cell density, depending on the cell types and the experimental endpoint	238
<b>3D with interface</b>	2D + 3D	Cell A is plated as a monolayer onto a gel suspension of cell B	Recapitulates some properties of cellular barriers (e.g. endothelium)	Interface will lose integrity in long term cultures as cell A migrates†	n + c -	- / +	Flow of medium may be applied to the system to introduce shear stress in this model	N/A
<b>RAFT™ system for 3D culture (Lonza)</b>	2D + 3D	Cell A is plated as monolayer onto a condensed gel suspension of cell B	- Realistic ECM density and depth of interstitial space - Relevant model of endothelial barrier - Gel concentrates may be stacked	- No control over cell organisation† - Poor removal of cell debris in the gel during culture† - Condensed ECM may hinder cell-cell contact & crosstalk	n - / + c +	- / +	N/A	N/A
<b>Organoid</b>	3D	Multiple types of stem cells are cultured to self-organise in ECM in micro-anatomically realistic manner	Recapitulation of the developmental process, and the complex network of cell-cell interaction	Stem cells may not develop functions seen <i>in vivo</i> †, and many properties cannot be modelled	n + c - / +	+	N/A	239,240
<b>Vascularised and perfusable construct</b>	3D + vasculature	EC are cultured in 3D matrices until they form a perfusable vascular network	- Flow of medium and intraluminal pressure are both applicable - Realistic delivery of medium and treatments (i.e. through vessels) - Less risk of cell hypoxia at the centre of construct	- Low control over vessel lumen size and branching density, which can be heterogenous within a sample - No negative controls (no EC) - Full development of vessels may require fibroblasts	n + c - / +	+ +	Accurate assessment of local shear stress and global vessel dimensions is challenging†	241,242

Name	Classification	Brief methodology	Strengths	Weaknesses	Throughput (n) & Cost (c)*	Physiological relevance*	Notes	References
<b>3D bioprints</b>	3D	Cells and ECM are plated/printed following strict 3D architecture	Complex shapes can be produced in 3D, separating cell types, or creating luminal structures	Precision of printing and cell viability are insufficient for other applications	n - - c + + +	+	Scaled reproduction of the heart anatomy is possible, allowing the modelling of cardiac chamber pressure variations	242
<b>Cells on slices</b>	Direct contact + native tissue	Cell A is plated as monolayer onto ultrathin slice of native tissue	Benefits from the presence of normal cardiac tissue, with all its cell types, complex ECM, and contractility of <i>in vivo</i> quality	- Cells plated onto the slice may only affect its superficial layer of tissue - Paracrine effects of plated EC may be diluted by endogenous EC	n - - - c +	- / +	N/A	N/A
<b>Decellularized scaffolds</b>	3D + native tissue	Native tissue is decellularized and re-populated with required cell types	- Cardiac ECM and ultrastructure are preserved - Unwanted cell types may be excluded from final co-culture product - Tissue stiffness may be preserved	The process of decellularisation can be incomplete or even cytotoxic, and may alter the ECM composition and its ultrastructure <sup>243</sup>	n - - - c +	+	N/A	244
<b>Culture of slices</b>	Native tissue	Native cardiac tissue is trimmed for <i>ex vivo</i> culture in chamber or bioreactor	Most relevant model to study the effects of a cell-cell crosstalk on cardiac function	- Within days contractility will greatly reduce <sup>†</sup> - Common issues of contaminations, undesired fibrosis, and poor viability over time <sup>†</sup>	n - - - c +	+ + +	N/A	N/A
<sup>†</sup> Observation obtained from tests performed in the lab (preliminary data or data not shown) <sup>*</sup> Score tiering has been performed subjectively N/A Non-available (for references: no relevant paper investigating the EC-CM crosstalk with this technique was found)								

Relevant systems were categorised and scored based on practicality, physiological relevance, overall cost, throughput, and limitations. Traditionally, a balance must be found subjectively between physiological relevance and practical limitations associated with each model. For this study, several criteria build up to restrict further the list of candidates. First, it must be possible to pre-condition EC prior to co-culture with CM, so that co-cultures may begin with EC of different phenotypes. The model should also allow the separation of the two cell types after co-culture, to characterise the function of CM or collect cell type-specific molecular samples. The current study is focused on the paracrine effects of EC on CM, so co-culture models which allow physical interaction between the two cell types must also be excluded. Finally, models which can only recapitulate parts of the paracrine interaction cannot be used, thus excluding the transfer of EC-derived exosomes, vesicles, or conditioned media (in which some soluble factors are unstable, such as nitric oxide). As seen in Table 3.1, the use of filters separating EC and CM (i.e. Transwells) most closely satisfies the experimental needs of this study.

To test the most physiologically relevant application of this method, ARVM were plated in the insert at a density of  $4.4 \times 10^4$  cells per  $\text{cm}^2$ , and HUVEC were plated on the opposite side of the filter (apical membrane facing down) (Greiner Bio-One, 12 well-plate inserts, 0.4  $\mu\text{m}$  pore size) (Figure 3.2B). In this model, EC and CM are only separated by the thickness of the filter, and pores connect directly the two cell types. However, after 24h of incubation, three washes with PBS in both compartments and a media change, there was a noticeable loss of ARVM in all replicates (data not shown).

Preliminary tests also helped determine that the shape of the well insert was not adapted to perform electrophysiological studies on CM. In-built customised inserts were ruled out and it was rapidly decided to adopt the original Transwell conformation (Figure 3.2A), with CM plated on glass coverslips in the lower compartment and EC plated into the insert and facing up. This technique is compatible with all the endpoint experiments required for this study and was thus used for further validation.

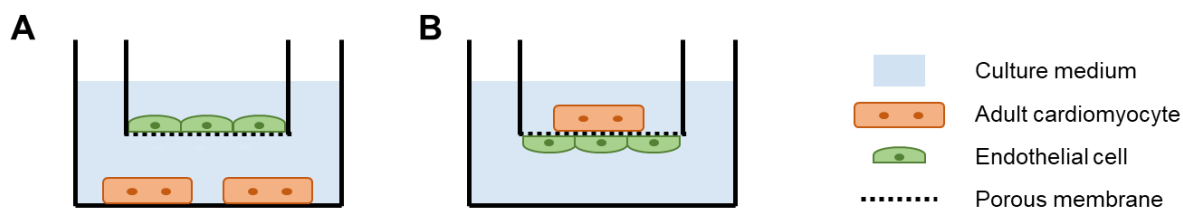


**Figure 3.2: Schematic view of the two main Transwell insert applications for use as EC-CM co-culture model**

**A.** Traditional application for transwell inserts. **B.** Plating cell types on either side of the membrane

### 3.3.3 Cardiac and non-cardiac EC might regulate calcium handling of CM differently

Many studies relying on EC-CM co-cultures have been published with HUVEC or other non-cardiac EC lines<sup>75,221,227,234,240,242,245,246</sup>. To determine if the response of CM to co-culture is affected by the origin of EC, ARVM were cultured under Transwell inserts plated with HUVEC, HAEC or HCMEC. Calcium transients were recorded in ARVM using the technique of optical mapping after 24h of co-culture. First, in Figure 3.3, it can be seen that none of these EC lines induced in CM a significant change of calcium transient amplitude (Figure 3.3A) or time to peak (Figure 3.3B) compared to CM alone (CTL). However, HAEC and HCMEC, but not HUVEC, induced a slower calcium reuptake compared to control (i.e. longer time to 90% decay, Figure 3.3C, and a rate of decay reduced by approximately 19%, 42% and 33% by HUVEC, HAEC and HCMEC respectively, Figure 3.3D). Increasing the N number might provide further insight on these effects and potential differences between EC conditions, as some of these comparisons produced p values near the threshold of significance.

### 3.3.4 HCMEC did not induce remodelling of cell dimensions and sarcomeres in ARVM after 24 hours in Transwell co-culture

Following confirmation that HCMEC could be used in co-cultures with ARVM to study the EC-CM interaction, the effects of EC on CM sarcomeric structures were investigated to test if the

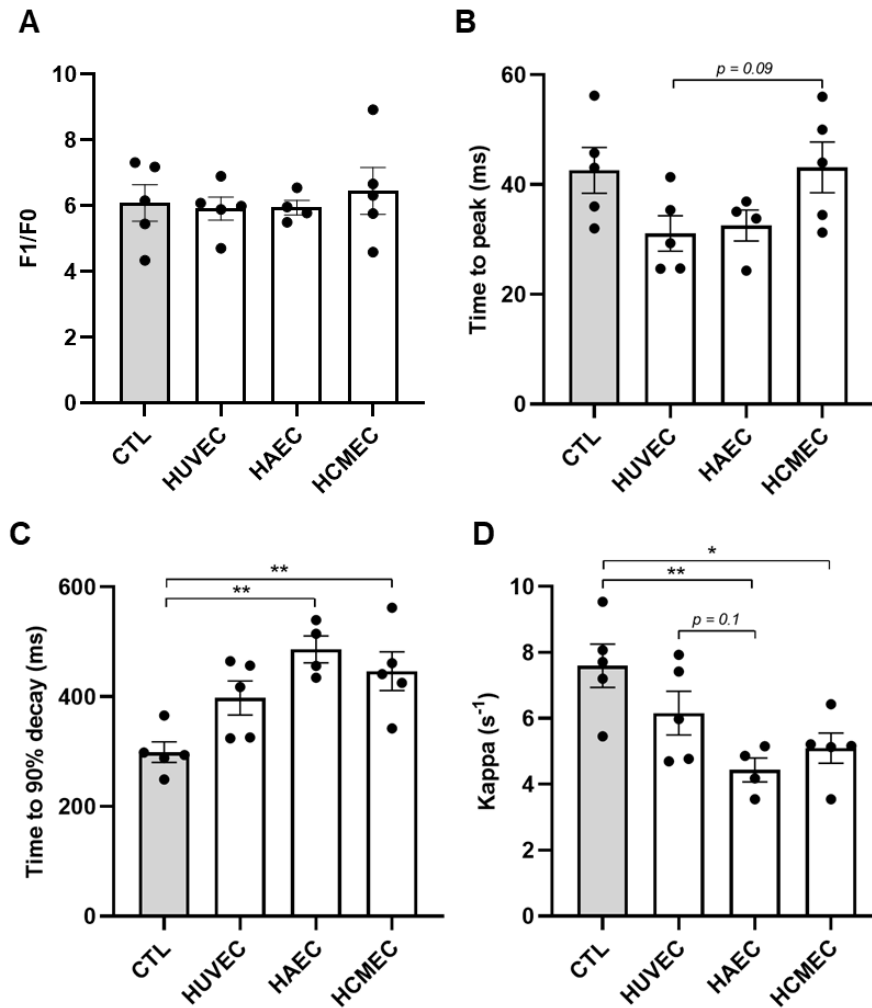


**Figure 3.3: Cardiac and non-cardiac EC might regulate calcium handling differently in adult rat CM**

Calcium transients in ARVM after 24h of co-culture with HUVEC, HAEC, HCMEC, or no co-cultured EC (CTL), recorded using optical mapping. **A.** Amplitude (F1/F0). **B.** Time to calcium transient peak. **C.** Time to 90% decay. **D.** Rate of decay expressed as kappa. Control “CTL” n/N = 20/5, HUVEC n/N = 20/5, HAEC n/N = 20/4, HCMEC n/N = 20/5 for all parameters analysed. n = average number of cells per biological replicate. N = biological replicates. Data are represented as mean +/- SEM. Each dot represents a biological replicate for which the values of all cells have been averaged. EC groups were compared to CTL using ordinary one-way ANOVA with Dunnett’s multiple comparisons test. EC groups were compared to each other using one-way ANOVA with Tukey’s multiple comparisons test in a separate analysis. \*  $p < 0.05$ , \*\*  $p < 0.01$ .



known pro-hypertrophic component of the EC-CM crosstalk<sup>66,247,248</sup> could be detected with this short-term co-culture model. Freshly isolated ARVM were plated under Transwell inserts with confluent HCMEC and co-cultured for 24 hours as described above. CM were then fixed and  $\alpha$ -actinin was stained for confocal imaging of sarcomeres. For planimetry, white light was used to delineate the boundaries of cells. In Figure 3.4A it can be seen that co-culture with HCMEC for 24 hours did not significantly alter the length (long axis), width (short axis) and aspect ratio

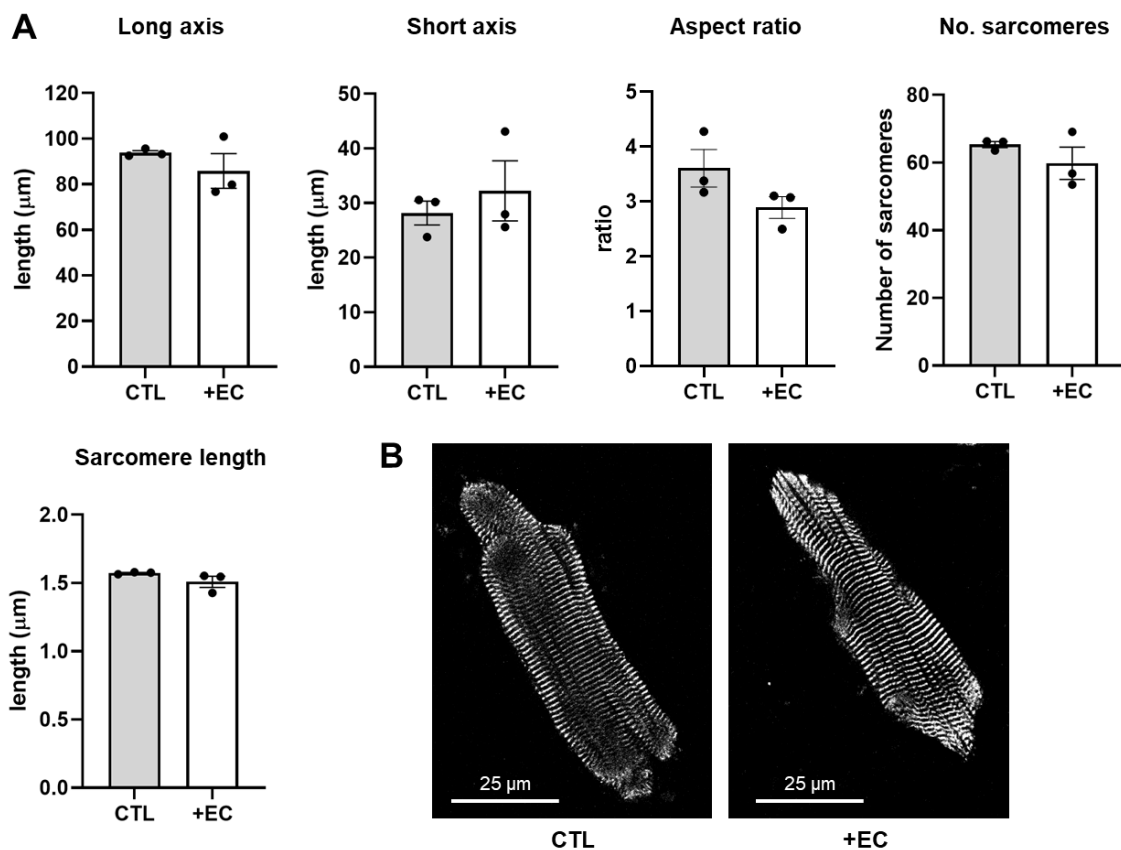


**Figure 3.4: Co-culture with HCMEC for 24 hours did not induce a remodelling of dimensions or sarcomere structures in ARVM**

Planimetric data and sarcomere properties in ARVM after 24 hours in co-culture with HCMEC. Data were collected from immunofluorescent staining of  $\alpha$ -actinin, imaged by confocal microscopy at 40x.

**A.** Quantification of CM dimensions and sarcomere number and length after co-culture (+EC) or in CM alone (CTL). n/N (images per replicate/biological replicates) = 20/3. Groups were compared with an unpaired two-tailed t-test with Welch's correction when standard deviations were not equal. No statistical indicator = no significant difference. Data points show N values (i.e. averaged n values). **B.** Representative confocal images (40x objective) of  $\alpha$ -actinin immunostaining (white). Bar = 25  $\mu\text{m}$ .

of ARVM, nor the average number of sarcomeres along the long axis and the length of these sarcomeres. This suggests the hypertrophic signalling of EC on CM is not present in this model of co-cultures, at least at this time-point.

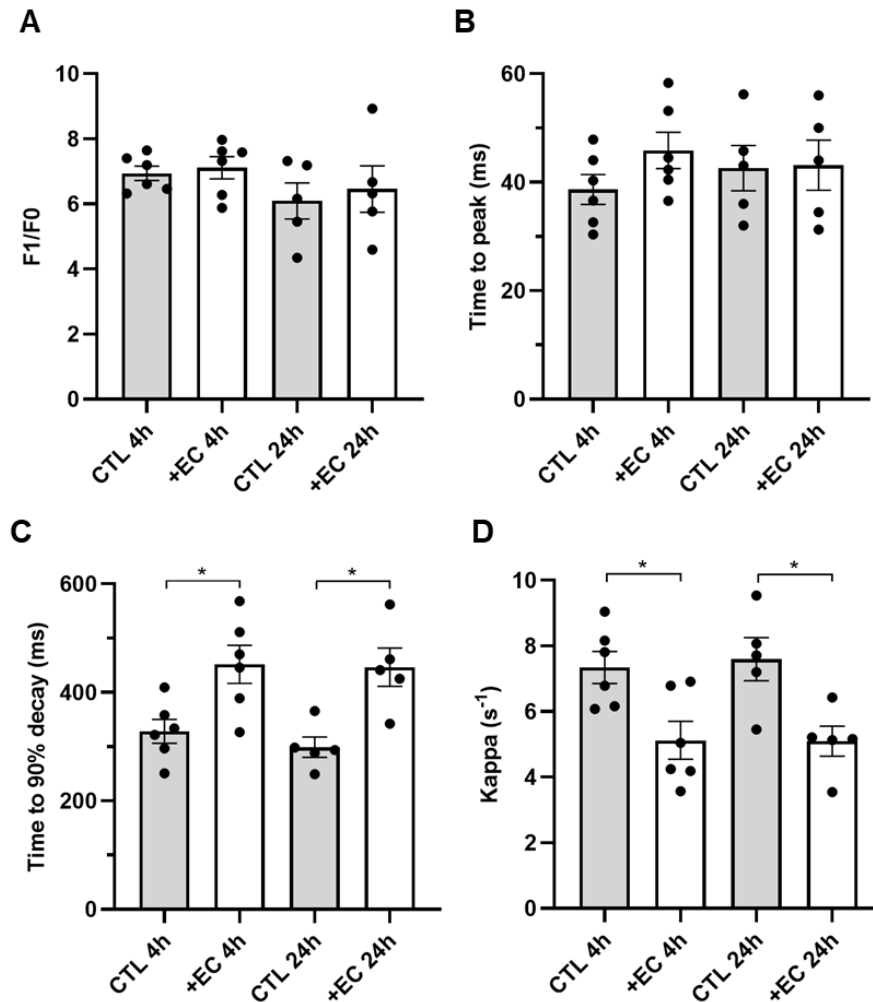


**Figure 3.5: EC induced the same effects on calcium handling of co-cultured CM after 4 and 24 hours**

Calcium transients in ARVM after 4 or 24h of co-culture with HCMEC (+EC), or no EC (CTL), recorded using optical mapping. **A.** Amplitude (F1/F0). **B.** Time to calcium transient peak. **C.** Time to 90% decay. **D.** Rate of decay expressed as kappa. CTL 4h n/N = 20/6, +EC 4h n/N = 20/6, CTL 24h n/N = 20/5, +EC 24h n/N = 20/5 for all parameters analysed. n = average number of cells per biological replicate. N = biological replicates. Data are shown as mean +/- SEM, with dots showing biological replicates for which the values of all cells have been averaged. EC groups were compared to CTL using ordinary one-way ANOVA with Tukey's multiple comparisons test. \* p < 0.05.

### **3.3.5 HCMEC produced the same paracrine effects on calcium handling in ARVM after 4 or 24 hours of Transwell co-culture**

Following the suggestion that sarcomeric remodelling was absent after 24 hours of co-culture, more attention was given to the functional response of CM to EC, and particularly to calcium handling. A shorter time-point for co-cultures was first tested to determine if the effect of EC on calcium reuptake was time-dependent. ARVM were therefore co-cultured for 4 or 24h under Transwell inserts containing confluent HCMEC, and calcium transients were recorded using optical mapping (Figure 3.5). In this experiment, co-culturing ARVM with HCMEC for 4 or 24 hours had the same effect on the morphology of their calcium transients, both increasing the time to 90% decay (Figure 3.5C) and reducing the rate of decay (Figure 3.5D) significantly and with the same magnitude (4h versus 24h:  $p > 0.98$ ). Thence co-cultures were performed for only 4 hours in order to limit the incidence of arrhythmic behaviour or agent contamination in cultures, as both issues were recurrent at 24 hours (data not shown).

### **3.3.6 HCMEC conserved their paracrine effects on calcium handling of ARVM isolated after myocardial infarction**

To determine if the effects of EC on CM described above are conserved when CM are isolated from infarcted myocardium, ARVM were isolated 16 weeks after permanent coronary ligation, and immediately co-cultured for 4h under Transwell inserts containing healthy HCMEC. Co-culture induced the same changes of calcium transient morphology in CM from infarcted tissue and healthy tissue (i.e. slower calcium uptake compared with CM alone, but no effect on the amplitude or time to peak) (Figure 3.6). The rate of decay was indeed reduced by 30% and 39% by co-culture of EC with control-CM and MI-CM respectively (Figure 3.6D). Surprisingly, there was no significant change of calcium handling properties after MI in this experiment, regardless of co-culture conditions.

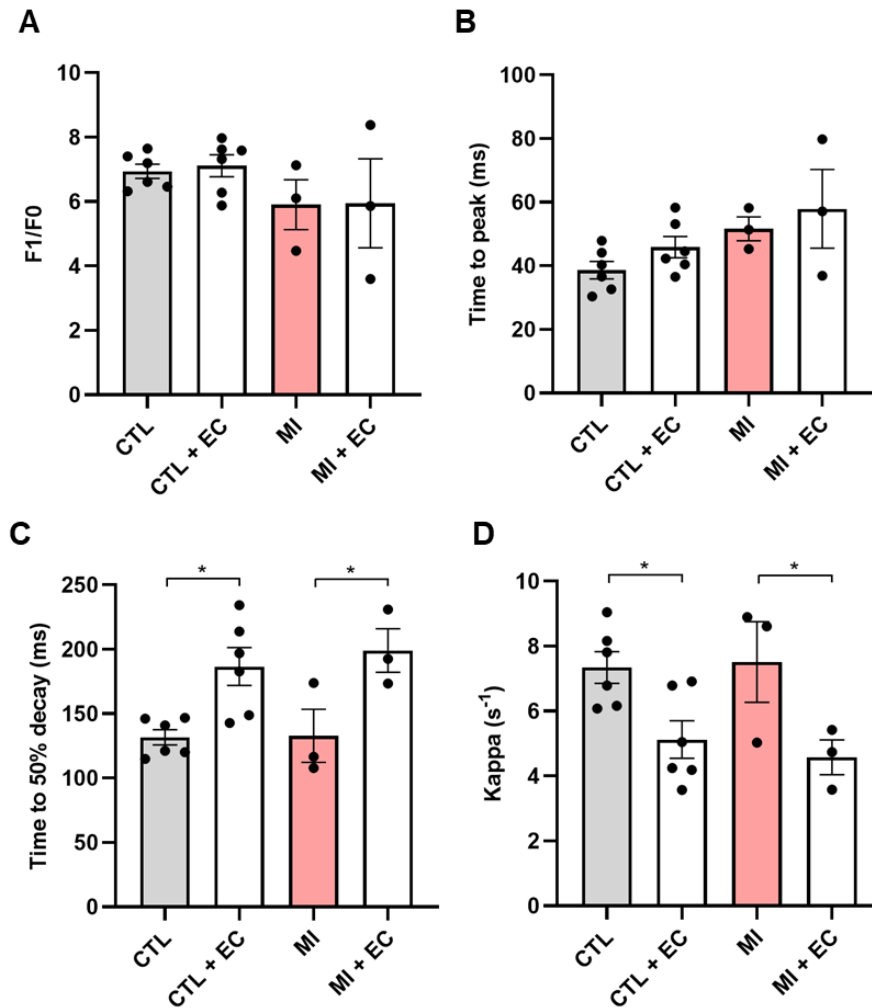


**Figure 3.6: EC induced the same effects on the calcium handling of co-cultured CM after myocardial infarction**

Calcium transients in ARVM isolated 16 weeks after permanent MI compared to control (no MI). Data were collected after 4 of co-culture with HCMEC (+EC) using optical mapping. **A.** Amplitude (F1/F0). **B.** Time to calcium transient peak. **C.** Time to 50% decay. **D.** Rate of decay expressed as kappa. CTL n/N = 20/6, CTL + EC n/N = 20/6, MI n/N = 20/3, MI + EC n/N = 20/3 for all parameters analysed. n = average number of cells per biological replicate. N = biological replicates. Data are shown as mean +/- SEM, with dots being biological replicates in which all cells have been averaged. Data were analysed using ordinary one-way ANOVA with Bonferroni's multiple comparisons test. \* p < 0.05.

### **3.3.7 Use of the custom designed co-culture media did not induce transdifferentiation of HCMEC into lymphatic EC or fibroblasts**

Because it is recommended to culture the commercially obtained HCMEC in their optimal kit culture medium, it was a concern that these microvascular cells might transdifferentiate into lymphatic EC or even into fibroblasts after incubation with the medium designed for co-culture with ARVM. To test this, HCMEC were cultured for 24 hours in 6-well plates in either the kit medium EGM-MV2 with 10% FBS or the custom medium (see Section 3.2.1). Cells were then detached, fixed, permeabilised and counted by flow cytometry with staining for the endothelial markers CD31 and CD144, the lymphatic marker Lyve-1, or  $\alpha$ -SMA (Figure 3.7). HUVEC and human adult cardiac fibroblasts served as controls for bona fide EC and non-EC, respectively. Although the N number was too low for appropriate statistical analysis, these pilot data suggest that HCMEC do not lose their expression of endothelial markers (N = 2) and do not express Lyve-1 after incubation with the custom media (Figure 3.7A). Of note,  $\alpha$ -SMA was expressed by >70% of cells in all groups but as expected fibroblasts did not express CD31 or CD144.

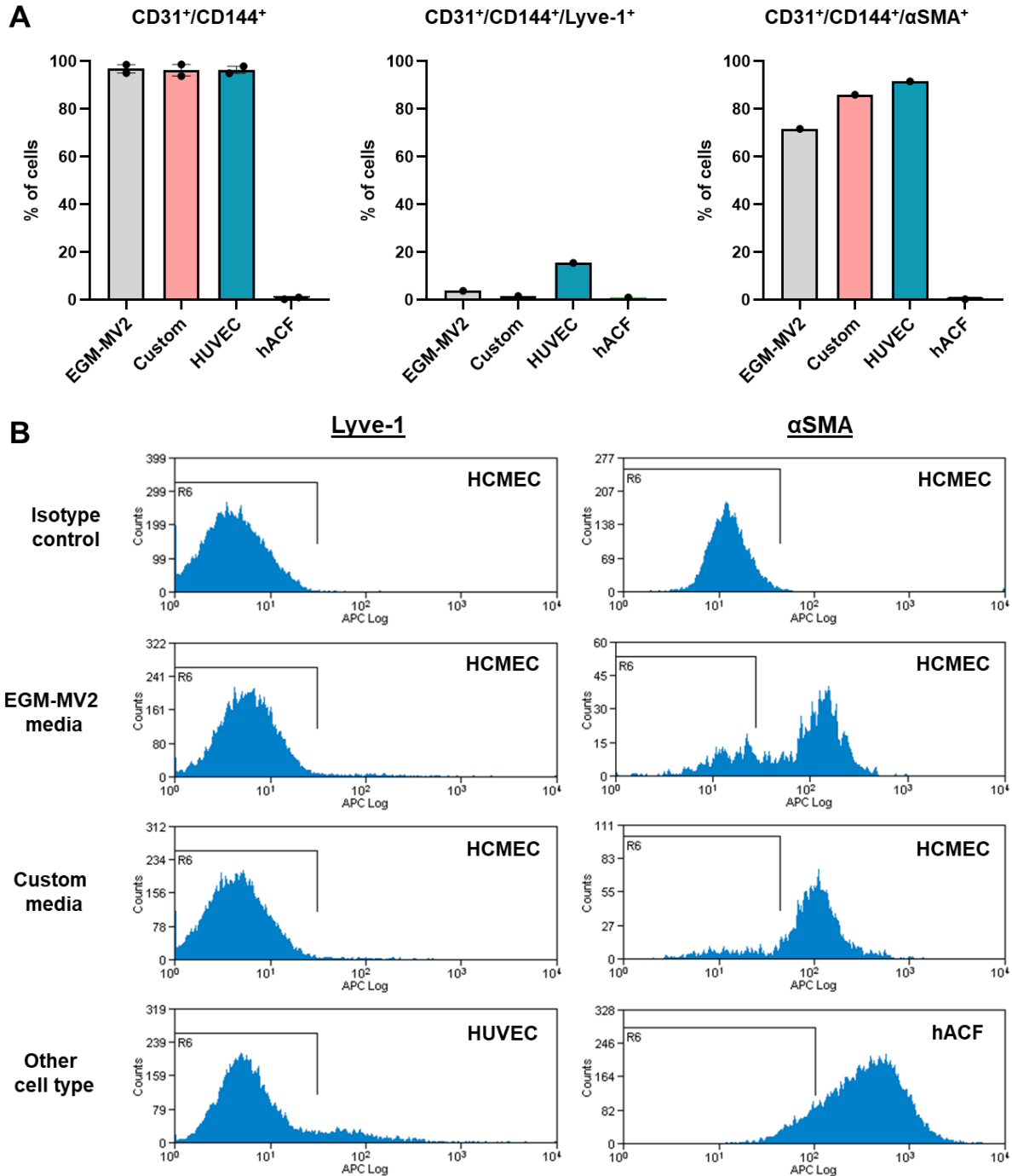


**Figure 3.7: HCMEC did not transdifferentiate into lymphatic EC or fibroblasts after 24 hours of incubation with the custom medium used for co-cultures**

Flow cytometric quantification of CD31, CD144, Lyve-1 and α-SMA expression in HCMEC after 24 hours in the recommended kit media (EGM-MV2) or the custom media used for EC-CM co-culture.

**A.** Percentage of double- and triple-positive cells for CD31, CD144, and Lyve-1 or α-SMA. CD31 and CD144: N = 2. Lyve-1 and α-SMA: N = 1. Due to low n number, data were not statistically compared.

**B.** Histograms of Lyve-1<sup>+</sup> or α-SMA<sup>+</sup> cells in the CD31<sup>+</sup>/CD144<sup>+</sup> gate (except for human adult cardiac fibroblasts (hACF)).

### 3.4 Discussion

Despite the multiplicity of articles and reviews which add every year to our knowledge on the subject of EC-CM interaction, there is surprisingly no consensus on: (1) the basic elements of methodology to study this crosstalk and (2) on the basal effects of EC on CM function. As a result, the first steps of this project were to determine the optimal means to model *in vitro* EC-CM crosstalk. After review of practices in the literature I determined that co-cultures using Transwells were most adapted to model the EC-CM paracrine crosstalk, without interference from intercellular mechanical coupling or partial loss of secretome content. The data presented subsequently demonstrate that co-culture with this model using unstimulated EC is sufficient to induce a change of calcium handling in CM.

In this chapter we show that: (1) there is no stereotypical model of EC-CM co-culture in the literature. (2) Co-culture with EC induce a slower calcium reuptake in CM and a prolongation of calcium transients without altering the amplitude or time to decay, but of note (3) HUVEC do not produce as strong an effect on CM calcium handling as cardiac microvascular EC. (4) Co-culture with EC do not induce hypertrophic or sarcomeric remodelling in CM after 24 hours. (5) The effect of HCMEC on CM is preserved between 4 and 24 hours of co-culture, and (6) conserved on CM isolated after myocardial infarction. (7) HCMEC do not transdifferentiate in the custom co-culture medium, further validating the robustness of the model used.

#### 3.4.1 Limitations and failures of published research with EC-CM co-cultures

To our knowledge there is currently no published analysis, discussion, or review of co-culture methodology to study the interaction of cardiac cells. Moreover, seminal reviews on the subject of EC-CM crosstalk have failed to examine previous studies in terms of co-culture quality and relevance, and have failed to address the inconsistency of reported effects of EC on CM<sup>66,197,247</sup>. As a result, starting a research project on EC-CM interaction is challenged by the multitude of possible co-culture protocols, by insufficient data to understand their inherent

value or inter-comparability, and by the lack of consensus on what can serve as gold standard for EC effects on CM. To illustrate this issue and better contextualise the future results in this project, articles published with EC-CM co-cultures were categorised by methodology. Figure 3.1 demonstrates that such methodology can be optimised for practicality rather than for physiological relevance, with non-cardiac EC from adult human donors cultured with CM isolated from neonatal rats<sup>232,234</sup> for example. The inherent limitations of such practices are still not fully understood and may contribute to a delay in the translation of results from co-cultures to clinic.

The multiplicity of co-culture methods which have been published is an issue also aggravated by inconsistent levels of protocol validation, correction of experimental variables, transparency of methods in publications, and even cogency of data interpretation. As an example, in Liu *et al.* (2014) it is unclear which medium was used in co-cultures, and the EC:CM cell ratio cannot be found<sup>227</sup>. There was also no justification provided for the use of rat aortic EC, no experiment testing other time-points, and curiously an experiment on CM viability after co-culture with EC did not include a CM-only group. Finally, the mechanism which was studied in this article (the role of endothelial vasostatin-1 on CM survival after hypoxia/reoxygenation injury) was only manipulated using adenoviral protein overexpression in EC, notwithstanding that endogenous expression was not ruled out in the article. Other articles share these practices<sup>203,249,250</sup>, while the mechanisms thus attributed to the EC-CM crosstalk are adopted in subsequent articles. As is shown in Figure 3.1 there is a high percentage of articles not providing crucial information for the reproducibility of experiments. This can only impair the relevance of such studies.

#### **3.4.2 Transwell inserts are most appropriate to study the paracrine interaction of EC and CM without mechanical or electrophysiological interference, or loss of secretome**

There is a substantial record of publications in which transwell inserts have been used for co-cultures<sup>75,225–227</sup>, making this approach one of the most widely accepted means of investigating a crosstalk *in vitro*. Having reviewed all major types of *in vitro* and *ex vivo* systems which could



be used in the current project (Table 3.1), the Transwell model was selected for the following reasons. First, in this model, CM face the basolateral membranes of EC (when EC are plated in the insert as in this project). Due to the known polarity of endothelial secretory pathways<sup>251–253</sup>, this conformation is more physiologically relevant than other published models, e.g. plating ARVM on top of EC monolayers<sup>226</sup>. The insert membrane physically separates both cell types, thus preventing cross-contamination during functional assays or when collecting samples, in addition to preventing mechanical or electrophysiological forces which might interfere with the paracrine crosstalk. This system is also well suited to the experimental set-up required for this project because: (1) EC can be grown to monolayer and pre-conditioned to given stimuli prior to co-culture with CM, (2) cells can be easily separated after co-culture, (3) it requires low cell numbers compared to 3D *in vitro* models (e.g. in vascularised organoids) and many more replicates can be run simultaneously, allowing test conditions to be better controlled.

The transfer of conditioned media can satisfy the requirements above. However, the Transwell model has the advantage in terms of the dynamics of secreted mediator activity on receptor cells. Indeed, when transferring conditioned media, the available concentration of EC-secreted cardiotropic factors cannot be maintained and thus decreases constantly at the rate of their respective half-life in solution or as a function of their interaction with CM or CM-secreted factors. Therefore, the method is much less physiologically relevant than the Transwell system in which these cardiotropic factors are secreted by EC continuously. This is likely to alter the response of CM to EC-derived products as, for example, bioavailability of cardiotropes such as NO might be different in the two models. Indeed, NO was reported to have a very short half-life in solution, ranging from milliseconds to minutes depending on the physiological and molecular conditions<sup>254</sup>, even after biotransformation into more stable species, and NO levels decrease more rapidly with increasing concentrations of cells in the system<sup>255</sup>. This suggests that the activity of NO on CM after the transfer of conditioned media can only be transient (if present at all after the processing of the culture supernatants), while NO is continuously released by EC in the Transwell configuration. The same issue can be raised for other factors,

including proteins, even though their half-life and consumption by CM may be slower than with NO. It has long been understood that cell signalling and functions were highly sensitive to temporal dynamics of stimuli<sup>256</sup>, thus questioning the relevance of transferring an unstable pool of proteins, vesicles and other soluble factors on CM. Furthermore, the EC-CM crosstalk is incompletely modelled by conditioned media, since the CM-to-EC communication axis is absent, abrogating potential feedback loops (note: this might be a desired property of the model, which admittedly is less difficult to interpret than Transwell systems).

There are however some limitations to using Transwells as a model. First, the physiological relevance of the system is inferior to more complex models (e.g. vascularised constructs, >2 cell types co-cultures, *ex vivo*). It is also difficult to determine which cell type is responsible for the secretion of a specific mediator. Finally, some experimental endpoints require the insert to be removed or the media to be changed, which eliminates all paracrine factors from the micro-environment of the target cell, potentially disrupting parts of the intercellular crosstalk.

### **3.4.3 HCMEC are most relevant for co-cultures with CM due to high EC heterogeneity**

With the development of microarrays and RNA sequencing many reports have been published in recent years to show that the phenotype of EC differs widely with their location *in situ*. This heterogeneity is notably demonstrable across different vascular beds, differentiating large vessels and microvasculature EC<sup>257,258</sup> but also EC from different organs<sup>215,259,260</sup>. Beyond its ability to discriminate expression profiles, EC heterogeneity was also seen in functional responses of the endothelium to stimuli, such as inflammation *in vivo*<sup>215</sup>. In face of this evidence, a study rapidly argued that the heterogeneity was lost after isolation, culturing and passaging of EC<sup>261</sup>. However, this study only compared two EC populations of arterial origin and more recent and more numerous papers have argued the opposite more convincingly<sup>257,259</sup>. It would therefore be somewhat questionable to consider EC of different sources as interchangeable for co-cultures with CM. Furthermore, as Figure 3.1A shows, the majority of EC-CM co-cultures contained EC of non-cardiac origin. To date there has been no

direct comparison of cardiac versus non-cardiac EC induced effects on CM in co-culture. In 2006 however, Lemmens *et al.* reported that co-culture with rat aortic EC had no effect on neonatal rat CM while (in a separate experiment) cardiac microvascular EC induced CM hypertrophy, a mechanism which the authors attributed to their differential expression of NRG-1<sup>262</sup>. The data were not included in the article.

It is beyond the scope of this discussion to reflect on possible reasons for non-cardiac EC of large veins or arteries being co-cultured with CM. However, since HUVEC, HAEC and HCMEC were available in Prof Mason's lab, this was an opportunity to directly compare their effect on CM in co-culture. Figure 3.3 shows the effect of co-culture on calcium handling in CM, where HAEC and HCMEC, but not HUVEC, induced a significantly slower calcium reuptake. More biological replicates would help refine the conclusions from this experiment, but these data suggest that these EC populations differ in their paracrine effects on calcium handling in CM, quantitatively more than qualitatively. To fully determine how the heterogeneity of EC modifies the endothelial crosstalk with CM, one would need to correlate transcriptomics or proteomics data from a variety of EC subpopulations with the expression profile of co-cultured CM. In this case, effector variables in EC can be correlated with receptor variables in CM, as is done with heterocellular ligand-receptor correlation analyses<sup>70</sup>. Until this type of experiment is performed and published, there will be no hard line between acceptable and unacceptable EC subsets, and physiologically relevant co-culture behaviours when modelling *in vitro* the cardiac EC-CM interaction. There is heterogeneity of EC within the myocardium itself<sup>66</sup>, refuting the possibility of a perfect *in vitro* model. From early *in vivo* studies of the EC-CM interaction it is established that myocardial capillary EC and endocardial EC are the subsets of EC most likely to exchange paracrine signals with CM<sup>66,85,87,92,263</sup>, validating further the use of HCMEC for this study.

#### **3.4.4 Using ARVM, a custom co-culture medium and a short time-point to circumvent the limitations of *in vitro* co-culture of EC and CM**

In the last decade CM derived from human pluripotent stem cells have been developed and utilized increasingly as a valuable and malleable resource for regenerative medicine, cardiac disease modelling *in vitro* and EC-CM co-cultures. However, these cells exhibit structural and functional properties which have been called “immature” in that they model inadequately the properties of primary adult human CM<sup>97,264</sup>, notably at the level of calcium handling<sup>265</sup>. This is an issue shared in many aspects with neonatal CM, which also lack the complex tubular network and calcium handling properties fit to generate optimal excitation-contraction coupling such as is seen in adult CM<sup>265</sup>. The paucity of access to healthy adult human CM is yet another challenge to *in vitro* CM models. Though theoretically ideal, such cells can only be isolated from healthy donor hearts that have been ruled out for transplantation. Because of this, electrophysiologists tend to rely preferably on adult primary CM isolated from mammals such as dog, pig, rabbit, guinea pig, mouse, rat, cat and ferret<sup>216,266</sup>. Importantly, CM phenotype can differ across these species and with human CM, and this impacts relaxation properties and calcium handling<sup>216,266,267</sup>.

*In vitro* culture conditions of CM have been long validated. Yet, there are still articles which go against traditional cardiac cell culture, introducing serum in the media of primary adult CM for example<sup>225</sup>. Since 1982 many reports have demonstrated that even though it could stabilise CM cultures for days, FBS also induced cell hypertrophy in ARVM<sup>268,269</sup>, neonatal rat CM<sup>270</sup> and human embryonic stem cells-derived CM or induced pluripotent stem cells-derived CM<sup>271</sup>. It is less well understood what effects serum has on other properties of CM. There is no guideline on EC-CM co-culture methodology with regards to serum content and media formulation. As a result, a multitude of media have been used and rarely validated. As shown in Figure 3.1D, some co-cultures have been performed in endothelial growth media, which typically contains growth factors such as VEGF and unknown concentrations of calcium chloride. It is still unclear how such media formulations can alter CM function *in vitro*. Because

of this, the composite medium which was designed for this project was first validated during preliminary experiments, and did not induce remodelling of calcium handling or hypertrophy compared with the optimal culture medium (i.e. medium-199 and ascorbic acid, creatinine, carnitine, taurine) (data not shown). In co-cultures the presence and absence of serum can be as problematic, notably due to the poor viability of EC in response to prolonged serum starvation. Preliminary experiments helped determine that 1% FBS was the minimum required to maintain HCMEC viability in co-culture for at least 24 hours without altering CM properties, as discussed above (data not shown). As shown in Figure 3.7 there is also evidence that the custom medium for co-cultures does not induce HCMEC to transdifferentiate into fibroblasts, nor increases the presence of lymphatic EC in culture. In this experiment, adult cardiac fibroblasts were predominantly categorised  $\alpha$ -SMA<sup>+</sup>/CD31<sup>-</sup>/CD144<sup>-</sup> while EC were  $\alpha$ -SMA<sup>+</sup>/CD31<sup>+</sup>/CD144<sup>+</sup>, including HCMEC cultured with the custom medium. HCMEC were also predominantly negative for the lymphatic EC marker Lyve-1<sup>272</sup>, in fact less so than HUVEC. Partial expression of Lyve-1 in HUVEC *in vitro* was reported previously<sup>212,273</sup>, so this finding was expected. However, this experiment was too underpowered for statistical analysis and access to lymphatic EC samples as positive controls for Lyve-1 staining, as well as additional markers for lymphatic EC (such as Prox-1<sup>272</sup>) would have increased the validity of these results. CD34 was also found to be absent in Lyve-1<sup>+</sup> cells<sup>272</sup> and thus would have been a good addition to this panel of antibodies for flow cytometry.

Finally, it is well accepted that primary CM undergo rapid de- and re-differentiation *in vitro* after isolation. In adult pig ventricular myocytes, T-tubule density was significantly reduced after the first 24 hours of culture post-isolation<sup>121</sup>. This was associated with a slower calcium rise, less efficient excitation-contraction coupling, and a depolarised resting membrane potential in CM, all in all resembling the electrophysiological and cytoarchitectural properties of CM in HF<sup>214</sup>. It was therefore important to control this phenotypic shift in co-cultures, testing the feasibility of shorter time points. As Figure 3.5 shows there was no effect of culturing ARVM for 4 or 24 hours at the level of calcium handling, whether in co-culture with HCMEC or not. This suggests

that the electrophysiological remodelling induced by de-differentiation was not yet significant in these settings. Such difference with previous reports<sup>121</sup> may be attributed to interspecies variability, as rat CM might be more resilient to remodelling once in culture than pig CM. As discussed in Section 3.3.5 the 4 hours time-point was however preferred for practical reasons.

### **3.4.5 No hypertrophy of ARVM was detected after co-culture with HCMEC**

At the beginning of the project it was not immediately clear which effect of EC on CM would serve as a primary experimental endpoint. Since the EC-induced hypertrophy of CM has been proposed and demonstrated in some pathophysiological conditions *in vivo*<sup>274</sup> and *in vitro*<sup>203,222,275</sup>, though disputed in others<sup>276</sup>, and in light of the link between inflammation and the expression of pro-hypertrophic cardiotropes such as ET-1 by EC<sup>277,278</sup>, hypertrophy of CM was naturally of interest in this project. In Figure 3.4 it can be seen that co-culture of ARVM with HCMEC for 24 hours did not induce hypertrophic remodelling or sarcomeric remodelling. As discussed in Sections 1.11 and 3.4.1 there is surprisingly little direct evidence for the effects of EC on CM and, where data exist, the overall quality of experiments or publication practices often lowers the possibility to translate such results in other models. However, there are a few reports to mention: in Lemmens *et al.* (2006), CM hypertrophy was investigated after 72 hours on NRVM cultures<sup>203</sup>. NRVM were also used in Higashikuni *et al.* (2011), though after 48 hours<sup>275</sup>. Yin *et al.* (2017) looked at neonatal mouse CM after 3 days in co-cultures<sup>279</sup>. Finally Kubin *et al.* (1999) measured protein synthesis in ARVM after 8 days in culture with EC-conditioned media<sup>222</sup>. Other articles, presenting EC-CM co-cultures at shorter time-points, did not test CM hypertrophy<sup>228,249</sup>. It is thus difficult to conclusively determine at which point in co-culture with EC the CM undergo hypertrophic remodelling. It is important to note that so far the majority of studies testing this signalling *in vitro* have done so using neonatal CM or CM derived from induced pluripotent stem-cells<sup>75</sup>, both inadequate to model the ultrastructure and cell dimensions of adult CM such as ARVM. The absence of hypertrophic remodelling in ARVM after 24 hours of co-culture with HCMEC, as shown above, might thus be explained by

the brevity of co-cultures and a lower response to hypertrophic stimuli in adult CM. However, it should be noted that this experiment was underpowered and would have greatly benefitted from a positive control for hypertrophy, for example with a treatment of ARVM alone with Ang-II<sup>276</sup>. Using techniques more sensitive to changes in cell hypertrophy would have also strengthened this experiment. For example, live membrane staining of ARVM would allow volumetric measurements of CM morphology, and the membrane capacitance obtained from the whole-cell configuration of the patch-clamping technique would provide highly accurate measurements of plasmalemma surface area (i.e. of the cell volume). Finally, protein expression for markers of cardiac hypertrophy (e.g. ANF/BNP, MyHC) would precede changes in cell morphology and thus might be a preferable endpoint for shorter time-points in co-cultures.

#### **3.4.6 MI did not affect the response of ARVM to EC co-culture**

Later experiments in this project rely on the pro-inflammatory conditioning of EC and the study of its effects on healthy (i.e. naïve) CM in co-cultures. There are two caveats to this approach. First, myocarditis or even myocardial dysfunction caused by systemic inflammatory diseases are not restricted to disrupting EC. Therefore, the effect of activated/dysfunctional EC on CM is likely to occur when CM are equally under pro-inflammatory stimulation (this is still poorly understood). Second, it is hypothesised in this project that the effect of “inflammatory” EC on CM will alter the phenotype of CM, in a way which might ultimately affect their response to EC, in the fashion of negative feedback loops. Because of this, it would be challenging to determine if a change in the effects of EC on CM is caused by phenotypic changes in EC, or in CM. To help solve this issue and determine if HF or a pro-inflammatory environment impacts the ability of CM to respond to EC, untreated HCMEC were co-cultured with ARVM freshly isolated 16 weeks after MI. This model was well optimised and performed by Peter O’Gara<sup>122</sup>, and was characterised by a significant infarct area in the LV, cardiac hypertrophy, reduced LVEF, and an elevated end-diastolic pressure consistent with the HF phenotype. In ARVM, this model

was shown to induce a lower amplitude of twitch contractions, prolonged time to peak and a slower rate of decay for calcium transients, an increased frequency of spontaneous calcium sparks, and a disruption of the T-tubule network<sup>122</sup>, also consistent with HF. Figure 3.6 shows that ARVM from MI responded to co-culture with EC identically to control-ARVM, suggesting that pathological remodelling in CM does not impair the EC-to-CM paracrine axis qualitatively or quantitatively. However, there was no significant difference of calcium handling between MI and control ARVM, as opposed to the findings listed above (though using the same model and same operator). In the article where ARVM from this MI model were characterised, calcium transient analysis was performed on freshly isolated cells, whereas in this experiment it was performed 6 hours after isolation, including 4 hours of culture in Ca<sup>2+</sup>-enriched medium. In the article CM were paced at 0.5 Hz whereas in this experiment they were paced at 1 Hz. This could explain differences of calcium handling between that published in Lyon *et al.* (2009) and that recorded in this project. Of note, this experiment does not test whether CM desensitisation to “inflamed” EC during co-culture can occur.

### **3.4.7 Summary the effects of EC on ARVM in these co-culture conditions**

In conclusion, with the *in vitro* co-culture model that was developed in this chapter, we have confirmed that EC regulate CM function. This was a critical step of the project, allowing further experiments to be performed to determine how this effect might be altered. Due to time-point restrictions, the alleged pro-hypertrophic effect of EC on CM was not investigated further. The change in calcium handling in CM after co-culture, however, was found to be a reliable starting point to: (1) establish when co-cultures misbehaved in future experiments, and (2) test whether the inflammatory response of EC altered this crosstalk, quantitatively or qualitatively.

To recapitulate the main finding in this chapter, beside the validation of the co-culture model, it was found that co-culture with EC prolonged the decay phase of calcium transients without changing the amplitude or time to peak in CM. In the next chapter, the aim will be to optimise and validate the pro-inflammatory intervention on HCMEC.



# 4.

**Pro-inflammatory treatment of cardiac microvascular endothelial cells with TNF $\alpha$ , IL-1 $\beta$  and hyper-IL-6**

## 4.1 Introduction

In Chapter 3, the model of EC-CM co-culture was optimised to study the paracrine effects of EC on CM. Before setting out to characterise these effects, and how they can be altered during endothelial inflammation, it is imperative to validate the pro-inflammatory treatment which will be applied on HCMEC. It remains a challenge to model endothelial inflammation *in vitro*, first because it involves many factors which cannot be realistically replicated fully in homotypic EC cultures (e.g. interactions with rapidly changing populations of immune cells, or hemodynamic changes and comorbidities), but also because inflammation is an umbrella term covering many distinct processes. These involve different soluble mediators, cell types, signalling pathways, and can drive the tissue to more injury or repair, with cell death or proliferation, all depending on intra- and extracellular conditions<sup>37</sup>. Using one cytokine as a pro-inflammatory intervention *in vitro*, as is done traditionally, can be problematic. TNF $\alpha$  and IL-6, for example, contribute to both acute (type-II) and chronic inflammation but their effect on EC can be easily described as anti-inflammatory or pro-inflammatory depending on which EC function is observed or the nature of other inflammatory signals<sup>37,280–282</sup>. In this chapter, the aim was to optimise a treatment of EC to model endothelial inflammation, at least in terms of paracrine activity on other cell types (CM in this project). Therefore, even in the case where not all aspects of inflammation are fully induced by this treatment, it is sufficient that EC are shown to release pro-inflammatory factors in response to cytokine treatment. To improve the relevance of this model, and the coverage of functions affected by this pro-inflammatory treatment of EC, a cocktail of three cytokines was tested for the first time (TNF $\alpha$ , IL-1 $\beta$ , hIL-6; the term “Cytomix” was coined to abbreviate the name of this treatment). These cytokines are most frequently expressed and correlated to cardiac disease progression, severity, and mortality, but also with vascular inflammation and endothelial dysfunction, all underlying HF<sup>39,283–290</sup>.

To validate the use of Cytomix, the effective concentration of each cytokine was determined and briefly characterised. It was necessary to confirm for example that IL-6 treatment of EC can induce a phosphorylation of STAT3<sup>285,291,292</sup> and induce the expression of pro-

inflammatory target genes such as ICAM-1<sup>47,293</sup>. EC do not express the receptor for IL-6, sIL-6R $\alpha$ , which is provided to EC by leucocytes during inflammation. A chimeric protein based on IL-6/sIL-6R $\alpha$  was produced by Fischer *et al.* (1997) and reported to be active at 100-1000-fold lower concentrations than unbound IL-6 and sIL-6R $\alpha$ <sup>294</sup>. I decided to test the effects of this fusion protein, known as hyper-IL-6 (hIL-6), alone and within Cytomix, comparing the effects on EC with those reported using other cells and concentrations<sup>295-297</sup>.

Thrombin was used in this project as a known stimulant of endothelial permeability and of NO synthesis by EC<sup>62</sup>. Thrombin signalling is mediated in EC by protease-activated receptors (predominantly PAR-1)<sup>62,298</sup>. PAR-1 activation leads to a transient increase of intracellular Ca<sup>2+</sup> (from intracellular stocks and the extracellular space), which in turn potentiates the activity of eNOS<sup>63</sup>, as a calcium-sensitive isoform of NOS<sup>81</sup>. This leads to NO synthesis, which induces a cytoskeletal remodelling of multiple proteins by S-nitrosylation (e.g.  $\beta$ -catenin, VE-cadherin,  $\alpha$ -/ $\beta$ -/ $\gamma$ -actin)<sup>299</sup>. The end result of this signalling is disassembly of cell-cell junctions and a higher paracellular permeability<sup>62</sup>. TNF $\alpha$  potentiates this effect by increasing the expression of Transient Receptor Potential Channel-1 (contributing to the calcium transients in EC)<sup>56</sup> and by regulating the expression and calcium-dependency of eNOS<sup>80</sup>. It is therefore hypothesised that Cytomix increases calcium releases, NO synthesis, and permeability of EC. Endothelial proliferation, contributing to angiogenesis and myocardial remodelling<sup>300,301</sup>, is also regulated by inflammatory cytokines (e.g. IL-1 $\beta$ )<sup>302,303</sup>. Although EC responses to cytokines can be altered by other cytokines, such as IL-6<sup>304</sup>, it is hypothesised that Cytomix also inhibits EC proliferation.

The work described in this chapter set out therefore to test the hypothesis that Cytomix is able to induce a multi-parametric pro-inflammatory response in HCMEC. This was tested at the levels of cell cycle progression (used as a marker of proliferation), permeability, transient calcium release, NO synthesis, and secretion of cytokines and chemokines.

## 4.2 Methods

The methods described in this chapter are described in full in Chapter 2.

### 4.2.1 Cell culture, cytokine treatments, and co-cultures

Human cardiac microvascular EC (HCMEC) were grown and maintained in EGM-MV2, up to passage 6. Adult rat ventricular myocytes (ARVM) were isolated from male Sprague-Dawley rats (refer to Chapter 2 for the protocol). This was kindly performed by Peter O’Gara. Primary human adult ventricular fibroblasts were isolated from the LV of hearts which were ruled out for transplantation. Cells were isolated, maintained and kindly provided by Brian Wang, PhD., with the help of Oisín King. Fibroblasts were used under passage 20.

For most experiments, unless stated otherwise, HCMEC were cultured for 24 hours in EGM-MV2 after plating before treatment started. At this point, medium was removed, cells washed three times with PBS, and co-culture medium added with cytokines when applicable. Except for concentration curve experiments, human recombinant TNF $\alpha$  and IL-1 $\beta$  were both used at 1 ng/ml. Hyper-IL-6 (hIL-6) was used at 25 ng/ml. The cytokine cocktail characterised in this chapter, which was coined “Cytomix”, consisted of TNF $\alpha$  (1 ng/ml), IL-1 $\beta$  (1 ng/ml) and hIL-6 (25 ng/ml). All cytokine treatments were performed for 24 hours unless stated otherwise.

For HCMEC-ARVM co-cultures, the protocol follows that optimised in the previous chapter. In short: 60,000 EC were cultured in 12-well Transwell inserts (at 60,000 cells per insert, Greiner Bio-One) for 24 hours in EGM-MV2. Media were then changed for co-culture medium (Section 2.2) and EC were cultured for 24 hours with individual cytokines or Cytomix. Freshly isolated ARVM were plated on laminin-coated 13 mm diameter glass coverslips (20,000 rod-shaped cells per coverslip) and cultured for 2 hours to allow cell attachment. ARVM were then gently washed with medium to remove calcium-intolerant CM, and the Transwell inserts containing EC were transferred on top of ARVM cultures. Co-cultures were stopped after 4 hours.

#### **4.2.2 SDS-PAGE and western blotting**

The protein expression of VCAM-1, ICAM-1, MnSOD, GAPDH, p-STAT3 S727, iNOS, eNOS, A20, HO-1, and TRAF6 was quantified by SDS-PAGE separation and western blotting, run as described in Section 2.4. All primary antibodies (listed in Section 2.9) were used at 1:1000 in blocking buffer, except the anti-GAPDH antibody which was used at 1:3000. The secondary antibodies, all HRP-conjugated, were diluted at 1:3000 in blocking buffer and used accordingly with the species of the primary antibodies (anti-mouse or anti-rabbit). The amounts of proteins were normalised to the level of GAPDH, which served as a loading control. Protein standards (i.e. ladders) were used to identify proteins by their molecular weight. ECL reaction was used to detect proteins, and images were captured on radiographic films. Quantification was done using ImageJ, after conversion of images in 8-bits.

#### **4.2.3 Cell cycle analysis by flow cytometry**

Cell cycle progression and proliferation of HCMEC were analysed by flow cytometry using a propidium iodide staining. Cells were cultured in 6-well plates at 100,000 cells per well for 24 hours in EGM-MV2. Cultures were then washed, and media were replaced by co-culture medium containing either 1% or 10% FBS. Some cells were collected before the media change, as a  $t_{(0h)}$  control. After 24 hours of culture, cells were trypsinised, washed with PBS three times, fixed with 70% ice-cold ethanol for 1 hour at 4°C, washed with ice-cold PBS three times, and incubated for 30 min at 37°C in permeabilization buffer which contained propidium iodide (P4170, Sigma; at 50 µg/ml) and RNase A (R5000, Sigma; at 0.4 mg/ml). This was performed in darkness. Cell suspensions were then processed through a CyAn™ APD cytometer (Beckman Coulter). Between 10,000-20,000 events were recorded from each sample. Debris and cell multiplets were excluded from the datasets. Analysis was carried out in FCS Express, using the in-built analytical tool to classify cells by cell cycle phase, based on an algorithmic processing of the propidium iodide staining. Only data collected from HCMEC plated at 100,000 cells per well are presented in this chapter.

#### **4.2.4 Endothelial permeability, by transmural diffusion of FITC-Dextran**

To measure the endothelial permeability of HCMEC, cells were plated at 60,000 cells per 12-well Transwell insert (Greiner Bio-One) and grown to confluence for 24 hours in EGM-MV2. Cells were then washed with PBS and the media replaced with co-culture media (+/- Cytomix) for 24 hours. The fluorescent tracer FITC-Dextran of 40 kDa (FD40, Sigma) was added at 0.1 mg/ml in the upper chamber of the inserts (500  $\mu$ l). Immediately after adding the FITC-Dextran, Thrombin from bovine plasma (T7572, Sigma) was added in the upper chamber of the inserts as well, at a final concentration of 0.1 U/ml. After 1 hour of treatment, medium from the lower compartment was sampled in triplicates (200  $\mu$ l). Intensity of fluorescence was measured on a plate reader, at 488 nm. Endothelial permeability was calculated using the equations 1-3 (Section 2.5.3) and expressed as  $m.s^{-1}$ .

#### **4.2.5 Thrombin-induced calcium transients in EC – Optical Mapping**

Intracellular calcium transients were imaged in HCMEC using epifluorescent imaging of Fluo-4 AM signals over time, recorded using the technique of Optical Mapping (Section 2.5.4). For this experiment, HCMEC were cultured on glass bottom dishes (7 mm  $\varnothing$ , MatTek) at 20,000 cells per dish, for 24 hours in EGM-MV2, followed by 24 hours in co-culture medium. Cells were then washed with normal Tyrode's solution and incubated for 15 min with Fluo-4, before bath solution was changed and left to equilibrate at 37°C for 10 min. Images were collected at 10x magnification using a CMOS camera (Hamamatsu, Japan), at 2 Hz for 20 min. After 120 seconds, Thrombin was injected at different concentrations in the Tyrode's solution, with a pipette near the site of recording. Traces were extracted in ImageJ and analysed in Clampfit (pClamp suite). Background noise was averaged in cell-free regions and subtracted from the Fluo-4 AM fluorescence in cells. Only one dish was used per thrombin-induced calcium wave.

#### **4.2.6 Confocal imaging of DAF-2 DA fluorescence**

To measure the intracellular levels of NO in HCMEC, the cell permeable fluorescent probe for NO, 4,5-Diaminofluorescein diacetate (DAF-2 DA), was added at 1  $\mu$ M in culture medium on 60,000 HCMEC (per well of a glass-bottom 12-well plate). Cells were incubated thus for 1 hour and medium was then changed to fresh Tyrode's solution. After 5 min of equilibration at 37°C, Thrombin (0-0.1 U/ml) and/or L-NAME (10  $\mu$ M) were added to the wells and incubated for 20 min. DAF-2 images were collected using a Zeiss LSM-780 inverted microscope, at 488/515 nm (ex./em.) and at a 63x magnification. The DAF-2 fluorescence intensity was corrected for background noise and averaged as pixel intensity for each cell using ImageJ.

#### **4.2.7 Human XL Cytokine Profiler™ Array**

To identify cytokines and chemokines differentially secreted by HCMEC after treatment with Cytomix, culture supernatants (1 ml) were collected from the lower compartment of Transwell cultures. Samples were centrifuged at 18,000 *g* for 12 min (at 4°C) to remove cells and debris, and were stored at -80°C until used. For UT and Cytomix, two biological samples were pooled together to be used on a single membrane and two membranes were used per conditions (i.e. 4 biological samples in total). For TNF $\alpha$ , IL-1 $\beta$  and hIL-6-treated HCMEC, only one membrane could be used (in this case three biological samples were pooled in each condition). The array kit was used as per manufacturer's recommendations (ARY022B, R&D), the array membranes were imaged by ECL using radiographic films, and data were analysed with ImageJ. Proteins detected by the array are listed in Table 4.1.

#### **4.2.8 Enzyme-Linked Immunosorbent Assay (ELISA)**

The level of CXCL5, CXCL1, G-CSF, GM-CSF and ET-1 were quantified in the supernatants of HCMEC, ARVM, HCMEC-ARVM Transwell co-cultures and adult cardiac fibroblasts using ELISA kits: DuoSet ELISAs for CXCL5 (DY254, R&D), CXCL1 (DY275, R&D), G-CSF (DY214,

R&D) and GM-CSF (DY215, R&D), were used with the DuoSet ancillary reagent kit (DY008, R&D). A Quantikine™ ELISA was used to detect ET-1 (DET100, R&D). The kits were all used as per manufacturer's recommendations. Cells were cultured (or co-cultured) for 4 hours, media were collected and processed as in Section 4.2.7. Samples were run in technical duplicates. Data were collected using a plate reader measuring optical density at 450 nm (with readings at 562 nm subtracted).

**Table 4.1: Analytes detected in the Proteome Human XL Cytokine Profiler™ Array kit**

<b>Adiponectin</b>	<b>CXCL4</b>	<b>IL-3</b>	<b>M-CSF</b>
<b>ApoA1</b> (Apolipoprotein A-1)	<b>CXCL5</b> (ENA-78)	<b>IL-4</b>	<b>MIF</b>
<b>Angiogenin</b>	<b>CXCL8</b> (IL-8)	<b>IL-5</b>	<b>MMP-9</b>
<b>Ang-1</b> (Angiopoietin-1)	<b>CXCL9</b>	<b>IL-6</b>	<b>MPO</b> (Myeloperoxidase)
<b>Ang-2</b> (Angiopoietin-2)	<b>CXCL10</b>	<b>IL-8</b> (CXCL8)	<b>OPN</b> (Osteopontin)
<b>BAFF</b>	<b>CXCL11</b>	<b>IL-10</b>	<b>PDGF-AA</b>
<b>BDNF</b> (Brain-derived Neurotrophic Factor)	<b>CXCL12</b>	<b>IL-11</b>	<b>PDGF-AA/BB</b>
Complement Component <b>C5/C5a</b>	<b>Cystatin C</b>	<b>IL-12 p70</b>	<b>Pentraxin-3</b>
<b>CCL2</b> (MCP-1)	<b>Dkk-1</b> (Dickkopf-1)	<b>IL-13</b>	<b>RAGE</b>
<b>CCL3/CCL4</b> (MIP-1 $\alpha$ /MIP-1 $\beta$ )	<b>EGF</b> (Epidermal Growth Factor)	<b>IL-15</b>	<b>RANTES</b>
<b>CCL7</b> (MCP-3)	<b>Fas Ligand</b>	<b>IL-16</b>	<b>RBP-4</b>
<b>CCL17</b>	<b>FGF basic</b>	<b>IL-17</b>	<b>Relaxin-2</b>
<b>CCL19</b> (MIP-3 $\beta$ )	<b>FGF-7</b>	<b>IL-18 Bpa</b>	<b>Resistin</b>
<b>CCL20</b> (MIP-3 $\alpha$ )	<b>FGF-19</b>	<b>IL-19</b>	<b>Serpin E1</b>
<b>CD14</b>	<b>Fit-3 Ligand</b>	<b>IL1RL1</b> (ST2)	<b>SHBG</b>
<b>CD26</b>	<b>G-CSF</b>	<b>IL-22</b>	<b>TFF3</b>
<b>CD30</b>	<b>GM-CSF</b>	<b>IL-23</b>	<b>TGF-<math>\alpha</math></b>
<b>CD31</b> (PECAM-1)	<b>Growth Hormone</b>	<b>IL-24</b>	<b>TSP-1</b> (Thrombospondin-1)
<b>CD 40 ligand</b> (TRAP)	<b>HGF</b>	<b>IL-27</b>	<b>TNF-<math>\alpha</math></b>
<b>CD71</b>	<b>ICAM-1</b> (CD54)	<b>IL-31</b>	<b>uPAR</b>
<b>CD105</b> (Endoglin)	<b>IFN-<math>\gamma</math></b>	<b>IL-32</b>	<b>VEGF</b>
<b>CD147</b> (Emmprin)	<b>IGFBP-2</b>	<b>IL-33</b>	<b>Vitamin D BP</b>
<b>Chitinase 3-like 1</b>	<b>IGFBP-3</b>	<b>IL-34</b>	<b>TIM-3</b>
<b>Complement Factor D</b>	<b>IL-1<math>\alpha</math></b>	<b>Kallikrein 3</b>	<b>VCAM-1</b> (CD106)
<b>CRP</b> (C-Reactive Protein)	<b>IL-1<math>\beta</math></b>	<b>Leptin</b>	<i>Negative Controls</i>
<b>Cripto-1</b>	<b>IL-1ra</b>	<b>LIF</b>	/
<b>CXCL1</b> (GRO $\alpha$ )	<b>IL-2</b>	<b>Lipocalin-2</b>	/



#### 4.2.9 Meta-analysis

CM cytokine and chemokine receptor mRNA expression was investigated using datasets available online: Tabula Muris is a single-cell transcriptomics dataset obtained from 20 mouse organs (7 mice)<sup>208</sup>. Gene count was derived from a SMART-Seq2 RNAseq library prepared from individually FACS sorted cells. Data were obtained from the open platform Figshare (find at <https://tabula-muris.ds.czbiohub.org/>). Besides the raw RNA count for each gene of interest, cells were also counted as positive for a certain gene when the cell RNA count was superior or equal to 10.

To use a different model and a different method of analysis, a microarray for mRNA expression in neonatal and adult Sprague-Dawley rat ventricular CM was examined<sup>209</sup>. This was performed at N = 6 using an Affymetrix GeneChip™ Rat Genome Array 230 2.0 (A-AFFY-43), covering 31,000 gene transcripts (Expression Atlas – E-MTAB-2832). Data were normalised by Robust Multi-array Average using the Oligo 1.36.1 package (R). Extraction of data was done with the help of Robert Maughan, PhD.

#### 4.2.10 Statistics

Data are shown as mean +/- SEM. A D'Agostino-Pearson test was used to test the normality of sample distributions. Statistical significance was then calculated to compare >2 groups with each other, or multiple samples to the control group, using an ordinary one-way ANOVA with Bonferroni's post-hoc test (parametric) or a Welch's ANOVA with Dunnett's T3 correction for multiple comparisons (non-parametric) were used. Significance is shown as: \* p < 0.05. \*\* p < 0.01. \*\*\* p < 0.001. \*\*\*\* p < 0.0001.

## 4.3 Results

### 4.3.1 Inflammatory signalling in EC after treatment with TNF $\alpha$ , IL-1 $\beta$ or hIL-6 alone

To establish the formulation of a suitable pro-inflammatory treatment for HCMEC, each of the three candidate cytokines was first validated separately. The aims were to keep the incubation period constant for all conditions and identify the concentrations capable of inducing significant expression of known pro-inflammatory target genes with the lowest probability of non-specific effects. This was demonstrated using western blotting. As depicted in Figures 4.1A-B, TNF $\alpha$  and IL-1 $\beta$  both induced a significant expression of VCAM-1 after 24h, at and above 1 ng/ml.

There is still some debate as to the presence of a canonical IL-6 signalling in endothelial cells. However, preliminary experiments failed to detect expression of the IL-6 target gene ICAM-1 in HCMEC after 24 hours treatment with human recombinant IL-6 alone, up to 100 ng/ml (data not shown). To allow for trans-signalling of IL-6 to occur, whereby IL-6 binds extracellularly to its soluble receptor prior to contact with target cells, HCMEC were treated with IL-6/sIL-6R $\alpha$ , a chimeric compound branded as Hyper-IL-6 (hIL-6) at 25 ng/ml, as described in Section 4.1. As shown in Figure 4.1C, there was a significant increase of STAT3 phosphorylation on S727 in HCMEC compared to untreated controls (4.3-fold,  $p < 0.05$ ) after a 30 min incubation with hIL-6. Interferon- $\alpha$  (IFN- $\alpha$ ) was used as a positive control for the phosphorylation of STAT3<sup>305</sup>, at 1 ng/ml (~100 U/ml). STAT3 phosphorylation was lost by 24h ( $p = 0.0096$  for hIL-6). However, after 24 hours of treatment with hIL-6 there was a significant induction of ICAM-1 expression (26-fold,  $p < 0.05$  vs UT) and unexpectedly also MnSOD (6-fold,  $p < 0.05$ ), as seen in Figure 4.1D. VCAM-1 expression was also increased by 4-fold but not significantly, while known target genes of TNF $\alpha$  or IL-1 $\beta$  signalling in EC were not affected by hIL-6 (eNOS, iNOS, A20, HO-1 and TRAF6:  $p > 0.2$ ). For further experiments, TNF $\alpha$ , IL-1 $\beta$  and hIL-6 were used at 1 ng/ml, 1 ng/ml and 25 ng/ml respectively, all for 24h.

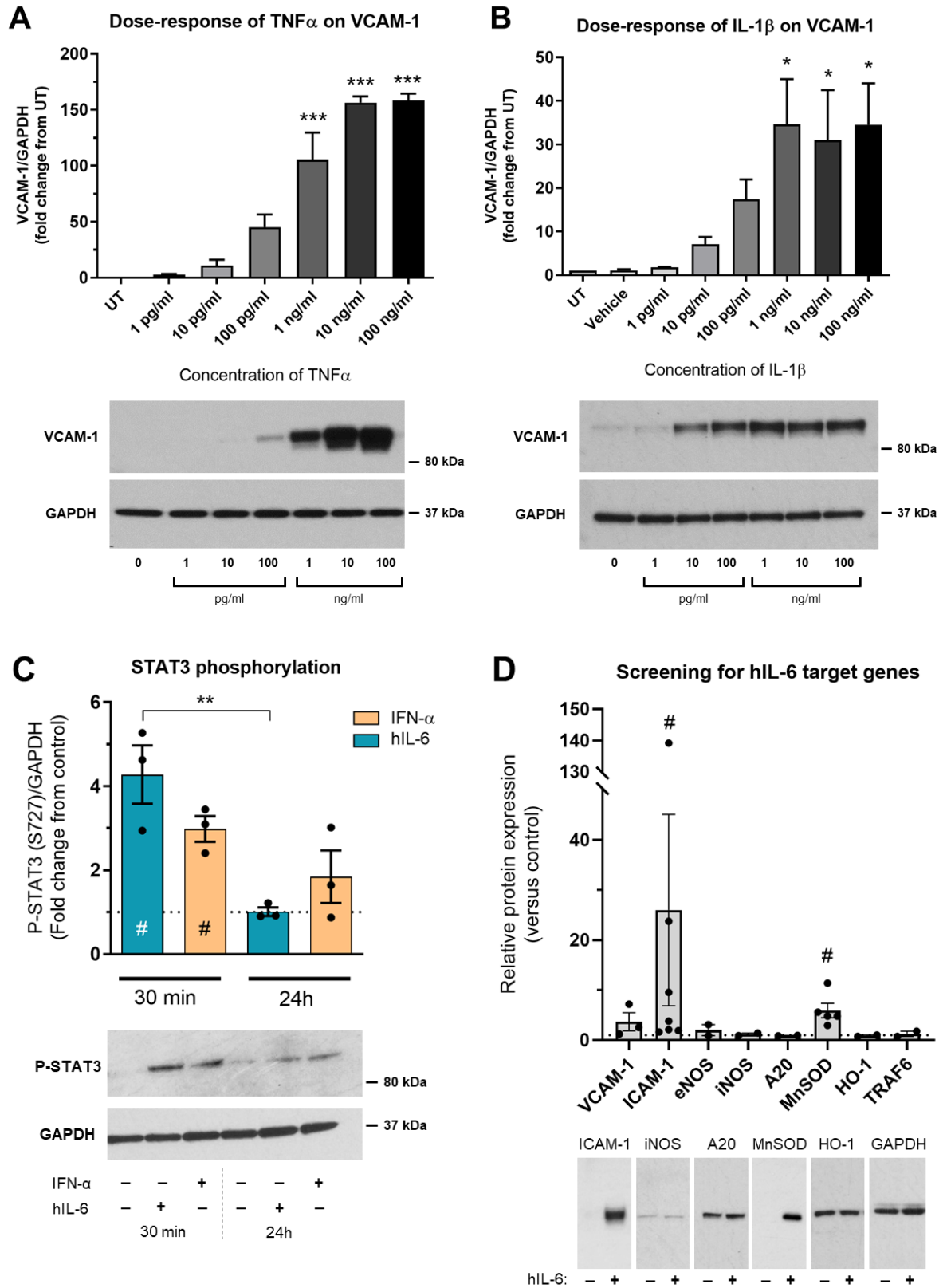


**Figure 4.1** (continued)

**Figure 4.1: Induction of pro-inflammatory markers validating the use of TNF $\alpha$ , IL-1 $\beta$  and hIL-6 at tested concentrations in HCMEC in vitro**

Quantification of protein expression by western blotting in HCMEC 24 hours after treatment with pro-inflammatory cytokines. **A-B.** Expression of VCAM-1 after TNF $\alpha$  (A) or IL-1 $\beta$  (B) treatment at various concentrations, and representative blots for VCAM-1 and loading control GAPDH. N = 3 (A), 5 (B). **C.** Phosphorylation of STAT3 on S727 after hIL-6 treatment for 30 min or 24 hours. IFN- $\alpha$  serves as a positive control. Data were compared with an ordinary one-way ANOVA and Bonferroni's correction. (lower panel) Representative blots. N = 3. **D.** Relative expression for a small panel of proteins known to be regulated in EC during inflammation: VCAM-1, ICAM-1, eNOS, iNOS, A20, MnSOD, HO-1, and TRAF6, with representative blots. N = 3, 7, 2, 2, 2, 5, 2, 2, respectively. Data are expressed as mean  $\pm$  SEM and compared to control (untreated) using a one-way ANOVA and Bonferroni's correction. \* p < 0.05. \*\* p < 0.01. \*\*\* p < 0.001. # p < 0.05 versus untreated.

**4.3.2 Protein expression of inflammatory markers in EC is cytokine-dependent and distinct in the cytokine co-treatment (Cytomix)**

Given the differences of cell signalling and protein expression profiles in response to TNF $\alpha$  or IL-1 $\beta$  and hIL-6, as shown above, it was of interest to determine if a co-treatment would induce a different inflammatory response in EC and to characterise this effect (e.g. based on additive, antagonistic or synergistic interactions of cytokine signalling). HCMEC were either treated with TNF $\alpha$ , IL-1 $\beta$ , hIL-6, individually or as a cocktail of all three (Cytomix). Protein expression was then measured by western blotting after 24 hours (Figure 4.2). First, only after treatments with TNF $\alpha$  or IL-1 $\beta$  was VCAM-1 expression significantly increased above that in untreated EC (p < 0.05 and 0.01 respectively). Surprisingly, VCAM-1 induction was markedly reduced after co-treatment of cytokines (3-fold with Cytomix compared to 85-fold with TNF $\alpha$ , p < 0.01), bringing VCAM-1 upregulation down to that seen with the hIL-6 treatment group (4-fold). TNF $\alpha$  also induced significantly more VCAM-1 expression than in IL-1 $\beta$ -treated EC (35-fold increase only, p < 0.05). In this experiment, expression of ICAM-1 was found significant compared to control after IL-1 $\beta$  treatment, though Cytomix treatment approached significance (p = 0.07) (as seen

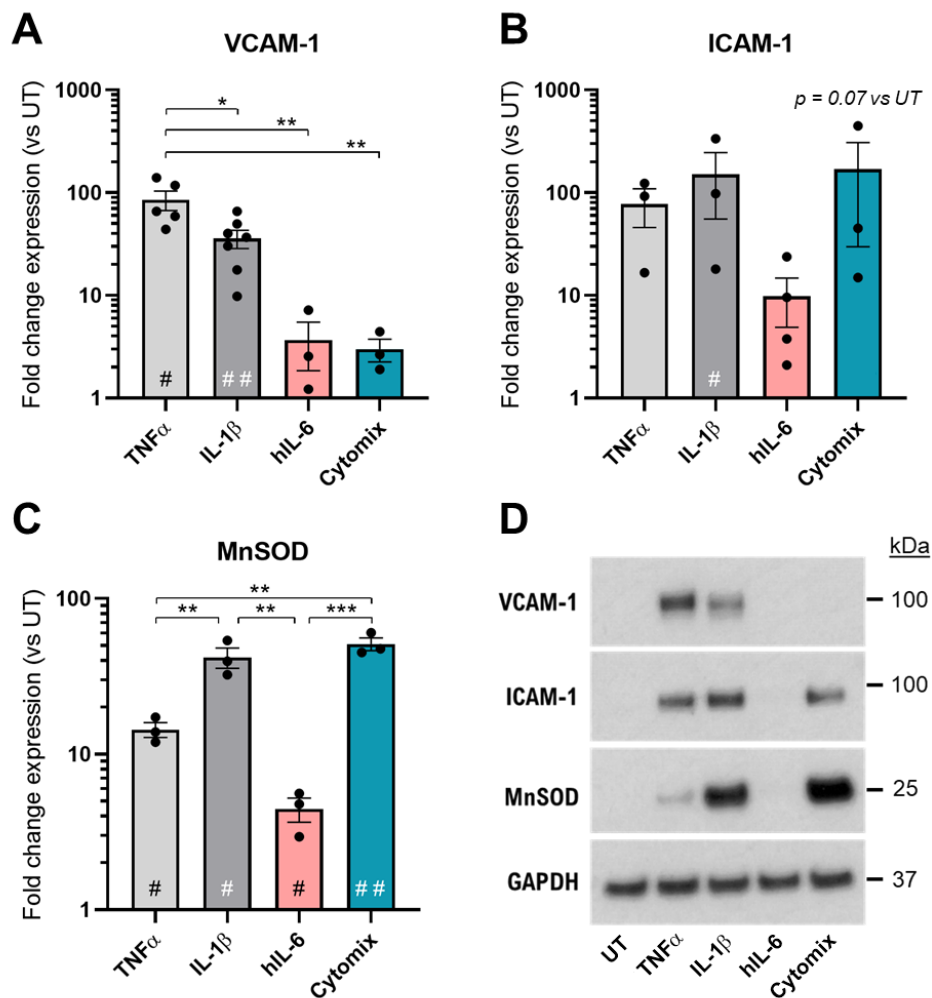


**Figure 4.2: Expression profiles of markers of cytokine activity were cytokine-specific, and the effect of cytokines co-treatment was not additive or synergistic**

Protein expression quantified in HCMEC 24 hours after treatment with TNF $\alpha$ , IL-1 $\beta$ , hIL-6 or Cytomix (TNF $\alpha$  + IL-1 $\beta$  + hIL-6), using Western blotting. Data are shown as fold change from the UT group.

**A-C.** Bar graphs showing respectively the mean relative expression of VCAM-1, ICAM-1 and MnSOD. N = 3-7. Data are expressed as mean +/- SEM. Statistical analysis was carried out with a one-way ANOVA with Bonferroni's post-hoc test \*  $p < 0.05$ . \*\*  $p < 0.01$ . \*\*\*  $p < 0.001$ . #  $p < 0.05$ , ##  $p < 0.01$  vs control. **D.** Representative blots for VCAM-1, ICAM-1, MnSOD and the loading control GAPDH.

in Figure 4.2B). Although the induction of ICAM-1 was reliably found to be lower after the hIL-6 treatment compared to other cytokines or Cytomix (9.8-fold vs 77-fold, 150-fold and 169-fold for TNF $\alpha$ , IL-1 $\beta$  and Cytomix respectively), this was not statistically confirmed, probably due to the low n number. As seen in Figure 4.2C, MnSOD expression was not specific to hIL-6, where expression was lower than after IL-1 $\beta$  or Cytomix treatment (4.5-fold vs 42-fold and 51-fold respectively,  $p < 0.01$  and  $p < 0.001$ ). Similarly, MnSOD induction by TNF $\alpha$  was of lesser magnitude than in IL-1 $\beta$  and Cytomix groups (with a 14-fold increase,  $p < 0.01$ ).

#### **4.3.3 Cell cycle progression was arrested at G1 in HCMEC after Cytomix treatment**

To determine if the cytokine co-treatment (Cytomix) introduced above recapitulates the effects of inflammation on EC proliferation, cell cycle progression was measured by flow cytometry in HCMEC (Figure 4.3). For this experiment, HCMEC were fixed, permeabilised and stained with propidium iodide at 0 hours ( $t_{(0)}$ ), or at 24 hours of culture in co-culture medium enriched with 10% FBS (as a positive control for proliferation) or in normal 1% FBS co-culture medium with or without Cytomix (TNF $\alpha$ , 1 ng/ml; IL-1 $\beta$ , 1 ng/ml; hIL-6, 25 ng/ml). Representative cytometric histograms with cell populations are shown in Figure 4.3A, with the G1, G2 and S phases of cell cycle differentiated by an algorithm (in-built in FSC Express). In Figure 4.3B it can be seen that the Cytomix treatment was characterised by a significantly lower percentage of HCMEC at the S or G2 phases than at  $t_{(0)}$ , but also compared to untreated cells grown in 1 or 10% FBS (16% cells at G2/S with Cytomix, versus 36% at  $t_{(0)}$  and 32% in UT group,  $p < 0.01$  and 0.05 respectively). Of note, there was no difference between 1% or 10% serum in this case, nor a change of proliferation between 0 and 24 hours of culture in the co-culture medium, whether enriched with FBS or not. This experiment was performed with HCMEC plated at low density (100,000 per well of 6-well plate). Cell cycle analysis was also performed at the usual HCMEC culture density of 320,000 cells per well, but this resulted in a dampened proliferation in basal conditions (including with 10% FBS) due to cell confluence (data not shown).

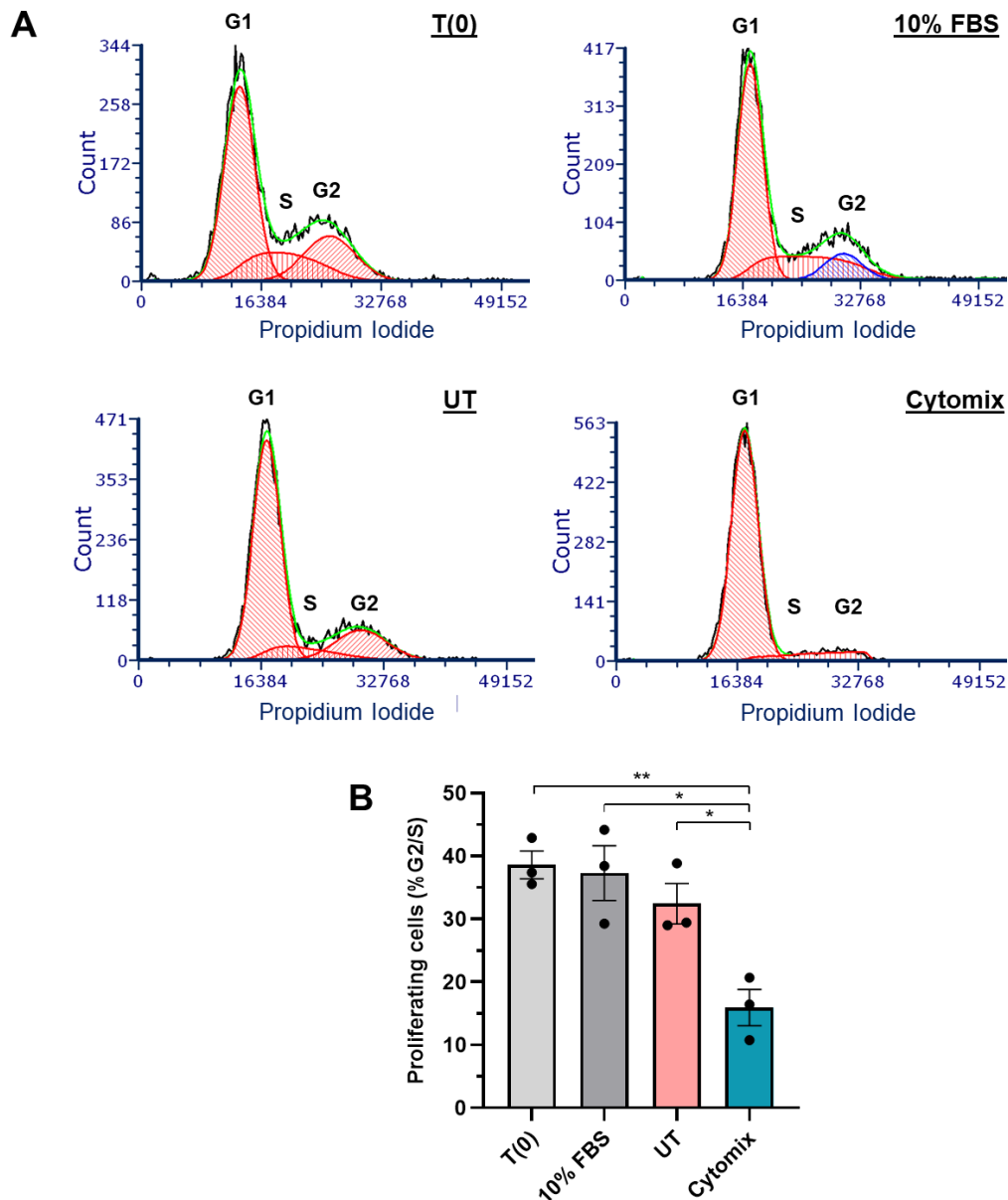


**Figure 4.3: Cytomix treatment induced cell cycle arrest at G1 in HCMEC**

Flow cytometric analysis of cell cycle progression in HCMEC after 24 hours of treatment with Cytomix *in vitro* compared to control (UT), 0 hours of treatment (T(0)), or 24 hours in co-culture medium with 10% FBS, by intracellular staining of Propidium Iodide. **A.** Representative flow cytometry histograms with automated classification of cells by their position in the cell cycle using FCS Excess algorithms. **B.** Percentage of HCMEC in the G2 or S phases after treatment, considered proliferative. N = 3. Data are represented as mean +/- SEM. Statistical analysis was carried out with a one-way ANOVA with Bonferroni's multiple comparisons test. \* p < 0.05. \*\* p < 0.01.

#### 4.3.4 Effect of Cytomix on basal and thrombin-induced endothelial permeability

Because pro-inflammatory conditions have been known to promote endothelial permeability, with fenestration of intercellular junctions and leakage from the vascular wall<sup>298,306</sup>, the effects of Cytomix on basal and thrombin-induced permeability of EC monolayers were investigated. To test this, the trans-endothelial diffusion of FITC-Dextran (40 kDa) was used as a measure of permeability (Figure 4.4). First, the limits of detection for FITC-Dextran were defined using a range of concentrations in medium (1 pg/ml to 1 mg/ml), as seen in Figure 4.4A. At least down to 1 pg/ml the detection of FITC was highly accurate ( $R^2 = 0.9967$ ). This was performed in technical triplicates. Next it was necessary to test if coating the insert membrane with gelatine hindered the basal diffusion of FITC-Dextran, even before cells could be plated. This was addressed by measuring “abluminal” concentration of FITC-Dextran, 1 hour after application in the “luminal” compartment of the Transwell system, i.e. diffusion from the insert to the lower compartment (Figure 4.4B). Plating HCMEC in the insert led to a 63% decrease of diffused FITC-Dextran compared to empty membranes ( $p < 0.001$ ), and a significant 57% reduction compared to the gelatine-coated inserts ( $p < 0.01$ ). There was no change of diffusion caused by the gelatine coating alone, compared to empty inserts ( $p = 0.32$ ). Measured FITC-Dextran concentrations ranged from  $4.5 \times 10^{-4}$  mg/ml, with HCMEC, to  $1.4 \times 10^{-3}$  mg/ml, in empty inserts. As demonstrated above, this is well within the limits of linearity for the quantification of FITC-Dextran. Finally, permeability of monolayers was measured 1 hour after 0.1 U/ml of thrombin was applied in the top compartment of inserts (Figure 4.4C). In untreated conditions, the calculated endothelial permeability  $P(EC)$  rose from  $9.4 \times 10^{-5}$  m.s<sup>-1</sup> to  $4.2 \times 10^{-4}$  m.s<sup>-1</sup> after thrombin application, a 4.47-fold change compared to control. However, due to variability in the thrombin group this was not statistically significant, and more repeats are thus warranted to confirm this effect. There was no statistical difference of basal  $P(EC)$  between the UT and Cytomix groups, and interestingly thrombin did not increase  $P(EC)$  in Cytomix pre-conditioned samples.



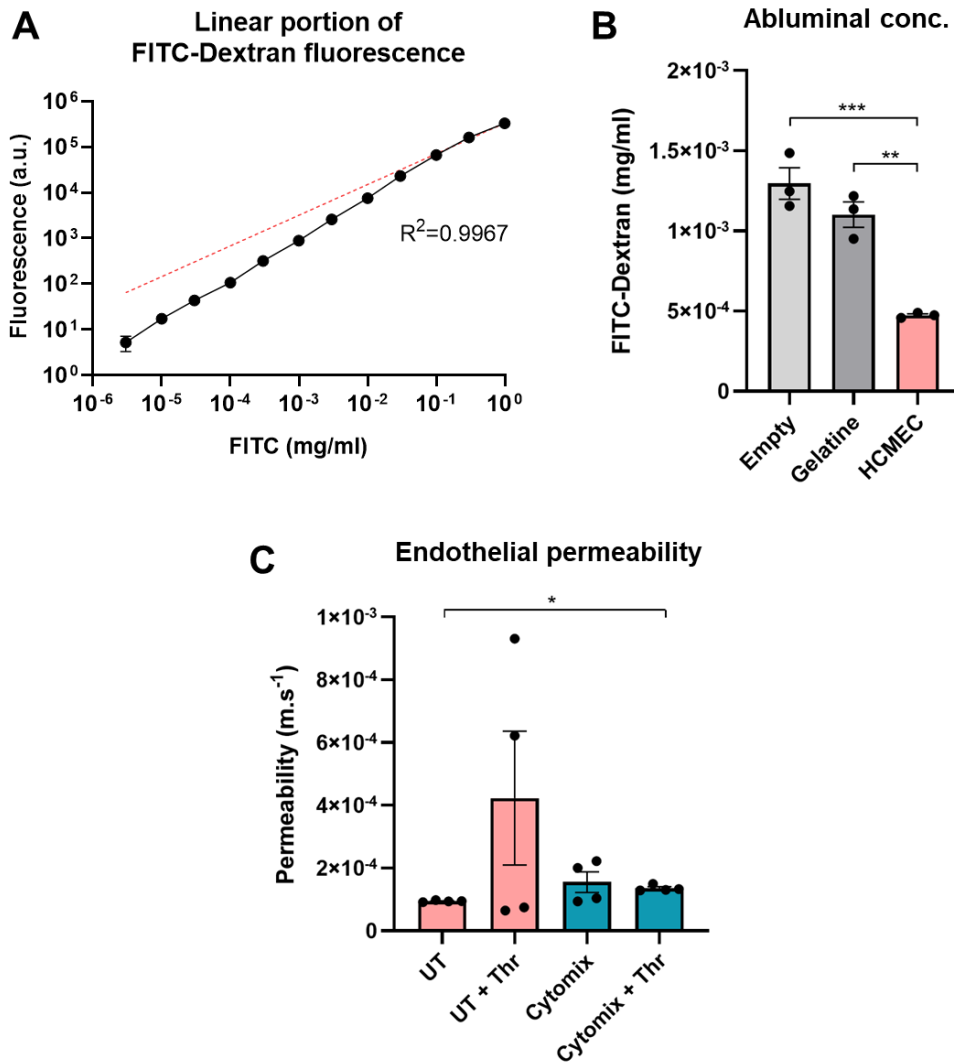


**Figure 4.4: Cytomix treatment did not affect basal permeability in HCMEC monolayers but might affect the response of EC to thrombin**

Endothelial permeability after Cytomix treatment for 24 hours, as measured by the diffusion of FITC-Dextran (40 kDa) across EC monolayers. **A.** Linear relationship between FITC-Dextran concentration (mg/ml) and fluorescence (a.u.). Red line = linear fit.  $R^2$  value is shown in the graph. **B.** Concentration of FITC-Dextran in the lower chamber of a Transwell system (abluminal side) after diffusion through a bare insert membrane (empty), after coating with gelatine, or through HCMEC monolayers.  $N = 3$ . Data were compared with a one-way ANOVA and Bonferroni's post-hoc test. **C.** Permeability of EC monolayers before and after treatment with thrombin (0.1 U/ml).  $N = 4$ . Due to unequal SD, statistical analysis was carried out here with Welch's ANOVA, and Dunnett's T3 multiple comparison test. Data are represented as mean  $\pm$  SEM. \*  $p < 0.05$ . \*\*  $p < 0.01$ . \*\*\*  $p < 0.001$ .

#### 4.3.5 Effect of Cytomix on thrombin-induced calcium transients in HCMEC

The release of  $\text{Ca}^{2+}$  from intracellular stores (and an influx of extracellular  $\text{Ca}^{2+}$ ) is responsible for the increased endothelial permeability that is seen in response to thrombin<sup>64</sup>. Moreover, this was shown to be regulated by inflammatory cytokines such as  $\text{TNF}\alpha$ <sup>61</sup>. To test if the absence of thrombin-induced permeability after Cytomix treatment could be explained by a change in calcium transient morphology in EC, free cytosolic  $\text{Ca}^{2+}$  was imaged in HCMEC using Fluo-4 AM. The frequency of spontaneous calcium transients in the UT and Cytomix groups was too low to provide data of sufficient quality (data not shown). However, as was expected, thrombin induced reproducible calcium transients in a concentration-dependent manner (Figure 4.5).

As seen in Figure 4.5B, the scale of thrombin-induced calcium transients was dramatically smaller after Cytomix pre-conditioning compared to UT conditions. As a result, the duration of transient was also greatly reduced compared to control, as illustrated in Figure 4.5C for which the transients were normalised to their amplitude. Figures 4.5D and 4.5E show that thrombin-induced calcium transients were only significantly affected by Cytomix at 0.1, 1, 10, but not at 0.05 U/ml of thrombin ( $p > 0.05$ ). Interestingly, the amplitude of transients in UT cultures rose from 11 to 20 between 0.05 and 10 U/ml of thrombin (note: not significantly) but it was mostly unaffected by thrombin concentration in the Cytomix group. Conversely, while the duration of the transient was mostly unaffected by thrombin concentration in the UT group (it increased non-significantly from 122 to 159 s), it was significantly reduced from 87 to 44 s between 0.05 and 10 U/ml of thrombin after Cytomix pre-conditioning.

This suggests that the adaptive response of endothelial calcium homeostasis to thrombin is disrupted by the treatment with Cytomix. Furthermore, the reduction in amplitude and shorter duration of calcium transients shown in this experiment may well explain the lack of thrombin-induced endothelial permeability which was described in the previous section.

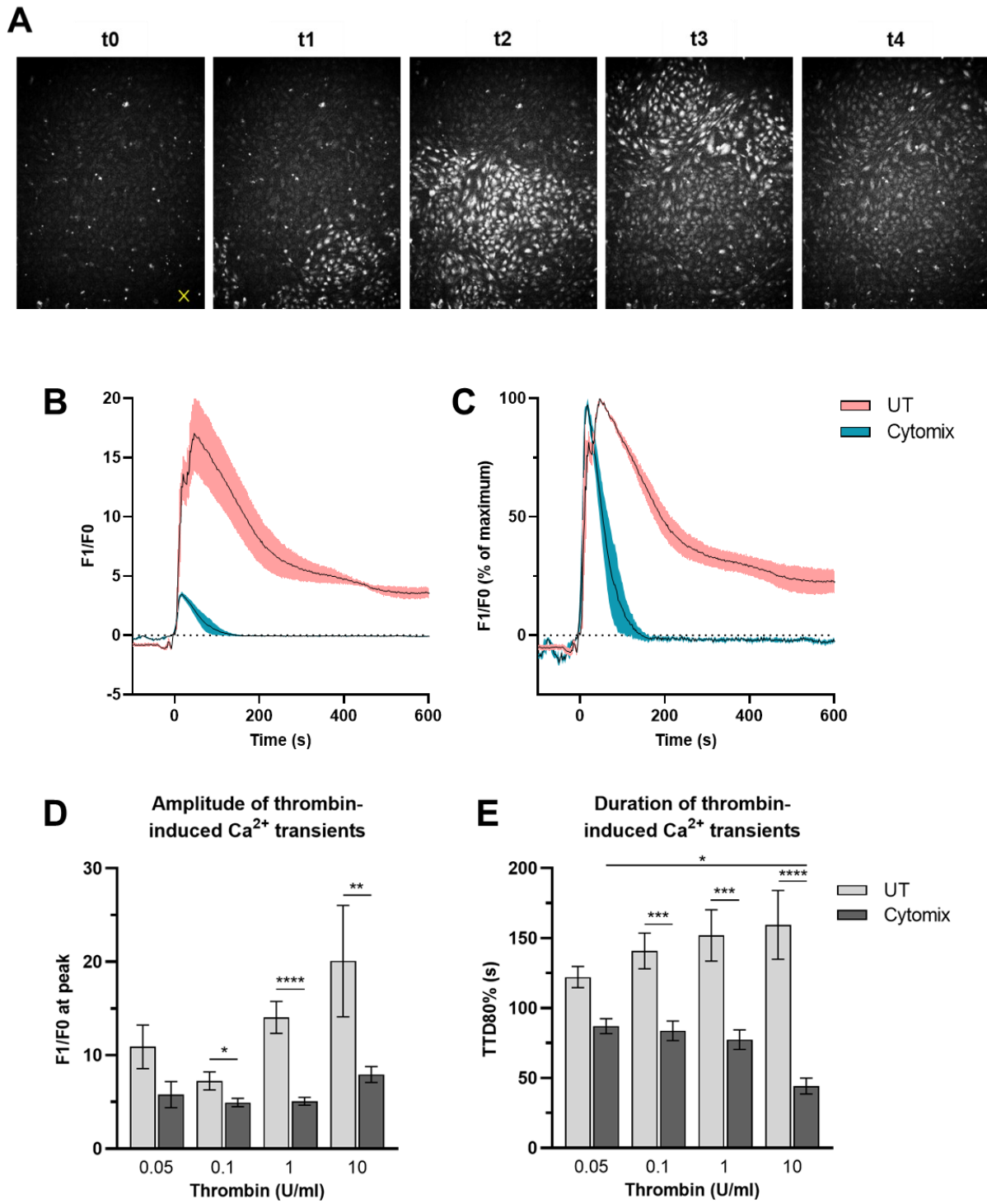


**Figure 4.5** (continued)

#### **Figure 4.5: Cytomix treatment attenuated both the amplitude and duration of thrombin-induced calcium transients in HCMEC**

Optical mapping recording of calcium transients in HCMEC *in vitro*, using Fluo-4 AM and following an acute delivery of thrombin. HCMEC were pre-conditioned with Cytomix for 24 hours before the experiment. **A.** Representative time course of calcium transients after thrombin application (at the yellow cross), during which images of Fluo-4 AM fluorescence were collected every minute at 10x magnification (t<sub>0</sub> to t<sub>4</sub>). **B.** Averaged representative traces of calcium transients with amplitude corrected for the basal Fluo-4 AM intensity and background noise (F<sub>1</sub>/F<sub>0</sub>). n = 3. SEM is shown as a coloured region. **C.** Averaged representative traces (n = 3) of calcium transients normalised to the peak amplitude. **D.** Amplitude of calcium transients after the treatment with thrombin at different concentrations. **E.** Duration of calcium transients expressed as the time to reach 80% of signal decay from the start of the transient (TTD<sub>80%</sub>), after thrombin treatment. n = 20 technical replicates. Data are expressed as mean +/- SEM and compared with Welch's ANOVA and Dunnett's T3 post-hoc test. \* p < 0.05. \*\* p < 0.01. \*\*\* p < 0.001. \*\*\*\* p < 0.0001.

#### **4.3.6 Effect of Cytomix on basal and thrombin-induced NO synthesis in HCMEC**

Thrombin is also known to stimulate eNOS activity, and therefore the synthesis of NO in EC<sup>64</sup>. Interestingly, this mechanism involves the intracellular calcium release which was investigated above<sup>63</sup>. Given the absence of thrombin-induced permeabilization (a signalling target of eNOS-produced NO<sup>62</sup>) and impaired calcium homeostasis in EC after treatment with Cytomix, it was hypothesised that thrombin-induced NO production would also be affected by Cytomix. It was also important to test the basal unstimulated synthesis of NO since any difference would have important repercussions for the interpretation of EC-CM co-culture effects. Using a cell-permeable fluorescent indicator for NO, DAF-2 DA, the intracellular NO level was imaged in living cells by confocal microscopy (Figure 4.6A).

Bradykinin was tested in preliminary experiments as an independent inducer of NO, at a range of concentrations from 10<sup>-10</sup> to 10<sup>-4</sup> M. Images were collected every 20 s for 20 min (data not shown). Surprisingly, there was no detectable increase of DAF-2 intensity in UT EC at any

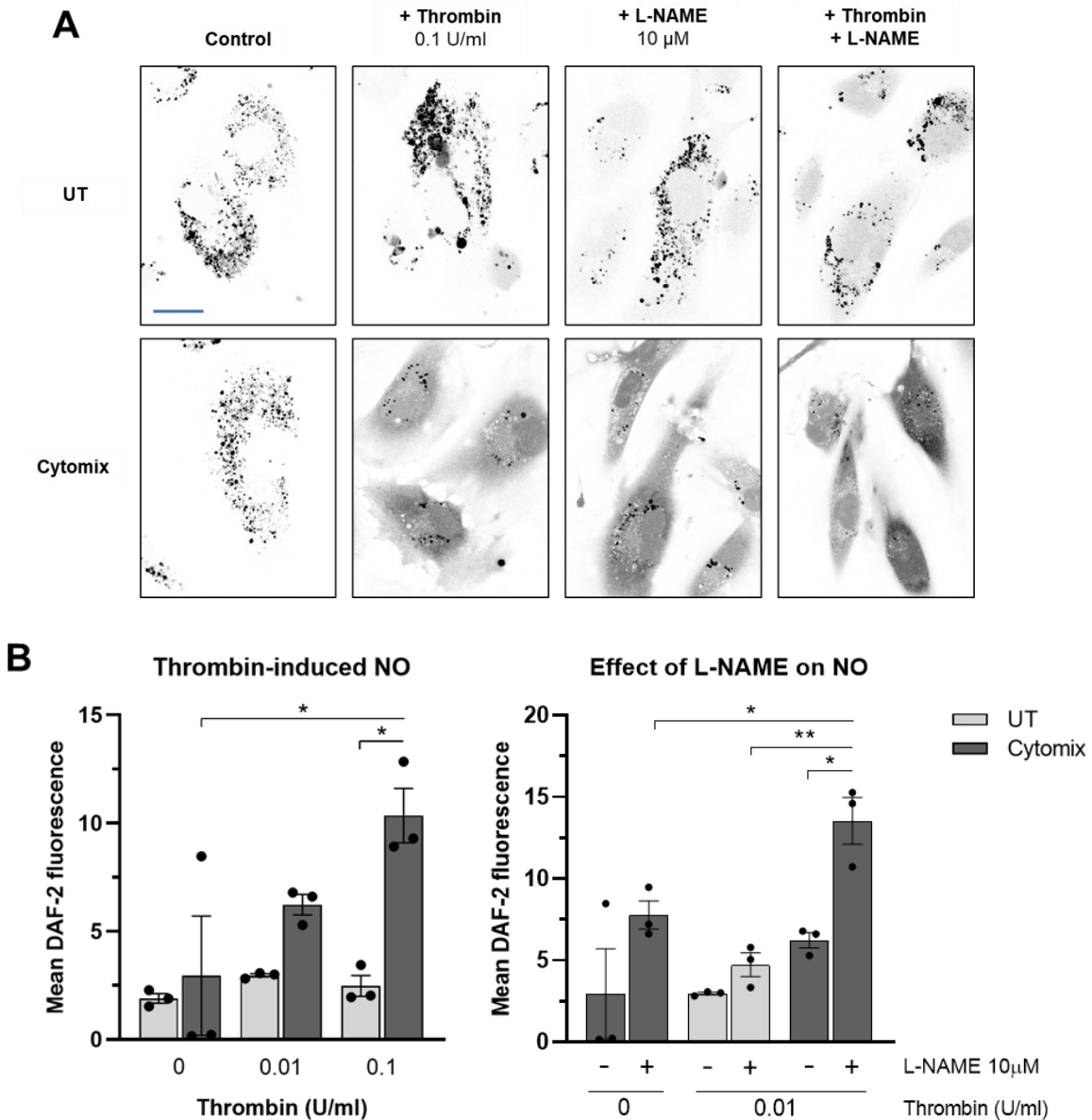


**Figure 4.6: Cytomix treatment increased the synthesis of NO in vitro after thrombin or after L-NAME application in HCMEC, but not the basal levels of intracellular NO**

Confocal microscopic imaging of DAF-2 DA fluorescence in HCMEC after Cytomix pre-conditioning, and treatment with thrombin and/or L-NAME. **A.** Representative images of DAF-2 DA fluorescence, at 63x magnification. Images are shown as inverted greyscale. Blue bar = 30 µm. **B.** (left panel) DAF-2 DA fluorescence (pixel densitometry) averaged per cell, 20 min after treatment with 0, 0.01 or 0.1 U/ml of thrombin. (right panel) DAF-2 DA fluorescence 20 min after treatment with 0 or 0.01 U/ml of thrombin, 10 µM of L-NAME, or thrombin + L-NAME co-treatments. n/N = 10/3 (images per replicate / technical replicates). Data are expressed as mean +/- SEM, and points show technical replicates (N). Analysis was done on N values using an ordinary one-way ANOVA and Bonferroni's post-hoc test. \* p < 0.05. \*\* p < 0.01.

concentration of bradykinin. As seen in Figure 4.6B, there was also no production of NO after 60 min treatments of UT EC with thrombin (at 0.01 and 0.1 U/ml), again contrary to published reports<sup>62</sup>. However, and even more surprisingly, application of thrombin at 0.1 U/ml induced a significant increase of DAF-2 fluorescence in HCMEC pre-treated with Cytomix, compared to the baseline fluorescence (3.5-fold change,  $p = 0.021$ ). As a result, NO synthesis was greater in the Cytomix group than in the UT group, with thrombin used at 0.1 U/ml (4.2-fold change,  $p = 0.013$ ). At 0.01 U/ml of thrombin, the effects of Cytomix and thrombin were not significant.

There was no detectable difference between the basal NO synthesis in UT and Cytomix-pre-treated EC, though this lack of effect is still statistically inconclusive due to high variability. To confirm that the Cytomix-specific increase of DAF-2 intensity by thrombin was indeed NO, the well-established NO synthase inhibitor L-NAME was used in cultures for 20 min, at 10  $\mu$ M. As shown in Figures 4.6A and 4.6B however, L-NAME increased NO levels in the Cytomix-treated cells compared to baseline, without any thrombin (2.6-fold change, though note that  $p = 0.14$ ), instead of decreasing DAF-2 signal intensity. When added to 0.01 U/ml of thrombin, L-NAME still induced a negligible and non-significant increase of DAF-2 signal in UT. After Cytomix pre-conditioning however, L-NAME + thrombin induced a significantly larger production of NO than thrombin alone (2.2-fold change,  $p = 0.013$ ), L-NAME alone (1.7-fold change,  $p = 0.05$ ) or in UT (2.9-fold change,  $p = 0.0032$ ). Due to timeline restrictions no other inhibitor of NO could be tested to investigate the counterintuitive effects of thrombin and L-NAME in this experiment.

#### **4.3.7 Screening for EC-secreted inflammatory markers and candidate mediators for the paracrine effects of EC on CM**

To further validate that the Cytomix treatment generates a pro-inflammatory phenotype in EC, at least with regards to their paracrine activity, and to potentially bring to light soluble mediators contributing to the effects of EC-CM co-culture in future experiments (Chapter 5), the culture

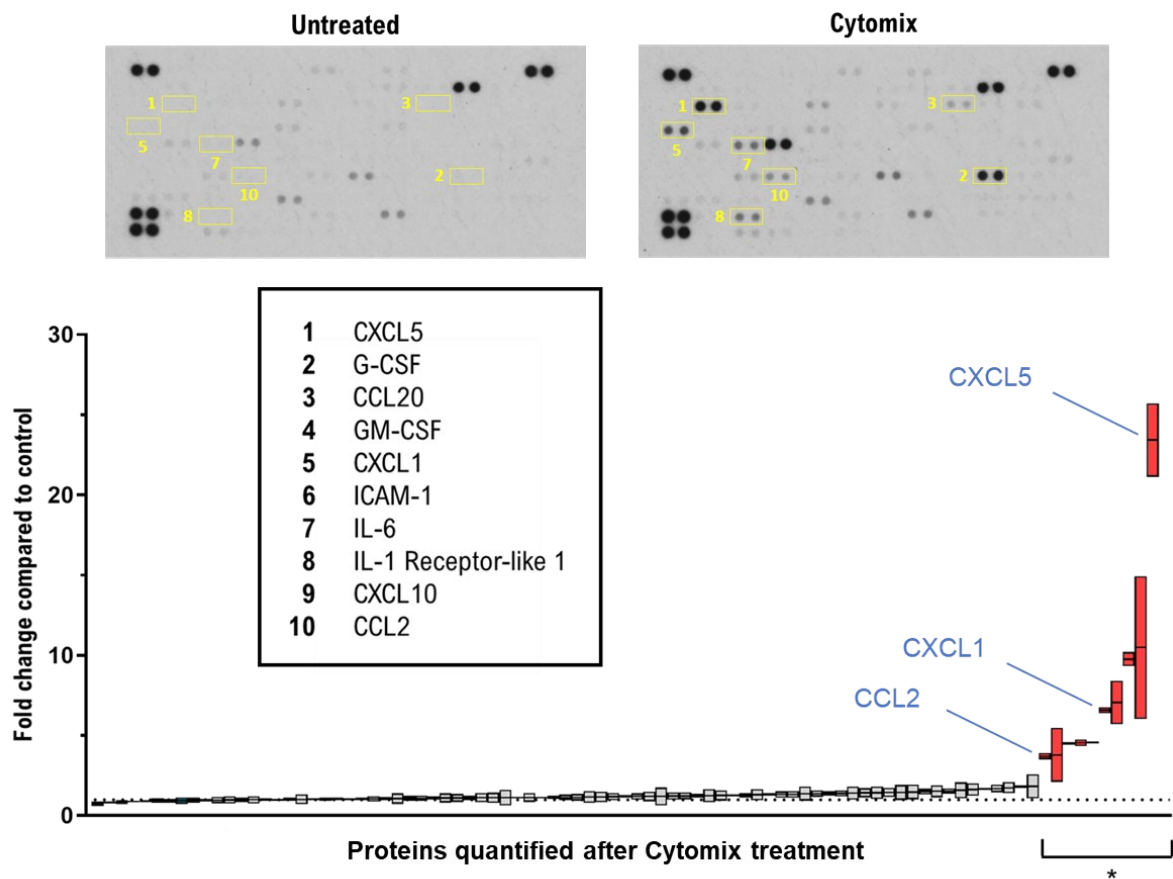


**Figure 4.7: Cytomix treatment stimulated the secretion of 10 pro-inflammatory proteins by HCMEC in vitro**

Densitometric quantification of the expression of 105 proteins in supernatants of HCMEC 24 hours after Cytomix treatment, obtained using the human XL Cytokine Profiler Array from R&D. (left panel) Representative array membranes showing duplicate spots for proteins and controls. Yellow markers identify some differentially expressed proteins between the two conditions. (right panel) Fold change of expression for each protein of the array after Cytomix treatment compared to UT. Red = statistical difference. N = 2 (number of arrays, with a pool of 2 biological replicates for each). Data are shown as mean +/- SEM and analysis was done using one-way ANOVA and Bonferroni's test. \*  $p < 0.05$ .

supernatants were collected from UT or Cytomix-treated HCMEC (after 24 hours). The relative expression of 105 secreted proteins was measured and analysed using a human XL Cytokine Profiler Array (R&D), which consists of capture and control antibodies spotted in duplicates on nitrocellulose membranes (Figure 4.7). Using this method, as is shown in Figure 4.7, 10 factors were identified as differentially expressed between conditions ( $p < 0.05$ ). These following were

**Table 4.2: Treatment with Cytomix or individual cytokines produced different profiles of secreted inflammatory proteins in HCMEC in vitro**

Quantification of protein expression in the supernatants of HCMEC after treatment with TNF $\alpha$ , IL-1 $\beta$ , hIL-6 or Cytomix for 24 hours, as measured by densitometry using the Cytokine Profiler Array (R&D). Data are shown as fold change (blue < 1 < red) compared to the group of reference shown in grey and in italics. Data are either compared to the top 10 proteins identified after treatment with UT (upper left), TNF $\alpha$  (upper right), IL-1 $\beta$  (middle left), hIL-6 (middle right), or with Cytomix (lower left); or compared by the top 10 differences of protein expression between UT and Cytomix (lower right). N = 2 (UT and Cytomix) and 1 (TNF $\alpha$ , IL-1 $\beta$ , hIL-6).

UT:	UT	TNF $\alpha$	IL-1 $\beta$	hIL-6	Cytomix
Serpin E1	102.50	1.00	0.99	0.99	0.99
EGF	98.69	0.99	0.87	0.98	1.03
Pentraxin-3	85.44	0.93	0.78	0.94	1.01
Vitamin D BP	75.98	0.87	0.22	0.86	1.00
MIF	75.33	0.96	0.58	0.90	1.04
IL-5	74.32	0.92	0.32	0.96	1.03
Lipocalin-2	74.01	0.93	0.30	0.93	1.39
MPO	73.91	0.89	0.28	0.85	1.03
Ang-2	73.63	0.88	0.50	0.79	0.95
IFN- $\gamma$	73.30	0.90	0.43	0.82	1.02

TNF $\alpha$ :	UT	TNF $\alpha$	IL-1 $\beta$	hIL-6	Cytomix
Serpin E1	1.00	102.77	0.98	0.99	0.99
IL-8	0.74	97.79	1.01	0.65	1.33
EGF	1.01	97.51	0.88	0.99	1.04
Pentraxin-3	1.07	79.55	0.84	1.01	1.08
CCL2	0.42	72.19	0.60	0.53	1.58
MIF	1.05	71.98	0.61	0.94	1.09
TSP-1	0.99	70.62	0.95	0.89	0.93
Lipocalin-2	1.08	68.78	0.33	1.00	1.49
CXCL1	0.31	68.43	1.30	0.48	2.02
IL-5	1.09	68.13	0.35	1.05	1.13

IL-1 $\beta$ :	UT	TNF $\alpha$	IL-1 $\beta$	hIL-6	Cytomix
Serpin E1	1.01	1.02	101.10	1.01	1.00
IL-8	0.73	0.99	99.22	0.64	1.31
CXCL1	0.24	0.77	89.04	0.37	1.55
EGF	1.15	1.13	86.17	1.13	1.18
TSP-1	1.04	1.05	67.39	0.93	0.97
Pentraxin-3	1.28	1.19	66.65	1.21	1.29
GM-CSF	0.17	0.20	60.37	0.13	1.13
IL-6	0.50	0.39	57.48	0.42	2.28
MIF	1.72	1.65	43.73	1.54	1.79
CCL2	0.71	1.67	43.10	0.89	2.64

hIL-6:	UT	TNF $\alpha$	IL-1 $\beta$	hIL-6	Cytomix
Serpin E1	1.01	1.01	0.99	101.81	1.00
EGF	1.02	1.01	0.89	96.94	1.05
Pentraxin-3	1.06	0.99	0.83	80.36	1.07
IL-5	1.04	0.95	0.33	71.61	1.07
Lipocalin-2	1.07	1.00	0.33	68.94	1.49
MIF	1.12	1.07	0.65	67.49	1.16
Vitamin D BP	1.16	1.01	0.26	65.70	1.15
IL-8	1.15	1.55	1.57	63.10	2.06
TSP-1	1.12	1.12	1.07	62.91	1.04
MPO	1.18	1.05	0.33	62.75	1.20

Cytomix:	UT	TNF $\alpha$	IL-1 $\beta$	hIL-6	Cytomix
Serpin E1	1.01	1.01	1.00	1.00	103.42
IL-8	0.55	0.75	0.76	0.48	96.78
EGF	0.97	0.96	0.85	0.96	95.08
CXCL5	0.04	0.30	0.24	0.06	91.74
CCL20	0.11	0.24	0.39	0.12	82.93
CXCL1	0.15	0.50	0.65	0.24	67.52
IL-6	0.22	0.17	0.44	0.19	60.65
IL1RL1	0.22	0.25	0.09	0.23	60.35
Pentraxin-3	0.99	0.93	0.78	0.93	59.88
MIF	0.96	0.92	0.56	0.86	58.49

versus UT:	UT	TNF $\alpha$	IL-1 $\beta$	hIL-6	Cytomix
CXCL5	3.96	6.91	5.59	1.47	23.17
G-CSF	4.52	1.34	4.39	1.32	9.74
CCL20	9.47	2.08	3.46	1.04	8.75
GM-CSF	4.62	1.19	5.95	0.78	6.74
CXCL1	10.26	3.26	4.25	1.57	6.58
ICAM-1	5.07	2.98	1.16	0.63	4.57
IL-6	13.40	0.77	1.99	0.84	4.53
IL1RL1	13.41	1.11	0.40	1.03	4.50
CXCL10	2.35	N/A	N/A	N/A	3.31
CCL2	12.35	2.35	1.41	1.25	3.71



the most enriched in supernatants after Cytomix treatment: CXCL5 (23.17-fold change vs UT), G-CSF (9.74-fold), CCL20 (8.75-fold), GM-CSF (6.74-fold), CXCL1 (6.58-fold), ICAM-1 (4.57-fold), IL-6 (4.53-fold), IL1RL1 (4.50-fold), CXCL10 (3.31-fold) and CCL2 (3.71-fold). There was no significant downregulation of secreted factors compared to UT. Of note, as shown in Table 4.2, these proteins were not necessarily among those which were detected at the highest intensities with the array. Indeed, the proteins with the highest raw values were (from the highest): Serpin E1, IL-8, EGF, CXCL5, CCL20, CXCL1, IL-6, IL1RL1, Pentraxin-3 and MIF; of which 4 were shared with the top 10 expressed proteins found in the UT condition. Raw values are not entirely physiologically relevant when read in isolation since they directly correlate to the sensitivity of each capture antibody. However, direct comparison of such highly expressed factors allows for additional insight on the effect of each treatment.

To further understand the contribution and interplay of TNF $\alpha$ , IL-1 $\beta$  and hIL-6 in the effects of Cytomix, and on the phenotype of EC, additional arrays were run with supernatants obtained from HCMEC treated with only TNF $\alpha$ , IL-1 $\beta$  or hIL-6 for 24 hours. These were included in the meta-analysis of UT versus Cytomix (Table 4.2). From the list of most highly expressed factors for each cytokine treatment, it can be observed that each condition produced a unique profile. For example, looking at the top rankers in UT samples, IL-1 $\beta$  stands out from other cytokines and Cytomix in that most of these proteins were downregulated (e.g. lower expression of MIF, EGF, Pentraxin-3). GM-CSF, IL-6 and CXCL1 were expressed at higher levels in IL-1 $\beta$ -treated EC than in TNF $\alpha$ - or hIL-6-treated cells, suggesting their induction by Cytomix originates from an IL-1 $\beta$  signalling. Similarly, CCL2 and ICAM-1 are predominantly induced by TNF $\alpha$ . Overall, the secretome response of HCMEC to hIL-6 is poorly reflected in the Cytomix response versus UT, with a negligible induction of CXCL5, CXCL1 or ICAM-1 compared to levels obtained from TNF $\alpha$  and IL-1 $\beta$  samples.

#### **4.3.8 Quantitative validation of soluble factors identified with the array as potentially enriched by Cytomix treatment on HCMEC**

The Cytokine Profiler Array represents a useful screen but can only provide semi-quantitative data, with much less accuracy than other methods. To further validate the secreted factors identified in the previous experiment and to determine if their differential release in EC after Cytomix pre-conditioning is maintained in co-cultures with CM, new culture supernatants were collected and analysed by ELISA. Before comparing experimental conditions, it was first necessary to identify the optimal dilution for the samples, as ELISA tests are much more sensitive to their targets than the Profiler Array. This was validated for CXCL5, CXCL1, G-CSF, GM-CSF, plus ET-1 (which was not included in the Array but is of interest for EC-CM paracrine interactions), using supernatant samples diluted at 1:1, 1:50, 1:100 and 1:200. As seen in Figure 4.8, in Cytomix-treated samples, for CXCL5 and GM-CSF, only the 1:1 dilution was found within the bounds of the recommended standard curve. For CXCL1, samples should not be diluted more than at 1:50. Finally, for G-CSF and ET-1, sample dilutions from 1:1 to 1:200 allowed detection along the recommended standard curve. At 1:1 dilution, the 5 targets were equally detected within the limits of the standard in supernatants collected from UT cultures. At higher dilution ratios, UT samples often produced values close to or below background noise. Therefore, this 1:1 sample dilution was preferred in subsequent ELISAs.

The concentrations of CXCL5, CXCL1, G-CSF, GM-CSF and ET-1 were measured by ELISA, in co-culture medium, in HCMEC, ARVM or adult human cardiac fibroblasts (FB) supernatants, or in HCMEC-ARVM transwell co-cultures (Figure 4.9). To prevent the secretome of EC at the end of their Cytomix pre-conditioning being carried over in the supernatants of co-cultures, all samples were collected 4 hours after Cytomix was removed, cells thoroughly washed and co-cultures started. First, CXCL5 was found enriched in HCMEC and co-culture supernatants in response to Cytomix, with no difference between EC and EC + CM (24-fold change vs UT and 13-fold,  $p = 0.0002$  and  $p = 0.0435$ , respectively). Cytomix did not induce CXCL5 release in ARVM, but significantly in FB (43-fold change vs UT FB,  $p < 0.0001$ ). In all cell types and after

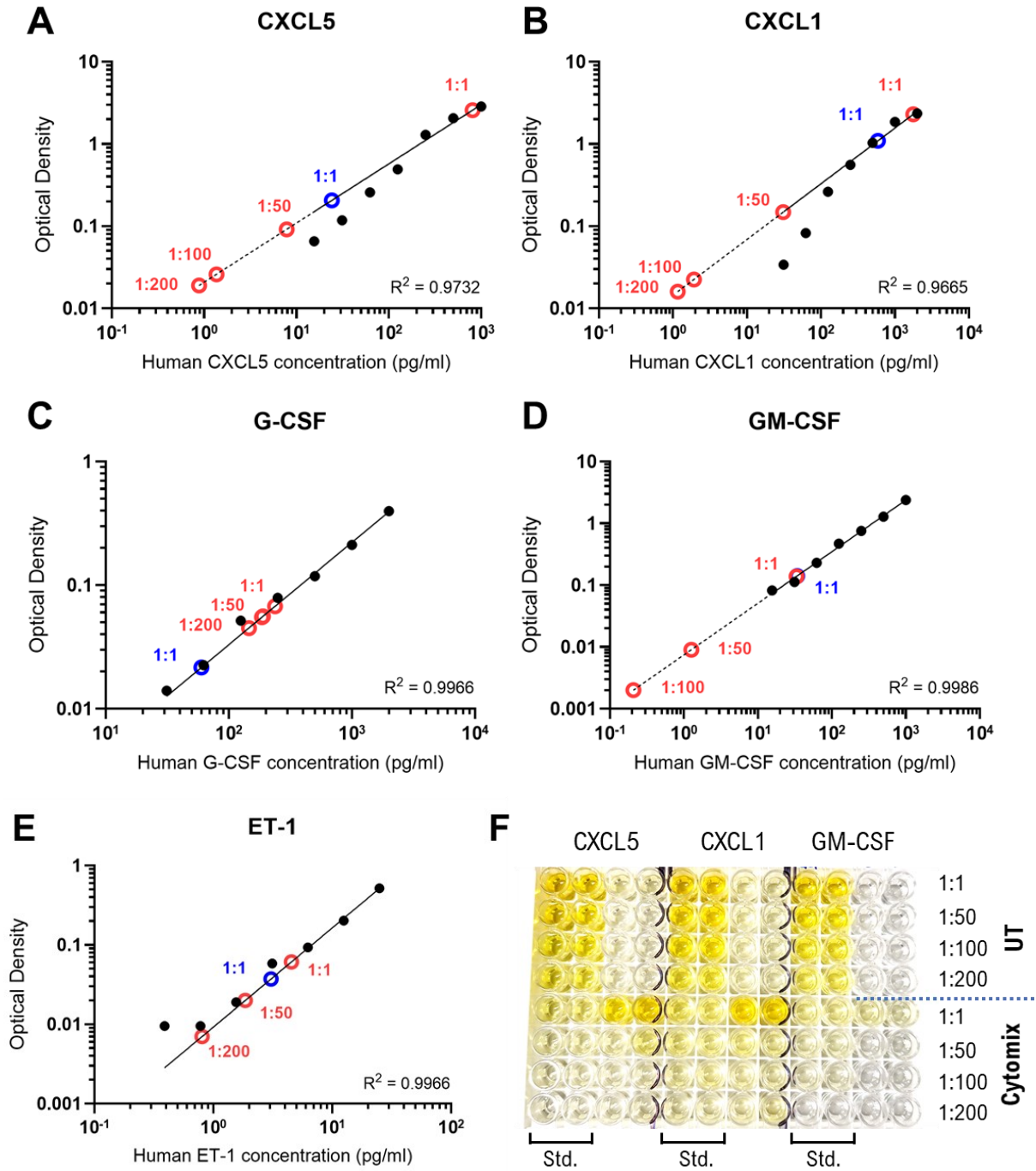


**Figure 4.8: Optimisation of sample dilution for ELISA quantification of candidate EC-secreted factors**

Quantification by ELISA of human CXCL5 (A), CXCL1 (B), G-CSF (C), GM-CSF (D) and ET-1 (E) in HCMEC supernatants 24 hours after Cytomix treatment, with samples diluted at 1:1, 1:50, 1:100, or 1:200. N = 1. A nonlinear regression fit has been applied to optical density values of the standard.  $R^2$  is given in each graph. The curve is dotted where extrapolated. Red dots = sample dilutions for Cytomix; blue dots = UT. F. Picture of ELISA plate after reaction has been stopped, with CXCL5, CXCL1 and GM-CSF, showing the standard (std.) and samples from UT or Cytomix treatments.

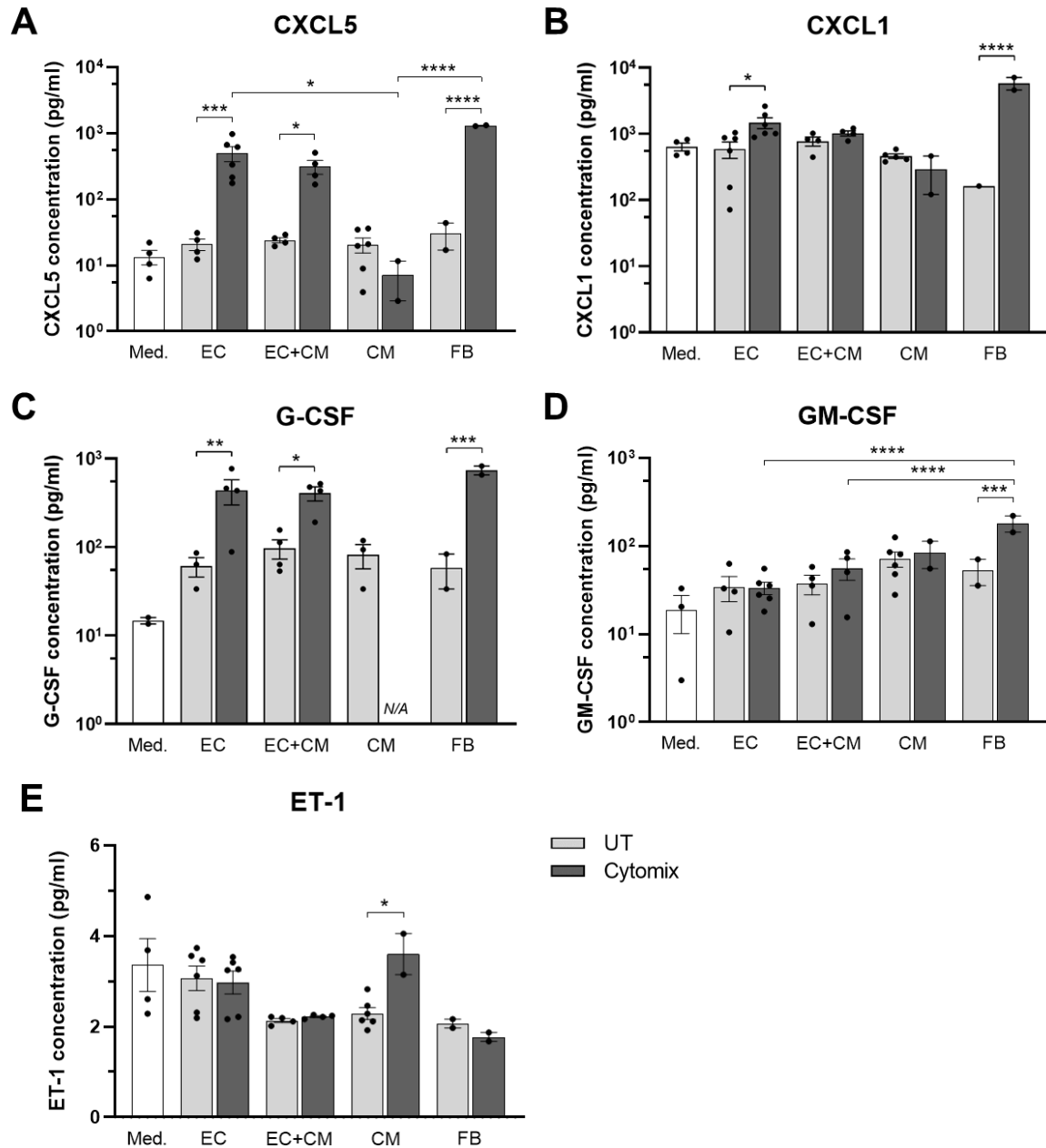


**Figure 4.9: CXCL5 and G-CSF, but not ET-1, CXCL1 and GM-CSF, were differentially released by EC alone and during EC:CM co-culture after Cytomix treatment**

Quantification by ELISA of CXCL5 (A), CXCL1 (B), G-CSF (C), GM-CSF (D) and ET-1 (E) in culture supernatants of HCMEC, ARVM, hACF (FB) or EC:CM co-cultures, collected after 4 hours of culture in fresh medium, following 24 hours of pre-conditioning with Cytomix N = 6 (EC; CM UT), 4 (medium alone; EC+CM), N = 2 (CM + Cytomix; FB). Values were excluded when measured below the limit of detection. Data are shown as mean +/- SEM and compared using an ordinary one-way ANOVA and Bonferroni's correction for multiple comparisons. \* p < 0.05. \*\* p < 0.01. \*\*\* p < 0.001. \*\*\*\* p < 0.0001. *Med*: culture medium alone. *N/A*: no data point available.

co-culture, UT levels were statistically indistinguishable from the levels detected in medium. Similarly, G-CSF was induced by Cytomix in EC, FB and in EC-CM co-cultures (7-fold change vs UT, 12-fold and 4-fold, respectively,  $p = 0.0095, 0.0006, 0.022$ ), and the UT concentrations were unchanged from medium alone. Levels in CM after Cytomix treatment could not be read within the limits of detection. There was no effect of co-culture with CM on the levels of EC-produced G-CSF. CXCL1 was only found induced by Cytomix treatment in EC or FB alone (2-fold and 36-fold, respectively,  $p = 0.0275, < 0.0001$ , compared to 1.3-fold at  $> 0.9999$  in co-cultures). Here again in UT samples the concentration of CXCL1 was indistinguishable from media levels. Surprisingly, GM-CSF was not induced by Cytomix in EC, CM or co-cultures (contrary to data from the profiler array) but was significantly enriched post-treatment in FB (3.5-fold change vs UT,  $p = 0.0003$ ). The GM-CSF concentration was also insignificant in all UT conditions. Finally, ET-1 was found enriched in the supernatants of CM, but not of EC, FB, or curiously in EC-CM co-cultures after a Cytomix treatment (1.5-fold change in CM vs UT,  $p = 0.0421$ ). To summarise, these data suggest that CXCL1, GM-CSF and ET-1 are unlikely to contribute to the paracrine effects of EC on CM. However, this confirmed the induction by Cytomix of CXCL5 and G-CSF secretion by EC, as detected with the profiler array.

#### **4.3.9 Meta-analytical assessment of ligand-receptor interactions in CM, based on the expression of specific receptors in published large datasets**

To determine if the paracrine mediators identified using the profiler array were likely to induce signal transduction in CM, the RNA expression of receptors for these factors was investigated using the Tabula Muris online resource (a single-cell RNA sequencing dataset, on mouse CM for example) and a published normalised RNA microarray dataset from Fuller *et al.* (2015) with the expression profile of adult compared to neonatal rat CM<sup>209</sup>. The expression of ligands was also quantified to better contextualise the data obtained with ELISA in CM. RNA expression was analysed for specific markers of CM (*TNNT2*, *MYL2*, and *ACTC1*), for the ligands *CXCL5*, *CXCL1*, *CCL2*, *CSF2* (GM-CSF), *CSF3* (G-CSF), *IL6*, *IL1RL1*, and the receptors *CCR2* and

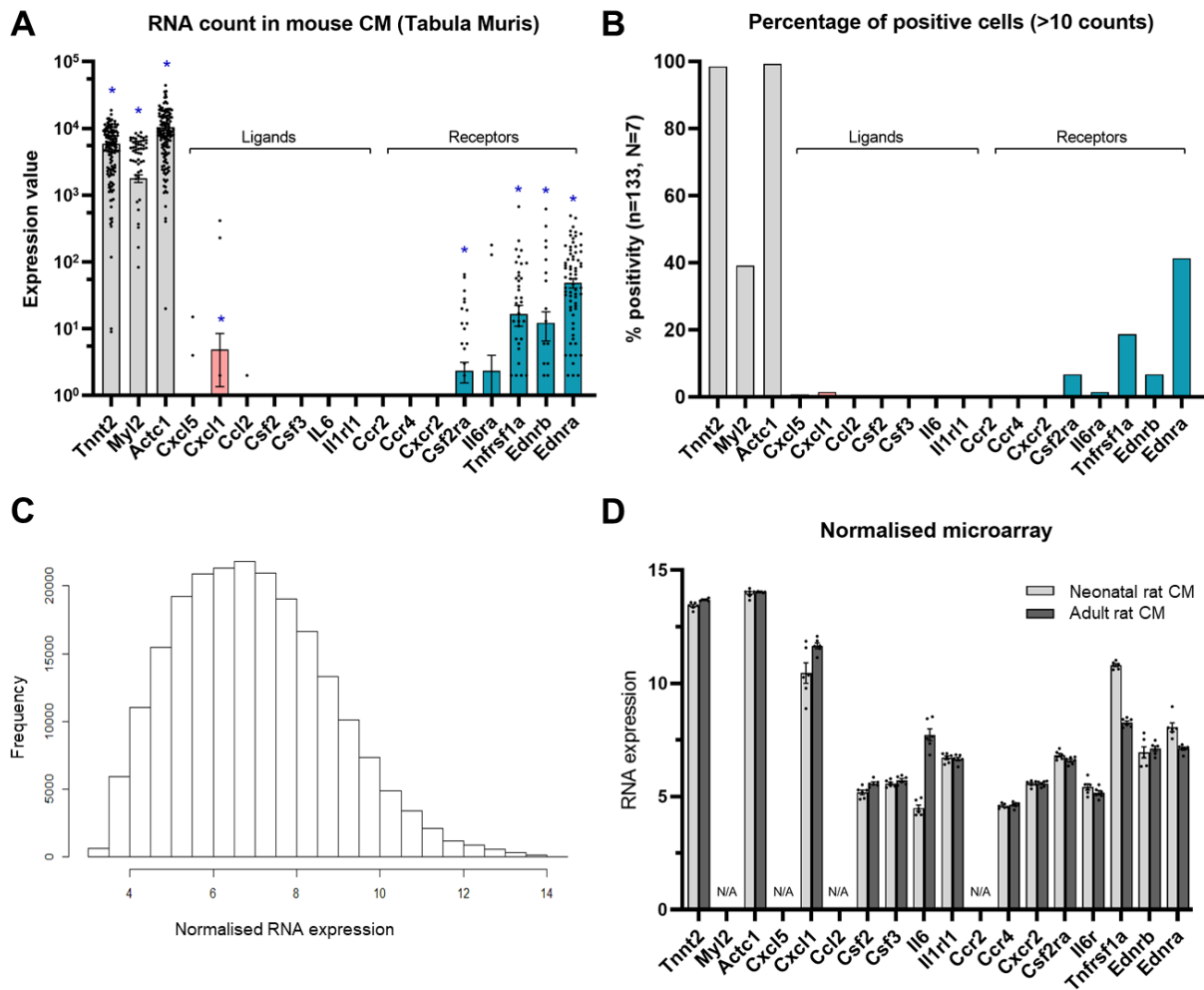


**Figure 4.10: RNA expression of candidate ligands (identified with the Profiler Array) and their canonical receptors in mouse and rat CM**

Meta-analysis of RNA count and normalised RNA expression for CM markers (*TNNT2*, *MYL2*, and *ACTC1*), or proteins identified with the profiler array and their main known receptors. **A.** Analysis of RNA levels in mouse CM in the Tabula Muris single-cell transcriptomic dataset.  $n = 133$  cells (these obtained from a total of 7 biological replicates). Gene expression is compared to zero using the Welch's ANOVA and Dunnett's correction. **B.** Percentage of CM positive for each gene of interest. The lower cut-off for expression in cells was 10 counts. **C.** Histogram of gene distribution per normalised RNA expression in neonatal and adult rat CM, as measured by RNA microarray (Fuller *et al.* 2015). Graph has been generated by Robert Maughan, PhD. **D.** Normalised RNA expression for all the genes of interest, shown as mean  $\pm$  SEM.  $N = 6$ . All samples passed normality test of D'Agostino & Pearson in this dataset. \*  $p < 0.05$ . N/A: gene was not tested in the microarray.

*CCR4* (activated by *CCL2*), *CXCR2* (targeted by *CXCL1*, *CXCL5* and *IL-8*), *CSFR2A* (for GM-CSF), *IL6R*, *TNFRSF1A* (receptor for  $\text{TNF}\alpha$ , which was used as a positive control for receptor expression in CM), *EDNRA* and *EDNRB* (ET-1 receptors).

As seen in Figure 4.10A, the RNA transcripts for ligands and receptors genes in Tabula Muris was much lower than the expression of the CM markers. For *CXCL1*, *CSF2RA*, *TNFRSF1A*, *EDNA* and *EDNB*, RNA expression was significantly greater than 0. Applying a cut-off of 10 RNA counts per cell, below which cells were considered negative for a given gene, the number of CM positively expressing each ligand and receptor was found to be much lower than for CM markers. Indeed, 98% and 99% of CM expressed *TNNT2* and *ACTC1* (although only 39% also expressed *MYL2*). Only 1.5% of cells expressed *CXCL1*, reflecting the absence of basal *CXCL1* secretion by CM measured by ELISA. *CSF2RA*, *TNFRSF1A*, *EDNA* and *EDNB* were only expressed significantly in 6.7%, 18.8%, 6.7% and 41.3% of all mouse CM (respectively).

Similar findings were obtained in rat CM, using the normalised data from the RNA microarray published in Fuller *et al.* (2015). Of note, *MYL2*, *CXCL5*, *CCL2* and *CCR2* were not included in the dataset. When using this type of microarray data it can be challenging to determine what constitutes high and low RNA expression. To help read the data from this meta-analysis, the distribution of all genes was plotted by RNA expression (Figure 4.10C). This histogram shows firstly that RNA expression in this microarray is confined between 3 and 14, with most genes detected between 5 to 9. Only *TNNT2*, *ACTC1*, *CXCL1* and, in neonatal CM, *TNFRSF1A* were detected above 9 (Figure 4.10D). Due to the experimental design for this microarray, it is not possible to quantify accurately the number of positive CM, as was done with Tabula Muris. It can be difficult to detect ligands and receptors at the level of both mRNA and protein, and this limits the possible interpretations of such results. The expression of these factors can be low, dynamic, and inducible. A low level of mRNA expression thus does not correlate necessarily with a low ligand or receptor activity. Further experimental protein expression data and most importantly functional analysis is required to investigate further the effects of these candidate EC-derived soluble factors on CM function.

## 4.4 Discussion

A lot remains to be understood about inflammatory signalling in EC, particularly regarding the complex interplay of stimuli that can occur to regulate the transcriptional or post-transcriptional activity of EC. In this chapter, data converge to illustrate how the phenotype of EC is regulated differently by similar cytokines, all of which have been categorised and widely used by us and others as pro-inflammatory treatments. To go beyond the differences of cytokine responses in EC, endeavouring to improve the physiological relevance of the models and to understand the intricate plasticity of endothelial behaviour in this process, an important aim for this chapter was to use TNF $\alpha$ , IL-1 $\beta$  and IL-6 in conjunction, instead of separately as is done traditionally. In many disease-related pro-inflammatory responses these cytokines are present together in the local microenvironment. Using this treatment strategy, my data indicate that the response of HCMEC to these cytokines is far from simply additive. Indeed, responses were sometimes antagonistic (VCAM-1 induction was lost in the co-treatment response) and synergistic (with a larger release of pro-inflammatory factors), this complicated cellular response has raised more questions than answers, so far. While characterising the physiology of EC after treatment with this cytokine cocktail (Cytomix), there was sufficient evidence that the EC response to this treatment was of an inflammatory nature.

A *sine qua non* to testing the subsequent paracrine effects of Cytomix-treated EC on CM in co-culture was some evidence that endothelial secretions were modulated by Cytomix (both quantitatively and qualitatively) and consistent with the phenotype of EC during inflammation. Using a Cytokine Profiler Array, pro-inflammatory proteins were found to be enriched in the culture supernatants of EC after Cytomix treatment and, among those, a number were further validated by ELISA. However, a brief meta-analysis of receptors mRNA expression in healthy CM suggested that these ligands are unlikely to transduce signals in a healthy CM population. This mRNA expression result must be interpreted very cautiously and cannot be considered the most sensitive way of investigating these ligand-receptor interactions. Protein expression



data in CM are required, and ultimately a direct analysis of CM functional responses following exposure to the individual cytokines and chemokines must be performed.

Perhaps the most interesting and perplexing finding in this chapter is the differential synthesis of NO after thrombin treatment in Cytomix pre-conditioned EC but not in untreated EC. This was associated with a decreased amplitude and duration of calcium transients in EC, a lack of endothelial permeability in response to thrombin, and greater NO synthesis (which in theory represents the intermediate link between calcium and EC permeability). Though the aim for this chapter was fulfilled, the data shown above warrant further characterisation of endothelial properties and signalling pathways. This will help determine how co-treatment with cytokines differs from individual cytokine treatments, and how this might be exploited therapeutically.

To summarise rapidly the results of this chapter, we show that: (1) TNF $\alpha$ , IL-1 $\beta$  and hIL-6 (but not IL-6) induced unique expression profiles of known pro-inflammatory proteins in EC. (2) Co-treatment of cytokines (Cytomix) induced a complex non-additive response for these markers. (3) Cytomix treatment provoked EC cycle arrest to G1. (4) Cytomix did not modulate basal EC permeability but attenuated the thrombin-induced EC permeability. (5) This is associated with smaller and shorter thrombin-induced calcium transients. (6) Basal NO was undetectable in UT or Cytomix-treated EC, but thrombin stimulated NO synthesis in Cytomix pre-conditioned EC only. (7) In this experiment, L-NAME had the effect of increasing NO synthesis. (8) A small group of factors was identified as differentially released by EC after Cytomix treatment. (9) Only some of these soluble factors could be validated quantitatively by ELISA. (10) The paracrine activity of EC on CM via these soluble factors merits further functional investigation.

#### **4.4.1 Modelling the trans-signalling of IL-6 in EC in vitro with hIL-6**

The caveat to using IL-6 *in vitro* on isolated EC is that IL-6 requires binding with its receptor sIL-6R $\alpha$ , a protein only expressed in hepatocytes and leucocytes<sup>44</sup>. As introduced earlier, this issue can be circumvented using hyper-IL-6 (hIL-6). Due to its composite nature it is possible

that hIL-6 behaves unexpectedly in HCMEC. This was ruled out in Figure 4.1C and 4.1D with hIL-6 (but not IL-6) being able to induce acutely STAT3 phosphorylation on S727 and, after 24 hours, to induce expression of ICAM-1 and MnSOD. Both targets have been shown to be inducible by hIL-6 or IL-6/sIL-6R $\alpha$  previously<sup>47,307,308</sup>. Other markers of inflammation, which were selected as targets more specific to TNF $\alpha$  and IL-1 $\beta$ , were not regulated by hIL-6 (VCAM-1, eNOS, iNOS, A20, HO-1, and TRAF6). The ability of IL-6 to regulate these proteins might be cell type-dependent. For example, HO-1 was found induced by IL-6 in myeloma cells<sup>309</sup> but not in macrophages<sup>310</sup>. The response of HCMEC to hIL-6 was however considered compatible with the canonical trans-signalling of IL-6.

#### **4.4.2 hIL-6 interfered with the TNF $\alpha$ and IL-1 $\beta$ signalling in EC**

Originally, the rationale for using three cytokines as co-treatment was to mirror a complex pro-inflammatory microenvironment. It was hypothesised that adding cytokines to the treatment of EC would generate synergistic effects. As discussed above, cytokine interactions are relatively rarely studied and so poorly understood. It was thus interesting to find a significantly lower induction of VCAM-1 after Cytomix treatment than after TNF $\alpha$  treatment alone (Figure 4.2A), although TNF $\alpha$  was used at the same concentration in Cytomix and added to IL-1 $\beta$ , which independently can also induce a significant increase in VCAM-1 expression. VCAM-1 was not induced by hIL-6. I propose that this absence of VCAM-1 induction by Cytomix is caused by hIL-6 directly interfering with the canonical response of EC to TNF $\alpha$  and IL-1 $\beta$ . This sort of effect, particularly when multiple cytokines are involved, is too often dismissed as “cytokine phenomenology” and thought difficult to relate to *in vivo* settings. However, it should be noted that this very effect has been reported previously. Indeed, treatment of astrocytes and human astrogloma cells with IL-6/sIL-6R $\alpha$  blunted TNF $\alpha$ -induced VCAM-1 expression, but not TNF $\alpha$ -induced ICAM-1 expression<sup>311</sup>. My data provide the first report of such a response in EC. The effect is poorly understood, and has been attributed to anti-inflammatory effects of IL-6, e.g. a synthesis of IL-1Ra (a potent antagonist of IL-1) and the release of soluble TNF $\alpha$  receptors<sup>304</sup>.

Despite this effect having anti-inflammatory ramifications, it would be too reductionist to categorise the hIL-6 signalling in Cytomix as purely anti-inflammatory (or antagonistic to TNF $\alpha$ /IL-1 $\beta$ ). Indeed, hIL-6 did not inhibit ICAM-1 or, as is shown in Table 4.2, was not able to prevent the synergistic release of pro-inflammatory factors by EC when added in Cytomix. Furthermore, even TNF $\alpha$  is not entirely pro-inflammatory, as it also exerts anti-inflammatory and antioxidant effects in the vascular endothelium (including induction of A20 and MnSOD). The pathophysiological implications of VCAM-1 expression in the microvasculature during the inflammatory response are still misunderstood. The density of CAM was reported to be greater in the venular endothelium than in arterioles or capillaries, causing leucocyte rolling, adhesion and diapedesis to occur preferentially in postcapillary venules<sup>312,313</sup>. In this the heart might even be an exception, with neutrophils adhering mostly to the walls of larger coronary veins<sup>314</sup>. The contribution of microvascular EC expressed CAM to cardiac inflammation is still undefined and might even be dispensable. The lack of VCAM-1 induction by Cytomix does not invalidate its use as a pro-inflammatory intervention. With IL-6 and endothelial STAT3 signalling correlating with and contributing to HF<sup>285,291,315</sup>, the value of such hIL-6 interference with TNF $\alpha$  or IL-1 $\beta$  activity should not be overlooked in any model of cardiovascular inflammation.

#### **4.4.3 Anti-proliferative properties of Cytomix treatment in HCMEC, recapitulating the pathophysiology of microvascular inflammation**

A commonly reported feature of vascular remodelling in disease is the defect of angiogenesis, which is dependent on EC proliferation. It is thus not surprising that low EC proliferation was found in *in vivo* models of diabetes<sup>316</sup>, vascular injury<sup>317</sup> and MI<sup>303,318</sup>, which are all characterised by an inflammatory response of the microvasculature. Cytomix treatment induced a significant arrest of cell cycle progression at G1, after 24 hours in HCMEC (Figure 4.3), suggesting it can model appropriately the anti-proliferative effect of microvascular inflammation. It would be also pertinent to test if this effect can be reproduced in more complex models of angiogenesis, in which EC proliferation is not the only cellular function measured.

A fibrin gel bead assay (also known as a bead sprouting assay) was tried in this project but could not be developed in time, mostly due to an absent sprouting in untreated conditions which prevented us from testing the effects of Cytomix (no data could be included). Other experimental approaches could be used to further demonstrate and explain this anti-proliferative effect of Cytomix. The expression of proteins involved in the cell cycle, such as cyclins, p21 and p53 could be measured by western blotting, for example. The respective anti-proliferative capacities of TNF $\alpha$ , IL-1 $\beta$  and hIL-6 (in isolation) could be tested to determine which cytokine contributes the most to this effect.

It is a limitation of this chapter that the endothelial phenotype of HCMEC was not re-confirmed after Cytomix treatment, even though it is unlikely that EC transdifferentiation occurred in such short durations of treatment. In this chapter, medium supplemented with 10% FBS was used as a positive control for proliferation and it showed no improvement over the normal 1% FBS-based co-culture medium. Inclusion of a negative control in this dataset would have helped determine how Cytomix treatment compares with known anti-proliferative agents or stimuli. To better grasp the limitations of this model, it should be noted that the link between inflammation and EC proliferation is not absolute and not immune to plasticity of EC to other elements of their environment. For example, mechanical strain applied dynamically to *in vitro* cultures of microvascular EC was able to completely inhibit the anti-proliferative effects of IL-1 $\beta$ <sup>302</sup>. Some anti-inflammatory agents (e.g. TGF- $\beta$ ) are also anti-proliferative in EC<sup>319</sup>. It is however safe to assume that the response of EC to Cytomix is compatible with an endothelial inflammatory response, at least in terms of cell proliferation.

#### **4.4.4 Lack of effect of Cytomix treatment on endothelial permeability**

Vascular permeability is another marker of endothelial activation in vascular inflammation<sup>54</sup>, contributing to thrombosis, interstitial oedema, diapedesis, endothelial dysfunction, and when excessive, to cardiovascular diseases aetiology<sup>55</sup>. TNF $\alpha$ , IL-1 $\beta$ , IFN- $\gamma$ , thrombin, bradykinin and histamine<sup>58</sup>, MASP-1, VEGF and LPS, but not IL-6<sup>320</sup>, have been shown to induce or

potentiate permeability in EC *in vitro*<sup>57-59,320,321</sup>. It was therefore surprising that Cytomix did not augment the permeability of HCMEC in Transwell inserts and, even more counterintuitively, that thrombin effects on EC permeability were abrogated by Cytomix.

Was the technique used not sensitive enough? To date the preferred technique relies on the measurement of impedance (i.e. the trans-endothelial electrical resistance, TEER), indeed a more accurate method than alternatives relying on the transmural diffusion of labelled tracers, radioactive or fluorescent. Both methods have limitations. TEER is adapted to detect minute changes of permeability, but larger openings in the monolayer tend to decrease the signal-to-noise ratio excessively. It also provides an integral measurement of EC permeability across the monolayer, but it cannot be used to test the sieving capacity for tracers of different sizes<sup>207</sup>. While this can be accomplished by measuring the diffusion of tracers through the monolayer (as in this project), this method cannot be used to detect fine temporal changes. Permeability peaks 20 min after treatment with thrombin and returns to baseline within an hour<sup>57</sup>. This would be difficult to illustrate with a cumulative signal. Siflinger-Birnboim *et al.* (1987) measured the baseline permeability of pulmonary arterial EC monolayers for molecules of sizes ranging from 182 Da (mannitol) to 340 kDa (fibrinogen) and reported that permeability was between 7.29 and 0.012 m.s<sup>-1</sup>, respectively (0.195 m.s<sup>-1</sup> at 43 kDa)<sup>207</sup>. This is orders of magnitude larger than the baseline permeability for 40 kDa FITC-Dextran that was measured in this project (9.4x10<sup>-5</sup> m.s<sup>-1</sup>). However, it should be noted that in this paper the filters had pores of 0.8 µm diameter, compared with 0.4 µm in this project. Pore density was not reported and might be different as well since it is dependent on the manufacturing process. Using membranes with 0.4 µm pores, Ehringer *et al.* (1996) reported EC permeability values more consistent with the results in this chapter: 1.59x10<sup>-4</sup> m.s<sup>-1</sup> in UT EC, rising to 4.92x10<sup>-4</sup> m.s<sup>-1</sup> 30 min after the thrombin treatment (calculated here at 4.22x10<sup>-4</sup> m.s<sup>-1</sup>, 1 hour post-treatment). This suggests that values obtained above, with or without thrombin, were measured within the range of expected EC permeability.

FITC-Dextran was collected and measured 1 hour after treatment with thrombin to allow for the transient increase of EC permeability to peak and decline fully (measuring the total diffused volume of tracer), and for longer transient events to be integrated as well. It is unlikely therefore that the lack of thrombin-induced permeability after Cytomix treatment is due to data collected too early after treatment. Measuring the TEER would be a first step to confirming this finding. Secondly, other stimulants of endothelial permeability (e.g. VEGF, bradykinin, PAR-agonists or even cytochalasin D, which disrupts the actin cytoskeleton) could be used instead of thrombin to determine which mechanisms are targeted by Cytomix. Finally, it would be of great interest to measure the protein expression of thrombin targets in HCMEC after Cytomix treatment, such as the members of the PAR family, which initiate the signalling of thrombin. Post-translational modifications might provide further insight into this effect and could be characterised by western blotting.

#### **4.4.5 Cytomix impaired the calcium release in EC after acute thrombin treatments**

As introduced above, transient intracellular calcium releases are integral to the control of EC permeability by extracellular agents such as thrombin. Consistently with the lack of thrombin-induced EC permeabilization described above, Cytomix treatment attenuated the thrombin-induced calcium transients in HCMEC. This dual response might be compliant with the paradigm of calcium-regulated EC permeability, it is still the opposite of what was expected from such a pro-inflammatory intervention.  $\text{TNF}\alpha$ , as an example, was shown to potentiate EC permeabilization by prolonging calcium release in EC (but amplitude was unaffected)<sup>56</sup>. Pre-conditioning HCMEC with  $\text{TNF}\alpha$  instead of Cytomix might be extremely useful in the future, as a positive control for variations of thrombin-induced calcium transients. As for the previous section, more needs to be done to understand how the response of EC to thrombin is disrupted by Cytomix. The data generated herein suggest the presence of important protective signalling pathways.

#### 4.4.6 On the “paradoxical” thrombin-induced increase of NO in Cytomix-treated EC

Given the abrogated response of EC to thrombin, at the levels of calcium transients and paracellular permeability, it was subsequently hypothesised that Cytomix treatment would also lower NO synthesis in EC. If true, this would model endothelial dysfunction more than the traditional endothelial inflammatory response (during which NO bioavailability is increased<sup>322</sup>), and make the effects of Cytomix-treated EC on CM less relevant to myocardial inflammation. Instead of finding less NO in EC, however: (1) no basal NO could be detected in UT and Cytomix-treated HCMEC, so as such the basal bioavailability of NO was unchanged, and (2) thrombin induced a larger synthesis of NO after the Cytomix treatment than in UT HCMEC. This is a paradoxical finding, at first glance, because a lower calcium release theoretically attenuates eNOS activity, leading to reduced generation of NO (assuming all other conditions are unchanged). The second issue is that increased NO synthesis in response to thrombin should translate to enhanced endothelial permeability, not an uncoupling between thrombin and endpoint permeability as was found in this project (as reviewed by Durán *et. al.*<sup>323,324</sup>).

This increase of detected NO, in conditions where calcium transients were smaller in duration and amplitude, can be simply explained by a shift from Ca<sup>2+</sup>-dependent to Ca<sup>2+</sup>-independent mechanisms of NO synthesis. This shift can take at least two forms. First, as discussed above iNOS is constitutively active and does not require intracellular calcium waves to synthesise NO in EC<sup>81</sup>. During inflammation, eNOS expression can be downregulated (additionally eNOS can be uncoupled, generating superoxide instead of NO), all while iNOS expression is upregulated, resulting in more NO being synthesised and less reliance on calcium<sup>78</sup>. Although it is a calcium-dependent isoform of NOS, eNOS can equally generate NO in response to stimuli which do not trigger calcium release<sup>325</sup>, and it has been shown to gain calcium-independency under pro-inflammatory conditions<sup>80</sup>. If the Cytomix treatment leads to iNOS replacing eNOS in HCMEC, there would have been a synthesis of NO even in conditions where thrombin was not applied. This effect was shown in one replicate. Reproducing the DAF-2 DA experiment appears thus essential to verify this finding. With more time allowed it

would be interesting to measure eNOS and iNOS protein expression by western blotting and examine the calcium-dependency of eNOS (in light of the calcium transients data). Using well established treatments as positive controls for the eNOS-iNOS shift could help validate this experiment as well. Next, to test if eNOS has been uncoupled by Cytomix treatment, the intracellular levels of superoxide or BH4 could be quantified (loss of BH4 contributes to NOS uncoupling). Finally, other methods of NO detection and quantification should be tried to confirm the lack of NO levels at baseline, under or without stimulation with Cytomix. Analysis of nitrite and nitrate levels in the supernatants of HCMEC in culture would be a good starting point, although this method is less accurate than fluorescent probes due to the dynamic and volatile nature of the molecular reactions involved. A better alternative would be to use the copper-based fluorescent probe CU2FL2E which may be more sensitive to low levels of NO (such as in EC) than DAF-2<sup>249</sup>.

L-NAME induced a significant increase of NO in both control and thrombin-treated cells, but only after Cytomix pre-conditioning. This result is extremely controversial given that L-NAME is commonly used as a non-specific inhibitor of NOS<sup>249</sup>. The aims for this part of the experiment were two-fold: (1) confirm that the DAF-2 DA fluorescent signal and its response to thrombin were indeed due to NO synthesis, and (2) to validate this method of inhibition for later use in EC-CM co-cultures where a manipulation of NO would have been of interest. However, to date these aims have not yet been completed. It is not the first report of L-NAME counterintuitively increasing NO<sup>326</sup>, with Liu *et al.* (2019) noticing a potentiation of this effect by macrophages<sup>109</sup>, suggesting inflammation could favour this reversal of function. Repeating this experiment with the NOS-inactive enantiomer D-NAME, other NOS inhibitors (e.g. L-NMMA), NO scavengers and finally NO donors would help define the bioavailability of NO in response to Cytomix and meet the two secondary aims mentioned above.

It is still unknown why thrombin did not induce NO synthesis in UT cells, why the increased NO after Cytomix did not result in an increased permeability, nor why Cytomix treatment had no impact on NO levels at baseline, compared to UT. These caveats and the rest of the data



shown above should therefore be interpreted with caution. If these results are true however, it should be considered that the effect of EC pre-conditioning by Cytomix on co-cultured CM is unlikely to involve a differential release of NO.

Until a quantitative assessment of NO generation is done it will remain difficult to conclude that the low DAF-2 DA signal measured above was normal or caused by inappropriate calibrations, or technical/biological issues. Should this NO release be indeed low (or too low in UT cells to detect even lower levels after Cytomix treatment), the effect of EC on CM would model more closely that of endothelial dysfunction than inflammation, a limitation to keep in mind when interpreting data from co-cultures.

#### **4.4.7 Screening and differential release by EC of markers of endothelial inflammation after treatment with Cytomix**

The Cytomix treatment altered the secretome profile of HCMEC in culture and induced the release of pro-inflammatory proteins which were not detected in control conditions. This was first observed using a proteome profiler cytokine array, which has become a popular option to study inflammatory responses *in vitro* or to phenotype the environment of biological samples<sup>327</sup>. The absence of detection (or relative enrichment) of TNF $\alpha$  and IL-1 $\beta$  from supernatants of EC pre-conditioned with TNF $\alpha$  or IL-1 $\beta$  validates the washing strategy observed in all experiments after treatment and before co-culture with CM. In other words, there is little evidence from this array that any carry-over of cytokines occurs from the treatment to the final cell culture system. IL-6 was only detected in the IL-1 $\beta$  and Cytomix samples, and the higher expression of IL-6 in Cytomix (compared to IL-1 $\beta$ ) cannot be attributed to carry-over from the hIL-6 in Cytomix since it was undetectable in the hIL-6 group.

Some proteins were detected strongly in all conditions, including in UT cells: Serpin E1, MIF, Pentraxin-3 and EGF. This subject of analysis is not ideal, considering that only few proteins (out of the 105 tested) were detected above background level in the UT group, allowing pro-

inflammatory factors such as IFN- $\gamma$  and Ang-2 to be construed as “relatively highly secreted” in UT conditions. Serpin E1 has been shown to be inducible in EC by IL-1 $\beta$ , LPS and IL-6<sup>328,329</sup>. Using the profiler array, however, Serpin E1 was conserved across all treatments. Pentraxin-3 was also detected at high levels in UT; a surprising find given its role in vascular inflammation, endothelial dysfunction and lowering NO synthesis<sup>330</sup>. Similarly, MIF is constitutively secreted by vascular EC, but its expression is stimulated by pro-inflammatory stimuli such as LPS<sup>331</sup> and this was not seen in the array. Another limitation of this array is the absence of many proteins known to contribute to the inflammatory response of EC and to the EC-CM crosstalk, such as ET-1, which have to be examined separately.

Of note, IL-8 was induced by TNF $\alpha$ , IL-1 $\beta$  and Cytomix, but slightly reduced by hIL-6, again demonstrating the complex nature of the inflammatory IL-6 response. However, some reports have shown the induction of IL-8 by IL-6<sup>332</sup>, while others have demonstrated that IL-6 promotes the release of additional inflammatory factors which were not found with the array<sup>38</sup>. Finally, it should be noticed that the pro-inflammatory cytokine IL-18, well known to require activation of the inflammasome<sup>333</sup> as IL-1 $\beta$ , was not detected in the array after Cytomix treatment. This was expected however because EC do not express IL-18<sup>334</sup>.

These data best demonstrate the plasticity of endothelial secretions to cytokines, and the potential value of studying Cytomix over individual cytokine treatments. Some proteins detected in Cytomix were indeed differentially induced by each cytokine, with G-CSF, GM-CSF, CCL20, IL-6 being more dominant in the IL-1 $\beta$  response, while ICAM-1 and CCL2 being induced preferentially by TNF $\alpha$ . This sort of dataset might eventually be translated clinically, where circulating markers of inflammatory activity are highly sought after. CXCL10, a known pro-inflammatory chemokine, was not detected in the supernatants of TNF $\alpha$ , IL-1 $\beta$  or hIL-6-treated EC, suggesting that the response of EC to Cytomix is more complex than necessarily additive. Of note, CXCL10 was shown to inhibit proliferation in EC<sup>335</sup>, echoing the G1 arrest of EC that was induced by Cytomix (Figure 4.3). IL1RL1, another pro-inflammatory factor, has been associated with HF and mortality after MI<sup>336</sup>, but also with hemodynamic improvement

following left ventricular assist device (LVAD) implantation<sup>337</sup>. So far, its secretion was only identified in CM and lung epithelial cells, in response to TNF $\alpha$  and IL-1 $\beta$ <sup>336,338</sup>, though its expression in EC has never been studied. Finally, CXCL5 was expressed in Cytomix samples at approximately twice the levels seen after TNF $\alpha$ , IL-1 $\beta$  or hIL-6 treatment combined, standing out from other additive/synergistic effects of Cytomix. CXCL5, a bona fide neutrophil chemoattractant, was shown to be inducible at least by IL-1 $\beta$ <sup>339</sup> and is often used as a marker for acute coronary syndrome<sup>340</sup>. Matsuo *et al.* (2009) demonstrated that treatment of EC with exogenous CXCL5 was however proliferative and pro-angiogenic<sup>341</sup>, a response not reflected in the cell cycle data obtained in our model.

CXCL5, CXCL1 and G-CSF, but not GM-CSF, were indeed quantitatively induced by Cytomix, as confirmed by ELISA. ET-1 was quantified as well and was not found to be regulated by the treatment, surprisingly<sup>277,278</sup>. Of note, the values calculated in all conditions were within the limits of detection for all ELISA, ensuring that this lack of effect was not due to low sensitivity. ELISA was preferred as a validation method over RT-qPCR or western blotting because it specifically tests the secreted portion of the cell proteome. This is an important distinction because some of the factors screened in the array can be constitutively expressed but only secreted in certain conditions<sup>342,343</sup>. When quantifying these soluble factors in co-cultures, the induction of CXCL1 was lost, unlike CXCL5 and G-CSF, indicating a possible feedback mechanism on the release of CXCL1 by CM-derived soluble mediators. ET-1 was found increased in CM after Cytomix treatment but not in EC or in co-culture media, suggesting that one effect of co-culture of CM with EC is to dampen the release of cardioactive and/or inflammatory proteins by CM. Finally, the release of CXCL5/1, G-/GM-CSF, but not of ET-1 in cardiac fibroblasts supernatants was also stimulated by Cytomix, indicating that these proteins cannot be used as specific markers of the EC response to inflammation in cardiac tissue.

The capture and detection antibodies included within the ELISA kits were equally reactive with human and rat protein homologues (a concern for the CM condition). It should be noted that vesicular bodies were excluded from the supernatants before performing the profiler array and

the ELISA. It is thus possible that some paracrine mediators responsible for effects on CM, or better markers of the EC response to Cytomix, were eliminated as part of vesicular cargoes. In this project the interest was first restricted to protein markers and mediators, but other types of paracrine signals may be investigated in future experiments (e.g. miRNA, lipids, exosomes). Finally, given the differential response of Cytomix-treated EC to thrombin (implicating calcium waves as shown above), and given the role of calcium in exocytosis<sup>344</sup>, it would be extremely interesting to test whether the secretome profile of EC differs quantitatively or qualitatively after thrombin treatments, in UT versus Cytomix-treated cells.

#### **4.4.8 Are the soluble factors secreted by Cytomix-treated HCMEC likely to affect the function of ARVM in co-culture?**

I have established that CXCL5 and G-CSF are secreted by EC in co-cultures with CM after Cytomix pre-conditioning and might be useful as soluble markers of EC inflammation (though non-specifically, as discussed previously). Further experiments are now required to determine whether these proteins contribute to the effects of EC on CM function. The mRNA expression of their canonical receptors in CM was found to be low (Figure 4.10). However, there are other large datasets which have been published openly and could have been used for this project. Only two were selected, first for practical reasons, but also because not all datasets have been produced appropriately (at least for the purpose of this meta-analysis). Fuller *et al.* (2015) was chosen for its use of adult rat CM and the fact that data were normalised and contained more replicates than other datasets<sup>209</sup>. A downside of this dataset was the absence of some genes of interest for this project. The Tabula Muris, on the other hand, provides high-quality data and data could be extracted for more relevant genes. In this analysis, usual CM markers served as positive controls. Even though CM in both datasets technically expressed the mRNA for the receptors of some chemokines and cytokines of interest (i.e. ET-1 and CSF receptors, but not the receptors for CXCL1/5 or for IL-6), the actual number of cells expressing significant levels of these mRNA was surprisingly low in Tabula Muris. This was consistent with the data

collected in the 2015 microarray, where transcription of these genes was also lower than the majority of other genes measured in CM. Importantly, these data do not indicate whether the low expression of some genes is compensated by a low turn-over of the proteins. It is also possible that expression is low at baseline but induced in co-culture with EC, for example. As described above, not all genes could be investigated with this method.

The next three steps should be to: (1) validate this result using RT-qPCR and western blotting in CM after co-culture with HCMEC with and without inhibitory antibodies, (2) determine if CM from HF patients express these genes differently, as this could facilitate novel effects of EC in co-culture, and (3) apply this sort of meta-analysis to datasets obtained from single-cell RNA sequencing, where cell-cell ligand-receptor correlation analyses are possible<sup>70</sup>. This last step may even highlight novel mediators implicated in the paracrine EC-CM crosstalk.

#### **4.4.9 Conclusions on the effects of Cytomix in EC**

In conclusion, the results in this chapter demonstrate that a 24-hours treatment with Cytomix induces a pro-inflammatory response in HCMEC, characterised by inhibition of proliferation and the secretion of cytokines and chemokines known to contribute to inflammation. Cytomix also modified the responses of EC to thrombin, with smaller calcium transients, enhanced NO synthesis, and a lack of endothelial permeabilization. Although more needs to be done to fully define this effect and its mechanisms, this might be a good starting point to expand further our understanding of the cardiotropic role of thrombin in sepsis, RA, or acute coronary syndrome, where it participates in the inflammatory environment of the vascular endothelium<sup>298</sup>.

In this chapter, data also converge to show how the phenotype of EC can differ in response to different cytokines. Cytomix was not the summation of cytokine responses but the result of a complex interplay between cytokine signalling pathways and targets. Future experiments might include the confirmation that the Cytomix-induced phenotype described in this chapter models appropriately the myocardial microvascular inflammation, by phenotyping in parallel

EC isolated from cardiac biopsies of HF patients and by replacing Cytomix by serum from HF or RA patients. Comparing the effects of individual cytokines with Cytomix would generate extremely valuable data as to the relevance of their use in isolation *in vitro*.

Co-culture of EC and CM dampened the secretion of CXCL1 by EC, and of ET-1 by CM. This suggests that the co-culture design optimised in the previous chapter allows for second degree autocrine/paracrine effects to occur, with potential feedback loops from CM to EC. This would not be achievable with the use of conditioned media and is an excellent finding to strengthen the relevance of the Transwell co-culture model. Although the main goal for this chapter has been completed, there are still no paracrine mediators which have been definitely shown to be involved in the effects of EC on CM in co-cultures. In the absence of thrombin, no significant NO was synthesised by HCMEC, and no secreted protein identified with the profiler array was matched with a high expression of its known receptors in CM, hence limiting the likelihood of a signal transduction in CM (though this needs to be confirmed experimentally). To best define the paracrine activity of EC on CM after Cytomix treatment, CM function needs to be assessed after co-culture with Cytomix-treated EC. This is described in the next Chapter.

# 5.

## **Effects of Cytomix-treated cardiac microvascular endothelial cells on co-cultured adult rat ventricular myocytes**

## 5.1 Introduction

Having validated the model of co-culture for EC and CM, and the pro-inflammatory intervention on EC (Cytomix) in the two previous chapters, it is now possible to test the original hypothesis in this project. We have established that there was no sarcomeric remodelling after 24 hours of co-culture. Although it cannot be entirely excluded that Cytomix pre-conditioning in EC might in fact introduce that sort of remodelling in CM, I have decided to focus on the excitation-contraction coupling properties of the CM.

Starting from the observation in Chapter 3 that co-culture with EC produces a prolongation of calcium transients in CM, the first aim of this Chapter is to determine if that effect is modified when EC are pre-conditioned by Cytomix. To validate the hypothesis that EC paracrine effects on CM change upon inflammatory stimulation, it is crucial that the effects of Cytomix are EC-specific, hence its use in pre-conditioning of EC and not as a treatment of co-cultures where CM could also respond directly to Cytomix and introduce a second variable to the crosstalk.

Other properties of the excitation-contraction coupling, i.e. upstream or downstream of calcium release, will be characterised to better define potential targets of paracrine mediators involved in the EC-CM crosstalk. NO, for example, has been proposed as a mediator able to regulate  $\text{Ca}^{2+}$  entry via the L-type calcium channel<sup>107</sup>, the efficiency of calcium-induced calcium release and the SR calcium loading<sup>112</sup> (i.e. the amplitude of calcium transients), the efficiency of the SR  $\text{Ca}^{2+}$  uptake via SERCA<sup>142</sup>, but also the  $\text{Ca}^{2+}$  sensitivity of myofilaments, the relaxation of cardiac tissue after systole, diastolic stiffness<sup>89,345,346</sup> and the response to increased preload<sup>347</sup>.

Should a Cytomix treatment in EC affect the rate of decay of calcium transients in co-cultured CM, it will be of interest to determine which mechanism(s) of  $\text{Ca}^{2+}$  efflux is targeted. SERCA and NCX, the main two mechanisms, have distinct roles in calcium homeostasis: while SERCA increases SR content, NCX extrudes  $\text{Ca}^{2+}$  to the extracellular space. It will thus be useful to determine if the relative activity of SERCA and NCX is affected by co-culture with Cytomix-



treated EC, as is the case in HF<sup>133</sup>. However, it should be kept in mind as a limitation that NCX exhibits lower expression in rat CM than in human CM, and inversely for SERCA<sup>111</sup>.

ERK1/2 and Akt signalling pathways respond to cytokines, ROS, EC-produced cardiotropes (e.g. ET-1). They are also known to be particularly responsive to factors such as Epidermal Growth Factor (EGF), which was found in the supernatants of both UT and Cytomix-treated EC (Table 4.2)<sup>348–350</sup>. Analysing their expression and activation by western blotting will help contextualise the response of CM to co-culture with EC, and with Cytomix-treated EC. Indeed, phosphorylation of ERK1/2 and/or Akt provides cytoprotection in CM and stimulates cardiac hypertrophy, but doing so also contributes to the development of HF when hypertrophy becomes less compensated by other mechanisms<sup>350–352</sup>. In addition to this pro-hypertrophic effect, and more relevantly to the focus of this chapter, ERK1/2 is also known to decrease SERCA expression *in vitro* and *in vivo*, to induce hypophosphorylation of PLB and to lower LTCC currents<sup>353,354</sup>. Conversely, activation of Akt was linked with higher SERCA expression and activity in cultured myocytes<sup>355</sup>.

To summarise, in this last chapter of results, I will aim to address the general hypothesis of this project, by: (1) testing whether pre-conditioning EC with Cytomix modifies their effect on Ca<sup>2+</sup> extrusion in co-cultured CM. (2) Determine if the expression and activity of SERCA and NCX are differentially regulated by co-cultures. (3) Test the efficiency of calcium release from the SR. (4) Measure the phosphorylation of regulators of SERCA, e.g. PLB, ERK1/2 and Akt. (5) Investigate whether Cytomix-treated EC alter the contractility of co-cultured CM. (6) Test the Ca<sup>2+</sup> sensitivity of myofilaments after co-culture.

## 5.2 Methods

The methods described in this chapter are described in full in Chapter 2.

### 5.2.1 Cell culture, cytokine treatments, and co-cultures

Human cardiac microvascular EC (HCMEC) and adult rat ventricular myocytes (ARVM) were purchased, isolated, grown, and co-cultured as described previously. Cytomix (1 ng/ml TNF $\alpha$ , 1 ng/ml IL-1 $\beta$ , and 25 ng/ml hIL-6) was used to treat HCMEC for 24 hours prior to co-culture in Transwell inserts with freshly isolated ARVM. CM alone served as negative control for co-cultures, and CM treated with Cytomix for 4 hours served as a secondary control. Co-cultures were stopped after 4 hours.

### 5.2.2 Optical Mapping, fractional release, and quantification of SERCA/NCX activity

Calcium transients were recorded in ARVM using the cytosolic free Ca<sup>2+</sup> indicator Fluo-4 AM, as described in previous chapters. Briefly, ARVM were loaded for 15 min with Fluo-4 AM while still in co-culture with HCMEC. Transwell inserts were then removed and ARVM transferred on the microscope stage to equilibrate for 15 min in superfused 37°C Tyrode's solution before the recording. Samples were paced continuously at 1 Hz. ImageJ was used to extract traces of Fluo-4 AM signals from individual cells. Background noise was corrected for each recording using cell-free regions. Traces were exported to Clampfit (pClamp suite) where the calcium transient parameters were measured manually. The amplitude, time to peak, time to 50% and 90% decay, and the time constant *tau* (from which the rate of decay *kappa* was calculated) were averaged for all cells within each biological replicate (20 cells minimum).

To calculate the fractional release of SR Ca<sup>2+</sup> during calcium transients at 1 Hz, caffeine was used at 40 mM and injected near cells of interest using a micropipette, while field stimulation was stopped. Max F<sub>1</sub>/F<sub>0</sub> of calcium transients at 1 Hz was divided by the max F<sub>1</sub>/F<sub>0</sub> of caffeine-induced calcium release.

The activity of SERCA was calculated as the difference of rates of decay between the caffeine and caffeine-free calcium transients. Switching to Na<sup>+</sup>-free and Ca<sup>2+</sup>-free Tyrode's solution, a new calcium release was induced using caffeine. NCX activity was calculated as the difference of rates of decay for caffeine-induced calcium releases obtained with the normal Tyrode's and the modified Tyrode's solutions. The remainder was attributed to slow extrusion mechanisms of calcium (e.g. mitochondrial Ca<sup>2+</sup> uniporter).

### **5.2.3 Western blotting**

Protein expression of PLB, phosphorylated PLB, NCX, ERK1/2 and phosphorylated ERK1/2 was quantified using SDS-PAGE separation and western blotting, run as described in Section 2.4 with GAPDH as loading control. All primary antibodies (listed in Section 2.9) were used at 1:1000 in blocking buffer, except the anti-GAPDH antibody which was used at 1:3000. The secondary antibodies, all HRP-conjugated, were diluted at 1:3000 in blocking buffer and used accordingly with the species of the primary antibodies (anti-mouse or anti-rabbit). The amounts of proteins were normalised to the level of GAPDH. ECL reaction was used to detect proteins, and blot images were captured on radiographic films. Quantification was done using ImageJ, after conversion of images in 8-bits.

### **5.2.4 CytoCypher™ MultiCell system – Contractility and calcium dual measurements**

Contractility of ARVM was measured with the fully automated CytoCypher™ MultiCell system, which is based on IonOptix technology. After co-culture, CM were washed and transferred to a glass bottom MatTek dish. Recordings were done in normal Tyrode's solution, after 15 min equilibration and under field stimulation at 1 Hz. Of note, at the time of these experiments, the system did not yet include a perfusion mechanism, so all recordings were performed in a static Tyrode's solution at 37°C. The ratiometric fluorescent Ca<sup>2+</sup> indicator Fura-2 AM was used to simultaneously record calcium transients. Cells were incubated with the dye for 15 min, while in co-cultures, prior to loading on stage. Analysis was automatically done in MultiCell.

### **5.2.5 Calcium-contraction hysteresis loops and calcium sensitivity of myofilaments**

The sensitivity of myofilaments to calcium, regulating the calcium-dependency of contractions, was measured as the slope of the linear segment of calcium-sarcomere length loops. These were generated by plotting the sarcomere shortening as a function of Fura-2 intensity, hence creating hysteresis loops.

### **5.2.6 Adult living ultrathin myocardial slices and force transducer**

Adult rat myocardial slices of 300  $\mu\text{m}$  thickness and approximately 7x7 mm, were cut from the left ventricle wall of Sprague-Dawley rats using a vibratome. Slices were randomly assigned to test groups and cultured for 24 hours in superfused 37°C oxygenated medium. Throughout, slices were kept at a 17% isometric stretch using custom-made stainless steel stretchers and 3D-printed rings glued to the extremities of slices, and paced at 1 Hz by field stimulation.

After 24 hours of culture, slices were removed from culture chambers and connected to a force transducer in isometric configuration. Recording was performed under 1 Hz field stimulation, while slices were superfused with an oxygenated Tyrode's solution. Starting from 0% stretch, slices were progressively stretched up to 30% and data collected at stable state. Baseline was read as passive tension and the amplitude (corrected for the cross-sectional area of slices) as contractility. Recording and analysis were performed with the pClamp suite.

### **5.2.7 Statistics**

A D'Agostino-Pearson test was used to test the normality of sample distribution. Statistical significance was then calculated with an ordinary one-way ANOVA with Bonferroni's post-hoc test (parametric) or a Kruskal-Wallis test with Dunn's correction for multiple comparisons (non-parametric). Significance is shown as: \*  $p < 0.05$ . \*\*  $p < 0.01$ . \*\*\*  $p < 0.001$ . \*\*\*\*  $p < 0.0001$ .

## 5.3 Results

### 5.3.1 Shortening of calcium transients in CM after co-culture with Cytomix-treated EC

To establish the effect of co-culture with Cytomix-treated EC (compared to untreated) on the calcium handling of CM, calcium transients were recorded using Fluo-4 and the technique of Optical Mapping. First, as seen in Figure 5.1, this experiment reproduced the findings shown in Figures 3.3, 3.5 and 3.6, in which co-culture with untreated EC had no effect on amplitude or time to decay of calcium transients, but prolonged significantly their return to baseline (i.e. longer time to 90% decay and smaller rate of decay  $\kappa$ ). Indeed, in this experiment, there was a 1.3-fold increase of the time to 90% decay ( $p = 0.0005$ ). Pre-conditioning HCMEC with Cytomix for 24 hours prior to co-culture, however, resulted in a significant shortening of the time to 50% and 90% decay, and of the rate of decay of transients in CM (0.71-fold change,  $p = 0.0063$ ; 0.59-fold change,  $p = 0.0021$ ; 1.74-fold increase,  $p = 0.0049$ , respectively). Because this is opposed to the basal effects of co-culture with EC, there was no statistical difference between the control (no EC) and Cytomix samples. There was also no change between the time to peak and amplitude of co-cultures with untreated and Cytomix-treated EC, although there was a significant reduction of baseline fluorescence ( $F_0$ ) in the Cytomix group (0.43-fold change,  $p = 0.0209$ ). This makes any interpretation of  $F_1/F_0$  amplitude difficult, due to the non-ratiometric properties of Fluo-4. To summarise, and as is shown in Figure 5.1B, Cytomix treatment in EC induced a narrowing of calcium transients in CM and a steeper return to baseline after the peak than after co-culture with untreated EC. The contribution of individual cytokines to this effect of Cytomix was investigated with cytokine-specific pre-conditioning. No parameter was significantly different between TNF $\alpha$ , IL-1 $\beta$  and hIL-6 pre-conditioning groups but hIL-6 was closest of all three to the Cytomix values, with a significant reduction of the time to 90% decay and an increase of the rate of decay compared to the untreated-EC group (0.74-fold change,  $p = 0.0274$ ; 1.36-fold change,  $p = 0.0424$ , respectively). Interestingly, hIL-6 was also characterised by a lower baseline fluorescence than UT, nearly reaching significance ( $p = 0.051$ ), while the TNF $\alpha$  and IL-1 $\beta$  samples could not be differentiated from the UT sample.

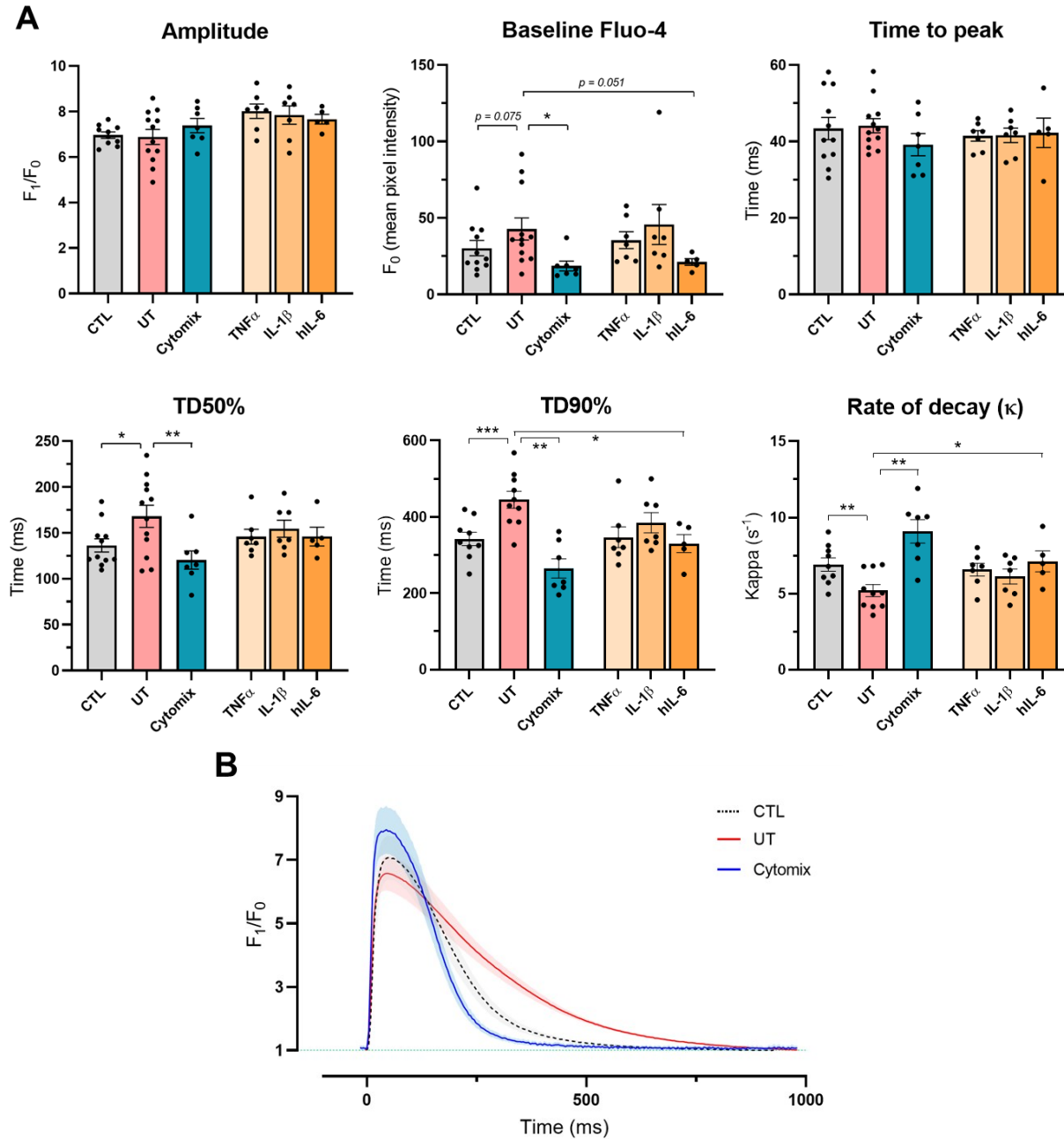


**Figure 5.1: Cytomix-treated EC shortened the calcium transients in co-cultured CM compared to untreated EC**

Calcium transient analysis in ARVM (Optical Mapping imaging of Fluo-4 AM), 4 hours after co-culture with HCMEC (UT), cytokine-treated HCMEC or no EC (CTL). **A.** Amplitude ( $F_1/F_0$ ), Baseline Fluo-4 intensity ( $F_0$ ), Time to peak, Time to 50% decay (TD50%), Time to 90% decay (TD90%) and Rate of decay (Kappa) of 1 Hz calcium transients. N = 5 (hIL-6), N = 7 (TNF $\alpha$ , IL-1 $\beta$ , Cytomix), N = 10 (CTL), 12 (UT). Data were compared with a one-way ANOVA and Bonferroni's post-hoc test. Data are shown as mean  $\pm$  SEM. \*  $p < 0.05$ . \*\*  $p < 0.01$ . \*\*\*  $p < 0.001$ . **B.** Representative calcium transients for the main three conditions, averaged from 6 traces each. Coloured shadows cover the SEM.

### 5.3.2 Efficiency of calcium release from the SR of CM after co-culture with EC

The amplitude of calcium transients is regulated by two properties: the amount of  $\text{Ca}^{2+}$  that is stored in the SR, and the proportion of that amount that is released into the cytosol during each calcium transient. To test if these properties were left unaffected by co-culture with EC and Cytomix treatment, which would explain the lack of change for the amplitude of transients (Figure 5.1), the fractional release of  $\text{Ca}^{2+}$  from the SR was quantified (Figure 5.2). Caffeine was used to deplete the SR, allowing direct comparison with the amplitude of calcium release produced at 1Hz. Due to the differences in  $F_0$  between conditions it is not recommended to compare the amplitude of caffeine-induced transients (i.e. SR calcium stores) across samples.

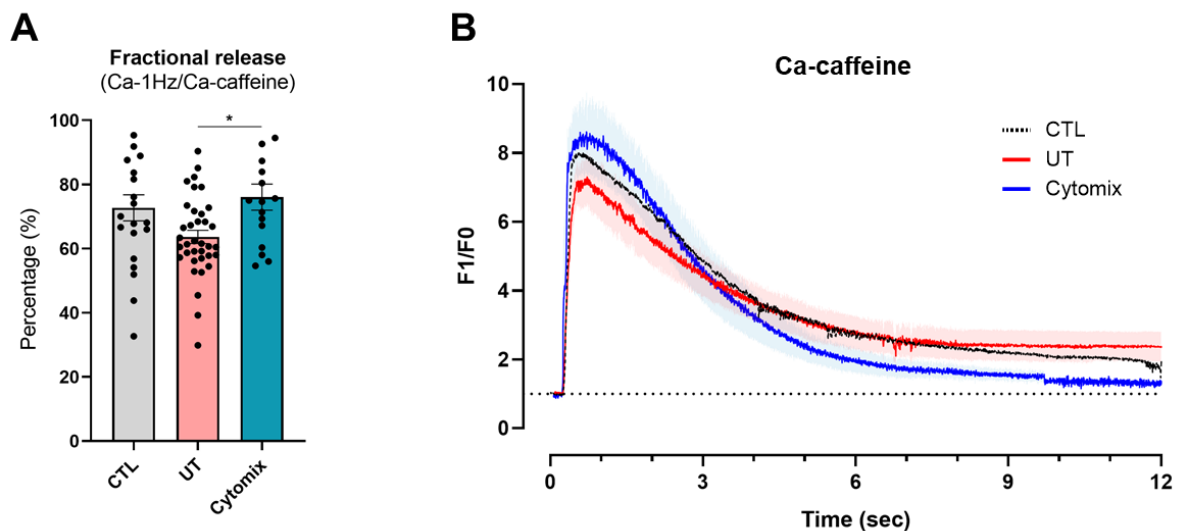


**Figure 5.2: Efficiency of SR  $\text{Ca}^{2+}$  release was improved in CM co-cultured with Cytomix-treated EC compared to untreated EC**

Calcium transient analysis in ARVM by Optical Mapping imaging of Fluo-4 AM, after acute perfusion with 40 mM caffeine, 4 hours after co-culture with HCMEC (UT), Cytomix-treated HCMEC or no EC (CTL). **A.** Fractional release of  $\text{Ca}^{2+}$  (percentage of SR stores), expressed as the ratio of amplitude of calcium transients at 1 Hz (no caffeine) over the amplitude of the caffeine-induced calcium release. Data were compared with a one-way ANOVA and Bonferroni's post-hoc test. Data are shown as mean  $\pm$  SEM, with data points representing 15-36 technical replicates (pooled from 3 biological samples). \*  $p < 0.05$ . **B.** Mean intensity of Fluo-4 signal over time, showing caffeine-induced calcium releases from the SR in each condition, averaged from 5 representative traces. Coloured shadows cover the SEM.

Regardless of the amplitude of caffeine-induced calcium releases, Figure 5.2A shows that the amplitude of calcium transients produced at 1 Hz represented only 63% of  $\text{Ca}^{2+}$  stores after co-culture with untreated EC, but 76% with Cytomix-treated EC (1.2-fold change,  $p = 0.0263$ ). This increase is suggestive of an improvement of calcium-induced calcium release in CM.

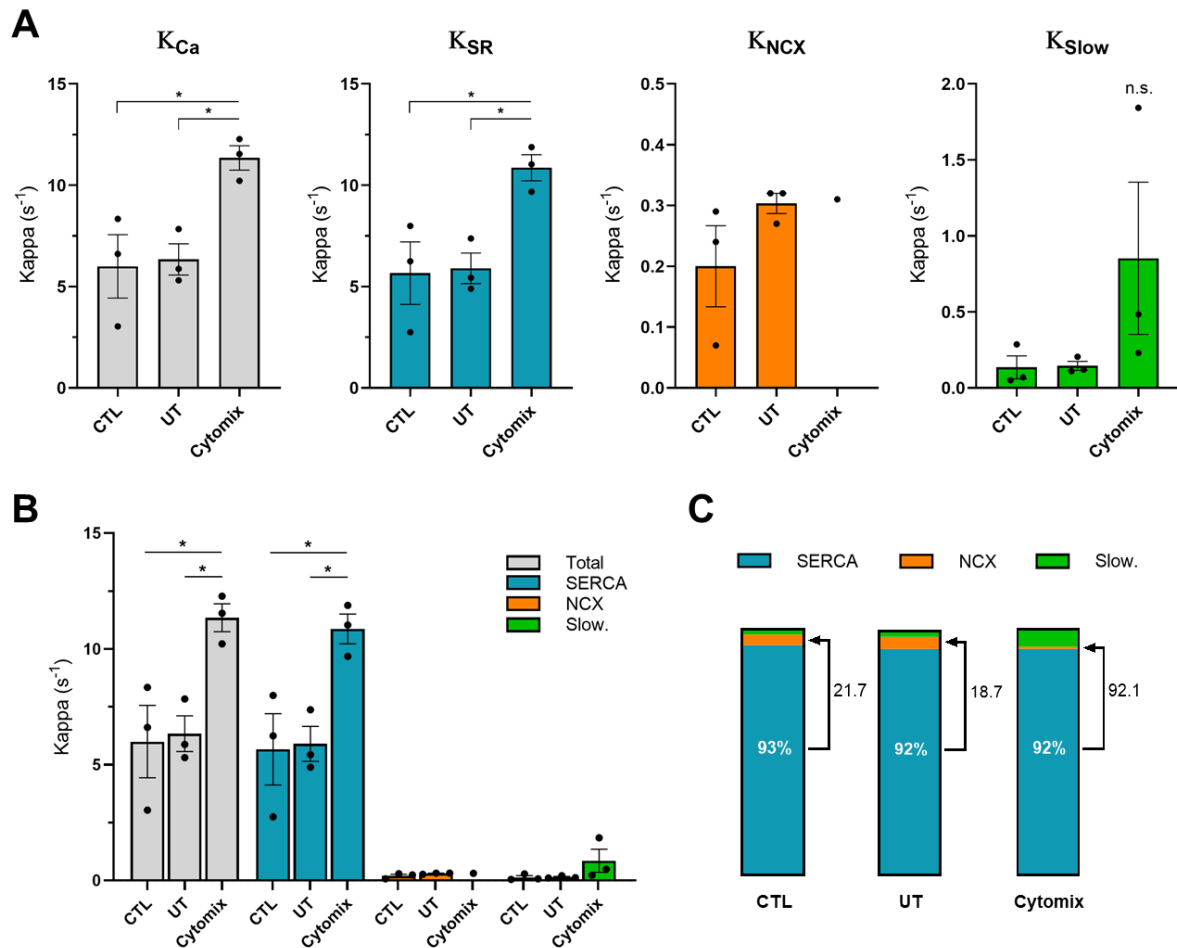


**Figure 5.3:  $\text{Ca}^{2+}$  extrusion involving SERCA but not NCX was increased in CM after co-culture with Cytomix-treated HCMEC**

Optical Mapping analysis of  $\text{Ca}^{2+}$  extrusion mechanisms in CM, comparing the rate of decay of 1 Hz, caffeine-induced, and  $0 \text{ Na}^+ / 0 \text{ Ca}^{2+}$  calcium transients, 4 hours after co-culture with HCMEC. **A.** Rates of decay of normal calcium transients ( $K_{Ca}$ ), SERCA ( $K_{SR}$ ), NCX ( $K_{NCX}$ ) and other mechanisms ( $K_{Slow}$ ).  $N = 3$  biological replicates. Data are expressed as mean  $\pm$  SEM and compared with the same scale in panel **(B)**. Data were compared with a one-way ANOVA and Bonferroni's post-hoc test. \*  $p < 0.05$ .

**C.** Contribution of each extrusion mechanism to the total rate of decay (percentage). The arrow and number shown on the graph indicate the SERCA:NCX ratio.



### **5.3.3 Cytomix-induced shortening of calcium transients in EC-CM co-cultures is due to higher SERCA activity**

To explain further the differences of calcium transient duration that were observed above, the contribution of SERCA, NCX and other (slower) mechanisms of  $\text{Ca}^{2+}$  extrusion was measured. This was achieved by measuring the rate of decay of normal calcium transients (1 Hz), calcium transients induced by caffeine at 40 mM, and caffeine-induced calcium release in conditions free of  $\text{Na}^+$  and extracellular  $\text{Ca}^{2+}$  (Figure 5.3). As seen in this figure, due to the low number of biological replicates which could be recorded and the variability in the control sample, the rate of decay was not affected by co-culture with untreated EC, therefore hindering analysis of the extrusion mechanism(s) responsible for this effect. However, importantly the Cytomix pre-conditioning of EC led to a significantly higher rate of decay than untreated EC (1.8-fold change,  $p = 0.0473$ ). SERCA-dependent extrusion of  $\text{Ca}^{2+}$  was found significantly improved in Cytomix samples, rising from 5.9 to 10.9  $\text{s}^{-1}$  (1.8-fold change,  $p = 0.0479$ ). As seen in Figure 5.3C, this indicates that the relative contribution of SERCA to the decay of calcium transients was similar between UT and Cytomix (92%), and that SERCA activity is potentiated by Cytomix treatment in co-cultured EC. Of note, the activity of NCX was so minimal that the rate of decay attributed to it could not be calculated with this method on multiple occasions, causing a relative increase of activity for slow mechanisms in the Cytomix group (not significant). Of note, the contribution of NCX to calcium transients was found to be only 4.3%, 4.9% and 1% in control, untreated-EC, and Cytomix-treated EC, respectively. Overall, these data indicate that the faster return to baseline in the Cytomix samples is caused by an increased activity of SERCA which outperforms the activity of other  $\text{Ca}^{2+}$  extrusion mechanisms (Figure 5.3B).

### **5.3.4 Changes of protein expression and phosphorylation in CM after co-culture**

To investigate the changes in SERCA activity shown above, but also the improved fractional release of  $\text{Ca}^{2+}$  shown in Figure 5.2 and the apparent lack of effect of NCX in some Cytomix samples, the protein expression of NCX, RyR2, SERCA and PLB was measured by western

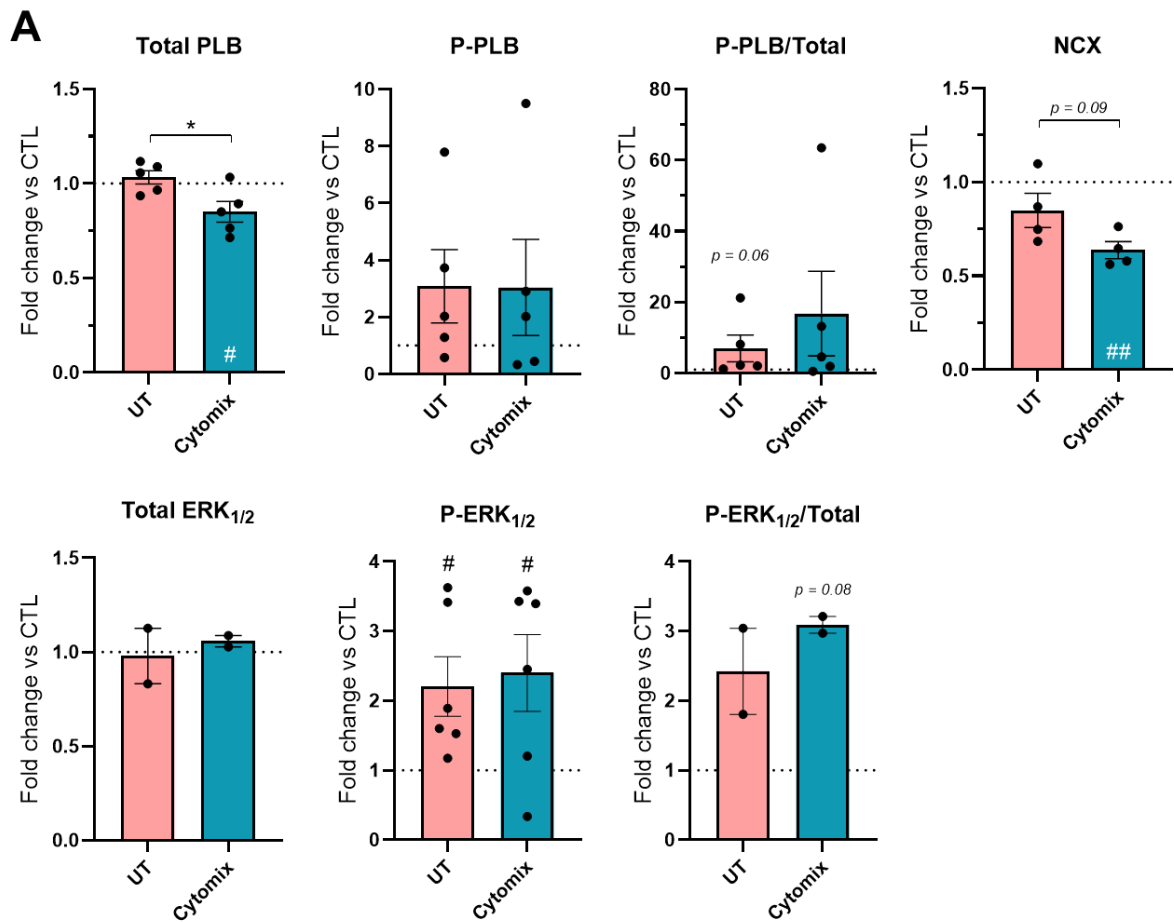


**Figure 5.4: Protein expression profile of CM after 4 hours of co-culture with EC**

Protein expression in ARVM, as measured by western blotting, 4 hours after co-culture with untreated or Cytomix-treated HCMEC. Biological replicates consist of three pooled technical replicates. Protein expression was normalised to the level of GAPDH. Data are then expressed as fold change of control (CM alone), shown as mean  $\pm$  SEM and compared with one-way ANOVA and Bonferroni's post hoc test. N = 5 for total-PLB, phosphorylated PLB and their ratio. N = 4 for NCX. N = 6 for total ERK<sub>1/2</sub>. N = 2 for phosphorylated ERK<sub>1/2</sub> and its relative expression compared to total ERK<sub>1/2</sub>. \*  $p < 0.05$ . #  $p < 0.05$  vs CTL. ##  $p < 0.01$  vs CTL.

blotting. However, RyR2 and SERCA were not detectable in ARVM using available antibodies and could not be included in this analysis. As can be seen in Figure 5.4, there was 0.6-fold reduction of NCX expression in Cytomix samples compared to control ( $p = 0.0055$ ), but not in the UT group where the level of NCX was higher than in the Cytomix group (1.3-fold change,  $p = 0.0942$ ). Total PLB expression in co-cultures with Cytomix-treated EC was significantly reduced by 15% and 18% from control and co-cultures with untreated EC, respectively ( $p = 0.0405$  and  $0.0135$ ). After normalisation with GAPDH, the levels of phosphorylated PLB were too variable to detect any significant difference between conditions.

Turning to other kinases, the levels of total and phosphorylated ERK1/2, and Akt, were also investigated. The available Akt antibody proved a poor detector of Akt in ARVM. To date, two blots for total ERK1/2 have been successful, and the level of phosphorylated ERK1/2 in co-cultures was found significantly higher than in the control group, regardless of pre-conditioning ( $p = 0.0289$  for UT,  $p = 0.05$  for Cytomix).

### **5.3.5 Co-culture with untreated or Cytomix-treated EC did not alter CM contractility**

Since co-culture of CM with Cytomix-treated EC provoked a narrowing of calcium transients compared to co-cultures with untreated EC, it was hypothesised that CM contractions would equally be affected. To test this, the contractility of ARVM (here the peak cell shortening) was recorded and automatically analysed using a CytoCypher™ MultiCell system, newly acquired for the benefits of the Cardiac Section at NHLI, and set up by Peter Wright, PhD. Surprisingly, there was no difference between UT and Cytomix samples, nor when compared to the control group (Figure 5.5). Of note, adding Cytomix to CM alone for 4 hours resulted in significantly smaller contractions than in co-cultures with Cytomix-treated EC, suggesting once again that the effects seen in the Cytomix sample are unlikely to be caused by cytokine carry-over.

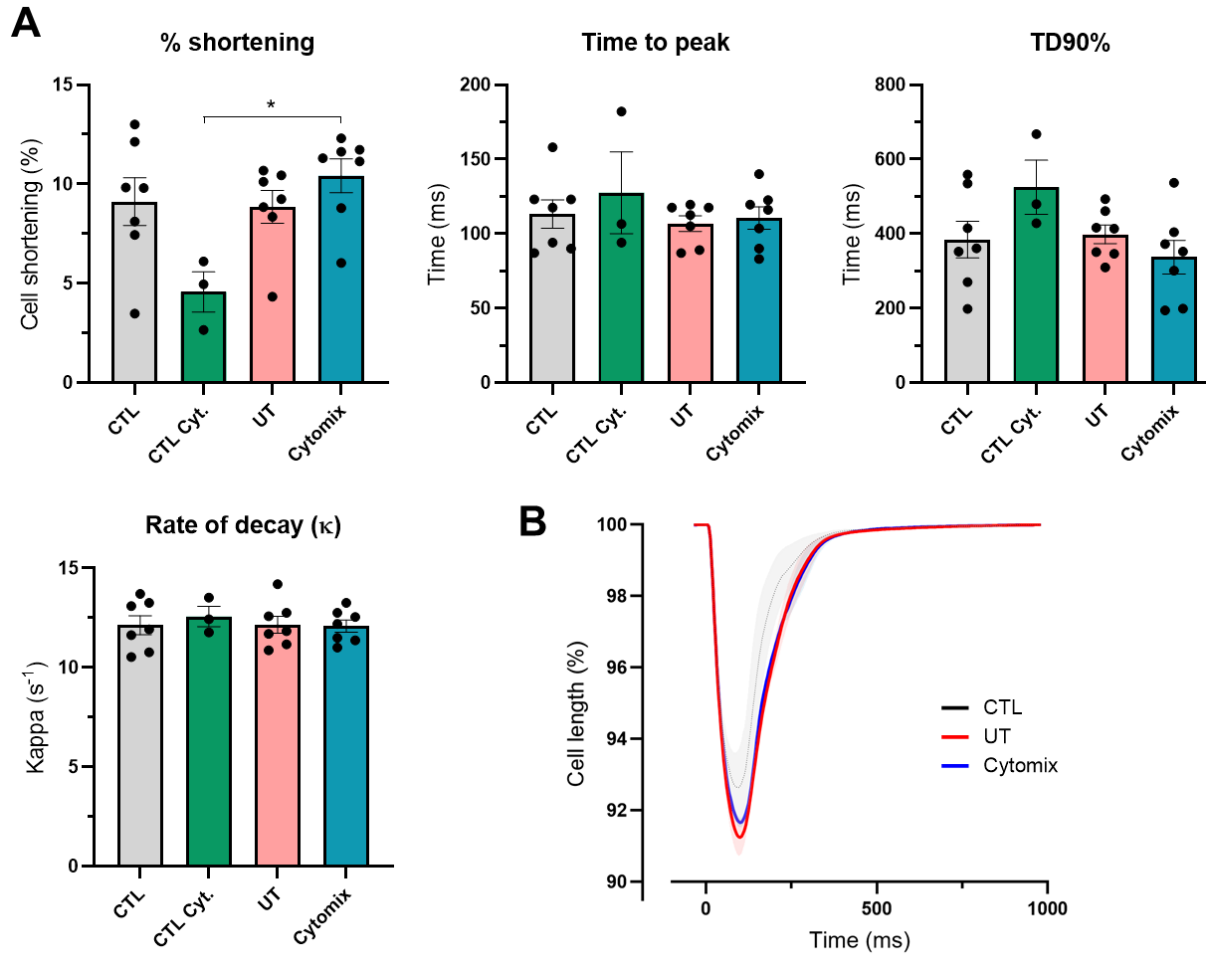


**Figure 5.5: Lack of effect of co-culture with untreated or Cytomix-treated EC on contractility of CM, using CytoCypher™**

Contractility of isolated ARVM (by automated IonOptix analysis), 4 hours after co-culture with HCMEC (UT), Cytomix-treated HCMEC or no EC (CTL). CM were also treated for 4 hours with Cytomix as an additional control (CTL Cyt.). **A.** Cell shortening at peak (% of cell length), Time to peak, Time to 90% decay (TD90%) and Rate of decay (Kappa) of 1 Hz contractions. N = 7 (CTL, UT, Cytomix) and N = 3 (CTL Cyt.). Data were compared with a one-way ANOVA and Bonferroni's post-hoc test and shown as mean +/- SEM. \* p < 0.05. **B.** Representative contractions averaged from 6 traces collected from a common biological replicate. Coloured shadows cover the SEM.

### **5.3.6 Co-culture of CM with untreated or Cytomix-treated EC did not alter the calcium sensitivity of myofilaments**

An advantage of the CytoCypher™ MultiCell system is the built-in Fura-2 imaging equipment to record calcium transients in parallel to contractions. Fura-2 is a ratiometric fluorescent dye sensitive to free-cytosolic  $\text{Ca}^{2+}$ , therefore more accurate for the detection of changes in  $\text{Ca}^{2+}$  levels than non-ratiometric dyes (such as Fluo-4). First, as shown in Figure 5.6A, the calcium transients recorded using Fura-2 mirrored the changes seen with Fluo-4. Indeed, Cytomix treatment of EC prior to co-culture was associated with a significantly faster return to baseline and thus a narrowing of calcium transients compared to co-cultures with untreated EC: TD90% fell from 494 to 272 ms in average ( $p < 0.0001$ ), while the rate of decay increased 1.5 fold ( $p < 0.0001$ ). Time to peak was unchanged across all samples, but interestingly the peak fluorescence was found to be lower in the UT group than in control cells or in the Cytomix group (0.87-fold compared to both,  $p = 0.0001$  and  $p < 0.0001$  respectively). For a small number of cells, the automated data collection from the MultiCell system allowed for calcium-contraction hysteresis loops to be constructed. Using these, no difference of slope (for the linear section of loops) was found between the UT and Cytomix samples, suggesting that the sensitivity of myofilaments to  $\text{Ca}^{2+}$  is unchanged during co-culture and unaltered by Cytomix pre-conditioning of EC. However, the small number of cells that could be used for this dataset warrants more biological repeats of this experiment before changes of calcium sensitivity are fully excluded.

### **5.3.7 Cytomix only affected the contractility of cardiac tissue at high levels of preload**

Given the effect of Cytomix on the duration of calcium transients in CM after co-cultures, why was this effect not translated into changes of contractility? To answer this question, we must take a step back and examine the effect of Cytomix on the contractility of cardiac tissue. Living rat myocardial slices were cultured for 24 hours with Cytomix and their contractility measured

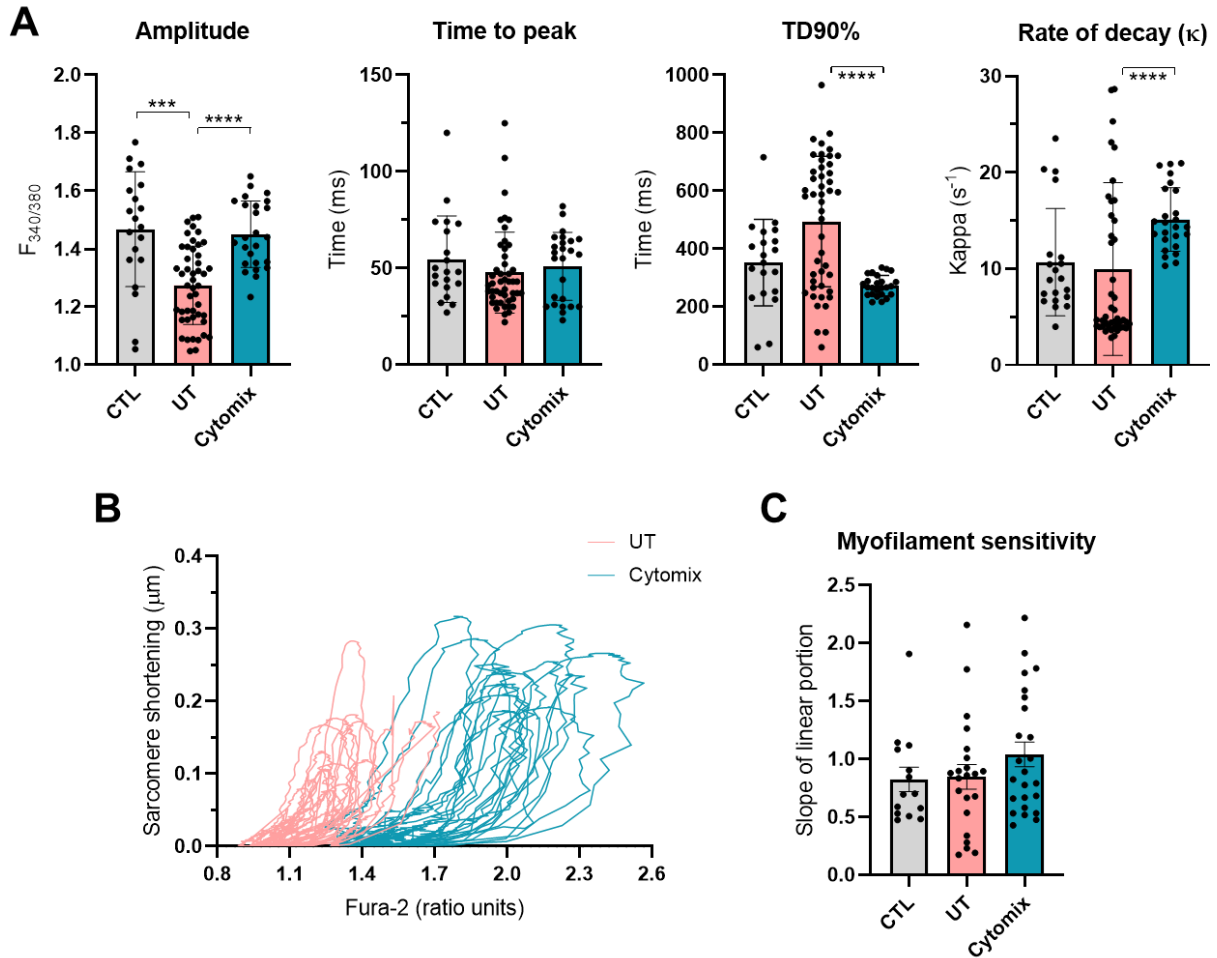


**Figure 5.6: Dual measurement of calcium and contractility in CM showed no significant effect of co-culture and Cytomix treatment on the sensitivity of myofilaments to  $Ca^{2+}$**

Analysis of calcium transients obtained with Fura-2 on the CytoCypher™ MultiCell automated system and hysteresis loops of calcium-contraction to extrapolate the sensitivity of myofilaments to  $Ca^{2+}$ . **A.** Amplitude (peak fluorescence), Time to peak, Time to 90% decay (TD90%) and Rate of decay ( $\kappa$ ) of calcium transients at 1 Hz.  $n = 20$  cells (CTL), 47 (UT) and 25 (Cytomix),  $N = 3$  biological replicates. Data are expressed as mean  $\pm$  SD, with data points showing individual cells ( $n$ ). **B.** Superposition of representative hysteresis loops for each condition. **C.** Myofilament sensitivity to  $Ca^{2+}$  (i.e. the slope of the linear portion in hysteresis loops).  $n = 14$  cells (CTL), 22 (UT) and 24 (Cytomix),  $N = 3$  biological replicates. Data are shown as mean  $\pm$  SEM, with data points showing individual cells ( $n$ ). For all panels, data were compared with a Kruskal-Wallis test with Dunn's multiple comparisons test, based on the  $n$  values. \*\*\*  $p < 0.001$ . \*\*\*\*  $p < 0.0001$ .

using a force transducer. Different levels of isometric stretch (0-30%) were applied to assess the stiffness of slices (passive tension) (Figure 5.7).

Interestingly, Cytomix had no effect on the passive tension developed by slices at all levels of stretch. However, while there no difference of contractility could be detected at a physiological load (20% stretch) and down to unloaded slices, the contractility of Cytomix-treated slices was significantly higher than control slices at 23% and up to 27% of stretch ( $p < 0.05$ ). Physiological load was therefore the branching point above which the effects of Cytomix were detected. In Figure 5.8, it can be seen that while the contractility of Cytomix-treated slices at 23% stretch increased 2.2-fold compared to control slices ( $p = 0.0471$ ), the time to peak, time to 90% decay and the rate of decay of contractions were unchanged by Cytomix at either level of stretch.

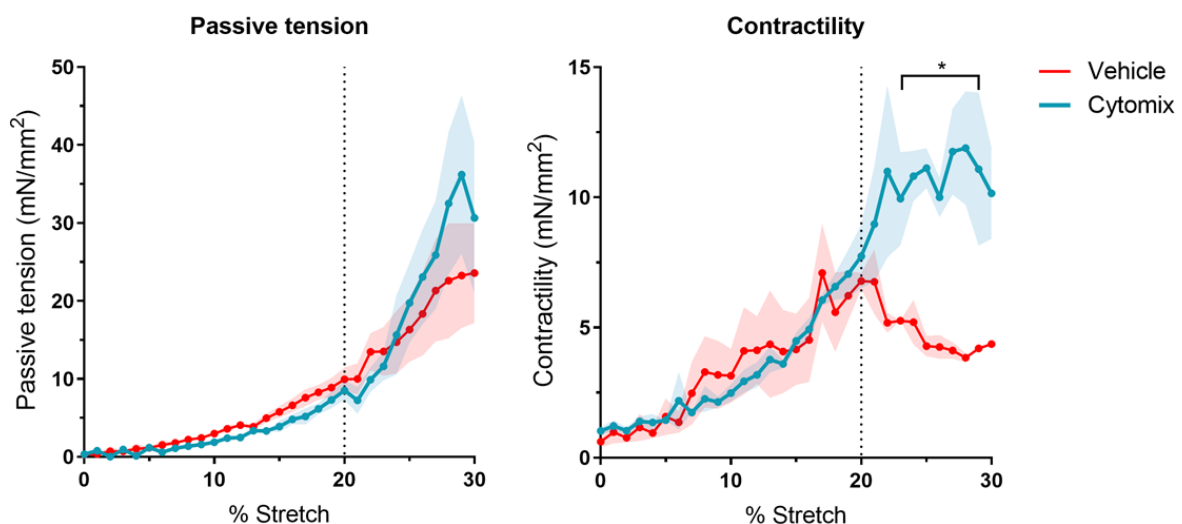


**Figure 5.7: Stretch-dependent effects of Cytomix on the contractility, but not passive tension of cultured rat myocardial slices**

Passive tension and contractility of adult rat myocardial slices, 24 hours after culture with Cytomix or vehicle (BSA) and recorded isometrically at 1 Hz with a force transducer at different levels of stretch (at 0-30% of unloaded slice length).  $n/N = 8/4$  (slices/animals). Data are expressed as mean  $\pm$  SEM. A t-test was used to compare the means. The  $n$  values were used for statistics and the graphics. The coloured shadows cover the SEM. \*  $p < 0.05$ .

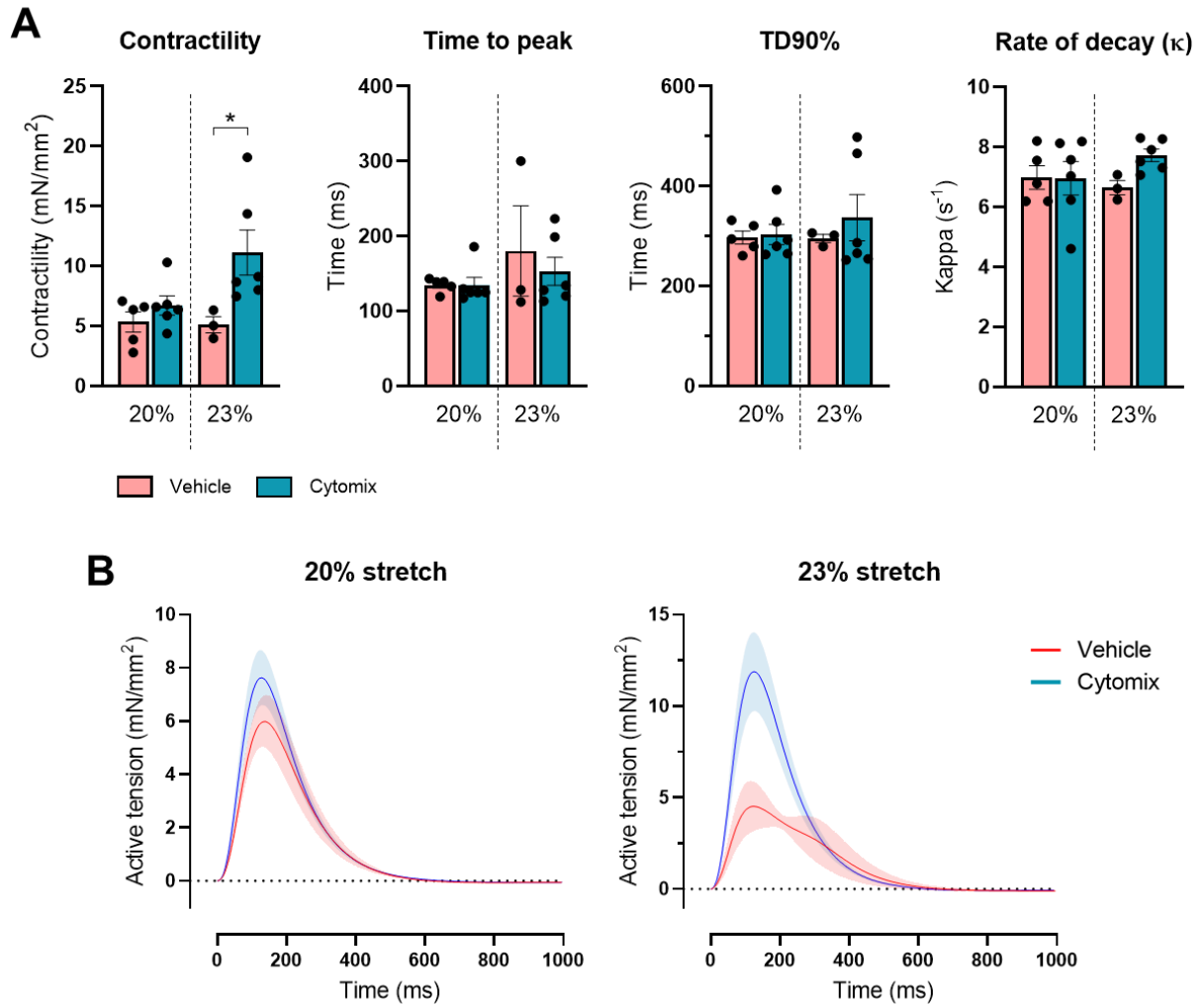


**Figure 5.8: Morphology of contractions at 20% and 23% isometric stretch of slices**

**A.** Contractility, time to peak, time to 90% decay and rate of decay ( $\kappa$ ) of slice contractions at 1 Hz, after 24 hours of culture with Cytomix or its vehicle (BSA) and recorded isometrically at 20% and 23% stretch (based on unloaded length). Cytomix: n/N = 6/4; Vehicle: 5/4 at 20%, 3/3 at 23% (slices/rats). Data are expressed as mean  $\pm$  SEM and compared with a one-way ANOVA and Bonferroni's test, using the values obtained from individual slices (n) which were also displayed as data points. \*  $p < 0.05$ . **B.** Contractility traces at 20% and 23% stretch, averaged from all replicates. The coloured shadows cover the SEM.



## 5.4 Discussion

In summary, the results in this chapter show that: (1) Cytomix pre-conditioning of EC in co-culture significantly accelerates the extrusion of  $\text{Ca}^{2+}$  during relaxation. (2) This is likely due to SERCA but not NCX activity, and is potentially correlated with reduced expression of PLB. (3) Co-culture with Cytomix-treated EC elevated the fractional release of  $\text{Ca}^{2+}$  from the SR and the amplitude of calcium transients compared to untreated-EC. (4) Surprisingly there was no effect of co-culture or Cytomix pre-conditioning on the amplitude or duration of contractions in isolated CM, nor differences of myofilament sensitivity to  $\text{Ca}^{2+}$ . (5) Cytomix increased the contractility of myocardial slices at high levels of mechanical load, but it did not affect diastolic stiffness or the duration of contractions.

### 5.4.1 Differential effects of untreated and Cytomix-treated EC on calcium extrusion in co-cultured CM: lost function or new function?

With Fluo-4 and Fura-2 (Figures 5.1 and 5.6), and in a third independent experiment (in Figure 5.3), the rate of decay of calcium transients was found increased after co-culture with Cytomix-treated EC compared to untreated EC. This result is the cornerstone of this thesis, representing the first evidence to confirm the original hypothesis, i.e. that an inflammatory response in EC can affect their paracrine effect on CM function. We could technically stop at this point, but this effect is not self-explanatory, and a more thorough investigation of CM functions is required to better understand the mechanisms involved, and the role that this intercellular signalling may take in inflammatory cardiac remodelling.

Given the basal effect of co-culture with EC on calcium handling in CM, the following question arises: is the effect of Cytomix pre-conditioning the result of a gain-of-function, loss-of-function, or both? Except in Figure 5.3 (where the rate of decay of calcium transients in control CM was unusually lower than in co-cultures with Cytomix-treated EC), no significant difference of calcium handling was found between the CM alone and CM after co-culture with Cytomix-

treated EC. At first glance, this raises the possibility that EC and CM become uncoupled when EC respond to Cytomix, resulting in EC “losing” their ability to regulate CM function. This itself would still comply with the hypothesis in this project, but is not supported by other data shown in this chapter. Indeed, ERK1/2 was found equally hyperphosphorylated in CM following co-culture with Cytomix-treated EC and with untreated EC. The lower expression of NCX in the Cytomix group compared to CM alone is further evidence that treatment of EC with Cytomix does not entirely deconstruct the EC-CM paracrine axis, but modifies its nature. Furthermore, no loss-of-function was found using the Profiler Array after Cytomix treatment (Chapter 4), suggesting that the paracrine activity of EC becomes richer, not poorer, in response to Cytomix. However, it will remain challenging to solve this discussion point until we know more of the paracrine mediators that are involved in these effects.

In this experiment, the effects of TNF $\alpha$ , IL-1 $\beta$  and hIL-6 could be individually compared to the effects of Cytomix (Figure 5.1). Except for the amplitude of calcium transients (the relevance of this measure is criticised later), each cytokine produced an effect on average between those of untreated and Cytomix-treated EC. Of note, only treatments with Cytomix and hIL-6 lead to a significant change of rate of decay and decay duration compared to control co-cultures. This contrasts with the results of the Profiler Array where treatment of EC with hIL-6 alone did not induce the secretion of many factors shared by the TNF $\alpha$ , IL-1 $\beta$  and Cytomix groups, and was closest of all treatments to the secretome profile of untreated EC. The lack of significant effect on calcium transient decay after TNF $\alpha$  and IL-1 $\beta$  treatments might be the result of intrasample variation and more replicates would increase the statistical power of this analysis.

#### **5.4.2 Increased SERCA activity mediates the lusitropic effects of Cytomix-treated EC on calcium handling in co-cultured CM**

Activity of SERCA, but not NCX, was found increased in co-cultures with Cytomix-treated EC compared to untreated EC (Figure 5.3). This finding is consistent with the accelerated calcium extrusion described above. The contribution of SERCA to calcium extrusion in this experiment

was consistently found at 92-93%, a value identical to that reported in adult rat CM in previous articles<sup>267</sup>. An accurate measurement of NCX contribution in co-cultures with Cytomix-treated EC could not be obtained in this experiment, thus interpreting the results presented above as evidence that NCX activity is clearly inhibited in such conditions would be unscientific. Even if this effect were true, the physiological consequences would be trivial in comparison to SERCA activity which, as is shown in Figure 5.3B, dwarfs that of all other mechanisms. Mirroring the difficulty to detect NCX activity in co-cultures with Cytomix-treated EC, the expression of NCX protein in CM was found to be significantly reduced in the Cytomix condition than in CM alone. It would be necessary to measure the NCX-specific current, using patch-clamping, to confirm that NCX activity is indeed lessened in this condition. The protocol that was used here is not adapted to detect accurately such minute changes of activity. It is also a limitation of this experiment that the SERCA:NCX ratio of expression and activity is higher in rat CM than in human CM. Testing the relative contribution of NCX and SERCA in other models, such as rabbit or guinea pig CM, would help contextualise the effects of co-cultures in a system where the basal activity of NCX is more substantial<sup>216,267</sup>.

Total levels of PLB were decreased in Cytomix-treated EC co-cultures compared to untreated EC. Phosphorylation of PLB was increased equally by co-culture, compared to control CM, in the majority of samples and up to 9-fold. However, due to intrasample variation this effect was not significant, and this experiment should be repeated along with another attempt to quantify the levels of SERCA. So far, it remains impossible to determine conclusively if Cytomix-treated EC increase SERCA activity by upregulating SERCA expression, by PLB phosphorylation, or solely by downregulating PLB expression (which results in a higher SERCA:PLB stoichiometry and potentially a lower inhibitory effect of PLB<sup>111</sup>). Of note, the levels of phosphorylated ERK1/2 were found to be increased in co-cultured CM than in CM alone, regardless of pre-conditioning for EC. Since ERK1/2 activity is associated with a lower SERCA expression and hypophosphorylation of PLB, resulting in lower SERCA activity, the effect of Cytomix-treated EC on SERCA activity cannot be explained by ERK1/2 phosphorylation<sup>353</sup>. Akt, however, is

known to increase SERCA activity and might be a more appropriate target of interest for future mechanistic studies of this apparent lusitropic effect of Cytomix on co-cultured EC<sup>355</sup>.

### **5.4.3 Inotropic effect of Cytomix-treated EC at the level of SR Ca<sup>2+</sup> release**

A higher SERCA activity is described as inotropic due to the increased SR Ca<sup>2+</sup> and peak of systolic Ca<sup>2+</sup> that it induces<sup>111,158</sup>. In this chapter, the amplitude of calcium transients was found to correlate with SERCA activity (using Fura-2 but not Fluo-4 however). Both were increased after co-culture with Cytomix-treated EC compared to untreated EC (Figure 5.6 and 5.3). Ca<sup>2+</sup> efflux from the SR was also proportionally increased in the Cytomix condition compared to the untreated, as shown by the fractional release of Ca<sup>2+</sup> induced by caffeine (Figure 5.2). In other words, while the SR filled up with more Ca<sup>2+</sup> during diastole, the RyR released proportionally more of that Ca<sup>2+</sup>. Increased SR Ca<sup>2+</sup> potentiates its release via the RyR in two main ways: (1) by increasing the driving force of Ca<sup>2+</sup> current through the RyR and, more indirectly, (2) by preventing stochastic attrition of RyR (as luminal calcium increase the opening probability of the channel), likely resulting in more channels being open<sup>158</sup>. A direct measurement of the SR Ca<sup>2+</sup> would help validate this mechanism. To circumvent the common issue of saturation of Ca<sup>2+</sup> indicators used to image SR Ca<sup>2+</sup>, low affinity dyes should be preferred over Fluo-4 or Fura-2<sup>356,357</sup>. The fractional release of Ca<sup>2+</sup> from the SR is not solely regulated by SR Ca<sup>2+</sup>, but also by the trigger Ca<sup>2+</sup> (from the L-type calcium channel current in dyads)<sup>358</sup>. Measuring  $I_{Ca}$  by patch-clamping would therefore be useful to determine if the trigger of calcium release in CM is also affected by Cytomix treatment in co-cultured EC. NCX is also thought to regulate RyR function when expressed near or at dyads, though this is still a matter of controversy<sup>359</sup>, and potentially it can affect the efficiency of calcium-induced calcium release and Ca<sup>2+</sup> leak from the SR. As discussed above, the activity of NCX in ARVM co-cultured with Cytomix-treated EC is possibly inhibited, so characterising the frequency of Ca<sup>2+</sup> sparks in CM would provide further details on the inotropic effects of Cytomix in co-cultures.

Using Fluo-4, the amplitude of calcium transients was found unchanged across all conditions (Figure 5.1), unlike the experiment where Fura-2 was used. This demonstrates the limitations of using non-ratiometric  $\text{Ca}^{2+}$  indicators for such purposes, despite correcting for background and baseline fluorescence. This is particularly true when there are differences of Fluo-4 at  $F_0$ , as was the case in this project. With regards to the amplitude of transients, therefore, the data obtained with Fura-2 are in theory more accurate than those obtained using Fluo-4.

#### **5.4.4 On the dissociation of calcium transient kinetics and contraction kinetics**

The inherent purpose of calcium release is to induce contraction of sarcomeres and shortening of CM in a concentration and time-dependent manner<sup>111</sup>. It was therefore unexpected that the effects of Cytomix-treated EC in co-culture on the amplitude and duration of calcium transients were not found to be translated into stronger and shorter CM contractions (Figure 5.5). It was first hypothesised that myofilaments reacted differently to  $\text{Ca}^{2+}$  in the Cytomix condition, thus compensating for changes of amplitude of  $\text{Ca}^{2+}$  release. However, their sensitivity to  $\text{Ca}^{2+}$  was unchanged by co-culture or by Cytomix pre-conditioning (Figures 5.6B and C), suggesting that another regulatory mechanism is responsible for the functional discrepancy described above. Such uncoupling of the calcium-contraction relationship is commonly associated with changes of myofilament sensitivity to calcium. Reports have indeed demonstrated that the amplitude of calcium transients can dissociate from force development, at least in the second phase of the Bowditch effect (force-frequency relation)<sup>360</sup>. In my experiment, frequency of stimulation was constant and preload null (a disadvantage of using isolated ARVM). It was therefore speculated that increasing the sensitivity of myofilaments to  $\text{Ca}^{2+}$  may improve the translation of calcium transient kinetics to contraction kinetics in co-cultures. The simplest way to achieve this would be to increase the preload of CM and this can be done by applying an axial stretch of CM using rigid posts attached to each extremity of the cell<sup>361</sup>.

#### **5.4.5 On the load-dependent effect of Cytomix on whole tissue contractility**

Contractility of myocardial slices is generally measured at physiological levels of mechanical load<sup>211</sup>. When this project started it was also customary in Terracciano's lab to record maximal contractility, regardless of the amount of load that had to be provided to each myocardial slice. This measure does not take into account the diastolic function of the tissue, so is less relevant. Testing the effect of Cytomix on contractility in slices was therefore the opportunity to improve this method and assess the force-length relationship of cardiac tissue in this model, as well to determine if Cytomix regulates diastolic properties which can only be studied properly when a mechanical load has been applied. A caveat to this approach is the high complexity of the model compared to co-cultures: Cytomix can activate all cell types present in slices and multidirectional crosstalks and feedback loops are allowed. This was however a necessary step back to be taken to better understand the effect of Cytomix in co-cultures.

Passive tension, as a measure of tissue stiffness and diastolic function, increased with stretch but was unchanged by Cytomix (Figure 5.7). Diastolic dysfunction, as a hallmark of HFpEF, is often attributed to the hypophosphorylation of titin that results from an impaired bioavailability of NO<sup>91</sup>. This leads to a stiffening of CM. Data presented in this project therefore suggest that the effect of Cytomix at 24 hours on cardiac tissue does not recapitulate this mechanism. To completely exclude this possibility, the next experiment would be to measure the levels of titin phosphorylation by western blotting, and the levels of NO produced within slices (by superficial imaging of DAF-2 or by analysis of nitrate/nitrite levels in the slice culture supernatants). The other defining feature of diastolic dysfunction is interstitial fibrosis. Since fibroblasts are also present in slices, the lack of difference for passive tension between conditions suggests that Cytomix does not induce fibroblast proliferation or collagen deposition in slices within 24 hours. This proposition could be tested by confocal imaging of vimentin and collagen type-I.

As expected, the active tension of slices, i.e. contractility, was load-dependent (Figure 5.7). It was moreover unaffected by Cytomix treatment up to 22% stretch, which covers physiological levels of load (20% stretch) and, naturally, unloaded slices. Interestingly, this is reminiscent of

the lack of effect of Cytomix-treated EC on CM contractility in co-culture. Indeed, it should not be forgotten that co-cultures were performed with mechanically unloaded CM. Of course, this is not to suggest that slices behave exactly as co-cultures. At 23% and above, curiously, there was a significantly higher contractility under Cytomix stimulation than in control slices. This is likely to be the result of different inflexion points in the force-tension relationship characterising these conditions. Above 20% stretch (i.e. approximately physiological preload<sup>210</sup>), contractility of vehicle-treated slices started declining with increasing load, in accordance with the Frank-Starling law which describes this shift and descending relationship at very high stretch (where the lattice spacing of myofilaments becomes too low). Interpreting these results would become easier by translating the level of stretch into sarcomere length, which is highly preferred when discussing such load-dependent mechanisms. In future experiments, it should be a priority to better define the sarcomere length after culture, and confirm that sarcomeric remodelling does not occur after Cytomix treatment (e.g. serial addition of sarcomeres would skew the validity of using macroscopic stretch as a reproducible amount of sarcomeric load).

Overall, these data can only serve as preliminary evidence that the effect of Cytomix can be investigated using slices as well, while suggesting that this effect is load-dependent and dominant in overloaded conditions. A limitation to measuring contractility of slices with an isometric force transducer is that ramping up stretch increases both preload and afterload in CM, hindering direct comparison of results with other models. This is still not well understood, and it is unclear if afterload-sensitive mechanisms are present during this sort of experiment (e.g. the Anrep effect).

The first two steps to bridge the findings from co-cultures and the response of slices to Cytomix should be: (1) to validate the activation of EC in slices after treatment, and (2) measure calcium transient amplitude and duration in slices, using Optical Mapping.

#### **5.4.6 Conclusion on the effect of Cytomix on the paracrine EC-CM crosstalk**

In support of the original hypothesis of this project, the data in this chapter converge to show that Cytomix-treated EC affect the properties of excitation-contraction coupling of co-cultured CM differently from untreated EC. The main function that was found to be regulated differently by Cytomix is the activity of SERCA, and this was associated with an increased amplitude of calcium transients as well as a more efficient clearing of  $\text{Ca}^{2+}$  during diastole. PLB expression was found decreased by co-cultured Cytomix-treated EC, concurring with the higher activity of SERCA. These data provide valuable insight into the plasticity of EC-CM crosstalk, and point to potential targets of EC-derived mediators (e.g. PLB, mechano-sensitivity) which have never been studied in the context of EC-CM interactions previously, at least not directly. Work remains to be done to bring to light the mechanisms involved in this effect, and to investigate other potential functions affected by co-culture and Cytomix pre-conditioning. For example, it would be valuable to test if the duration of action potentials is also affected, and to assess the susceptibility of CM to develop arrhythmia in these conditions.

The dissociation of calcium and contraction amplitudes and kinetics was the most surprising finding in this project, and by far the most challenging to address. The effect of Cytomix on the contractility of slices only at high levels of mechanical load raises the possibility that Cytomix affects the load-dependency of  $\text{Ca}^{2+}$  sensitivity in CM myofilaments. With more time allowed, the project would aim to: (1) apply uniaxial load to isolated CM after co-culture with untreated or Cytomix-treated EC and determine if the calcium-contraction relationship is restored in such conditions, and (2) examine the properties of the EC-CM crosstalk, and the effects of Cytomix, in myocardial slices to conclude on the relevance of findings obtained with co-cultures.

The pathophysiological relevance of findings presented above is discussed more in depth in Chapter 6. As a conclusion from this chapter, we have confirmed that the paracrine effects of EC on CM are subject to plasticity and that a prototypical inflammatory response in EC results in a positively inotropic and lusitropic calcium handling in CM, hence validating our hypothesis.



# 6.

## **General discussion**

## 6.1 Recapitulation and implications of results

This project tested the hypothesis that the paracrine effects of EC on the excitation-contraction coupling of CM are modulated during the inflammatory response of EC. To investigate this, a model of EC-CM co-culture was first validated. To increase the physiological relevance of our model, cardiac microvascular EC and freshly isolated adult ventricular CM were preferred over cell types which are more frequently used for EC-CM co-cultures. The calcium handling of CM was used as the principal experimental endpoint for co-cultures, aiming to complement other studies which have focused mostly on CM contractility, hypertrophy, metabolism, proliferation (when applicable), and maturation. Next, a cocktail of cytokines (Cytomix) was validated as a pro-inflammatory treatment for EC. The reason for using three cytokines instead of one, as is usually done, was two-fold: (1) to improve the pathophysiological relevance of the treatment, and (2) to provide some needed insight into cytokine interplay on EC function and on EC-CM crosstalk. Data converged to indicate that each cytokine produced a unique response in EC, while Cytomix produced a cellular response that was not additive, reinforcing the importance of cytokine interactions in inflammatory disease modelling. Calcium handling in CM was tested after co-culture with untreated or Cytomix-treated EC and, in line with our working hypothesis, was found to be different between conditions.

First, it was found at multiple occasions that untreated EC induced a prolongation of calcium transient decay in co-cultured CM compared to CM alone. This served as the baseline to study the effects of Cytomix. After co-culture with Cytomix-treated EC, the effects of co-culture were reversed: with an accelerated calcium extrusion and increased amplitude of calcium transients observed, surprisingly suggestive of positively inotropic and lusitropic effects from inflamed EC (at least relatively to the effects of untreated EC). The activity of SERCA, but not NCX, was found to be responsible for this Cytomix-induced acceleration of calcium clearing, and this was associated with a more efficient calcium-induced calcium release from the SR. Contractility and relaxation rate of CM after co-culture were also measured, in light of these results, but found unaffected by untreated or Cytomix-treated EC. Moreover, there was no

evidence for a modulation of the sensitivity of myofilaments to calcium. A possible explanation for this lack of effect was found in myocardial slices, in which a Cytomix treatment only affected tissue contractility at high levels of stretch, corresponding to cardiac overload (a parameter that could not be applied in co-cultures in this project). Further work is required to understand how the effects of co-culture on CM function relate to the properties of myocardial slices.

### **6.1.1 Limitations of interpreting changes of CM function in co-culture with EC**

So far, I have avoided interpreting the effects of EC on CM (before or after Cytomix treatment) as being either beneficial or detrimental to cardiac function. It is a common preconception that inflamed EC have a “bad” effect on CM function. However, this is likely the result of a confusion between cardiac endothelial inflammation and dysfunction. If numerous studies have helped define the effects of dysfunctional EC on CM function (i.e. diastolic dysfunction caused by lost NO bioavailability from EC) very little is known about the effects of inflamed EC on CM, where NO levels and other endothelial functions are distinct from both normal and dysfunctional EC. Furthermore, not all cardiac remodelling is pathological, as even strong indicators of HF such as ventricular hypertrophy can be part of physiological adaptations (e.g. leading to increased LV stroke volume in response to long-term aerobic exercise<sup>362</sup>). Even in a pathological context, it could be argued that hypertrophy has a protective effect, compensating the loss of contractility in portions of the LV wall after MI for example. I show in this report that Cytomix-treated EC induce an acceleration of calcium extrusion and a larger amplitude of calcium transients in co-cultured CM, compared to untreated EC. This is diametrically opposed to changes of calcium handling observed in HF<sup>24,363</sup>, which would suggest that inflamed EC have a beneficial effect on CM function in the conditions of this study. That these changes were not associated with a modulation of CM contractility and relaxation is still unexplained, and might have been caused by suboptimal recording conditions (for example too late after removal of EC from co-cultures) rather than biological mechanisms with physiological or clinical ramifications. Since co-culture with untreated EC produced a decreased rate of calcium SR uptake compared to CM alone,

i.e. in the direction of changes observed during HF, we would be at risk to conclude that EC have at baseline a detrimental effect on CM calcium handling. Here lie the limitations of such dichotomous interpretations of CM responses to stimuli, which should only be done cautiously.

### **6.1.2 Potential mediators of the paracrine effects of untreated and Cytomix-treated EC on calcium handling in CM**

The effects of EC on CM which we described in this study remain unexplained mechanistically, and more work is needed to identify potential soluble mediators of these effects. The secretion profile of EC was found highly affected by Cytomix treatment (Chapter 4), but a meta-analysis of gene expression in CM raised doubts over the involvement of these secreted factors in the paracrine effects of EC on CM. The Profiler Array that was used in this project is limited to 105 inflammatory factors, so paracrine pathways which are less related to inflammatory responses remain to be tested and excluded in EC-CM co-cultures. With NO being the candidate soluble mediator of choice in many studies of EC-CM interactions, if not the only paracrine factor that is investigated<sup>249</sup>, we ought to reflect on its potential activity in the model of this study. First, we must assume that the effects of intramyocardial NO are lost in CM after isolation, considering the numerous changes of media and the delay between isolation and the start of experiments. Next, if NO is involved in the paracrine effects of untreated EC or Cytomix-treated EC on the calcium handling of CM in co-culture, this would mirror the effects of NO donors on CM. The effect of NO on calcium handling is poorly understood when compared to its effect on the contractile properties of CM, but previous studies have shown that endogenous NO inhibits SR Ca<sup>2+</sup> uptake<sup>142</sup> as well as  $I_{Ca}$  and peak systolic calcium<sup>112</sup>, while exogenous NO (provided by NO donors) can accelerate calcium transient decay<sup>90</sup>. Other reported effects of NO include an increased calcium-induced calcium release by NO-mediated S-nitrosylation of L-type calcium channels<sup>364</sup> and RyR2<sup>128</sup>, but some studies have also failed to detect an effect of NO on calcium transient amplitude or kinetics<sup>89</sup>. In light of these inconsistent reports and given the limitations of NO detection in this study, it is not possible to

determine with certainty if the acceleration of calcium uptake in the SR caused by Cytomix-treated EC (compared to untreated EC) is due to a loss of inhibitory effects of NO on the activity of SERCA, to an increase of stimulatory effects of NO, or to NO-independent mechanisms. As discussed below, further work is needed to define the role of NO in EC-CM co-cultures and after Cytomix pre-conditioning of EC.

### **6.1.3 Additional remarks**

This work adds to the growing understanding of how EC can modulate the function of CM and how endothelial inflammation can affect myocardial function. The effect of EC on the calcium handling of CM is extremely novel, so far only hypothesised from indirect evidence. This may therefore eventually provide new markers of vascular inflammation in the myocardium, as well as new therapeutic targets to be investigated. The EC-CM paracrine signalling pathway that we propose in this project might eventually be exploited therapeutically, for example to prevent cardiac remodelling or dysfunction in myocardial or systemic inflammatory diseases.

Moreover, the pro-inflammatory treatment of EC that was optimised and validated in Chapter 4 was in response to multiple cytokines, which is still a highly irregular and progressive practice in cardiovascular research. This work may therefore lead to new understanding of cytokine interplay on the function of EC and CM during inflammation, or more generally in myocardial remodelling, and open up new strategies for the control of inflammation in cardiology.

Finally, I have focused on the effect of endothelial inflammation on CM function, in contrast to the growing number of studies investigating the role of endothelial dysfunction on CM remodelling (especially in the context of HFpEF). This is an important distinction to make, as our data may ultimately provide a new and unique insight on direct paracrine mechanisms which have been underestimated so far. Further work is however required to better define the transition between vascular inflammation and dysfunction, in terms of paracrine activity on CM function, and how this may be exploited therapeutically.

## 6.2 Comparison with a recently published study

In September 2019, the journal *JACC: Basic to Translational Science* published an article titled “Cardiac Microvascular Endothelial Enhancement of Cardiomyocyte Function is Impaired by Inflammation and Restored by Empagliflozin”, by Juni, PhD., and colleagues<sup>249</sup>. At this point of the discussion, we must address the many similarities and discrepancies between the work of these competitors and the methods and findings in this project. Indeed, both studies aim to address the paracrine effect of EC on properties of the excitation-contraction coupling of CM, and the disruption of that effect by an inflammatory response in EC. In both studies, EC were cultured in Transwell inserts and treated with pro-inflammatory cytokines. Expression of CAM was used to validate the treatment and intracellular levels of NO were measured by fluorescent imaging. Cytokines were eliminated prior to co-culture with adult CM, which lasted between 2-4 hours. Another common feature is the measurement of contractility (and relaxation) of CM, that was done with the novel system CytoCypher. Despite these similarities, however, effects of co-culture and of the pro-inflammatory conditioning of EC were physiologically inconsistent.

### 6.2.1 Comparison of general methods

As shown in Figure 3.1 and as discussed at length in Chapter 3, the characteristics of EC-CM co-culture systems that have been published, so far, differ greatly. It was therefore surprising, although somewhat validating as well, to find an uncanny resemblance between the co-culture method used in this project and that published by Juni *et. al.* (Table 6.1).

In Chapter 3, we found that the effect of EC on the calcium handling of co-cultured CM after 4 hours is identical to that of co-culture for 24 hours, but we could not find an effect of co-culture on CM contractility at 4 hours. In Juni *et. al.* (2019) the duration of co-culture was much shorter (2 hours). With no other data to suggest that this effect is stable, or at least that it can be seen at other time-points, it remains a possibility that changes of CM contractility are only transient in co-cultures.

**Table 6.1: Comparison of methodology for cell culture, co-culture, and characterisation of CM functions in this project and in Juni et. al. (2019)**

	<b>This project</b>	<b>Juni et. al. (2019)</b>
<b>EC type</b>	HCMEC (Promocell) – Passage 4 to 6	HCMEC (Lonza) – Passage 5 to 7
<b>CM type</b>	Freshly isolated ARVM (Sprague-Dawley)	Freshly isolated ARVM (Wistar)
<b>Coating</b>	1% gelatine (EC) and 1% laminin (CM)	1% gelatine (EC) and 1% laminin (CM)
<b>Co-culture system</b>	0.4 µm pores inserts (GBO) – 12-well format	3 µm pores inserts (GBO) – 24-well format
<b>Conditioned medium</b>	N/A	30 min, 1 hour, 1.5 hour, 2 hours
<b>Co-culture medium</b>	Custom - 1% FBS, no VEGF	EGM-2MV (Lonza) – 5% FBS, plus VEGF
<b>Inflammatory treatment</b>	1 ng/ml TNF $\alpha$ , 1 ng/ml IL-1 $\beta$ , 25 ng/ml hIL-6	10 ng/ml TNF $\alpha$ or 10 ng/ml IL-1 $\beta$
<b>Pre-conditioning</b>	<ul style="list-style-type: none"> <li>- EC seeded for 24 hours</li> <li>- 24 hours treatment</li> <li>- Media changed to prevent carry over</li> </ul>	<ul style="list-style-type: none"> <li>- EC seeded overnight</li> <li>- 6 hours treatment</li> <li>- Media changed to prevent carry over</li> </ul>
<b>Duration of co-culture</b>	4 or 24 hours	2 hours
<b>Calcium transients</b>	Fluo-4 and Fura-2	N/A
<b>Contractility</b>	CytoCypher (15 min incubation on stage)	CytoCypher (immediately after co-culture)
<b>Field stimulation</b>	1 Hz, 10 ms, 40 V	2 Hz, 4 ms, 25 V
<b>Recording bath solution</b>	Fresh Tyrode's solution	Unchanged culture medium (EGM-2MV)
<b>NO measurements</b>	DAF-2 DA	Copper-based probe (CU <sub>2</sub> FL2E)

In Juni *et. al.*, Transwell inserts containing EC were removed and CM imaged immediately. In my experiments however, preliminary data suggested that the duration of decay for contraction is unstable during the first 15 min after transferring CM on the CytoCypher stage (Figure 6.1). This is likely due to the handling of Transwell inserts, temperature changes, and introduction of field stimulation. Data were therefore collected between 15 and 30 min. In Juni *et. al.*, data were however collected “within a relatively short period of time” after transfer of CM on stage, i.e. potentially before stable state.

There are other technical differences (sources of cells, co-culture medium, pore size in inserts, seeding duration for EC), but in the interest of simplicity we should assume that the discrepant effects of co-culture described in both studies were not influenced by these parameters.

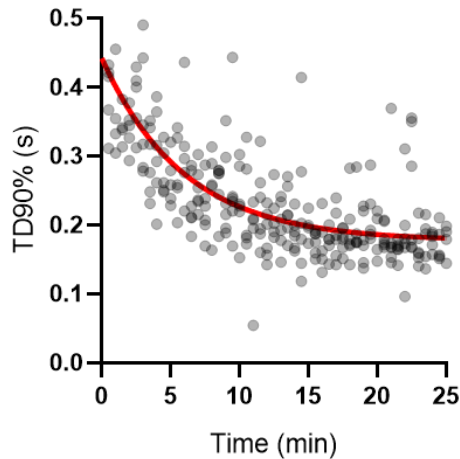


**Figure 6.1: Time-dependency of CM contraction decline duration with the CytoCypher set-up**

Time to 90% decay of cell shortening in ARVM from 0 to 25 min after transferring CM cultures to the set-up of CytoCypher. A one-phase exponential curve fit is shown in red. Data were taken from 3 independent experiments ( $n = 277$  cells in total). Half-life = 4 min. Time constant ( $\tau$ ) = 5.9 min.

### 6.2.2 The effects of pro-inflammatory treatment on endothelial NO bioavailability

In Juni *et. al.*, it can be argued that the authors somewhat conflate inflammatory endothelial activation and endothelial dysfunction, a distinction that we have established in Chapter 1. As a result, a decrease in NO synthesis by EC after TNF $\alpha$  treatment was interpreted as both a relevant sign of inflammatory response for EC and simultaneously an effect relevant to HFpEF, which semantically is paradoxical. Bioavailability of NO is known to be increased in a balanced endothelial response to inflammation, while NO imbalance defines endothelial dysfunction and contributes to the vascular and myocardial stiffening that are characteristic of HFpEF<sup>322</sup>.

In Juni *et. al.*, the TNF $\alpha$  treatment: (1) lowered mRNA levels of eNOS, (2) had no effect on the protein levels of dimeric eNOS but, according to the authors, lowered the monomeric form of the protein (this was not quantified), (3) increased phosphorylation of eNOS on S1177 (again quantification was not provided), and (4) inhibited NO synthesis in EC. While a TNF $\alpha$ -induced reduction of eNOS expression is expected<sup>365</sup>, it should also be accompanied by an uncoupling of eNOS (ergo a higher proportion of monomeric eNOS, contributing to ROS generation). Total protein levels of eNOS were also unchanged by TNF $\alpha$ , despite the change at the mRNA level. Phosphorylated eNOS on S1177, which was increased by TNF $\alpha$  in this article, is also known to potentiate NO synthesis<sup>366,367</sup>. Overall, these circumstances would indicate an increase in NO synthesis, not the decrease which was reported. As the authors rightfully suggest, this can simply be explained by the NO scavenging properties of ROS. To validate this, treatment of



EC with anti-oxidants rescued the TNF $\alpha$ -inhibited NO synthesis. In Juni *et. al.*, the probe which was used to measure NO levels in EC was more specific than DAF-2, which could explain the discrepancy of these findings with the results shown in Chapter 4. Using this probe to measure the basal effects of Cytomix on NO synthesis in EC appears thus essential to categorise this treatment as a model of either endothelial inflammation or endothelial dysfunction. This would also help confirm the suspected increase of NO induced by thrombin and its potentiation by Cytomix treatment. Of note, the radical scavenging enzyme MnSOD was here found induced by Cytomix at higher levels than after TNF $\alpha$  treatment, and more work should be done to test the levels and activity of ROS in our model. It is possible that an early TNF $\alpha$  response (in the article) and Cytomix have opposite effects on NO synthesis.

### **6.2.3 The effects of co-culture and EC pre-conditioning on CM contractility**

The effect of co-culture on CM contractile functions, as reported in Juni *et. al.*, is two-fold: (1) an increased fractional shortening and sarcomere length shortening compared to CM alone, and (2) an increased return velocity and decreased tau (i.e. increased rate of decay kappa) of relaxation. In contrast, we saw no effect of co-culture on contraction or relaxation of CM, and at the level of calcium handling, a lower amplitude and prolongation of return to baseline. Juni *et. al.* did not include an analysis of calcium transients, or of the sensitivity of myofilaments to calcium, which would have been helpful to fully compare the two studies.

In the same study, the effect of co-culture was statistically significant, but representative traces were not shown, thus making any interpretation of physiological significance difficult. Ignoring this, TNF $\alpha$  treatment of EC was reported by the authors to reverse the effects of co-culture (a shared observation with the current project). As shown in Figure 6.2 (reproduced from Figure 2 of the article), this results in a reduction of shortening amplitude and longer relaxation time compared to untreated EC, i.e. negatively inotropic and lusitropic. This is consistent with the reduction of NO generation in EC shown after TNF $\alpha$  treatment, but in a clear contrast to the positively inotropic and lusitropic effects of Cytomix treatment on the calcium handling of co-

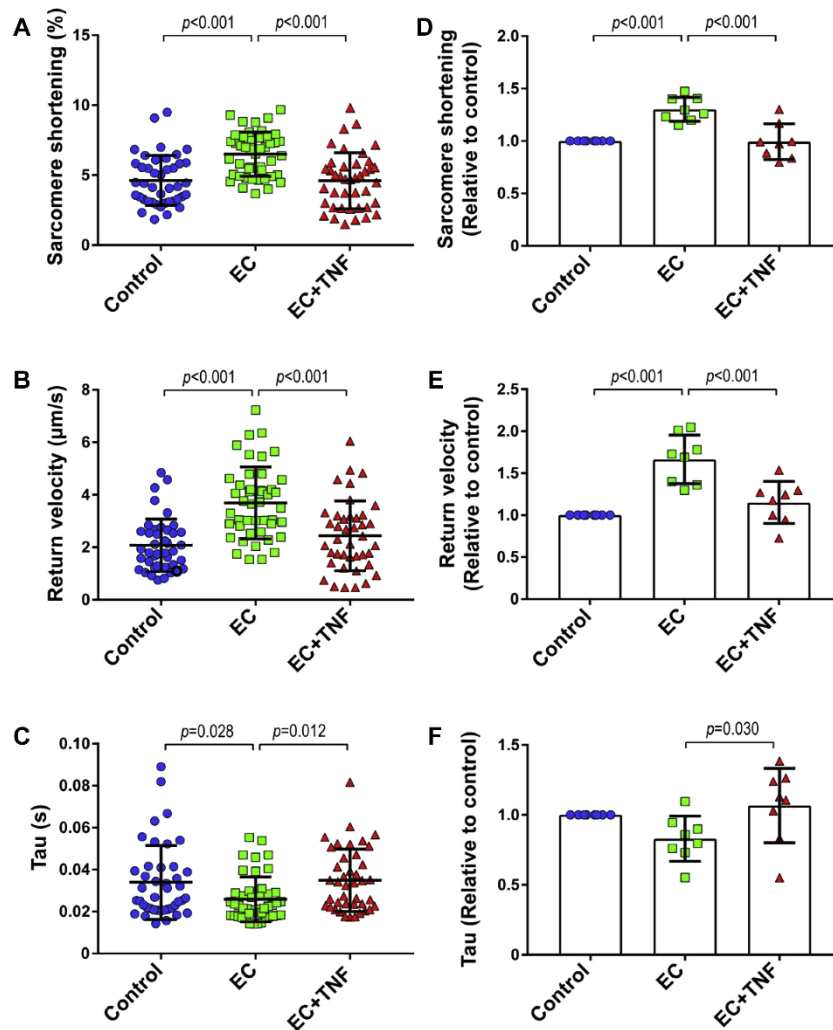


**Figure 6.2: Published effects of Transwell co-culture and of TNF $\alpha$  pre-conditioning of EC on the contractility and relaxation rate of contractions in CM**

Reproduced from Juni *et. al.* (2019). Original title: “CMECs Enhance CM Function”, legend: “CM contraction and relaxation were evaluated under basal conditions (control) and after co-culture with untreated (endothelial cells [ECs]) or tumor necrosis factor (TNF)- $\alpha$  pre-treated CMEC (EC+TNF). (A and D) Co-culture of CMs with ECs increased CM contraction (proportion sarcomere shortening), and (B and E) improved CM relaxation as shown by increased speed of relaxation (return velocity) and (C and F) shortened time constant of relaxation (tau). (A and D) Pre-treatment of CMECs with TNF- $\alpha$  (EC+TNF) abolished the beneficial effect of CMECs on CM contraction and (B, C, E, and F) relaxation. (A to C) Graphs representing single CMs isolated from 1 individual rat, distributed into the 3 corresponding experimental conditions; 40 to 45 CMs were measured per condition. (D to F) Data are representative of 8 independent experiments. (D to F) Graphs of combined average values obtained from 8 independent experiments corresponding to 8 individual rats. All data are represented as mean  $\pm$  SD.” (Under CC BY NC ND License – Permission not required by Elsevier)

cultured CM. Again, a direct comparison of contractility in a study with calcium properties in another should be done with great caution. As the NO scavenger 2-(4-carboxyphenyl)-4,4,5,5-tetramethylimidazoline-1-oxyl-3-oxide (c-PTIO) and L-NAME both inhibited the effects of EC on CM, the authors concluded that NO was likely to be the only mediator of those effects, and this was consistent with the effects of TNF $\alpha$  on NO synthesis in EC.

The transfer of conditioned media from untreated EC culture supernatants produced the same effect as Transwell co-cultures on the amplitude and relaxation of CM contraction, but this was lost between 30 min and 1 hour after the incubation of CM with conditioned media had started. Of note, this experiment was only done on CM from 1 rat. The half-life of NO in media varies depending on pH, oxidative species, endogenous buffers, and density of cells in culture, but is estimated to be degraded within seconds in physiological conditions<sup>254,255</sup>. It is thus surprising that the effects of co-culture and EC conditioned media on CM were completely abrogated by NO inhibitors 30 min after media had been transferred. S-Nitrosothiols formed by interaction of NO with redox-activated thiols have been proposed by others as active and stable reserves of NO (at least *in vivo*)<sup>254</sup>. The plasma half-life of S-Nitrosoalbumin, for example, is between 15 and 45 min<sup>254</sup>, so such reserves might allow the effects of NO to persist after removal of EC in co-culture. This remains highly speculative, and this proposition is based on two assumptions: that c-PTIO is equally efficient to scavenge biotransformed NO as free NO in culture medium, and that NO can be biotransformed in co-culture conditions. Finally, the effect of endogenous NO on the response of CM to EC-derived factors is not known. As a result, L-NAME or c-PTIO alone might not affect CM contractility directly but it remains a possibility that these treatments could influence the quality or degree of endogenous NO-dependent responses of CM to EC-derived factors. It is known, for example, that endogenous NO inhibits the response of CM to other hormonal stimuli, such as the  $\beta$ -adrenergic signalling which is dampened by endogenous NO in CM<sup>113,346</sup>.

In the current project, determining the levels of NO synthesis in EC before and after Cytomix treatment was limited by the overall quality of DAF-2 imaging, which was not sensitive enough

to detect basal NO levels. Originally, an aim of the present project was to use L-NAME, cPTIO, and a NO donor (NOC-5) in co-cultures or on CM alone to better define the contribution of NO signalling to the effects discussed above. However, with L-NAME increasing DAF-2 intensity disproportionately after Cytomix treatment compared to untreated controls, and given the lack of detectable NO in basal conditions, this treatment could not be used in co-cultures and this issue could not be resolved in time for this thesis.

#### **6.2.4 Conclusions from this comparison**

Titin hypophosphorylation and stiffened stretch-dependent passive force in CM, i.e. markers of endothelial dysfunction in HFpEF<sup>91,368</sup>, were not investigated by Juni *et. al.*, and could not be studied in time during my project. As a result, it remains difficult to categorise the signalling observed in both studies as particularly specific to HFpEF or to other inflammatory myocardial remodelling and dysfunction. In Juni *et. al.*, the EC response elicited by the pro-inflammatory treatment, the EC-CM paracrine axis, and its effects on CM function were strongly consistent with the diastolic dysfunction that can be induced by EC dysfunction. The title of the paper is perhaps misleading when suggesting that endothelial “inflammation” impairs the EC-mediated improvement of CM function. That an EC dysfunction was induced experimentally using a pro-inflammatory cytokine is not sufficient to interpret its effects as primarily inflammatory.

Before we can safely use the aforementioned study as a reference point for the interpretation of the results in this thesis, it would be necessary to attempt the replication of these results. In other words, it would be pertinent to test the same concentration of TNF $\alpha$  and to measure CM function at the same time-point after co-culture. If this effect can indeed be replicated, the next step would be to investigate how calcium handling is altered in this model, thus allowing a direct comparison of both models. Until this is done, it will remain difficult to identify common ground and differences between these two reports of EC-CM interaction.

### 6.3 Strengths and limitations

The main objective of my PhD project was to investigate how the paracrine activity of EC on CM was altered in response to pro-inflammatory cytokines. As such, how these cytokines affect the response of CM to EC signals, physiological or pathological, was of interest but beyond the scope of the project. This is both a strength and a limitation. Indeed, it is much easier to dissect the crosstalk of EC and CM with unidirectional pathways, but on the other hand the lack of co-stimulation for CM could mask pathologically relevant compensatory mechanisms, and limit the direct translation of results in *in vivo* models of myocardial inflammation where, by definition, the crosstalk is all but unidirectional.

Freshly isolated adult CM were used throughout in this project. This is a major asset compared to numerous previous studies which have used neonatal CM, induced-pluripotent stem cells-derived CM, or CM from immortalised cell lines. This was particularly important in my efforts to characterise the properties of excitation-contraction coupling in CM, a feature that is often said to be “immature” and therefore less physiologically relevant in non-adult CM and cultured CM<sup>265</sup>. The relative contribution of SERCA and NCX to Ca<sup>2+</sup> clearing is the biggest caveat to using rat CM to model calcium handling<sup>216</sup>, and it should be noted that NCX activity in response to co-culture and pro-inflammatory conditioning in EC might be underestimated in this study (in comparison to its activity in human CM). Moreover, as discussed at length in Chapter 3, the heterogeneity of EC phenotype is often overlooked in studies which make use of EC-CM co-cultures. It is therefore a strength of this project that HCMEC were used instead of HUVEC (or another non-cardiac source of EC). While NO and its signalling pathway are highly conserved across species, there remains a risk that other elements of EC-CM crosstalk were not maximally effective due to differences of protein sequences between human and rat, causing undesirable ligand-receptors mismatches. To control for this in future experiments, human CM derived from induced pluripotent stem cells, or rat cardiac microvascular EC, could be used in co-culture.

It was a major limitation of the experimental design in this study that the co-culture interactions had to be severed before measurements of CM properties, especially in light of the possibility that some effects of EC on CM could be transient and lost rapidly after EC removal. We know that this cannot be true for all effects of EC since the effects of co-culture on calcium transients in CM were preserved for up to 30 min. Only the measurement of CM contractile functions in co-culture (i.e. without EC removal), which would require new and costly equipment, can solve this issue and should be a consideration for future experiments.

The effect of Cytomix treatment on EC paracrine functions, as tested on CM calcium handling and contractility or relaxation, were only tested after 4 hours of co-culture. We show in Chapter 3 that the effect of co-culture with untreated EC is unchanged from 4 to 24 hours, but this was not confirmed for the lack of effect on CM contractile properties. Given the differences of result and of the duration of co-culture used in this project and in Juni *et. al.* (2019), as we discussed in the previous section, it is possible that other time-points (e.g. 30 min, 2-48 hours, or 7 days) could be defined by qualitatively and quantitatively different effects of EC on CM. This should be addressed in further experiments.

The mechanical exchange between EC and CM might influence their functional crosstalk, and this is a limitation of using Transwell inserts as a co-culture model in this project. The inserts used were the most adapted to investigate the paracrine axis of the crosstalk, specifically, but future models should aim to integrate biomechanical interactions between EC and CM.

Finally, there are limitations associated with using multiple cytokines as a co-treatment of EC. This is almost uncharted territory in vascular biology, and complicates any comparison of cell responses to Cytomix to the effects described in the literature with other treatment conditions. Yet, this type of “complication” can only lower the attrition rate of result translation from *in vitro* models of inflammatory diseases to clinical practice. With more research on the intricacies of cytokine interactions, the value of cytokine cocktails such as Cytomix could potentially trump that of single cytokine treatments in future research in cardiovascular biology.

## 6.4 Future work

To contextualise the effects of Cytomix on the paracrine activity of EC more conclusively, in terms of inflammatory cardiac disease modelling, I would like to: (1) measure the bioavailability of NO in co-cultures with more sensitive and specific methods than DAF-2, and (2) measure the phosphorylation of titin and the levels of cGMP in co-cultured CM. First, this would create an opportunity to validate properly a panel of chemical interventions to manipulate NO in co-cultures (L-NAME, negatively controlled using the inactive enantiomer D-NAME, c-PTIO, and NO donor NOC-5), and use these to assess the contribution of NO to the effects of untreated or Cytomix-treated EC on co-cultured CM. It remains possible that NO-independent paracrine pathways contribute to the effects of untreated EC or Cytomix-treated EC on CM function after co-culture. However, these can only be confirmed experimentally after their soluble mediators have been identified. Using a library of inhibitory antibodies in EC-CM co-cultures represents a potential approach to identify a small list of candidate mediators, but since calcium handling needs to be used as a main experimental outcome the throughput of such screening can only be limited. A better solution, less costly and more time-efficient, would be to analyse single-cell transcriptomics or proteomics datasets (available online) to correlate ligand expression in EC and receptor activation in CM (or proteins involved in CM function generally). With datasets collected using cardiac cells from HF patients and healthy donors, previous studies have been able to generate different EC-CM interactome maps between the normal and HF conditions<sup>70</sup>. This sort of unbiased correlation analysis would be an extremely valuable first step to propose non-NO mediators of the paracrine effects of EC on CM, although all factors would have to be eventually confirmed more thoroughly in co-cultures in future experiments.

Next, to ramp up the pathophysiological relevance of this study, it would be interesting to use serum purified from patients for whom systemic inflammation has been clinically confirmed (e.g. in RA), used as a pre-conditioning for EC prior to co-culture and in comparison to serum from healthy donors. To produce co-cultures in which the phenotype of EC matches best the EC functions in HF however, the next step would be to isolate microvascular EC from biopsies

of HF patients. Given the opportunity, it would also be interesting to compare the effects of EC on CM when isolated from different types of HF or, similarly, compare the effects of EC from HF patients and patients with systemic inflammatory diseases. Endothelial colony forming cells (already in use in the Mason lab) isolated from HF patients, might provide an alternative source of relevant EC in this setting.

These experiments however rely on the assumption that the paracrine effects of diseased EC on healthy CM are relevant to pathology, which as we have discussed previously is not entirely correct. A necessary test to be performed in future experiments would be to compare calcium handling properties in CM after Transwell co-culture with EC in the following conditions: (1) Cytomix-treated EC + CM, (2) Cytomix-treated EC + CM + Cytomix, (3) untreated EC + CM + Cytomix, (4) EC + CM, (5) CM + Cytomix, (6) CM only. This would address two possibilities: that untreated EC have a protective effect on the response of CM to inflammatory stimuli, and that this is lost or altered when EC and CM are responding to inflammatory conditions.

In Chapter 5, we show that Cytomix treatment induces a change of contractility of myocardial slices at high levels of mechanical load. This model is perfect to bridge co-cultures and *in vivo* experiments, due to all the physiological parameters which can be controlled in cultured slices. It would therefore be an important element of future work to validate the results obtained from co-cultures with myocardial slices, and confirm that the presence of structured ECM, other cell types (e.g. fibroblasts), and biomechanical interplay between cells do not abrogate the effects observed in simpler models. Before this can be accomplished however, more work is required to confirm that: (1) EC viability and microvascular structures (i.e. lumen, continuity of vessels) are preserved in cultured slices, and (2) EC respond to Cytomix added to slices in a similar fashion to HCMEC *in vitro*. Next, inhibitory antibodies could be used in the medium of cultured slices to attenuate elements of EC-CM crosstalk, though these elements might not be specific to EC and CM. EC-specific treatments or interventions are challenging in slices, as much as *in vivo*. Plasmids can be designed to deliver RNA-interfering siRNA or miRNA hairpins to EC specifically<sup>369</sup>, for example by placing the interfering RNA sequence under control of the VE-



cadherin promoter. With this technique, all cells in slices are infected but only those expressing VE-cadherin will express the interfering hairpins, resulting in an EC-specific downregulation of the gene of interest. This cannot be applied for too many targets however, considering the high cost of such plasmids and the time required to validate the efficiency and the EC-specificity of such RNA interference. With the same method, it would be interesting to block a candidate EC-secreted mediator of the EC-CM crosstalk in slices isolated from rat models of systemic inflammation, at a time point when cardiac microvasculature is not yet dysfunctional. HF models could be also used (e.g. Zucker diabetic fatty and spontaneously hypertensive HF F1 hybrid rats, known as ZSF1, which have on numerous occasions been used as a model of HFpEF<sup>11,91,370,371</sup>).

Ultimately, even the findings obtained using myocardial slices need to be confirmed *in vivo*. It would therefore be logical to use the same rat models of inflammatory diseases or HF that we discussed above for this *in vivo* study, and apply an EC-specific knockdown method validated in slices (e.g. RNA interference) by intra-myocardial injection of the plasmids, as was done by others<sup>372</sup>. This experiment would be the opportunity to integrate important elements of cardiac and inflammatory pathophysiology to our model (e.g. myocardial capillary resistance, changes of blood pressure, macrophage infiltration, a more complex stimulatory microenvironment for EC and CM, arrhythmia, thrombosis, LV and non-LV cardiac remodelling, etc.).

## 6.5 Concluding remarks

In this thesis, I have shown that EC modulate the calcium handling of CM in co-culture, and that this is altered when EC are pre-conditioned with a cocktail of pro-inflammatory cytokines. This shows that the paracrine activity of EC on CM is plastic, and modulated during myocardial or systemic inflammation. Further work is needed to fully characterise the response of CM to inflamed EC and the signalling pathways involved in these effects. Except for the reduction of NO bioavailability, little is known about how the shift from inflamed endothelium to endothelial dysfunction affects the paracrine activity of EC on other cell types, notably on CM. By focusing on the initial inflammatory response of EC, i.e. before the shift to endothelial dysfunction, new mechanisms of the EC-CM crosstalk, myocardial markers of onset-HF, and targets for novel therapeutic interventions might be brought to light. Eventually, this work might also be of great use for preventing cardiac complications in patients with systemic inflammatory disorders.

## Reference list

1. Ponikowski, P. *et al.* 2016 ESC Guidelines for the diagnosis and treatment of acute and chronic heart failure: The Task Force for the diagnosis and treatment of acute and chronic heart failure of the European Society of Cardiology (ESC) Developed with the special contribution of. *Eur. Heart J.* **37**, 2129–2200 (2016).
2. van Riet, E. E. S. *et al.* Prevalence of unrecognized heart failure in older persons with shortness of breath on exertion. *Eur. J. Heart Fail.* **16**, 772–777 (2014).
3. Badano, L. P. *et al.* Prevalence, clinical characteristics, quality of life, and prognosis of patients with congestive heart failure and isolated left ventricular diastolic dysfunction. *J. Am. Soc. Echocardiogr.* **17**, 253–261 (2004).
4. Owan, T. E. *et al.* Trends in Prevalence and Outcome of Heart Failure with Preserved Ejection Fraction. *N. Engl. J. Med.* **355**, 251–259 (2006).
5. Bonsu, K. O., Arunmanakul, P. & Chaiyakunapruk, N. Pharmacological treatments for heart failure with preserved ejection fraction—a systematic review and indirect comparison. *Heart Fail. Rev.* **23**, 147–156 (2018).
6. A., P. M., M., S. A. & A., B. B. Heart Failure With Preserved Ejection Fraction In Perspective. *Circ. Res.* **124**, 1598–1617 (2019).
7. Tomoyuki, T., Masatsugu, N., Kazuya, H., Hidenobu, K. & Akira, Y. Improved Diastolic Function Is Associated With Higher Cardiac Output in Patients With Heart Failure Irrespective of Left Ventricular Ejection Fraction. *J. Am. Heart Assoc.* **6**, e003389 (2020).
8. Tan, Y. T. *et al.* The Pathophysiology of Heart Failure With Normal Ejection Fraction: Exercise Echocardiography Reveals Complex Abnormalities of Both Systolic and Diastolic Ventricular Function Involving Torsion, Untwist, and Longitudinal Motion. *J. Am. Coll. Cardiol.* **54**, 36–46 (2009).
9. Paulus, W. J. & Tschöpe, C. A novel paradigm for heart failure with preserved ejection fraction: comorbidities drive myocardial dysfunction and remodeling through coronary microvascular endothelial inflammation. *J. Am. Coll. Cardiol.* **62**, 263–271 (2013).
10. Mohammed, S. F. *et al.* Coronary microvascular rarefaction and myocardial fibrosis in heart failure with preserved ejection fraction. *Circulation* **131**, 550–559 (2015).
11. Nguyen, I. T. N. *et al.* Both male and female obese ZSF1 rats develop cardiac dysfunction in obesity-induced heart failure with preserved ejection fraction. *PLoS One* **15**, e0232399–e0232399 (2020).

12. Zile, M. R., Baicu, C. F. & Gaasch, W. H. Diastolic Heart Failure — Abnormalities in Active Relaxation and Passive Stiffness of the Left Ventricle. *N. Engl. J. Med.* **350**, 1953–1959 (2004).
13. Kitzman, D. W. *et al.* Pathophysiological Characterization of Isolated Diastolic Heart Failure in Comparison to Systolic Heart Failure. *JAMA* **288**, 2144–2150 (2002).
14. Vedin, O. *et al.* Significance of Ischemic Heart Disease in Patients With Heart Failure and Preserved, Midrange, and Reduced Ejection Fraction: A Nationwide Cohort Study. *Circ. Heart Fail.* **10**, (2017).
15. Khatibzadeh, S., Farzadfar, F., Oliver, J., Ezzati, M. & Moran, A. Worldwide risk factors for heart failure: A systematic review and pooled analysis. *Int. J. Cardiol.* **168**, 1186–1194 (2013).
16. Y., E. I., Dhruv, M. & J., P. C. Medical Therapy for Heart Failure Caused by Ischemic Heart Disease. *Circ. Res.* **124**, 1520–1535 (2019).
17. John, S. M. G. St. & Norman, S. Left Ventricular Remodeling After Myocardial Infarction . *Circulation* **101**, 2981–2988 (2000).
18. López-Cuenca, A. *et al.* Comparison between type-2 and type-1 myocardial infarction: clinical features, treatment strategies and outcomes. *J. Geriatr. Cardiol.* **13**, 15–22 (2016).
19. E., T.-H. J. *et al.* Contemporary Diagnosis and Management of Patients With Myocardial Infarction in the Absence of Obstructive Coronary Artery Disease: A Scientific Statement From the American Heart Association. *Circulation* **139**, e891–e908 (2019).
20. Leurent, G. *et al.* Diagnostic contributions of cardiac magnetic resonance imaging in patients presenting with elevated troponin, acute chest pain syndrome and unobstructed coronary arteries. *Arch. Cardiovasc. Dis.* **104**, 161–170 (2011).
21. Montone, R. A. *et al.* Patients with acute myocardial infarction and non-obstructive coronary arteries: safety and prognostic relevance of invasive coronary provocative tests. *Eur. Heart J.* **39**, 91–98 (2018).
22. Hjort, M. *et al.* Increased Inflammatory Activity in Patients 3 Months after Myocardial Infarction with Nonobstructive Coronary Arteries. *Clin. Chem.* **65**, 1023–1030 (2019).
23. Torsten, D. *et al.* PCI and CABG for Treating Stable Coronary Artery Disease. *J. Am. Coll. Cardiol.* **73**, 964–976 (2019).

24. Pironti, G. *et al.* Cardiomyopathy, oxidative stress and impaired contractility in a rheumatoid arthritis mouse model. *Heart* **0**, 1–9 (2018).
25. Sallam, K., Kodo, K. & Wu, J. C. Modeling Inherited Cardiac Disorders. *Circ. J.* **78**, 784–794 (2014).
26. Dick, S. A. & Epelman, S. Chronic Heart Failure and Inflammation What Do We Really Know? *Circ. Res.* **119**, 159–177 (2016).
27. Krejci, J., Mlejnek, D., Sochorova, D. & Nemecek, P. Inflammatory Cardiomyopathy: A Current View on the Pathophysiology, Diagnosis, and Treatment. *Biomed Res. Int.* **2016**, 4087632 (2016).
28. Caforio, A. L. P. *et al.* Current state of knowledge on aetiology, diagnosis, management, and therapy of myocarditis: a position statement of the European Society of Cardiology Working Group on Myocardial and Pericardial Diseases. *Eur. Heart J.* **34**, 2636–48, 2648a–2648d (2013).
29. Breinholt, J. P. *et al.* Viral epidemiologic shift in inflammatory heart disease: the increasing involvement of parvovirus B19 in the myocardium of pediatric cardiac transplant patients. *J. Hear. lung Transplant. Off. Publ. Int. Soc. Hear. Transplant.* **29**, 739–746 (2010).
30. Ho, J. S., Sia, C.-H., Chan, M. Y., Lin, W. & Wong, R. C. Coronavirus-induced myocarditis: A meta-summary of cases. *Heart Lung* **49**, 681–685 (2020).
31. Siripanthong, B. *et al.* Recognizing COVID-19-related myocarditis: The possible pathophysiology and proposed guideline for diagnosis and management. *Hear. Rhythm* **17**, 1463–1471 (2020).
32. Ruan, Q., Yang, K., Wang, W., Jiang, L. & Song, J. Clinical predictors of mortality due to COVID-19 based on an analysis of data of 150 patients from Wuhan, China. *Intensive care medicine* **46**, 846–848 (2020).
33. Esfandiarei, M. & McManus, B. M. Molecular biology and pathogenesis of viral myocarditis. *Annu. Rev. Pathol.* **3**, 127–155 (2008).
34. Lee, D. W. *et al.* Current concepts in the diagnosis and management of cytokine release syndrome. *Blood* **124**, 188–195 (2014).
35. Mocan, M. *et al.* Biomarkers of Inflammation in Left Ventricular Diastolic Dysfunction. *Dis. Markers* **2019**, 7583690 (2019).
36. Bordy, R. *et al.* Microvascular endothelial dysfunction in rheumatoid arthritis. *Nat. Rev.*

*Rheumatol.* (2018). doi:10.1038/s41584-018-0022-8

37. Pober, J. S. & Sessa, W. C. Evolving functions of endothelial cells in inflammation. *Nat. Rev. Immunol.* **7**, 803–815 (2007).
38. Marin, V. *et al.* The IL-6-soluble IL-6R $\alpha$  autocrine loop of endothelial activation as an intermediate between acute and chronic inflammation: an experimental model involving thrombin. *J. Immunol.* **167**, 3435–3442 (2001).
39. Lee, J. *et al.* Interaction of IL-6 and TNF- $\alpha$  contributes to endothelial dysfunction in type 2 diabetic mouse hearts. *PLoS One* **12**, e0187189 (2017).
40. Xing, Z. *et al.* IL-6 is an antiinflammatory cytokine required for controlling local or systemic acute inflammatory responses. *J. Clin. Invest.* **101**, 311–320 (1998).
41. Schrader, L. I., Kinzenbaw, D. A., Johnson, A. W., Faraci, F. M. & Didion, S. P. IL-6 Deficiency Protects Against Angiotensin II-Induced Endothelial Dysfunction and Hypertrophy. *Arterioscler. Thromb. Vasc. Biol.* **27**, 2576–2581 (2007).
42. Hilfiker-Kleiner, D., Hilfiker, A. & Drexler, H. Many good reasons to have STAT3 in the heart. *Pharmacol. Ther.* **107**, 131–137 (2005).
43. Fattori, E. *et al.* Defective inflammatory response in interleukin 6-deficient mice. *J. Exp. Med.* **180**, 1243–1250 (1994).
44. Reeh, H. *et al.* Response to IL-6 trans- and IL-6 classic signalling is determined by the ratio of the IL-6 receptor  $\alpha$  to gp130 expression: fusing experimental insights and dynamic modelling. *Cell Commun. Signal.* **17**, 46 (2019).
45. Didion, S. P. Cellular and Oxidative Mechanisms Associated with Interleukin-6 Signaling in the Vasculature. *International Journal of Molecular Sciences* **18**, (2017).
46. Watson, C. *et al.* IL-6 acts on endothelial cells to preferentially increase their adherence for lymphocytes. *Clin. Exp. Immunol.* **105**, 112–119 (1996).
47. Wung, B. S., Ni, C. W. & Wang, D. L. ICAM-1 induction by TNF $\alpha$  and IL-6 is mediated by distinct pathways via Rac in endothelial cells. *J. Biomed. Sci.* **12**, 91–101 (2005).
48. Saura, M. *et al.* Stat3 mediates interleukin-6 [correction of interelukin-6] inhibition of human endothelial nitric-oxide synthase expression. *J. Biol. Chem.* **281**, 30057–30062 (2006).
49. Hung, M.-J., Cherng, W.-J., Hung, M.-Y., Wu, H.-T. & Pang, J.-H. S. Interleukin-6 inhibits endothelial nitric oxide synthase activation and increases endothelial nitric

- oxide synthase binding to stabilized caveolin-1 in human vascular endothelial cells. *J. Hypertens.* **28**, 940–951 (2010).
50. Liu, T., Zhang, L., Joo, D. & Sun, S.-C. NF- $\kappa$ B signaling in inflammation. *Signal Transduct. Target. Ther.* **2**, 17023 (2017).
  51. Al-Lamki, R. S. & Mayadas, T. N. TNF receptors: signaling pathways and contribution to renal dysfunction. *Kidney Int.* **87**, 281–296 (2015).
  52. Egawa, G. *et al.* Intravital analysis of vascular permeability in mice using two-photon microscopy. *Sci. Rep.* **3**, 1932 (2013).
  53. Claesson-Welsh, L. Vascular permeability--the essentials. *Ups. J. Med. Sci.* **120**, 135–143 (2015).
  54. Park, S. A., Jeong, S., Choe, Y. H. & Hyun, Y.-M. Sensing of Vascular Permeability in Inflamed Vessel of Live Animal. *J. Anal. Methods Chem.* **2018**, 5797152 (2018).
  55. Sukriti, S., Tauseef, M., Yazbeck, P. & Mehta, D. Mechanisms regulating endothelial permeability. *Pulm. Circ.* **4**, 535–551 (2014).
  56. Paria, B. C. *et al.* Tumor necrosis factor- $\alpha$ -induced TRPC1 expression amplifies store-operated Ca<sup>2+</sup> influx and endothelial permeability. *Am. J. Physiol. Lung Cell. Mol. Physiol.* **287**, L1303-13 (2004).
  57. Debreczeni, M. L. *et al.* MASP-1 Increases Endothelial Permeability . *Frontiers in Immunology* **10**, 991 (2019).
  58. Thibeault, S. *et al.* S-nitrosylation of beta-catenin by eNOS-derived NO promotes VEGF-induced endothelial cell permeability. *Mol. Cell* **39**, 468–476 (2010).
  59. Ehringer, W. D., Edwards, M. J. & Miller, F. N. Mechanisms of  $\alpha$ -thrombin, histamine, and bradykinin induced endothelial permeability. *J. Cell. Physiol.* **167**, 562–569 (1996).
  60. Vanhauwe, J. F. *et al.* Thrombin receptors activate G(o) proteins in endothelial cells to regulate intracellular calcium and cell shape changes. *J. Biol. Chem.* **277**, 34143–34149 (2002).
  61. Tiruppathi, C., Naqvi, T., Sandoval, R., Mehta, D. & Malik, A. B. Synergistic effects of tumor necrosis factor- $\alpha$  and thrombin in increasing endothelial permeability. *Am. J. Physiol. Cell. Mol. Physiol.* **281**, L958–L968 (2001).
  62. Choi, S. *et al.* Regulation of endothelial barrier integrity by redox-dependent nitric oxide signaling: Implication in traumatic and inflammatory brain injuries. *Nitric oxide Biol.*



- Chem.* **83**, 51–64 (2019).
63. D., M. E. *et al.* Mechanism of Endothelial Nitric Oxide Synthase Phosphorylation and Activation by Thrombin. *Hypertension* **49**, 577–583 (2007).
  64. Sandoval, R. *et al.* Ca(2+) signalling and PKC $\alpha$  activate increased endothelial permeability by disassembly of VE-cadherin junctions. *J. Physiol.* **533**, 433–445 (2001).
  65. Desai, T. R., Leeper, N. J., Hynes, K. L. & Gewertz, B. L. Interleukin-6 causes endothelial barrier dysfunction via the protein kinase C pathway. *J. Surg. Res.* **104**, 118–123 (2002).
  66. Brutsaert, D. L. Cardiac endothelial-myocardial signaling: its role in cardiac growth, contractile performance, and rhythmicity. *Physiol. Rev.* **83**, 59–115 (2003).
  67. Shah, A. M. & MacCarthy, P. A. Paracrine and autocrine effects of nitric oxide on myocardial function. *Pharmacol. Ther.* **86**, 49–86 (2000).
  68. Davidson, S. M. *et al.* Endothelial cells release cardioprotective exosomes that may contribute to ischaemic preconditioning. *Sci. Rep.* **8**, 15885 (2018).
  69. Pinto, A. R. *et al.* Revisiting Cardiac Cellular Composition. *Circ. Res.* (2015). doi:10.1161/CIRCRESAHA.115.307778
  70. Wang, L. *et al.* Single-cell reconstruction of the adult human heart during heart failure and recovery reveals the cellular landscape underlying cardiac function. *Nat. Cell Biol.* **22**, 108–119 (2020).
  71. Freeman, B. D., Machado, F. S., Tanowitz, H. B. & Desruisseaux, M. S. Endothelin-1 and its role in the pathogenesis of infectious diseases. *Life Sci.* **118**, 110–119 (2014).
  72. Molet, S., Furukawa, K., Maghazechi, A., Hamid, Q. & Giaid, A. Chemokine- and cytokine-induced expression of endothelin 1 and endothelin-converting enzyme 1 in endothelial cells. *J. Allergy Clin. Immunol.* **105**, 333–338 (2000).
  73. Thorin, E. & Webb, D. J. Endothelium-derived endothelin-1. *Pflugers Arch.* **459**, 951–958 (2010).
  74. Boulanger, C. & Lüscher, T. F. Release of endothelin from the porcine aorta. Inhibition by endothelium-derived nitric oxide. *J. Clin. Invest.* **85**, 587–590 (1990).
  75. Jiang, F., Mohr, F., Ullrich, N. D., Hecker, M. & Wagner, A. H. Endothelial cell modulation of cardiomyocyte gene expression. *Exp. Cell Res.* **383**, 111565 (2019).
  76. Yan, G., You, B., Chen, S.-P., Liao, J. K. & Sun, J. Tumor necrosis factor- $\alpha$

- downregulates endothelial nitric oxide synthase mRNA stability via translation elongation factor 1- $\alpha$  1. *Circ. Res.* **103**, 591–597 (2008).
77. Spillmann, F. *et al.* LXR agonism improves TNF- $\alpha$ -induced endothelial dysfunction in the absence of its cholesterol-modulating effects. *Atherosclerosis* **232**, 1–9 (2014).
  78. Kleinert, H., Pautz, A., Linker, K. & Schwarz, P. M. Regulation of the expression of inducible nitric oxide synthase. *Eur. J. Pharmacol.* **500**, 255–266 (2004).
  79. Kuhr, F., Lowry, J., Zhang, Y., Brovkovych, V. & Skidgel, R. A. Differential regulation of inducible and endothelial nitric oxide synthase by kinin B1 and B2 receptors. *Neuropeptides* **44**, 145–154 (2010).
  80. Lowry, J. L., Brovkovych, V., Zhang, Y. & Skidgel, R. A. Endothelial nitric-oxide synthase activation generates an inducible nitric-oxide synthase-like output of nitric oxide in inflamed endothelium. *J. Biol. Chem.* **288**, 4174–4193 (2013).
  81. Förstermann, U. & Sessa, W. C. Nitric oxide synthases: regulation and function. *Eur. Heart J.* **33**, 829–837d (2012).
  82. Mayourian, J. *et al.* Physiologic, Pathologic, and Therapeutic Paracrine Modulation of Cardiac Excitation-Contraction Coupling. *Circ. Res.* **122**, 167–183 (2018).
  83. Meulemans, A. L., Sipido, K. R., Sys, S. U. & Brutsaert, D. L. Atriopeptin III induces early relaxation of isolated mammalian papillary muscle. *Circ. Res.* **62**, 1171–1174 (1988).
  84. Brutsaert, D. L., Meulemans, A. L., Sipido, K. R. & Sys, S. U. Effects of damaging the endocardial surface on the mechanical performance of isolated cardiac muscle. *Circ. Res.* **62**, 358–366 (1988).
  85. Smith, J. A., Shah, A. M. & Lewis, M. J. Factors released from endocardium of the ferret and pig modulate myocardial contraction. *J. Physiol.* **439**, 1–14 (1991).
  86. Grocott-Mason, R., Anning, P., Evans, H., Lewis, M. J. & Shah, A. M. Modulation of left ventricular relaxation in isolated ejecting heart by endogenous nitric oxide. *Am. J. Physiol.* **267**, H1804-13 (1994).
  87. Paulus, W. J., Vantrimpont, P. J. & Shah, A. M. Paracrine coronary endothelial control of left ventricular function in humans. *Circulation* **92**, 2119–2126 (1995).
  88. Kojda, G. *et al.* Low increase in cGMP induced by organic nitrates and nitrovasodilators improves contractile response of rat ventricular myocytes. *Circ. Res.* **78**, 91–101

- (1996).
89. Layland, J., Li, J.-M. & Shah, A. M. Role of cyclic GMP-dependent protein kinase in the contractile response to exogenous nitric oxide in rat cardiac myocytes. *J. Physiol.* **540**, 457–467 (2002).
  90. Sabine, B. *et al.* Cyclic GMP-mediated phospholamban phosphorylation in intact cardiomyocytes. *Biochem. Biophys. Res. Commun.* **214**, 75–80 (1995).
  91. Hamdani, N. *et al.* Myocardial titin hypophosphorylation importantly contributes to heart failure with preserved ejection fraction in a rat metabolic risk model. *Circ. Heart Fail.* **6**, 1239–1249 (2013).
  92. Li, K., Stewart, D. J. & Rouleau, J. L. Myocardial contractile actions of endothelin-1 in rat and rabbit papillary muscles. Role of endocardial endothelium. *Circ. Res.* **69**, 301–312 (1991).
  93. Mebazaa, A. *et al.* Paracrine effects of endocardial endothelial cells on myocyte contraction mediated via endothelin. *Am. J. Physiol.* **265**, H1841-6 (1993).
  94. Konrad, D. *et al.* Positive inotropic and negative lusitropic effects of endothelin receptor agonism in vivo. *Am. J. Physiol. Heart Circ. Physiol.* **289**, H1702-9 (2005).
  95. Sakai, S. *et al.* Endogenous endothelin-1 participates in the maintenance of cardiac function in rats with congestive heart failure. Marked increase in endothelin-1 production in the failing heart. *Circulation* **93**, 1214–1222 (1996).
  96. Pandey, A. S. *et al.* Chronic endothelin-1 blockade preserves myocardial contractility in dilated cardiomyopathy. *J. Cardiovasc. Pharmacol.* **31 Suppl 1**, S306-8 (1998).
  97. Kane, C., Couch, L. & Terracciano, C. M. N. Excitation – contraction coupling of human induced pluripotent stem cell-derived cardiomyocytes. *Front. Cell Dev. Biol.* **3**, 1–8 (2015).
  98. Blaustein, M. P. & Lederer, W. J. Sodium/calcium exchange: its physiological implications. *Physiol. Rev.* **79**, 763–854 (1999).
  99. T., C. M. *et al.* Coronary Endothelial Dysfunction Is Associated With Increased Risk of Incident Atrial Fibrillation. *J. Am. Heart Assoc.* **9**, e014850 (2020).
  100. Lin, L. & Yuan, W.-J. Involvement of endothelin-1 in acute ischaemic arrhythmias in cats and rats. *Clin. Sci. (Lond).* **103 Suppl**, 228S–232S (2002).
  101. Hassanabad, Z. F., Furman, B. L., Parratt, J. R. & Aughey, E. Coronary endothelial

- dysfunction increases the severity of ischaemia-induced ventricular arrhythmias in rat isolated perfused hearts. *Basic Res. Cardiol.* **93**, 241–249 (1998).
102. Pabla, R. & Curtis, M. J. Nitric oxide fails to confer endogenous antiarrhythmic cardioprotection in the primate heart in vitro. *Br. J. Pharmacol.* **150**, 893–898 (2007).
  103. Ravinder, P. & J., C. M. Effects of NO Modulation on Cardiac Arrhythmias in the Rat Isolated Heart. *Circ. Res.* **77**, 984–992 (1995).
  104. Fei, L., Baron, A. D., Henry, D. P. & Zipes, D. P. Intrapericardial delivery of L-arginine reduces the increased severity of ventricular arrhythmias during sympathetic stimulation in dogs with acute coronary occlusion: nitric oxide modulates sympathetic effects on ventricular electrophysiological properti. *Circulation* **96**, 4044–4049 (1997).
  105. Piotr, M., Ming, L., F., B. H., J., P. D. & Barbara, C. Nitric Oxide Can Increase Heart Rate by Stimulating the Hyperpolarization-Activated Inward Current, If. *Circ. Res.* **81**, 60–68 (1997).
  106. Balligand, J. L., Kelly, R. A., Marsden, P. A., Smith, T. W. & Michel, T. Control of cardiac muscle cell function by an endogenous nitric oxide signaling system. *Proc. Natl. Acad. Sci.* **90**, 347 LP-351 (1993).
  107. Wang, H., Kohr, M. J., Wheeler, D. G. & Ziolo, M. T. Endothelial nitric oxide synthase decreases beta-adrenergic responsiveness via inhibition of the L-type Ca<sup>2+</sup> current. *Am. J. Physiol. Heart Circ. Physiol.* **294**, H1473-80 (2008).
  108. Giacomelli, E. *et al.* Three-dimensional cardiac microtissues composed of cardiomyocytes and endothelial cells co-differentiated from human pluripotent stem cells. *Development* **144**, 1008–1017 (2017).
  109. Liu, T. *et al.* L-NAME releases nitric oxide and potentiates subsequent nitroglycerin-mediated vasodilation. *Redox Biol.* **26**, 101238 (2019).
  110. Gaudesius, G., Miragoli, M., Thomas, S. P. & Rohr, S. Coupling of cardiac electrical activity over extended distances by fibroblasts of cardiac origin. *Circ. Res.* **93**, 421–428 (2003).
  111. Bers, D. M. Cardiac excitation-contraction coupling. *Nature* **415**, 198–205 (2002).
  112. Junhui, S. *et al.* Hypercontractile Female Hearts Exhibit Increased S-Nitrosylation of the L-Type Ca<sup>2+</sup> Channel  $\alpha$ 1 Subunit and Reduced Ischemia/Reperfusion Injury. *Circ. Res.* **98**, 403–411 (2006).
  113. Han, X., Kobzik, L., Balligand, J. L., Kelly, R. A. & Smith, T. W. Nitric oxide synthase

- (NOS3)-mediated cholinergic modulation of Ca<sup>2+</sup> current in adult rabbit atrioventricular nodal cells. *Circ. Res.* **78**, 998–1008 (1996).
114. Ricardo, G. *et al.* Nitric Oxide Increases Cardiac IK1 by Nitrosylation of Cysteine 76 of Kir2.1 Channels. *Circ. Res.* **105**, 383–392 (2009).
115. Bai, C.-X., Takahashi, K., Masumiya, H., Sawanobori, T. & Furukawa, T. Nitric oxide-dependent modulation of the delayed rectifier K<sup>+</sup> current and the L-type Ca<sup>2+</sup> current by ginsenoside Re, an ingredient of Panax ginseng, in guinea-pig cardiomyocytes. *Br. J. Pharmacol.* **142**, 567–575 (2004).
116. Gómez, R. *et al.* Nitric oxide inhibits Kv4.3 and human cardiac transient outward potassium current (I<sub>to1</sub>). *Cardiovasc. Res.* **80**, 375–384 (2008).
117. Taglialatela, M., Pannaccione, A., Iossa, S., Castaldo, P. & Annunziato, L. Modulation of the K(+) channels encoded by the human ether-a-gogo-related gene-1 (hERG1) by nitric oxide. *Mol. Pharmacol.* **56**, 1298–1308 (1999).
118. Yu, L. *et al.* Endothelin-1 stimulates the expression of L-type Ca<sup>2+</sup> channels in neonatal rat cardiomyocytes via the extracellular signal-regulated kinase 1/2 pathway. *J. Membr. Biol.* **246**, 343–353 (2013).
119. Damron, D. S., Van Wagoner, D. R., Moravec, C. S. & Bond, M. Arachidonic acid and endothelin potentiate Ca<sup>2+</sup> transients in rat cardiac myocytes via inhibition of distinct K<sup>+</sup> channels. *J. Biol. Chem.* **268**, 27335–27344 (1993).
120. Wang, J. X., Paik, G. & Morgan, J. P. Endothelin 1 enhances myofilament Ca<sup>2+</sup> responsiveness in aequorin-loaded ferret myocardium. *Circ. Res.* **69**, 582–589 (1991).
121. Louch, W. E. *et al.* Reduced synchrony of Ca<sup>2+</sup> release with loss of T-tubules—a comparison to Ca<sup>2+</sup> release in human failing cardiomyocytes. *Cardiovasc. Res.* **62**, 63–73 (2004).
122. Lyon, A. R. *et al.* Loss of T-tubules and other changes to surface topography in ventricular myocytes from failing human and rat heart. *Proc. Natl. Acad. Sci. U. S. A.* **106**, 6854–6859 (2009).
123. Levesque, P. C., Leblanc, N. & Hume, J. R. Release of calcium from guinea pig cardiac sarcoplasmic reticulum induced by sodium-calcium exchange. *Cardiovasc. Res.* **28**, 370–378 (1994).
124. Sipido, K. R., Carmeliet, E. & Pappano, A. Na<sup>+</sup> current and Ca<sup>2+</sup> release from the sarcoplasmic reticulum during action potentials in guinea-pig ventricular myocytes. *J.*

- Physiol.* **489** ( Pt 1, 1–17 (1995).
125. Bouchard, R. A., Clark, R. B. & Giles, W. R. Role of sodium-calcium exchange in activation of contraction in rat ventricle. *J. Physiol.* **472**, 391–413 (1993).
  126. Scriven, D. R., Dan, P. & Moore, E. D. Distribution of proteins implicated in excitation-contraction coupling in rat ventricular myocytes. *Biophys. J.* **79**, 2682–2691 (2000).
  127. Kushnir, A. & Marks, A. R. The ryanodine receptor in cardiac physiology and disease. *Adv. Pharmacol.* **59**, 1–30 (2010).
  128. Xu, L., Eu, J. P., Meissner, G. & Stamler, J. S. Activation of the Cardiac Calcium Release Channel (Ryanodine Receptor) by Poly-S-Nitrosylation. *Science* (80-. ). **279**, 234 LP-237 (1998).
  129. Barouch, L. A. *et al.* Nitric oxide regulates the heart by spatial confinement of nitric oxide synthase isoforms. *Nature* **416**, 337–339 (2002).
  130. Ogrodnik, J. & Niggli, E. Increased Ca(2+) leak and spatiotemporal coherence of Ca(2+) release in cardiomyocytes during beta-adrenergic stimulation. *J. Physiol.* **588**, 225–242 (2010).
  131. Ginsburg, K. S. & Bers, D. M. Modulation of excitation-contraction coupling by isoproterenol in cardiomyocytes with controlled SR Ca<sup>2+</sup> load and Ca<sup>2+</sup> current trigger. *J. Physiol.* **556**, 463–480 (2004).
  132. Periasamy, M. & Kalyanasundaram, A. SERCA pump isoforms: their role in calcium transport and disease. *Muscle Nerve* **35**, 430–442 (2007).
  133. Hasenfuss, G. Alterations of calcium-regulatory proteins in heart failure. *Cardiovasc. Res.* **37**, 279–289 (1998).
  134. Arai, M., Alpert, N. R., MacLennan, D. H., Barton, P. & Periasamy, M. Alterations in sarcoplasmic reticulum gene expression in human heart failure. A possible mechanism for alterations in systolic and diastolic properties of the failing myocardium. *Circ. Res.* **72**, 463–469 (1993).
  135. Dash, R., Frank, K. F., Carr, A. N., Moravec, C. S. & Kranias, E. G. Gender influences on sarcoplasmic reticulum Ca<sup>2+</sup>-handling in failing human myocardium. *J. Mol. Cell. Cardiol.* **33**, 1345–1353 (2001).
  136. Frank, K. F., Bölck, B., Brixius, K., Kranias, E. G. & Schwinger, R. H. G. Modulation of SERCA: implications for the failing human heart. *Basic Res. Cardiol.* **97 Suppl 1**, 172-8 (2002).

137. Mercadier, J. J. *et al.* Altered sarcoplasmic reticulum Ca<sup>2+</sup>(+)-ATPase gene expression in the human ventricle during end-stage heart failure. *J. Clin. Invest.* **85**, 305–309 (1990).
138. Movsesian, M. A., Karimi, M., Green, K. & Jones, L. R. Ca<sup>2+</sup>-transporting ATPase, phospholamban, and calsequestrin levels in nonfailing and failing human myocardium. *Circulation* **90**, 653–657 (1994).
139. Münch, G. *et al.* Unchanged protein expression of sarcoplasmic reticulum Ca<sup>2+</sup>-ATPase, phospholamban, and calsequestrin in terminally failing human myocardium. *J. Mol. Med. (Berl)*. **76**, 434–441 (1998).
140. Cohen, R. A. & Adachi, T. Nitric-oxide-induced vasodilatation: regulation by physiologic s-glutathiolation and pathologic oxidation of the sarcoplasmic endoplasmic reticulum calcium ATPase. *Trends Cardiovasc. Med.* **16**, 109–114 (2006).
141. Wu, K. D., Bungard, D. & Lytton, J. Regulation of SERCA Ca<sup>2+</sup> pump expression by cytoplasmic Ca<sup>2+</sup> in vascular smooth muscle cells. *Am. J. Physiol. Cell Physiol.* **280**, C843-51 (2001).
142. Xu, K. Y., Huso, D. L., Dawson, T. M., Bredt, D. S. & Becker, L. C. Nitric oxide synthase in cardiac sarcoplasmic reticulum. *Proc. Natl. Acad. Sci.* **96**, 657 LP-662 (1999).
143. Adachi, T. *et al.* S-Glutathiolation by peroxynitrite activates SERCA during arterial relaxation by nitric oxide. *Nat. Med.* **10**, 1200–1207 (2004).
144. Sipido, K. R., Acsai, K., Antoons, G., Bito, V. & Macquaide, N. T-tubule remodelling and ryanodine receptor organization modulate sodium-calcium exchange. *Adv. Exp. Med. Biol.* **961**, 375–383 (2013).
145. Ottolia, M., Torres, N., Bridge, J. H. B., Philipson, K. D. & Goldhaber, J. I. Na/Ca exchange and contraction of the heart. *J. Mol. Cell. Cardiol.* **61**, 28–33 (2013).
146. Pott, C., Eckardt, L. & Goldhaber, J. I. Triple threat: the Na<sup>+</sup>/Ca<sup>2+</sup> exchanger in the pathophysiology of cardiac arrhythmia, ischemia and heart failure. *Curr. Drug Targets* **12**, 737–747 (2011).
147. Mattiello, J. A., Margulies, K. B., Jeevanandam, V. & Houser, S. R. Contribution of reverse-mode sodium-calcium exchange to contractions in failing human left ventricular myocytes. *Cardiovasc. Res.* **37**, 424–431 (1998).
148. E., S. C. *et al.* Cardiac Neuronal Nitric Oxide Synthase Isoform Regulates Myocardial Contraction and Calcium Handling. *Circ. Res.* **92**, e52–e59 (2003).

149. Richards, M. A. *et al.* Nitric oxide modulates cardiomyocyte pH control through a biphasic effect on sodium/hydrogen exchanger-1. *Cardiovasc. Res.* (2019). doi:10.1093/cvr/cvz311
150. Pavlovic, D. *et al.* Nitric oxide regulates cardiac intracellular Na<sup>+</sup> and Ca<sup>2+</sup> by modulating Na/K ATPase via PKC $\epsilon$  and phospholemman-dependent mechanism. *J. Mol. Cell. Cardiol.* **61**, 164–171 (2013).
151. Cheung, J. Y. *et al.* Phospholemman: a novel cardiac stress protein. *Clin. Transl. Sci.* **3**, 189–196 (2010).
152. Shao-kui, W. *et al.* Protein Kinase A Hyperphosphorylation Increases Basal Current but Decreases  $\beta$ -Adrenergic Responsiveness of the Sarcolemmal Na<sup>+</sup>-Ca<sup>2+</sup> Exchanger in Failing Pig Myocytes. *Circ. Res.* **92**, 897–903 (2003).
153. Haworth, R. S., McCann, C., Snabaitis, A. K., Roberts, N. A. & Avkiran, M. Stimulation of the plasma membrane Na<sup>+</sup>/H<sup>+</sup> exchanger NHE1 by sustained intracellular acidosis. Evidence for a novel mechanism mediated by the ERK pathway. *J. Biol. Chem.* **278**, 31676–31684 (2003).
154. Ballard, C. & Schaffer, S. Stimulation of the Na<sup>+</sup>/Ca<sup>2+</sup> exchanger by phenylephrine, angiotensin II and endothelin 1. *J. Mol. Cell. Cardiol.* **28**, 11–17 (1996).
155. Lu, X. *et al.* Measuring local gradients of intramitochondrial [Ca(2+)] in cardiac myocytes during sarcoplasmic reticulum Ca(2+) release. *Circ. Res.* **112**, 424–431 (2013).
156. Finkel, T. *et al.* The ins and outs of mitochondrial calcium. *Circ. Res.* **116**, 1810–1819 (2015).
157. Drago, I., De Stefani, D., Rizzuto, R. & Pozzan, T. Mitochondrial Ca<sup>2+</sup> uptake contributes to buffering cytoplasmic Ca<sup>2+</sup> peaks in cardiomyocytes. *Proc. Natl. Acad. Sci. U. S. A.* **109**, 12986–12991 (2012).
158. Eisner, D. A., Caldwell, J. L., Kistamás, K. & Trafford, A. W. Calcium and Excitation-Contraction Coupling in the Heart. *Circ. Res.* **121**, 181–195 (2017).
159. Bers, D. M., Bassani, J. W. & Bassani, R. A. Competition and redistribution among calcium transport systems in rabbit cardiac myocytes. *Cardiovasc. Res.* **27**, 1772–1777 (1993).
160. Negretti, N., O'Neill, S. C. & Eisner, D. A. The relative contributions of different intracellular and sarcolemmal systems to relaxation in rat ventricular myocytes.



- Cardiovasc. Res.* **27**, 1826–1830 (1993).
161. Williams, G. S. B., Boyman, L., Chikando, A. C., Khairallah, R. J. & Lederer, W. J. Mitochondrial calcium uptake. *Proc. Natl. Acad. Sci. U. S. A.* **110**, 10479–10486 (2013).
  162. Hüser, J., Blatter, L. A. & Sheu, S. S. Mitochondrial calcium in heart cells: beat-to-beat oscillations or slow integration of cytosolic transients? *J. Bioenerg. Biomembr.* **32**, 27–33 (2000).
  163. Griffiths, E. J., Balaska, D. & Cheng, W. H. Y. The ups and downs of mitochondrial calcium signalling in the heart. *Biochim. Biophys. Acta - Bioenerg.* **1797**, 856–864 (2010).
  164. Ljubojevic, S. & Bers, D. M. Nuclear calcium in cardiac myocytes. *J. Cardiovasc. Pharmacol.* **65**, 211–217 (2015).
  165. Hunton, D. L., Zou, L., Pang, Y. & Marchase, R. B. Adult rat cardiomyocytes exhibit capacitative calcium entry. *Am. J. Physiol. Heart Circ. Physiol.* **286**, H1124-32 (2004).
  166. Kojima, A., Kitagawa, H., Omatsu-Kanbe, M., Matsuura, H. & Nosaka, S. Presence of store-operated Ca<sup>2+</sup> entry in C57BL/6J mouse ventricular myocytes and its suppression by sevoflurane. *Br. J. Anaesth.* **109**, 352–360 (2012).
  167. Uehara, A., Yasukochi, M., Imanaga, I., Nishi, M. & Takeshima, H. Store-operated Ca<sup>2+</sup> entry uncoupled with ryanodine receptor and junctional membrane complex in heart muscle cells. *Cell Calcium* **31**, 89–96 (2002).
  168. Zhao, G., Li, T., Brochet, D. X. P., Rosenberg, P. B. & Lederer, W. J. STIM1 enhances SR Ca<sup>2+</sup> content through binding phospholamban in rat ventricular myocytes. *Proc. Natl. Acad. Sci. U. S. A.* **112**, E4792-801 (2015).
  169. Hanft, L. M., Korte, F. S. & McDonald, K. S. Cardiac function and modulation of sarcomeric function by length. *Cardiovasc. Res.* **77**, 627–636 (2008).
  170. Millman, B. M. The filament lattice of striated muscle. *Physiol. Rev.* **78**, 359–391 (1998).
  171. Farman, G. P., Allen, E. J., Gore, D., Irving, T. C. & de Tombe, P. P. Interfilament spacing is preserved during sarcomere length isometric contractions in rat cardiac trabeculae. *Biophys. J.* **92**, L73-5 (2007).
  172. Fuchs, F. & Martyn, D. A. Length-dependent Ca(2+) activation in cardiac muscle: some remaining questions. *J. Muscle Res. Cell Motil.* **26**, 199–212 (2005).
  173. Fukuda, N. & Granzier, H. L. Titin/connectin-based modulation of the Frank-Starling

- mechanism of the heart. *J. Muscle Res. Cell Motil.* **26**, 319–323 (2005).
174. Solaro, R. J., Henze, M. & Kobayashi, T. Integration of troponin I phosphorylation with cardiac regulatory networks. *Circ. Res.* **112**, 355–366 (2013).
  175. Wijnker, P. J. M., Murphy, A. M., Stienen, G. J. M. & van der Velden, J. Troponin I phosphorylation in human myocardium in health and disease. *Neth. Heart J.* **22**, 463–469 (2014).
  176. Li, L., Desantiago, J., Chu, G., Kranias, E. G. & Bers, D. M. Phosphorylation of phospholamban and troponin I in beta-adrenergic-induced acceleration of cardiac relaxation. *Am. J. Physiol. Heart Circ. Physiol.* **278**, H769-79 (2000).
  177. Herron, T. J., Korte, F. S. & McDonald, K. S. Power output is increased after phosphorylation of myofibrillar proteins in rat skinned cardiac myocytes. *Circ. Res.* **89**, 1184–1190 (2001).
  178. Fukuda, N., Wu, Y., Nair, P. & Granzier, H. L. Phosphorylation of titin modulates passive stiffness of cardiac muscle in a titin isoform-dependent manner. *J. Gen. Physiol.* **125**, 257–271 (2005).
  179. Krüger, M. & Linke, W. A. Protein kinase-A phosphorylates titin in human heart muscle and reduces myofibrillar passive tension. *J. Muscle Res. Cell Motil.* **27**, 435–444 (2006).
  180. Stelzer, J. E., Patel, J. R. & Moss, R. L. Protein kinase A-mediated acceleration of the stretch activation response in murine skinned myocardium is eliminated by ablation of cMyBP-C. *Circ. Res.* **99**, 884–890 (2006).
  181. Pi, Y., Zhang, D., Kemnitz, K. R., Wang, H. & Walker, J. W. Protein kinase C and A sites on troponin I regulate myofilament Ca<sup>2+</sup> sensitivity and ATPase activity in the mouse myocardium. *J. Physiol.* **552**, 845–857 (2003).
  182. Cuello, F. *et al.* Protein kinase D selectively targets cardiac troponin I and regulates myofilament Ca<sup>2+</sup> sensitivity in ventricular myocytes. *Circ. Res.* **100**, 864–873 (2007).
  183. duBell, W. H. *et al.* The cytosolic calcium transient modulates the action potential of rat ventricular myocytes. *J. Physiol.* **436**, 347–369 (1991).
  184. Sipido, K. R., Stankovicova, T., Flameng, W., Vanhaecke, J. & Verdonck, F. Frequency dependence of Ca<sup>2+</sup> release from the sarcoplasmic reticulum in human ventricular myocytes from end-stage heart failure. *Cardiovasc. Res.* **37**, 478–488 (1998).
  185. Balcazar, D. *et al.* SERCA is critical to control the Bowditch effect in the heart. *Sci. Rep.* **8**, 12447 (2018).

186. Gerd, H. *et al.* Relationship Between Na<sup>+</sup>-Ca<sup>2+</sup>-Exchanger Protein Levels and Diastolic Function of Failing Human Myocardium. *Circulation* **99**, 641–648 (1999).
187. Wijnker, P. J. M. *et al.* Length-dependent activation is modulated by cardiac troponin I bisphosphorylation at Ser23 and Ser24 but not by Thr143 phosphorylation. *Am. J. Physiol. Circ. Physiol.* **306**, H1171–H1181 (2014).
188. Mamidi, R., Gresham, K. S., Verma, S. & Stelzer, J. E. Cardiac Myosin Binding Protein-C Phosphorylation Modulates Myofilament Length-Dependent Activation . *Frontiers in Physiology* **7**, 38 (2016).
189. Ait-Mou, Y. *et al.* Titin strain contributes to the Frank–Starling law of the heart by structural rearrangements of both thin- and thick-filament proteins. *Proc. Natl. Acad. Sci.* **113**, 2306 LP-2311 (2016).
190. Édes, I. F. *et al.* Rate of tension redevelopment is not modulated by sarcomere length in permeabilized human, murine, and porcine cardiomyocytes. *Am. J. Physiol. Integr. Comp. Physiol.* **293**, R20–R29 (2007).
191. Cingolani, H. E., Pérez, N. G., Cingolani, O. H. & Ennis, I. L. The Anrep effect: 100 years later. *Am. J. Physiol. Heart Circ. Physiol.* **304**, H175-82 (2013).
192. von Anrep, G. On the part played by the suprarenals in the normal vascular reactions of the body. *J. Physiol.* **45**, 307–317 (1912).
193. Petroff, M. G. *et al.* Endogenous nitric oxide mechanisms mediate the stretch dependence of Ca<sup>2+</sup> release in cardiomyocytes. *Nat. Cell Biol.* **3**, 867–873 (2001).
194. Zhang, Y. H., Dingle, L., Hall, R. & Casadei, B. The role of nitric oxide and reactive oxygen species in the positive inotropic response to mechanical stretch in the mammalian myocardium. *Biochim. Biophys. Acta* **1787**, 811–817 (2009).
195. Katrien, L., Paul, F., U., S. S., L., B. D. & W., D. K. G. Neuregulin-1 Induces a Negative Inotropic Effect in Cardiac Muscle. *Circulation* **109**, 324–326 (2004).
196. Ashley, E. A. *et al.* The endogenous peptide apelin potently improves cardiac contractility and reduces cardiac loading in vivo. *Cardiovasc. Res.* **65**, 73–82 (2005).
197. Segers, V. F. M., Brutsaert, D. L. & Keulenaer, G. W. De. Cardiac Remodeling: Endothelial Cells Have More to Say Than Just NO. *Front. Physiol.* **9**, (2018).
198. Shimano, M. *et al.* Cardiac myocyte follistatin-like 1 functions to attenuate hypertrophy following pressure overload. *Proc. Natl. Acad. Sci.* **108**, E899 LP-E906 (2011).

199. Lara-Pezzi, E. *et al.* Expression of Follistatin-Related Genes Is Altered in Heart Failure. *Endocrinology* **149**, 5822–5827 (2008).
200. Yuichi, O. *et al.* Follistatin-Like 1 Is an Akt-Regulated Cardioprotective Factor That Is Secreted by the Heart. *Circulation* **117**, 3099–3108 (2008).
201. Tanaka, K. *et al.* Follistatin-Like 1 Regulates Hypertrophy in Heart Failure With Preserved Ejection Fraction. *JACC Basic to Transl. Sci.* **1**, 207 LP-221 (2016).
202. Hedhli, N. *et al.* Endothelium-derived neuregulin protects the heart against ischemic injury. *Circulation* **123**, 2254–2262 (2011).
203. Lemmens, K., Segers, V. F. M., Demolder, M. & De Keulenaer, G. W. Role of neuregulin-1/ErbB2 signaling in endothelium-cardiomyocyte cross-talk. *J. Biol. Chem.* **281**, 19469–19477 (2006).
204. István, S. *et al.* Apelin, the Novel Endogenous Ligand of the Orphan Receptor APJ, Regulates Cardiac Contractility. *Circ. Res.* **91**, 434–440 (2002).
205. Brutsaert, D. L. Cardiac endothelial-myocardial signaling: its role in cardiac growth, contractile performance, and rhythmicity. *Physiol. Rev.* **83**, 59–115 (2003).
206. Vila-Petroff, M. G., Younes, A., Egan, J., Lakatta, E. G. & Sollott, S. J. Activation of distinct cAMP-dependent and cGMP-dependent pathways by nitric oxide in cardiac myocytes. *Circ. Res.* **84**, 1020–1031 (1999).
207. Siflinger-Birnboim, A. *et al.* Molecular sieving characteristics of the cultured endothelial monolayer. *J. Cell. Physiol.* **132**, 111–117 (1987).
208. Schaum, N. *et al.* Single-cell transcriptomics of 20 mouse organs creates a Tabula Muris. *Nature* **562**, 367–372 (2018).
209. Fuller, S. J. *et al.* Cardiac protein kinases: the cardiomyocyte kinome and differential kinase expression in human failing hearts. *Cardiovasc. Res.* **108**, 87–98 (2015).
210. Watson, S. A. *et al.* Preparation of viable adult ventricular myocardial slices from large and small mammals. *Nat. Protoc.* **12**, 2623–2639 (2017).
211. Watson, S. A. *et al.* Biomimetic electromechanical stimulation to maintain adult myocardial slices in vitro. *Nat. Commun.* **10**, 2168 (2019).
212. Cooley, L. S. *et al.* Reversible transdifferentiation of blood vascular endothelial cells to a lymphatic-like phenotype in vitro. *J. Cell Sci.* **123**, 3808–3816 (2010).
213. Chrobak, I., Lenna, S., Stawski, L. & Trojanowska, M. Interferon- $\gamma$  promotes vascular

- remodeling in human microvascular endothelial cells by upregulating endothelin (ET)-1 and transforming growth factor (TGF)  $\beta$ 2. *J. Cell. Physiol.* **228**, 1774–1783 (2013).
214. Louch, W. E., Sheehan, K. A. & Wolska, B. M. Methods in cardiomyocyte isolation, culture, and gene transfer. *J. Mol. Cell. Cardiol.* **51**, 288–298 (2011).
215. Jambusaria, A. *et al.* Endothelial heterogeneity across distinct vascular beds during homeostasis and inflammation. *Elife* **9**, (2020).
216. Sham, J. S., Hatem, S. N. & Morad, M. Species differences in the activity of the Na(+)-Ca<sup>2+</sup> exchanger in mammalian cardiac myocytes. *J. Physiol.* **488** ( Pt 3, 623–631 (1995).
217. Gilsbach, R. *et al.* Distinct epigenetic programs regulate cardiac myocyte development and disease in the human heart in vivo. *Nat. Commun.* **9**, 391 (2018).
218. Ribeiro-Rodrigues, T. M. *et al.* Exosomes secreted by cardiomyocytes subjected to ischaemia promote cardiac angiogenesis. *Cardiovasc. Res.* **113**, 1338–1350 (2017).
219. Zhang, Q. *et al.* Microvesicles derived from hypoxia/reoxygenation-treated human umbilical vein endothelial cells promote apoptosis and oxidative stress in H9c2 cardiomyocytes. *BMC Cell Biol.* **17**, 25 (2016).
220. Sniegón, I., Prieß, M., Heger, J., Schulz, R. & Euler, G. Endothelial Mesenchymal Transition in Hypoxic Microvascular Endothelial Cells and Paracrine Induction of Cardiomyocyte Apoptosis Are Mediated via TGF $\beta$ <sub>1</sub>/SMAD Signaling. *Int. J. Mol. Sci.* **18**, (2017).
221. Zhang, Y., Pasparakis, M., Kollias, G. & Simons, M. Myocyte-dependent regulation of endothelial cell syndecan-4 expression. Role of TNF- $\alpha$ . *J. Biol. Chem.* **274**, 14786–14790 (1999).
222. Kubin, T. *et al.* Microvascular endothelial cells remodel cultured adult cardiomyocytes and increase their survival. *Am. J. Physiol.* **276**, H2179-87 (1999).
223. van Wamel, A. J., Ruwhof, C., van der Valk-Kokshoorn, L. J., Schrier, P. I. & van der Laarse, A. Rapid effects of stretched myocardial and vascular cells on gene expression of neonatal rat cardiomyocytes with emphasis on autocrine and paracrine mechanisms. *Arch. Biochem. Biophys.* **381**, 67–73 (2000).
224. Zheng, W., Seftor, E. A., Meininger, C. J., Hendrix, M. J. & Tomanek, R. J. Mechanisms of coronary angiogenesis in response to stretch: role of VEGF and TGF- $\beta$ . *Am. J. Physiol. Heart Circ. Physiol.* **280**, H909-17 (2001).

225. Wang, X. *et al.* Cardiomyocytes mediate anti-angiogenesis in type 2 diabetic rats through the exosomal transfer of miR-320 into endothelial cells. *J. Mol. Cell. Cardiol.* **74**, 139–150 (2014).
226. Kuramochi, Y. *et al.* Cardiac endothelial cells regulate reactive oxygen species-induced cardiomyocyte apoptosis through neuregulin-1beta/erbB4 signaling. *J. Biol. Chem.* **279**, 51141–51147 (2004).
227. Liu, J. *et al.* Overexpression of vasostatin-1 protects hypoxia/reoxygenation injuries in cardiomyocytes-endothelial cells transwell co-culture system. *Cell Biol. Int.* **38**, 26–31 (2014).
228. Yue, X., Acun, A. & Zorlutuna, P. Transcriptome profiling of 3D co-cultured cardiomyocytes and endothelial cells under oxidative stress using a photocrosslinkable hydrogel system. *Acta Biomater.* **58**, 337–348 (2017).
229. Zhang, Y. *et al.* Endothelial cells regulate cardiac myocyte reorganisation through  $\beta$ 1-integrin signalling. *Cell. Physiol. Biochem. Int. J. Exp. Cell. Physiol. Biochem. Pharmacol.* **35**, 1808–1820 (2015).
230. Kurokawa, Y. K., Shang, M. R., Yin, R. T. & George, S. C. Modeling trastuzumab-related cardiotoxicity in vitro using human stem cell-derived cardiomyocytes. *Toxicol. Lett.* **285**, 74–80 (2018).
231. Leucker, T. M. *et al.* Endothelial-cardiomyocyte crosstalk enhances pharmacological cardioprotection. *J. Mol. Cell. Cardiol.* **51**, 803–811 (2011).
232. Liu, Y., Xu, G., Wei, J., Wu, Q. & Li, X. Cardiomyocyte coculture on layered fibrous scaffolds assembled from micropatterned electrospun mats. *Mater. Sci. Eng. C. Mater. Biol. Appl.* **81**, 500–510 (2017).
233. Dunn, K. K. *et al.* Coculture of Endothelial Cells with Human Pluripotent Stem Cell-Derived Cardiac Progenitors Reveals a Differentiation Stage-Specific Enhancement of Cardiomyocyte Maturation. *Biotechnol. J.* **14**, e1800725 (2019).
234. Condorelli, G. *et al.* Cardiomyocytes induce endothelial cells to trans-differentiate into cardiac muscle: implications for myocardium regeneration. *Proc. Natl. Acad. Sci. U. S. A.* **98**, 10733–10738 (2001).
235. Liu, Y. *et al.* Vascular endothelial growth factor regulation of endothelial nitric oxide synthase phosphorylation is involved in isoflurane cardiac preconditioning. *Cardiovasc. Res.* **115**, 168–178 (2019).

236. Nishida, M., Springhorn, J. P., Kelly, R. A. & Smith, T. W. Cell-cell signaling between adult rat ventricular myocytes and cardiac microvascular endothelial cells in heterotypic primary culture. *J. Clin. Invest.* **91**, 1934–1941 (1993).
237. Sekine, H. *et al.* Endothelial cell coculture within tissue-engineered cardiomyocyte sheets enhances neovascularization and improves cardiac function of ischemic hearts. *Circulation* **118**, S145-52 (2008).
238. Narmoneva, D. A., Vukmirovic, R., Davis, M. E., Kamm, R. D. & Lee, R. T. Endothelial cells promote cardiac myocyte survival and spatial reorganization: implications for cardiac regeneration. *Circulation* **110**, 962–968 (2004).
239. Kitsuka, T. *et al.* 2-Cl-C.OXT-A stimulates contraction through the suppression of phosphodiesterase activity in human induced pluripotent stem cell-derived cardiac organoids. *PLoS One* **14**, e0213114 (2019).
240. Garzoni, L. R. *et al.* Dissecting coronary angiogenesis: 3D co-culture of cardiomyocytes with endothelial or mesenchymal cells. *Exp. Cell Res.* **315**, 3406–3418 (2009).
241. Su, T. *et al.* Cardiac Stem Cell Patch Integrated with Microengineered Blood Vessels Promotes Cardiomyocyte Proliferation and Neovascularization after Acute Myocardial Infarction. *ACS Appl. Mater. Interfaces* **10**, 33088–33096 (2018).
242. Maiullari, F. *et al.* A multi-cellular 3D bioprinting approach for vascularized heart tissue engineering based on HUVECs and iPSC-derived cardiomyocytes. *Sci. Rep.* **8**, 13532 (2018).
243. Gilpin, A. & Yang, Y. Decellularization Strategies for Regenerative Medicine: From Processing Techniques to Applications. *Biomed Res. Int.* **2017**, 9831534 (2017).
244. Tong, C. *et al.* Generation of bioartificial hearts using decellularized scaffolds and mixed cells. *Biomed. Eng. Online* **18**, 71 (2019).
245. Rogozhnikov, D., O'Brien, P. J., Elahipanah, S. & Yousaf, M. N. Scaffold Free Bio-orthogonal Assembly of 3-Dimensional Cardiac Tissue via Cell Surface Engineering. *Sci. Rep.* **6**, 39806 (2016).
246. Ravenscroft, S. M., Pointon, A., Williams, A. W., Cross, M. J. & Sidaway, J. E. Cardiac Non-myocyte Cells Show Enhanced Pharmacological Function Suggestive of Contractile Maturity in Stem Cell Derived Cardiomyocyte Microtissues. *Toxicol. Sci.* **152**, 99–112 (2016).
247. Lim, S. L., Lam, C. S. P., Segers, V. F. M., Brutsaert, D. L. & De Keulenaer, G. W.

- Cardiac endothelium-myocyte interaction: clinical opportunities for new heart failure therapies regardless of ejection fraction. *Eur. Heart J.* **36**, 2050–2060 (2015).
248. Kivela, R. *et al.* Endothelial Cells Regulate Physiological Cardiomyocyte Growth via VEGFR2-Mediated Paracrine Signaling. *Circulation* **139**, 2570–2584 (2019).
249. Juni, R. P. *et al.* Cardiac Microvascular Endothelial Enhancement of Cardiomyocyte Function Is Impaired by Inflammation and Restored by Empagliflozin. *JACC. Basic to Transl. Sci.* **4**, 575–591 (2019).
250. Lew, R. A. & Baertschi, A. J. Endothelial cells stimulate ANF secretion from atrial myocytes in co-culture. *Biochem. Biophys. Res. Commun.* **163**, 701–709 (1989).
251. Lopes da Silva, M. & Cutler, D. F. von Willebrand factor multimerization and the polarity of secretory pathways in endothelial cells. *Blood* **128**, 277–285 (2016).
252. van Buul-Wortelboer, M. F., Brinkman, H. J., Reinders, J. H., van Aken, W. G. & van Mourik, J. A. Polar secretion of von Willebrand factor by endothelial cells. *Biochim. Biophys. Acta* **1011**, 129–133 (1989).
253. Narahara, N., Enden, T., Wiiger, M. & Prydz, H. Polar expression of tissue factor in human umbilical vein endothelial cells. *Arterioscler. Thromb. a J. Vasc. Biol.* **14**, 1815–1820 (1994).
254. Kelm, M. Nitric oxide metabolism and breakdown. *Biochim. Biophys. Acta - Bioenerg.* **1411**, 273–289 (1999).
255. Thomas, D. D., Liu, X., Kantrow, S. P. & Lancaster, J. R. J. The biological lifetime of nitric oxide: implications for the perivascular dynamics of NO and O<sub>2</sub>. *Proc. Natl. Acad. Sci. U. S. A.* **98**, 355–360 (2001).
256. Marshall, C. J. Specificity of receptor tyrosine kinase signaling: transient versus sustained extracellular signal-regulated kinase activation. *Cell* **80**, 179–185 (1995).
257. Chi, J.-T. *et al.* Endothelial cell diversity revealed by global expression profiling. *Proc. Natl. Acad. Sci. U. S. A.* **100**, 10623–10628 (2003).
258. Cleuren, A. C. A. *et al.* The in vivo endothelial cell transcriptome is highly heterogeneous across vascular beds. *Proc. Natl. Acad. Sci. U. S. A.* **116**, 23618–23624 (2019).
259. Marcu, R. *et al.* Human Organ-Specific Endothelial Cell Heterogeneity. *iScience* **4**, 20–35 (2018).
260. Nolan, D. J. *et al.* Molecular signatures of tissue-specific microvascular endothelial cell



- heterogeneity in organ maintenance and regeneration. *Dev. Cell* **26**, 204–219 (2013).
261. Burrige, K. A. & Friedman, M. H. Environment and vascular bed origin influence differences in endothelial transcriptional profiles of coronary and iliac arteries. *Am. J. Physiol. Heart Circ. Physiol.* **299**, H837–46 (2010).
262. Lemmens, K., Doggen, K. & Keulenaer, G. W. De. Neuregulin-1 and its potential role in the control of cardiac function. *Heart Fail. Monit.* **5**, 119–124 (2008).
263. Kichuk, M. R. *et al.* Regulation of nitric oxide production in human coronary microvessels and the contribution of local kinin formation. *Circulation* **94**, 44–51 (1996).
264. Hartman, M. E., Dai, D.-F. & Laflamme, M. A. Human pluripotent stem cells: Prospects and challenges as a source of cardiomyocytes for in vitro modeling and cell-based cardiac repair. *Adv. Drug Deliv. Rev.* **96**, 3–17 (2016).
265. Louch, W. E., Koivumäki, J. T. & Tavi, P. Calcium signalling in developing cardiomyocytes: implications for model systems and disease. *J. Physiol.* **593**, 1047–1063 (2015).
266. Bassani, R. A., Altamirano, J., Puglisi, J. L. & Bers, D. M. Action potential duration determines sarcoplasmic reticulum Ca<sup>2+</sup> reloading in mammalian ventricular myocytes. *J. Physiol.* **559**, 593–609 (2004).
267. Bassani, J. W., Bassani, R. A. & Bers, D. M. Relaxation in rabbit and rat cardiac cells: species-dependent differences in cellular mechanisms. *J. Physiol.* **476**, 279–293 (1994).
268. Piper, H. M., Jacobson, S. L. & Schwartz, P. Determinants of cardiomyocyte development in long-term primary culture. *J. Mol. Cell. Cardiol.* **20**, 825–835 (1988).
269. Nippert, F., Schreckenber, R. & Schlüter, K.-D. Isolation and Cultivation of Adult Rat Cardiomyocytes. *J. Vis. Exp.* (2017). doi:10.3791/56634
270. Simpson, P., McGrath, A. & Savion, S. Myocyte hypertrophy in neonatal rat heart cultures and its regulation by serum and by catecholamines. *Circ. Res.* **51**, 787–801 (1982).
271. Dambrot, C. *et al.* Serum supplemented culture medium masks hypertrophic phenotypes in human pluripotent stem cell derived cardiomyocytes. *J. Cell. Mol. Med.* **18**, 1509–1518 (2014).
272. Podgrabinska, S. *et al.* Molecular characterization of lymphatic endothelial cells. *Proc. Natl. Acad. Sci.* **99**, 16069 LP-16074 (2002).

273. Banerji, S. *et al.* LYVE-1, a new homologue of the CD44 glycoprotein, is a lymph-specific receptor for hyaluronan. *J. Cell Biol.* **144**, 789–801 (1999).
274. Heiden, S. *et al.* Vascular endothelium derived endothelin-1 is required for normal heart function after chronic pressure overload in mice. *PLoS One* **9**, e88730–e88730 (2014).
275. Yasutomi, H. *et al.* The ATP-Binding Cassette Transporter ABCG2 Protects Against Pressure Overload–Induced Cardiac Hypertrophy and Heart Failure by Promoting Angiogenesis and Antioxidant Response. *Arterioscler. Thromb. Vasc. Biol.* **32**, 654–661 (2012).
276. Ritchie, R. H., Schiebinger, R. J., LaPointe, M. C. & Marsh, J. D. Angiotensin II-induced hypertrophy of adult rat cardiomyocytes is blocked by nitric oxide. *Am. J. Physiol.* **275**, H1370-4 (1998).
277. Martínez-Miguel, P. *et al.* Tweak up-regulates endothelin-1 system in mouse and human endothelial cells. *Cardiovasc. Res.* **113**, 207–221 (2017).
278. Adamopoulos, C. *et al.* Advanced glycation end products upregulate lysyl oxidase and endothelin-1 in human aortic endothelial cells via parallel activation of ERK1/2-NF- $\kappa$ B and JNK-AP-1 signaling pathways. *Cell. Mol. Life Sci.* **73**, 1685–1698 (2016).
279. Yin, J. C. *et al.* Cellular interplay via cytokine hierarchy causes pathological cardiac hypertrophy in RAF1-mutant Noonan syndrome. *Nature communications* **8**, 15518 (2017).
280. Madge, L. A. & Pober, J. S. TNF Signaling in Vascular Endothelial Cells. *Exp. Mol. Pathol.* **70**, 317–325 (2001).
281. Gabay, C. Interleukin-6 and chronic inflammation. *Arthritis Res. Ther.* **8**, S3 (2006).
282. Su, H., Lei, C.-T. & Zhang, C. Interleukin-6 Signaling Pathway and Its Role in Kidney Disease: An Update . *Frontiers in Immunology* **8**, 405 (2017).
283. Porter, K. E. & Turner, N. a. Cardiac fibroblasts: At the heart of myocardial remodeling. *Pharmacol. Ther.* **123**, 255–278 (2009).
284. Fontes, J. A., Rose, N. R. & Cihakova, D. The varying faces of IL-6: From cardiac protection to cardiac failure. *Cytokine* **74**, 62–68 (2015).
285. Wang, M. *et al.* Endothelial STAT3 plays a critical role in generalized myocardial proinflammatory and proapoptotic signaling. *Am. J. Physiol. Circ. Physiol.* **293**, H2101–H2108 (2007).

286. Bironaite, D. *et al.* Molecular mechanisms behind progressing chronic inflammatory dilated cardiomyopathy. *BMC Cardiovasc. Disord.* **15**, 26 (2015).
287. Kalogeropoulos, A. *et al.* Inflammatory markers and incident heart failure risk in older adults: the Health ABC (Health, Aging, and Body Composition) study. *J. Am. Coll. Cardiol.* **55**, 2129–2137 (2010).
288. Bujak, M. & Frangogiannis, N. G. The role of IL-1 in the pathogenesis of heart disease. *Arch. Immunol. Ther. Exp. (Warsz).* **57**, 165–176 (2009).
289. Dubnika, A. *et al.* Cytokines as therapeutic agents and targets in heart disease. *Cytokine Growth Factor Rev.* **43**, 54–68 (2018).
290. Wu, C. *et al.* Plasma levels of tumor necrosis factor-alpha and interleukin-6 are associated with diastolic heart failure through downregulation of sarcoplasmic reticulum Ca<sup>2+</sup> ATPase. *Crit Care Med* **39**, (2011).
291. Zouein, F. A., Booz, G. W. & Altara, R. STAT3 and Endothelial Cell-Cardiomyocyte Dialog in Cardiac Remodeling. *Front. Cardiovasc. Med.* **6**, 50 (2019).
292. Romano, M. *et al.* Role of IL-6 and its soluble receptor in induction of chemokines and leukocyte recruitment. *Immunity* **6**, 315–325 (1997).
293. Romano, M. *et al.* Role of IL-6 and its soluble receptor in induction of chemokines and leukocyte recruitment. *Immunity* **6**, 315–325 (1997).
294. Fischer, M. *et al.* I. A bioactive designer cytokine for human hematopoietic progenitor cell expansion. *Nat. Biotechnol.* **15**, 142–145 (1997).
295. Garbers, C. *et al.* Inhibition of classic signaling is a novel function of soluble glycoprotein 130 (sgp130), which is controlled by the ratio of interleukin 6 and soluble interleukin 6 receptor. *J. Biol. Chem.* **286**, 42959–42970 (2011).
296. Brunssen, S. H., Moy, S. S., Toews, A. D., McPherson, C. A. & Harry, G. J. Interleukin-6 (IL-6) receptor/IL-6 fusion protein (Hyper IL-6) effects on the neonatal mouse brain: possible role for IL-6 trans-signaling in brain development and functional neurobehavioral outcomes. *Brain. Behav. Immun.* **27**, 42–53 (2013).
297. Rakemann, T. *et al.* The designer cytokine hyper-interleukin-6 is a potent activator of STAT3-dependent gene transcription in vivo and in vitro. *J. Biol. Chem.* **274**, 1257–1266 (1999).
298. Takashi, M. *et al.* Thrombin and Phenotypic Modulation of the Endothelium. *Arterioscler. Thromb. Vasc. Biol.* **24**, 41–53 (2004).

299. Horenberg, A. L., Houghton, A. M., Pandey, S., Seshadri, V. & Guilford, W. H. S-nitrosylation of cytoskeletal proteins. *Cytoskeleton* **76**, 243–253 (2019).
300. Gogiraju, R. *et al.* Endothelial Leptin Receptor Deletion Promotes Cardiac Autophagy and Angiogenesis Following Pressure Overload by Suppressing Akt/mTOR Signaling. *Circ. Heart Fail.* **12**, e005622 (2019).
301. Ferraro, B. *et al.* Pro-Angiogenic Macrophage Phenotype to Promote Myocardial Repair. *J. Am. Coll. Cardiol.* **73**, 2990 LP-3002 (2019).
302. Liu, J. & Agarwal, S. Mechanical Signals Activate Vascular Endothelial Growth Factor Receptor-2 To Upregulate Endothelial Cell Proliferation during Inflammation. *J. Immunol.* 93660 (2010). doi:10.4049/jimmunol.0903660
303. Bonauer, A. *et al.* MicroRNA-92a Controls Angiogenesis and Functional Recovery of Ischemic Tissues in Mice. *Science (80-. )*. **324**, 1710 LP-1713 (2009).
304. Tilg, H., Trehu, E., Atkins, M. B., Dinarello, C. A. & Mier, J. W. Interleukin-6 (IL-6) as an anti-inflammatory cytokine: induction of circulating IL-1 receptor antagonist and soluble tumor necrosis factor receptor p55. *Blood* **83**, 113–118 (1994).
305. Tsai, M.-H., Pai, L.-M. & Lee, C.-K. Fine-Tuning of Type I Interferon Response by STAT3 . *Frontiers in Immunology* **10**, 1448 (2019).
306. Bae, J.-S., Kim, Y.-U., Park, M.-K. & Rezaie, A. R. Concentration dependent dual effect of thrombin in endothelial cells via Par-1 and Pi3 Kinase. *J. Cell. Physiol.* **219**, 744–751 (2009).
307. DOUGALL, W. C. & NICK, H. S. Manganese Superoxide Dismutase: A Hepatic Acute Phase Protein Regulated by Interleukin-6 and Glucocorticoids\*. *Endocrinology* **129**, 2376–2384 (1991).
308. Brown, C. O. *et al.* Interleukin-6 counteracts therapy-induced cellular oxidative stress in multiple myeloma by up-regulating manganese superoxide dismutase. *Biochem. J.* **444**, 515–527 (2012).
309. Wang, J. *et al.* Potential Crosstalk of Interleukin-6-Heme Oxygenase-1 Dependent Mechanism Involved in Resistance to Lenalidomide in Multiple Myeloma Cells. *Blood* **126**, 4856 (2015).
310. Lee, T.-S. & Chau, L.-Y. Heme oxygenase-1 mediates the anti-inflammatory effect of interleukin-10 in mice. *Nat. Med.* **8**, 240–246 (2002).
311. Oh, J. W., Van Wagoner, N. J., Rose-John, S. & Benveniste, E. N. Role of IL-6 and the

- soluble IL-6 receptor in inhibition of VCAM-1 gene expression. *J. Immunol.* **161**, 4992–4999 (1998).
312. Granger, D. N. & Kubes, P. The microcirculation and inflammation: modulation of leukocyte-endothelial cell adhesion. *J. Leukoc. Biol.* **55**, 662–675 (1994).
313. Kriegelstein, C. F. & Granger, D. N. Adhesion molecules and their role in vascular disease. *Am. J. Hypertens.* **14**, 44S–54S (2001).
314. Li, W. *et al.* Intravital 2-photon imaging of leukocyte trafficking in beating heart. *J. Clin. Invest.* **122**, 2499–2508 (2012).
315. Lino, D. O. C. *et al.* Interleukin-6 and adhesion molecules VCAM-1 and ICAM-1 as biomarkers of post-acute myocardial infarction heart failure. *Brazilian Journal of Medical and Biological Research* **52**, (2019).
316. Wang, X. H. *et al.* MicroRNA-320 EXPRESSION IN MYOCARDIAL MICROVASCULAR ENDOTHELIAL CELLS AND ITS RELATIONSHIP WITH INSULIN-LIKE GROWTH FACTOR-1 IN TYPE 2 DIABETIC RATS. *Clin. Exp. Pharmacol. Physiol.* **36**, 181–188 (2009).
317. Iaconetti, C. *et al.* Inhibition of miR-92a increases endothelial proliferation and migration in vitro as well as reduces neointimal proliferation in vivo after vascular injury. *Basic Res. Cardiol.* **107**, 296 (2012).
318. Virag, J. I. & Murry, C. E. Myofibroblast and Endothelial Cell Proliferation during Murine Myocardial Infarct Repair. *Am. J. Pathol.* **163**, 2433–2440 (2003).
319. Fräter-Schröder, M., Müller, G., Birchmeier, W. & Böhlen, P. Transforming growth factor-beta inhibits endothelial cell proliferation. *Biochem. Biophys. Res. Commun.* **137**, 295–302 (1986).
320. Sedgwick, J. B., Menon, I., Gern, J. E. & Busse, W. W. Effects of inflammatory cytokines on the permeability of human lung microvascular endothelial cell monolayers and differential eosinophil transmigration. *J. Allergy Clin. Immunol.* **110**, 752–756 (2002).
321. Wyman, A. E. *et al.* SIRT7 deficiency suppresses inflammation, induces EndoMT, and increases vascular permeability in primary pulmonary endothelial cells. *Sci. Rep.* **10**, 12497 (2020).
322. Marti, C. N. *et al.* Endothelial dysfunction, arterial stiffness, and heart failure. *J. Am. Coll. Cardiol.* **60**, 1455–1469 (2012).
323. Durán, W. N., Beuve, A. V & Sánchez, F. A. Nitric oxide, S-nitrosation, and endothelial

- permeability. *IUBMB Life* **65**, 819–826 (2013).
324. Durán, W. N., Breslin, J. W. & Sánchez, F. A. The NO cascade, eNOS location, and microvascular permeability. *Cardiovasc. Res.* **87**, 254–261 (2010).
  325. Devika, N. T. & Jaffar Ali, B. M. Analysing calcium dependent and independent regulation of eNOS in endothelium triggered by extracellular signalling events. *Mol. Biosyst.* **9**, 2653–2664 (2013).
  326. Kopincová, J., Púzserová, A. & Bernátová, I. L-NAME in the cardiovascular system – nitric oxide synthase activator? *Pharmacol. Reports* **64**, 511–520 (2012).
  327. Dubey, S. *et al.* Withaferin A Associated Differential Regulation of Inflammatory Cytokines . *Frontiers in Immunology* **9**, 195 (2018).
  328. Mestries, J. C. *et al.* In vivo modulation of coagulation and fibrinolysis by recombinant glycosylated human interleukin-6 in baboons. *Eur. Cytokine Netw.* **5**, 275–281 (1994).
  329. Emeis, J. J. & Kooistra, T. Interleukin 1 and lipopolysaccharide induce an inhibitor of tissue-type plasminogen activator in vivo and in cultured endothelial cells. *J. Exp. Med.* **163**, 1260–1266 (1986).
  330. Zlibut, A., Bocsan, I. C. & Agoston-Coldea, L. Pentraxin-3 and endothelial dysfunction. *Adv. Clin. Chem.* **91**, 163–179 (2019).
  331. Nishihira, J., Koyama, Y. & Mizue, Y. Identification of macrophage migration inhibitory factor (MIF) in human vascular endothelial cells and its induction by lipopolysaccharide. *Cytokine* **10**, 199–205 (1998).
  332. Modur, V., Li, Y., Zimmerman, G. A., Prescott, S. M. & McIntyre, T. M. Retrograde inflammatory signaling from neutrophils to endothelial cells by soluble interleukin-6 receptor alpha. *J. Clin. Invest.* **100**, 2752–2756 (1997).
  333. Fenini, G., Contassot, E. & French, L. E. Potential of IL-1, IL-18 and Inflammasome Inhibition for the Treatment of Inflammatory Skin Diseases . *Frontiers in Pharmacology* **8**, 278 (2017).
  334. Gerdes, N. *et al.* Expression of interleukin (IL)-18 and functional IL-18 receptor on human vascular endothelial cells, smooth muscle cells, and macrophages: implications for atherogenesis. *J. Exp. Med.* **195**, 245–257 (2002).
  335. Campanella, G. S. V, Colvin, R. A. & Luster, A. D. CXCL10 Can Inhibit Endothelial Cell Proliferation Independently of CXCR3. *PLoS One* **5**, e12700 (2010).

336. O., W. E. *et al.* Expression and Regulation of ST2, an Interleukin-1 Receptor Family Member, in Cardiomyocytes and Myocardial Infarction. *Circulation* **106**, 2961–2966 (2002).
337. Caselli, C. *et al.* IL-33/ST2 Pathway and Classical Cytokines in End-Stage Heart Failure Patients Submitted to Left Ventricular Assist Device Support: A Paradoxical Role for Inflammatory Mediators? *Mediators Inflamm.* **2013**, 498703 (2013).
338. Mildner, M. *et al.* Primary sources and immunological prerequisites for sST2 secretion in humans. *Cardiovasc. Res.* **87**, 769–777 (2010).
339. Duchene, J. *et al.* A novel inflammatory pathway involved in leukocyte recruitment: role for the kinin B1 receptor and the chemokine CXCL5. *J. Immunol.* **179**, 4849–4856 (2007).
340. Zineh, I. *et al.* Epithelial neutrophil-activating peptide (ENA-78), acute coronary syndrome prognosis, and modulatory effect of statins. *PLoS One* **3**, e3117–e3117 (2008).
341. Matsuo, Y. *et al.* CXC-chemokine/CXCR2 biological axis promotes angiogenesis in vitro and in vivo in pancreatic cancer. *Int. J. cancer* **125**, 1027–1037 (2009).
342. Sanada, S. *et al.* IL-33 and ST2 comprise a critical biomechanically induced and cardioprotective signaling system. *J. Clin. Invest.* **117**, 1538–1549 (2007).
343. Lopez-Castejon, G. & Brough, D. Understanding the mechanism of IL-1 $\beta$  secretion. *Cytokine Growth Factor Rev.* **22**, 189–195 (2011).
344. Zupancic, G., Ogden, D., Magnus, C. J., Wheeler-Jones, C. & Carter, T. D. Differential exocytosis from human endothelial cells evoked by high intracellular Ca<sup>2+</sup> concentration. *J. Physiol.* **544**, 741–755 (2002).
345. Paulus, W. J. & Bronzwaer, J. G. F. Nitric oxide's role in the heart: control of beating or breathing? *Am. J. Physiol. Heart Circ. Physiol.* **287**, H8-13 (2004).
346. Cotton, J. M., Kearney, M. T. & Shah, A. M. Nitric oxide and myocardial function in heart failure: friend or foe? *Heart* **88**, 564–566 (2002).
347. Prendergast, B. D., Sagach, V. F. & Shah, A. M. Basal release of nitric oxide augments the Frank-Starling response in the isolated heart. *Circulation* **96**, 1320–1329 (1997).
348. Clerk, A. *et al.* Signaling pathways mediating cardiac myocyte gene expression in physiological and stress responses. *J. Cell. Physiol.* **212**, 311–322 (2007).

349. Garay, C. *et al.* Epidermal growth factor-stimulated Akt phosphorylation requires clathrin or ErbB2 but not receptor endocytosis. *Mol. Biol. Cell* **26**, 3504–3519 (2015).
350. F., B. O. & D., M. J. Involvement of Extracellular Signal-Regulated Kinases 1/2 in Cardiac Hypertrophy and Cell Death. *Circ. Res.* **91**, 776–781 (2002).
351. Kehat, I. & Molkenstin, J. D. Extracellular signal-regulated kinase 1/2 (ERK1/2) signaling in cardiac hypertrophy. *Ann. N. Y. Acad. Sci.* **1188**, 96–102 (2010).
352. Chaanine, A. H. & Hajjar, R. J. AKT signalling in the failing heart. *Eur. J. Heart Fail.* **13**, 825–829 (2011).
353. Zheng, M. *et al.* Sarcoplasmic reticulum calcium defect in Ras-induced hypertrophic cardiomyopathy heart. *Am. J. Physiol. Heart Circ. Physiol.* **286**, H424-33 (2004).
354. Ho, P. D. *et al.* The Raf-MEK-ERK Cascade Represents a Common Pathway for Alteration of Intracellular Calcium by Ras and Protein Kinase C in Cardiac Myocytes\*. (1998).
355. Kim, Y.-K. *et al.* Mechanism of Enhanced Cardiac Function in Mice with Hypertrophy Induced by Overexpressed Akt. *J. Biol. Chem.* **278**, 47622–47628 (2003).
356. Venetucci, L. A., Trafford, A. W., Díaz, M. E., O'Neill, S. C. & Eisner, D. A. Reducing ryanodine receptor open probability as a means to abolish spontaneous Ca<sup>2+</sup> release and increase Ca<sup>2+</sup> transient amplitude in adult ventricular myocytes. *Circ. Res.* **98**, 1299–1305 (2006).
357. Picht, E. *et al.* Dynamic calcium movement inside cardiac sarcoplasmic reticulum during release. *Circ. Res.* **108**, 847–856 (2011).
358. Bassani, J. W., Yuan, W. & Bers, D. M. Fractional SR Ca release is regulated by trigger Ca and SR Ca content in cardiac myocytes. *Am. J. Physiol.* **268**, C1313-9 (1995).
359. Jayasinghe, I. D., Cannell, M. B. & Soeller, C. Organization of ryanodine receptors, transverse tubules, and sodium-calcium exchanger in rat myocytes. *Biophys. J.* **97**, 2664–2673 (2009).
360. Haizlip, K. M. *et al.* Dissociation of Calcium Transients and Force Development following a Change in Stimulation Frequency in Isolated Rabbit Myocardium. *Biomed Res. Int.* **2015**, 468548 (2015).
361. Iribe, G., Helmes, M. & Kohl, P. Force-length relations in isolated intact cardiomyocytes subjected to dynamic changes in mechanical load. *Am. J. Physiol. Heart Circ. Physiol.* **292**, H1487-97 (2007).



362. Lee, B.-A. & Oh, D.-J. The effects of long-term aerobic exercise on cardiac structure, stroke volume of the left ventricle, and cardiac output. *J. Exerc. Rehabil.* **12**, 37–41 (2016).
363. Pogwizd, S. M., Qi, M., Yuan, W., Samarel, A. M. & Bers, D. M. Upregulation of Na(+)/Ca(2+) exchanger expression and function in an arrhythmogenic rabbit model of heart failure. *Circ. Res.* **85**, 1009–1019 (1999).
364. Campbell, D. L., Stamler, J. S. & Strauss, H. C. Redox modulation of L-type calcium channels in ferret ventricular myocytes. Dual mechanism regulation by nitric oxide and S-nitrosothiols. *J. Gen. Physiol.* **108**, 277–293 (1996).
365. Steyers, C. M. & Miller, F. J. Endothelial Dysfunction in Chronic Inflammatory Diseases. *Int. J. Mol. Sci.* **15**, 11324–11349 (2014).
366. McCabe, T. J., Fulton, D., Roman, L. J. & Sessa, W. C. Enhanced electron flux and reduced calmodulin dissociation may explain ‘calcium-independent’ eNOS activation by phosphorylation. *J. Biol. Chem.* **275**, 6123–6128 (2000).
367. Eroglu, E., Saravi, S. S. S., Sorrentino, A., Steinhorn, B. & Michel, T. Discordance between eNOS phosphorylation and activation revealed by multispectral imaging and chemogenetic methods. *Proc. Natl. Acad. Sci.* **116**, 20210 LP-20217 (2019).
368. Koliijn, D. *et al.* Empagliflozin improves endothelial and cardiomyocyte function in human heart failure with preserved ejection fraction via reduced pro-inflammatory-oxidative pathways and protein kinase G $\alpha$  oxidation. *Cardiovasc. Res.* (2020). doi:10.1093/cvr/cvaa123
369. Cao, J. *et al.* Lentiviral-human heme oxygenase targeting endothelium improved vascular function in angiotensin II animal model of hypertension. *Hum. Gene Ther.* **22**, 271–282 (2011).
370. Franssen, C. *et al.* Myocardial Microvascular Inflammatory Endothelial Activation in Heart Failure With Preserved Ejection Fraction. *JACC Hear. Fail.* **4**, 312–324 (2016).
371. Valero-Muñoz, M., Backman, W. & Sam, F. Murine Models of Heart Failure with Preserved Ejection Fraction: a ‘Fishing Expedition’. *JACC. Basic to Transl. Sci.* **2**, 770–789 (2017).
372. Pérez, N. G. *et al.* Silencing of NHE-1 blunts the slow force response to myocardial stretch. *J. Appl. Physiol.* **111**, 874–880 (2011).



## Appendix

## SPRINGER NATURE LICENSE

### TERMS AND CONDITIONS

Nov 01, 2020

This Agreement between Mr. Jerome Fourre ("You") and Springer Nature ("Springer Nature") consists of your license details and the terms and conditions provided by Springer Nature and Copyright Clearance Center.

License Number	4912581228718
License date	Sep 19, 2020
Licensed Content Publisher	Springer Nature
Licensed Content Publication	Nature
Licensed Content Title	Cardiac excitation–contraction coupling
Licensed Content Author	Donald M. Bers
Licensed Content Date	Jan 10, 2002
Type of Use	Thesis/Dissertation
Requestor type	academic/university or research institute
Format	print and electronic
Portion	figures/tables/illustrations
Number of figures/tables/illustrations	1
High-res required	no
Will you be translating?	no
Circulation/distribution	1 - 29
Author of this Springer Nature content	no
Title	Paracrine crosstalk between endothelial cells and cardiomyocytes during inflammation
Institution name	Imperial College London
Expected presentation date	Oct 2020
Portions	Figure 1